Technology for the Stars:
Extending Our Reach

DISTRIBUTION STATEMENT A
Approved for public release;
Distribution Unlimited

Research and Technology
1995 Annual Report
of the
Marshall Space Flight Center

DISCLAIMER NOTICE

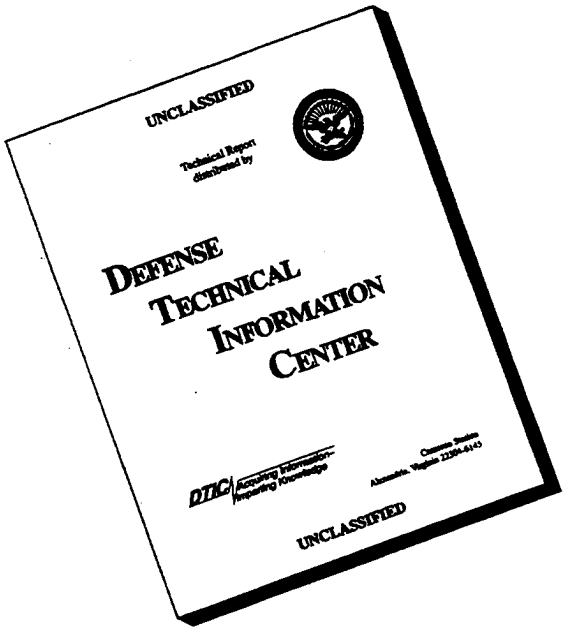

THIS DOCUMENT IS BEST QUALITY AVAILABLE. THE COPY FURNISHED TO DTIC CONTAINED A SIGNIFICANT NUMBER OF PAGES WHICH DO NOT REPRODUCE LEGIBLY.

For further information regarding this report,
contact Mr. Harry Craft, Jr., Director of the
Technology Transfer Office, Mail Stop LA01,
Marshall Space Flight Center, AL 35812.
The telephone number is 205–544–5418.

Research and Technology 1995

Annual Report of the Marshall Space Flight Center

NASA TM–108501

19960904 010

National Aeronautics and
Space Administration

George C. Marshall Space Flight Center
Marshall Space Flight Center, Alabama 35812

DTIC QUALITY INSPECTED 1

DISTRIBUTION STATEMENT A
Approved for public release;
Distribution Unlimited

Introduction

Marshall Space Flight Center's greatest assets are its people—highly qualified engineers and scientists who perform the daily analysis, development, and engineering necessary to extend humankind's grasp. Propulsion is the foundation that enables America's future in space. MSFC's talented team continues to achieve new advances through focused efforts in space propulsion, materials and processes, structures and dynamics, and avionics. Microgravity at MSFC provides invaluable insights into biotechnology processes and materials science/technology which are enabled by and exploit the unique space-flight environment. Dedicated scientific experts are making it possible to continue exploration of the physics of the Earth and the Universe. The Advanced Studies, Research, Technology, and Technology Transfer projects summarized in this report represent a sampling of MSFC's contributions to inspire and serve America and to benefit the quality of life for humankind.

J. Wayne Littles

Wayne Littles
Director
Marshall Space Flight Center

Acknowledgments

The point of contact and coordinator at MSFC for this report is H.C. Stinson, Technology Investment Office, (LA40/205–544–7239). She was assisted by an editorial committee consisting of E. Cothran, R. Chappell, J.M. McMillion, A. Roth, and G.R. Wallace. Detailed editorial support and production assistance was provided by MSI, a Division of The Bionetics Corporation. The research technology work at MSFC is a cooperative effort; however, due to space restrictions, it is impossible to list all those involved in the projects described in this report.

To assist the reader, the MSFC contact, office code, and telephone number are included at the beginning of each article. The sponsoring organization and university and industry involvement are given at the end of each article. An abbreviations and acronyms list, an alphabetical index of contacts, and an index of key words are presented at the end of this report.

Table of Contents

Technology for the Stars: Extending Our Reach ix

Advanced Studies

Introduction Axel Roth 1

Space Systems

Atmospheric and Ionospheric Research Using a Small Expendable Deployed Satellite — C. Les Johnson — 2

Very Fine-Line Lithography for Extreme Ultraviolet and Soft X-Ray Optics — C. Les Johnson — 3

Ultra-Lightweight Telescope, Integrated Missions for Astronomy — Edward E. Montgomery — 4

Tether Applications on the Space Station — Vernon W. Keller — 5

Global Emergency Observation Warning and Relief Network — Angelia P. Bukley — 7

Survivable Space Tethers — Charles C. Rupp — 8

Space Science

The Magnetosphere Imager Mission — C. Les Johnson — 10

Passively Cooled Reconnaissance of the Interstellar Medium — Jonathan W. Campbell — 11

Hard X-Ray and Gamma-Ray Imaging System — Jonathan W. Campbell — 12

Space Transportation

Maglifter — Joe T. Howell — 13

Solar Thermal Propulsion — Alan Adams — 17

Research

Virtual Keyboard for Hands-Free Operations — Jonnathan Kim — 18

Research Programs

Introduction Gregory S. Wilson 21

Microgravity Science

Electromagnetic Field Effects in Semiconductor Crystal Growth — Martin P. Volz — 22

Magnetic-Damping Test of Convective Flows in Microgravity — Frank R. Szofran — 23

High-Brilliance X-Ray Source for Protein Crystallography — Daniel C. Carter — 25

Protein Crystal-Growth Apparatus for Microgravity Facility Hardware — Daniel C. Carter — 26

Phase-Shifting Interferometric Analysis of Protein Crystal-Growth Boundaries and Convective Flows — William K. Witherow — 27

Diode-Laser Holographic-Imaging System Applied to the Study of Fluids in Microgravity — William K. Witherow — 28

Investigation of Local Effects on Microstructure Evolution — Donald O. Frazier — 29

Polydiacetylene Thin Films for Photonic Applications — Donald O. Frazier — 31

Prediction of Nonlinear Optical Properties of Organic Materials — Craig E. Moore — 32

Earth System Science

Numerical Modeling of Nonlinear Baroclinic Fluid Systems — Timothy L. Miller — 34

Global Modeling of Surface Boundary Forcing — Daniel E. Fitzjarrald, Franklin R. Robertson — 35

Global Multiphase Water Analysis — Franklin R. Robertson — 37

Astrophysics

The Third Burst and Transient Source Experiment Catalog of Gamma-Ray Bursts — Charles A. Meegan — 38

Gamma-Ray Bursts as a Tool for Cosmology	John M. Horack	39
Measurements With a Superconducting Magnet Spectrometer	Thomas A. Parnell James H. Derrickson	41
Solar Physics		
Newly Discovered Flows on the Sun's Surface	David H. Hathaway	44
Heating Magnetic Structures in the Solar Corona	Jason G. Porter	45
Solar Magnetic Fields	Mona J. Hagyard	47
The Fine-Scale Structure of the Interplanetary Magnetic Field	Steven T. Suess	48
Three-Dimensional Magnetic Field-Line Topology in the Outer Heliosphere	Steven T. Suess	49
Solar Flares	Ronald L. Moore	51
Three-Dimensional Rendering and Image Analysis of Coronal Loops	G. Allen Gary	52
Space Physics		
Particle Transport From the Magnetosphere's Low-Latitude Boundary Layer	Barbara L. Giles	54
MSFC Thermal Plasma Instrumentation Probing the Topside, Cleft Ionosphere	Craig J. Pollack	55
Cold Plasma in the Earth's Magnetosphere	Dennis L. Gallagher	57
The Dusty Plasma Experiment	James F. Spann	59
Quantitative Determination of the Rate of Hydrogen-Ion Heating by an Argon-Ion Beam	Michael O. Chandler	61
Helium- to Hydrogen-Ion Ratios in the Inner Magnetosphere	Paul D. Craven	62
Plasma Tornadoes	Thomas E. Moore	65
Absolute Sensitivity Measurement for the Thermal Ion Dynamics Experiment	Victoria N. Coffey	67
Technology Programs		
Introduction	James M. McMillion	71
Propulsion and Fluid Management		
Low-Cost Turbomachinery Technology	Matthew W. Marsh	72
Low-Cost Combustion Devices Component Design Verification	David L. Sparks	73
Magnetically Actuated Propellant Orientation	George Schmidt	76
Main and Preburner Injector Technology	John Hutt	78
Tripropellant Injector and Combustion Technology	Huu P. Trinh	79
Effects of Hydrogen Addition on RP–1 Droplet Burning in Oxygen Environment	Huu P. Trinh	80
Unielement, Oxygen-Rich Preburner	Huu P. Trinh	82
Ultrasonic Fuel Regression Measurement in Hybrid Rocket Motors	Dan M. Holt	84
Results of an 11-Inch Liquid-Oxygen Hybrid Rocket Motor Combustion Instability Study	Charles Martin	86
Pressure Oscillations in Hybrid Rocket Motors	Dan M. Holt	88
Solid Rocket Motor Asbestos-Free Insulation	John O. Funkhouser	90
Hybrid Rocket Cold-Flow Modeling	Wendy Cruit	91
Development and Demonstration of a 250-Kilopound-Force Hybrid Rocket Test-Bed	Dan M. Holt	92
Solid Rocket Combustion Simulation Using the Hybrid Combustion Process	Dan M. Holt	94
Solar Thermal Propulsion Thrusters and Cryogenic Fluid Management	Leon J. Hastings	96
A Lightweight, Composite, Liquid-Hydrogen Feedline	Philip Tygielski	98

Structures and Dynamics

Suppression of Transient Acceleration by Levitation Evaluation	Gerald S. Nurre	101
Reusable Launch Vehicle Lander Guidance and Control Research	Dan J. Coughlin Don R. Krupp Michael W. Gallaher	102
TREETOPS Structural Dynamics and Controls Simulation System Upgrade	George Myers	104
Segmented Mirror Adaptive Optics	John M. Rakoczy	105
Automated Rendezvous and Capture Technology Description	Richard W. Dabney	107
Experimental Determination of Preswirl Effects on Damping Seal Performance	Eric M. Earhart	111
System for Anomaly and Failure Detection	Thomas H. Fox	112
Flight-Control Augmentation for Aft Center-of-Gravity Launch Vehicles	Chris Barret	112
Composite Integrally Bladed Turbine	Katherine K. Mims	116
Damping Measurement of Advanced Composite Materials for Turbomachinery Applications	Donald L. Harris	117
Synchronous Phase-Averaging Method for Machinery Diagnostics	Tony R. Fiorucci	119
Single-Cycle Versus Multicycle Proof Testing	Henry M. Lee	122
Development of State-of-the-Art Proof-Test Methodology	Charles L. Denniston	122
Hybrid Method for Measurement of Rotational Structural Dynamic Properties	Michael L. Tinker	125
Life Prediction of Ceramic- and Metal-Matrix Composites	James B. Min	127
Elastic-Plastic and Fully Plastic Fatigue Crack Growth	Wayne Gregg	129
Life-Prediction Methodology for Ceramic-Matrix Composites	Rene Ortega	130
Coherent-Phase Cavitation-Monitoring System for Turbomachinery	Tom E. Nesman	131
Investigation of Inducer Steady and Unsteady Blade Loads	Stephen W. Gaddis	134
Investigation of Flow Through a Powering-Steering Flow-Control Valve	Stephen E. Skelley	135
Experimental Microthruster Evaluation at Simulated Orbital Conditions	Andrew W. Smith	136
Determination of Composite Material Sensitivity to Permeability Depending Upon Lay-Up Configuration	Robert W. Carrigan	138
Composite Intertank	Donald B. Ford Pete I. Rodriguez	138
Orbital Debris Penetration Effects in Spacecraft Interiors	Joel E. Williamsen	140
Nonautoclave Curing of Composite Flight Structures	Jeffrey L. Finckenor	143
Orbital Debris Penetration Resistance of Reusable Launch Vehicles	Jennifer H. Robinson	144
Composite Redesign of Obstetrical Forceps	Stan S. Smeltzer, III	145
Composite Dome and Polar-Boss Leakage Validation	Stan S. Smeltzer, III	146
Poisoning Characteristics of a Palladium-Based Trace Contaminant Control System Catalyst	Jay L. Perry Mary S. Traweek	147
Trace Chemical Contaminant Control System Performance Simulation	Jay L. Perry Charles Ray	148

Small, Efficient Metal-Substrate Catalytic Converter for Trace Contaminant Control — Jay L. Perry — 149
Catalysts for the Oxidation of Trace Contaminants — Jay L. Perry — 151
Trace Chemical Contaminant Generation Rates for System Design of Closed Habitats — Jay L. Perry — 151
Urine Pretreatment Methods for Microgravity — Cindy F. Hutchens — 152
Developing a Microbial Monitor With Polymerase Chain-Reaction Technology — Monserrate C. Roman — 154
Development of a Packed-Bed Adsorption Model With Predictive Capabilities — James C. Knox — 156
Pulse-Tube Refrigeration for Spacecraft and Commercial Applications — Douglas G. Westra — 158
Low-Temperature Stirling-Cycle Refrigerator for Spacecraft Refrigeration Systems — Douglas G. Westra — 159

Materials and Manufacturing Processes

Localized Corrosion in Aluminum Alloys by the Scanning Reference Electrode Technique — Merlin D. Danford — 162
Development of Low Thermal Conductivity, Polyacrylonitrile-Based Fibers — Raymond G. Clinton, Jr. — 164
Improved Single-Crystal Superalloys Tailored for Hydrogen Service — Deborah D. Schmidt — 167
Characterizing Metal Brittleness — Arthur C. Nunes, Jr. — 168
Casting Modeling Technology — Douglas N. Wells — 169
Development of a High-Strength, Low-Cost Aluminum Piston Alloy — Jonathan A. Lee — 170

Avionics

Clamp-On Flow-Velocity and Density Transducers for Cryofluids in Thin-Walled Conduits — William T. Powers — 171
Ground-Based Optical Leak Detection — William T. Powers — 172
In-Flight Leak Detection: a Hydrogen/Oxygen Leak-Imaging Sensor — William T. Powers — 174
Installation Integrity Measurement for Various Sensors — Morrison R. Burns, Jr. — 176
Optical Plume Anomaly Detection Engine Diagnostic Filtering System — William T. Powers — 178
Flight-Qualifiable, Three-Point Docking Mechanism Control Electronics for Automated Docking — William Jacobs — 181
Modular Rocket Engine Control Software — Richard H. Beckham — 182

Mission Operations

The Use of Virtual Reality in the Design Analysis of a Space Station Control Room — Joseph P. Hale, II — 183

Technology Transfer

Introduction — Harry G. Craft, Jr. — 187
MSFC Small Business Innovation Research — Helen C. Stinson, Timothy A. Self — 188
Dual-Use Hydrostatic Bearing Technology — Christopher J. Bramon — 190
Space Vehicle to Save Launch Costs — Vernotto C. McMillan — 193
Structural Ceramics for Advanced Turbomachinery Applications — Christopher J. Bramon, Gary G. Genge — 195
New Technology Targets Eye Disease — Robert J. Lessels — 197
Space-Age Training Program Technologies Offered to Commercial Industries — Robert J. Lessels — 198

NASA Welding Technology Transfer to Private Industry	Robert J. Lessels	200
Waterjet-Stripping Technology	Robert J. Lessels	201
Rapid Prototyping	Robert J. Lessels	201
Composites Technologies	Robert J. Lessels	202
Composite Piping for Offshore Oil and Gas Industry	Robert J. Lessels	203
NASA Assistance to the Physically Challenged	Robert J. Lessels	204
Marine Jet-Propulsion Technology	Robert J. Lessels	205
Portable Lifting Seat	Robert J. Lessels	207
Ocular Screening System	Robert J. Lessels	207
Hybrid Rocket Motor Technology	Robert J. Lessels	209
Quick-Connect Nut and Bolt	Robert J. Lessels	209
Improvements for Firefighters	Robert J. Lessels	211

MSFC Propulsion Center of Excellence is Built on Solid Foundation — Michael D. Wright — 212

Abbreviations and Acronyms — 223

Index of Contacts — 229

Index of Key Words — 236

Technology for the Stars:

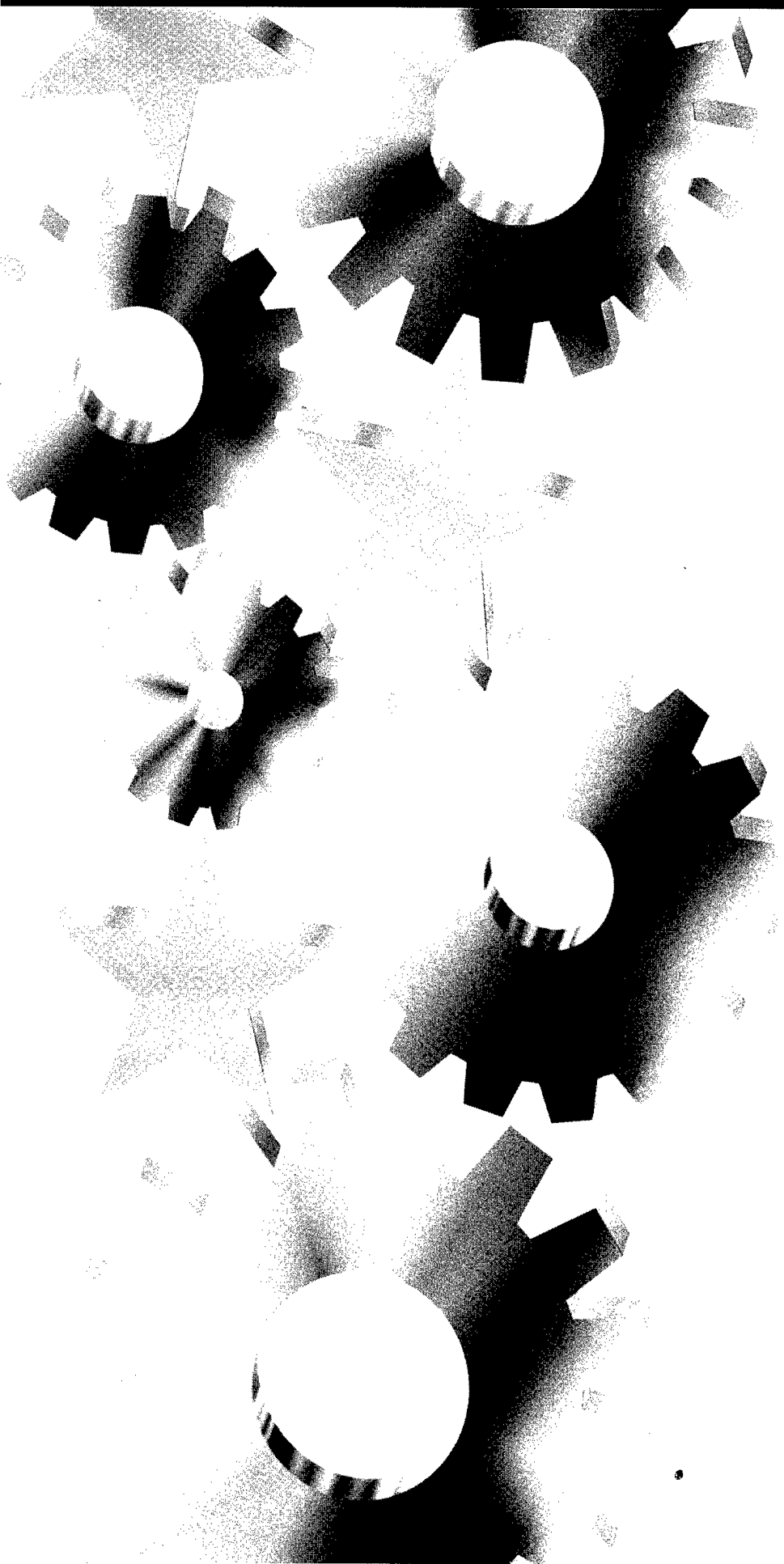

Extending Our Reach

The theme for this year's Research and Technology report is most appropriate in today's international scene in which the world's nations find themselves in a transitional and highly competitive mode, especially in the development and marketing of new products and technologies. NASA, with its traditional strength in the management of highly technical and complex programs, can be of tremendous service to our Nation in this area of global restructuring. NASA does this by continuing to manage a strong and successful space program and by working closely with the private sector to strengthen technology at all levels of research and industry. Fittingly, three interrelated areas of focus at NASA's Marshall Space Flight Center (MSFC) in 1995 were: (1) development of advanced space transportation technology that enhances NASA's own programs and makes space more affordable and accessible to U.S. commercial and academic interests; (2) microgravity research to continue to expand our knowledge of how the effects of low gravity can benefit man's search for new and improved materials and processes; and (3) technology transfer, which provides direct access to NASA's technical expertise in solving all types of problems encountered in commerce, industry, and public and private research. Common to all of these areas is a NASA commitment to form partnerships with—and make the U.S. space program accessible to—all Americans who can benefit from it.

Space transportation has increasingly broad implications to America's competitive position in the international market place. Basic to a successful space program is the capability to transport payloads and research facilities, as well as humans, into space and maneuver once there. MSFC's vision is to be the world's leader in space transportation. In 1995, MSFC formed a Task Team to develop a strategic plan that focuses and advances propulsion and space transportation technology and that stimulates NASA—as well as non-NASA—governmental agencies and researchers (industry, academia, etc.) to participate in developing innovative and revolutionary space transportation technology.

The overall goals are to build upon current technologies and to develop new space transportation technologies that will effect orders of magnitude reductions in Earth-to-orbit and in-space transportation costs. The planned cost savings will benefit not only NASA and other Government agencies, but also commercial and academic interests and will stimulate their participation. In this way, NASA's advanced space transportation program is envisioned as a national imperative.

In coming months, the effort will focus on further refining future national space goals; identifying the classes of transportation systems needed to meet these goals; determining the underlying types of technologies needed to support these systems, both singly and in combination; establishing a collaboration plan for including non-NASA elements in the process; formulating schedules, budgets, and road maps for accomplishing the goals; and establishing the plan in the national arena.

The second major area of focus is microgravity research. NASA's mission of microgravity research is composed of a microgravity science and applications program and a space processing program. The former is comprised of the research areas of combustion, fluid physics and transport phenomena, biotechnology, and materials science, as well as the infrastructure discipline programs of acceleration measurement and glovebox flight research.

MSFC's peer-reviewed, research-driven microgravity program is executed through science investigation management, flight and ground hardware development, and technical and mission support activities. Investigations are conducted aboard KC–135 parabolic aircraft, shuttle middeck, Spacelab and Spacehab, and the Mir Space Station.

The commercial component of the microgravity program also seeks to promote industry participation and to facilitate the use of space for commercial products and services. The industry-driven, space-based, high technology research and development program supports goals of implementing research and development to enable commercial space advances and expansion of current markets and to enable U.S. industry to develop new, profitable space industries. Currently, access to microgravity for commercial entities is via KC–135 parabolic aircraft, suborbital rockets, shuttle middeck, Spacelab and Spacehab, and the Mir Space Station.

Microgravity programs are performing extensive space station utilization planning in support of applied science and commercial user accommodations. In addition to new hardware developments, some existing payloads will transition for research and applications aboard the *International Space Station*.

NASA continues to directly benefit the American public through its technology transfer program that has provided solutions for thousands of private-sector needs in the areas of medicine, transportation, energy, construction, law enforcement, communications, public safety, appliances, sports and recreation, food products, manufacturing, agriculture, and others.

As its own realization of its importance as a national asset in this area has grown, NASA has improved delivery of its expertise to potential beneficiaries and expanded public awareness of this service. It has accomplished this through development of regional alliances that minister to needs in their immediate areas. MSFC has been a leader in the formation of NASA's Southeast Alliance for Technology Transfer. The primary effort of this alliance is an outreach program in which NASA representatives, together with NASA prime contractors and the academic community, join with state and local economic development officials to identify needs in their areas.

Technology transfer agreement requests are considered from such diverse

applicants as industry, individual entrepreneurs, the academic community, and other research-type organizations. In 1995, approximately 1,500 requests were considered by the southeast regional office. Government and private-sector engineers and scientists, working side-by-side, pursue scientific and engineering technologies needed in both industry and government. MSFC is dedicated to working technical and business arrangements with industry partners for space-flight projects. In addition, MSFC provides assistance in technology reinvestment projects operated by other government agencies.

The results have been impressive. Approved surveys show that 13,200 jobs have been added or saved, 775 new products developed, and an economic impact of $1.23 billion projected as a result of the Southeast Alliance's actions in a recent 3-year period.

NASA's leadership in space exploration is well documented. Its emerging importance as a national economic resource is an important part of its quest for new heights.

Advanced Studies

Innovative technologies are making it possible to expand our understanding of the world in which we live. Yet, the vastness of the Universe strengthens our desire for new discoveries and encourages further study in many scientific fields. A renewed emphasis on improving our quality of life has brought advanced studies "down to Earth," as well as beyond our atmosphere. It is these ideals that continue to inspire new developments and lay the foundation for future missions.

Scientific missions include making the first-ever global image of the Earth's magnetosphere, investigating the interstellar medium for information on where new stars are forming and the evolutionary process at work in our galaxy, and providing global disaster management support through a network of computers and communications satellites. Space tether technology will support missions in atmospheric and ionospheric research, and studies continue on the use of tethers for advanced propulsion, power generation, deboost and recovery of small space station payloads, and the disposal of space station waste. Solar thermal propulsion is a promising concept for transferring payloads from low-Earth orbit to geostationary Earth orbit, while superconducting magnetically levitated and propelled vehicles may reduce the cost for access to space. Technologies supporting space telescopes with large apertures and adaptive optics are being developed, and advances in achromatic lithography can achieve cost reductions in the production of extreme-ultraviolet and x-ray diffraction gratings. Equally important is the research to develop an intelligent, hands-free computer interface which could result in an improvement in the lives of individuals with physical impairments.

From the advanced studies underway within Program Development, future space science and application missions and technologies are being born. The missions that arise will take what is not understood and enlighten us as never before. MSFC's passion for the future continues to yield benefits for the Nation and enhance our understanding of the world and Universe around us.

Axel Roth
Director
Program Development

Space Systems

Atmospheric and Ionospheric Research Using a Small Expendable Deployed Satellite

C. Les Johnson/PS02
205–544–0614

MSFC is defining potential future tether missions; one of which is the proposed Atmospheric and Ionispheric Research Using a Small Expendable Deployed Satellite Mission. This mission, which is based on NASA's successful and proven Small Expendable Deployer System program, will collect atmospheric information in the altitude range of 260 to 125 kilometers via a tethered satellite lowered from the space shuttle orbiter. This region of near-Earth space is inaccessible by high-altitude balloons, aircraft, or orbiting spacecraft and is often called the "ignorosphere." The scientific and engineering information to be gained from the mission is essential to understanding and modeling atmospheric and ionospheric phenomena, including satellite drag, the effect of relativistic electrons on upper-atmospheric chemistry and ozone depletion, the energy deposition from magnetospheric currents and particle precipitation, and the spatial and temporal gradients in ionospheric properties.

MSFC is working in partnership with The Michigan Technic Corporation, Holland, Michigan, in mission definition and planning. In addition to the ground-breaking science to be accomplished by the mission itself, the innovative consortium being assembled for the effort exemplifies one aspect of the new philosophy under which NASA is seeking to do business and conduct scientific research. Michigan Technic is working to secure nongovernmental funding of the instruments, probe, tether, and tether deployer. The consortium would then provide this payload to NASA in exchange for launch aboard the space shuttle orbiter. All science data gathered during the mission will be treated in accordance with standard NASA practices. While no commitments for launch have yet been made, both MSFC and its potential partner are studying the technical and programmatic aspects of the mission and working toward such an arrangement.

The payload consists of three primary components—the probe, the tether deployer, and the tether. The payload is designed to be integrated with either the Hitchhiker-C, or the multipurpose experiment support structure pallet, and fit within the envelope of the orbiter. The probe capsule will contain scientific instruments, while the boom/wing assembly will provide separation between the global positioning system receiver antennas, supplemental instrument mountings, aerodynamic stiffness, as well as assist in control system desaturation in the yaw motion for flight below 185 kilometers.

The instrument suite includes an anemometer to measure pressure, heat flux sensors to measure heat transfer to the surface of the probe, a three-axis accelerometer, a mass spectrometer for characterizing atmospheric constituents, Langmuir probes to determine plasma density and temperature, a medium-energy particle detector, and a high-energy electron detector.

The mission will not only advance our understanding of this little-studied region of the Earth's upper atmosphere and demonstrate the use of advanced tether technology for science applications, but it may also serve as a pathfinder for a new type of government and industry partnership for performing high-value science at a lower cost.

Santangelo, A.D. April 1995. Atmospheric and Ionispheric Research Using a Small Expendable Deployed Satellite (AIRSEDS–II): A Tethered Satellite System (TSS–2) Precursor Mission to Test and Demonstrate Tethered Systems in the Earth's Upper Atmosphere. Proceedings of the Fourth International Conference on Tethers in Space, Smithsonian Institution, Washington, D.C.

Sponsor: Office of Space Flight

Industry Involvement: The Michigan Technic Corporation, Holland, Michigan

University Involvement: University of Texas at Dallas, University of New Hampshire

Very Fine-Line Lithography for Extreme Ultraviolet and Soft X-Ray Optics

C. Les Johnson/PS02
205–544–0614

The Very Fine-Line Grating Lithography Project is a phase II Small Business Innovation Research contract directed toward the development of technology to lithograph 0.1-micron- (1,000-angstrom-) period diffraction-grating patterns. Gratings with a period this small have 10,000 lines per millimeter in their pattern and cannot currently be produced in large areas at a reasonable cost. The goal of the research is to develop technology that can be used to produce large-scale (greater than 10 square centimeters) area patterns affordably. Patterns produced by this technology would be used as the starting point for production of extreme ultraviolet and x-ray diffraction gratings for NASA space science missions and such commercial applications as microscopy calibration gratings and grids, fine-scale positioner grids and gratings, and wire-grid polarizers.

Achromatic holographic lithography, a basic optical technique, has been demonstrated previously, but is currently little more than a laboratory curiosity. Earlier demonstrations using this technique have produced a few square millimeters of grating pattern per exposure. The cost of these experiments is prohibitive, thus precluding commercialization or practical application. One reason for their impracticality is their use of deep ultraviolet and x-ray radiation sources, which are expensive to operate and/or are poorly suited to the optical requirements of the technique, but are required to use radiation with a wavelength smaller than 200 nanometers.

The purpose of the Very Fine-Line Grating Lithography effort is to explore the possibility of developing achromatic holographic lithography into a practical technology. Phase I work led to a conceptual design for a practical lithography system. During phase II, MOXTEK, Inc., will build a system based on this concept and demonstrate its feasibility. (MOXTEK is currently building a prototype lithography system.) The deliverable of the phase II program will be a set of optical quality substrates to be patterned using achromatic holography (a 0.097-micron pitch grating is expected).

Following the successful completion of the research, MOXTEK expects to use very fine-line gratings as integral components of small, portable, soft x-ray fluorescence devices. Very fine-line gratings would critically enhance such devices, making it easier to produce high-performance instruments. Additional uses of the lithography technique include light polarizers or reflective beam-splitters, which are indicative of the potentially large commercial market applications.

Wire-grid polarizers are common in such long-wavelength applications as millimeter waves and the infrared, where they can even be produced by wrapping wire strands over a form. With visible light, the pitch of the wire grid must be less than 0.12 micron—a requirement that can be met with this new lithography technique. However, since the grating period must be about one-sixth of the shortest operating wavelength to achieve high extinction ratios to completely cover the entire visible spectrum, a pitch of about 0.08 micron is actually required, which also appears to be achievable with the system being developed.

The development of high-performance optics for use in the extreme ultraviolet and soft x-ray regions of the electromagnetic spectrum is technologically difficult. Reflecting optics, often based on multilayer reflection, are currently the only practical optic for most applications. Recent advances in achromatic lithography offer the potential for a commercially viable technique with application to NASA space science missions, as well as the commercial instrumentation and sensing industries. The successful completion of this Small Business Innovation Research will be an important step toward that end.

Hansen, D.P.; Reyes-Mena, A.; Colton, J.; Knight, L.; and Allred, D.D. 1992. Multilayer Phase-Diffraction Gratings Modeled as a Structure in Three Dimensions. Society of Photo-optical Engineers, 1742.

Hansen, D.P.; Reyes-Mena, A., and Knight, L. February 1993. Diffractive X-Ray Optics. Soft X-Rays in the 21st Century, Provo, Utah.

Sponsor: Small Business Innovation Research

Industry Involvement: MOXTEK, Inc., Orem, Utah

Ultra-Lightweight Telescope, Integrated Missions for Astronomy

Edward E. Montgomery/PS02
205–544–1767

The objective of the Ultra-Lightweight Telescope, Integrated Missions for Astronomy program is to achieve near-diffraction-limited images of astronomical objects at visible and/or infrared wavelengths with a space telescope having an ultra-lightweight primary mirror combined with large-amplitude, adaptive, correction optics. The program approach is to apply a stepwise process of technology developments on the ground and in space to advance the feasibility of constructing a very large aperture space telescope.

The technologies being developed will provide a system that can be transported to space in densely packaged form to fit existing launcher-payload envelopes, and then will be constructed/deployed to form space telescopes with large apertures. Such a system would also continually compensate for image distortions due to imperfections, natural disturbances, and equipment-induced vibrations/deflections. The goal will be to make possible very large primary reflectors of low mass and cost.

Proceeding from a set of telescope requirements established by a scientific working group from current needs in astronomy that includes cosmological investigations and the search for extra-solar planets, the technology program is going forward in two main thrusts: (1) large-aperture, thin-film mirror technology and (2) segmented adaptive correctors. The objective of the first thrust is to demonstrate the ability to form and maintain a thin-membrane primary reflector so that near-diffraction-limited performance is achieved over large areas sufficient to fill large primary apertures. The second objective is to demonstrate the ability to form and maintain a segmented quaternary mirror into a quasicontinuous surface with individual subapertures phased so that optical errors are compensated for and near-diffraction-limited performance is achieved in the telescope system.

Figure 1 shows several generations of adaptive, segmented-mirror technology developed over the last 5 years. In the upper left is a 7-centimeter-diameter, 4-centimeter-tall Phased-Array Mirror, Extendible Large Aperture—a half-meter aperture, 36-segment telescope demonstrator developed by Kaman under contract to the U.S. Army from 1988 to 1992. The round spiral patterns on the edge are inductive-edge sensor coils, and the cylindrical areas contain three voice-coil actuators.

Three years ago, MSFC produced a smaller mirror segment (to the right of the Phased-Array Mirror segment in fig. 1) based on electrostrictive actuators. Its diameter was reduced to 3 centimeters, although it has roughly the same height. Decreasing the diameter of the mirror surface makes it possible to compensate for increasingly finer scale aberrations. Reducing the height of the segment

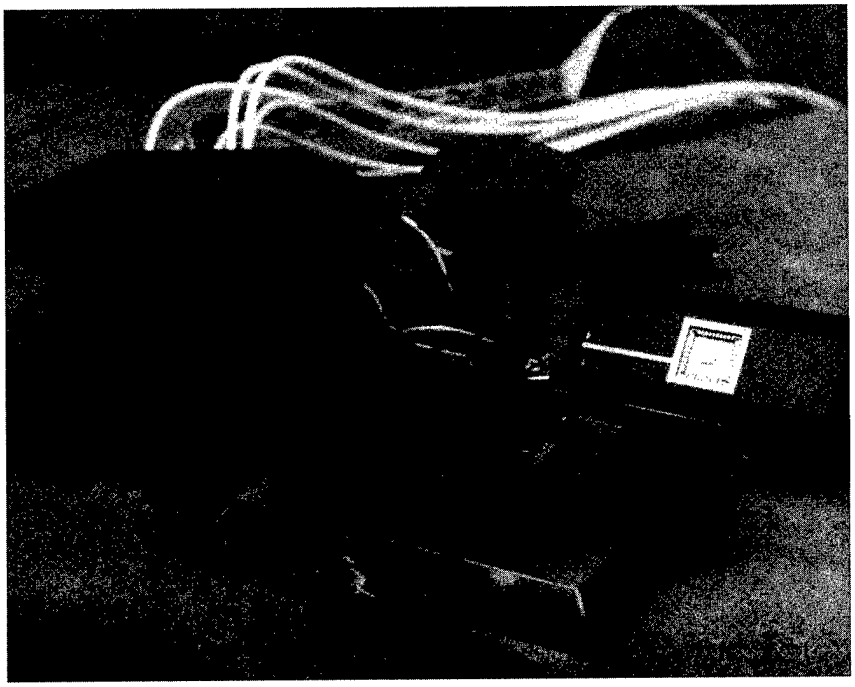

FIGURE 1.—Several generations of adaptive, segmented-mirror technology.

lowers the overall weight of the system. The latest generation of segmented-mirror technology (in the foreground of fig. 1) is a 3-centimeter segment, less than a centimeter in height, developed by Blue Line Engineering. The size reduction has been made possible by clever mechanical linkages in the actuators. Of the several segments, only the Phased-Array Mirror, Extendible Large Aperture has edge sensors installed.

In a parallel effort, edge-sensor technologies are being advanced. The computer chip shown in the photograph (the small gray area at the very center of the circuit module) contains a complete edge-sensor electronics package developed by SY Technology, serving in place of a 3-foot by 9-inch surface-mount electronics card in the Phased-Array Mirror system and improving such features as digital and analog outputs.

The existing method of building telescopes using monolithic slabs of glass is reasonable up to a meter or so in size. Since the mass of the mirror scales with the square of the diameter, the monolithic glass approach quickly becomes too heavy for consideration for larger mirrors. Segmentation allows the weight growth to be more manageable between 25 and 40 kilograms per square meter of mirror surface. If the film technology can be improved to achieve optical qualities, the mass could be reduced to a few kilograms or less per square meter.

Most scientists agree that the next step in astronomy calls for greater resolution beyond the Hubble Space Telescope, which has a 2.4-meter primary mirror. Since resolution is proportional to primary mirror size, future science is driving the need for technologies that enable large apertures of 20 meters or greater. The larger aperture will also provide more light gathering and, as a result, the ability to see objects thousands of times more faint than ever before—maybe an extra-solar planet.

Sponsors: Office of Space Access and Technology; Center Director's Discretionary Fund; Small Business Innovation Research

Industry Involvement: Blue Line Engineering; SY Technology, Inc.

Tether Applications on the Space Station

Vernon W. Keller/PS02
205–544–2470

Over the past several years, numerous tether-utilization concepts for space have been discussed. Recent progress in implementing tethers in space has revived enthusiasm for specific near-term tether applications, some of which are applicable to the *International Space Station*. The Office of Advanced Concepts and Technology is currently funding a study to assess the feasibility of using tether systems for deboost and recovery of small payloads (via sample return capsules) from the space station; deboost and burn-up of waste and disposable carriers; reboost of the *International Space Station* via momentum exchange from deboosted masses; and reboost of the *International Space Station* via orbiter towing. Interest has also been expressed in utilizing tethers to facilitate the reservicing of a proposed space station-based operational Wake-Shield Facility. In addition, the Office of Space Flight is currently sponsoring a study to assess the feasibility of using tethers and plasma contactors to augment electrical power generation for the *International Space Station*.

Several space tether systems have recently flown and others are scheduled to fly in the near future. The Small Expendable Deployer System has now flown twice as a secondary payload from Delta II expendable launch vehicles. Both flights successfully deployed a 26-kilogram mass to a length of 20 kilometers. A space shuttle-based SEDSAT flight is

scheduled for 1997. The Plasma Motor Generator, flown in 1993, deployed an insulated, conducting wire to a distance greater than 400 meters. The Tether Satellite System, first flown on the space shuttle in 1992, deployed a 500-kilogram Italian scientific satellite to a distance of 250 meters and retrieved it. This same system is scheduled for reflight on the space shuttle in early 1996, with plans to deploy the 500-kilogram satellite to a distance of 20 kilometers and then retrieve it. In addition, the Naval Research Laboratory is planning to fly a tether physics experiment in June 1996. Several other tether application flights are also in early planning stages.

Team participants in the current *International Space Station* tether application study include: MSFC, The Boeing Company, and Tether Applications Company. The midterm review for this study was held in August 1995. Since return flights from the *International Space Station* will be infrequent (typically only five per year), the use of sample return capsules would greatly facilitate the timely return of microgravity materials-processing samples and products; crew medical samples for checkups, diet, and other research; time-critical payloads for return directly to foreign users; computer diskettes, videocassettes, film, and other high-density data; environmental samples exposed inside or outside the station; small items needing prompt repair and return; etc.

Preliminary study indicates that a miniature expendable tether-deployment system can be utilized to deorbit lightweight sample return capsules capable of returning approximately 50-kilogram, 0.18-cubic-meter payloads to almost any recovery site on Earth. Parachutes and soft mid-air recovery by helicopter limits the forces experienced by the payload to the 8 units of gravitational force typically experienced during reentry by a nonlifting body, as compared to the 90 units experienced by a parachute-assisted Earth-impact return capsule (such as Raduga). Approximately 20 of these lightweight (10-kilogram) sample return capsules could be simultaneously stored within the space of one-half of a logistics rack and utilized as needed.

An additional potential application of tethers for the *International Space Station* is their use to reboost the station itself. This is important from two aspects: (1) It could serve as an emergency reboost capability, or (2) it could be used routinely to reduce the required reboost propellant, potentially saving launches. Reboost of the *International Space Station* can be accomplished by deorbiting substantial masses, such as with the Progress resupply spacecraft, the Soyuz spacecraft, or even the space shuttle itself. A tether connecting two satellites in different altitude orbits experiences a tension due to the fact that the orbital rate of the upper satellite is speeded up by the tether and that of the lower satellite is slowed down. When the tether is severed, the lower satellite will drop into a lower orbit, with the release point as the apogee of its new orbit. The upper satellite, when released, will go into a higher orbit in which its point of release is the perigee for the new orbit.

Reboost of the *International Space Station* can also be accomplished via orbital towing. In this case, the orbiter flies below and forward of the space station with an approximately 3-kilometer tether connecting them. When orbiter fuel from the orbital maneuvering system is burned by the reaction control system in short pulses, the station can be reboosted in excess of 20 kilometers, while maintaining low tether tension throughout the two to three orbits required to accomplish this reboost. Station propellant savings from orbiter towing are significant even for nominal amounts of orbital maneuvering system fuel.

The feasibility of using a conducting tether to generate supplemental electrical power is being studied by the Office of Space Flight. An insulated, conducting tether deployed from the *International Space Station* will experience an induced electromotive force from its motion through the Earth's geomagnetic field. Through the use of plasma contactors at each end of the tether and the connection to an electrical load on the station, a current will flow through the tether and produce useful electrical power for the space station. Two previous tether flights, the Plasma Motor Generator and the first flight of the Tethered Satellite System, demonstrated that electrical power can be generated in space using conducting tethers. Building upon these experiments, it now appears feasible to generate 3 to 5 kilowatts of power using a tether scalable from that used on the Tether Satellite System. Several issues remain to be resolved, however, before tethers can be assured of success in generating power for the *International Space Station*. The most significant of these results from the

potential impact of the tether system on the station's center of mass and on the microgravity environment in the laboratory modules. However, if tethers are properly located on the space station structures, they can be used to shift the station's center of mass and actually improve the microgravity environment in the laboratory modules.

A significant drag force is experienced by the system during power generation, resulting from the flow of electrical current through the tether. The physics that produces this drag force can also, in principle, be used to provide an alternative reboost capability. If power generated by solar arrays were channeled through the tether, flowing in a direction opposite to that used for power generation, an accelerating force would be experienced by the tether and the *International Space Station*—thus providing reboost.

Sponsors: Office of Advanced Concepts and Technology; Office of Space Flight

Industry Involvement: The Boeing Company, Tether Applications Company

Global Emergency Observation Warning and Relief Network

Angelia P. Bukley/PS02
205–544–0054

The Global Emergency Observation Warning and Relief Network is a proposed concept that optimizes the use of existing remote-sensing resources and data-processing centers linked together via a computer network and communications satellites to perform the task of providing global disaster management support. Its development is motivated by a significant number of recent devastating disasters and the United Nations proclamation of the 1990's as the International Decade for Natural Disaster Reduction.

In this study, MSFC developed information requirements and investigated the remote-sensing data needs of the disaster management community. A broad survey of current and planned projects and programs that support disaster management efforts, both in applications and research, was performed to assess what gaps exist, determine where NASA could best contribute to disaster mitigation activities, and avoid any potential duplication of effort in future NASA studies and projects. An extensive data base with over 430 entries was developed cataloguing the findings of the survey. A set of recommendations for the Agency was developed based on the results of the requirements study and the project survey. These addressed suggested courses of action for future support of hazards research and management efforts and how the Agency might interface with other domestic and international efforts. The findings were compiled in a white paper delivered to the Oceans, Solid Earth, and Natural Hazards Branch in the Science Division of the Office of Mission to Planet Earth.

Sponsor: Office of Mission to Planet Earth

Survivable Space Tethers

Charles C. Rupp/PS04
205–544–0627

The two recent successful flights of the Small Expendable Deployer System (SEDS) have demonstrated the capability of tethers to deorbit payloads (SEDS–1) and to support scientific experiments in space (SEDS–2). This system was launched as a Delta secondary payload on an Air Force mission into a 350-kilometer, 35-degree inclination orbit. The 20-kilometer tether deployed a 35-kilogram instrumentated payload from the second stage downward into a stable, local, vertical orientation. This orbit afforded many stargazers a unique sight, as the tether was visible shortly after sunset or before sunrise as the Delta traveled overhead. Five days after the active portion of the mission was over, the tether was cut by a micrometeoroid or space debris, and the 7 kilometers of tether that remained attached to the Delta's second stage reentered approximately 60 days later. The severing emphasized the mission risk associated with flying tethers in space for long periods of time. Tethers can be built to survive a space environment according to work by R.L. Forward and R.P. Hoyt.[1] The Small Expendable Deployer System tethers are built with very large factors of safety, such as 80, so that they can survive hits by very small debris and micrometeoroids. As shown by Forward and Hoyt, a space tether can

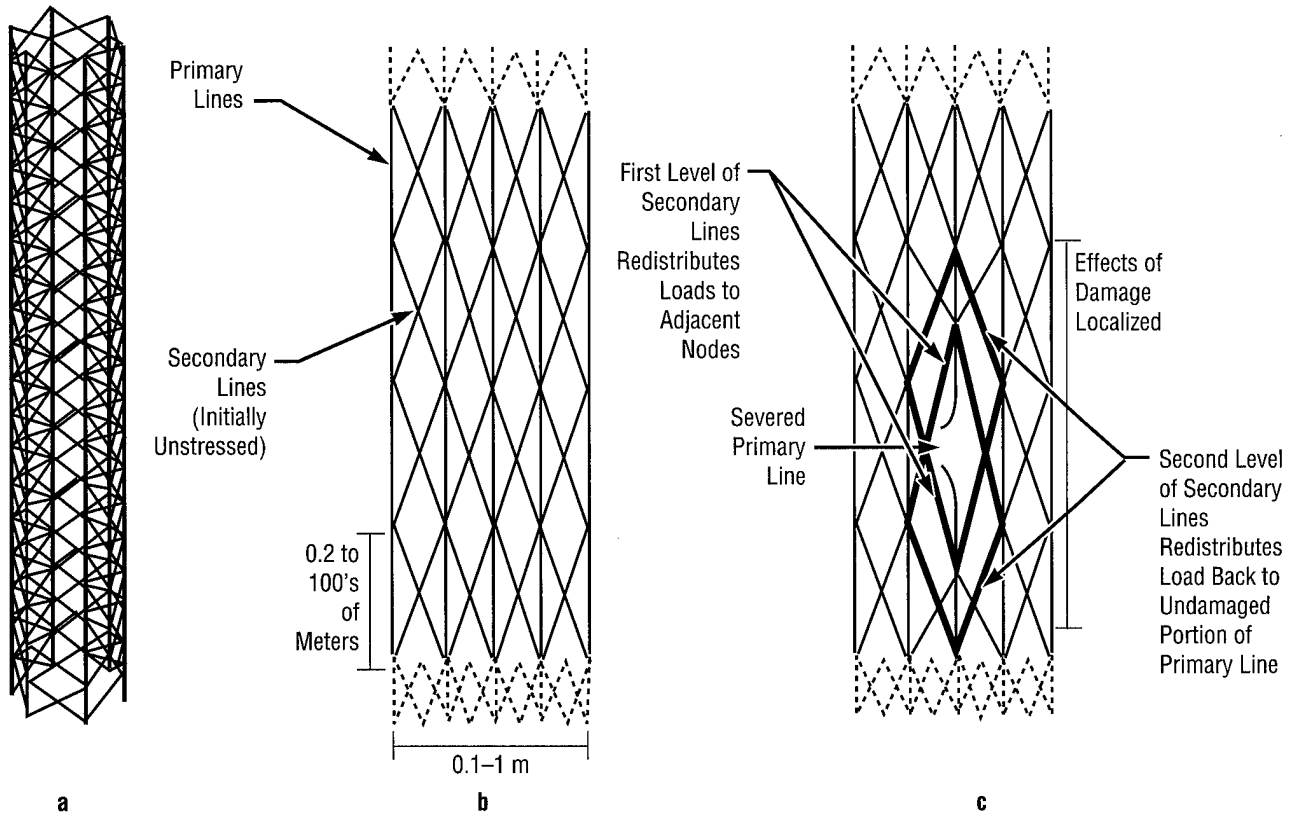

FIGURE 2.—(a) Section of Hoytether, (b) schematic of undisturbed Hoytether, (c) secondary lines redistributing load around a failed primary line without collapsing structure. Note that horizontal scale is expanded relative to vertical scale; in reality, the secondary lines are nearly parallel to the primary lines.

be built of many separated but interconnected strands in which the total cross section is relatively large. Named after its inventor, "Hoytether survivability" (fig. 2) is improved because it takes a larger particle to completely sever a tether built in this configuration.

For missions in which the tether safety factor can be relatively high, as in the first two Small Expendable Deployer System missions, micrometeoroid and debris survivability can be improved many orders of magnitude (fig. 3). The improved survivability can also be used as a justification for reducing the safety factor, thus lowering the weight of high-performance tether configurations.

[1]Forward, R.L. 1992. Fail-safe Multistrand Tether Structures for Space Propulsion. Twenty-Eighth Joint Propulsion Conference, Nashville, Tennessee. American Institute of Aeronautics and Astronautics, paper 92–3214.

Sponsor: Small Business Innovation Research

Industry Involvement: Tethers Unlimited

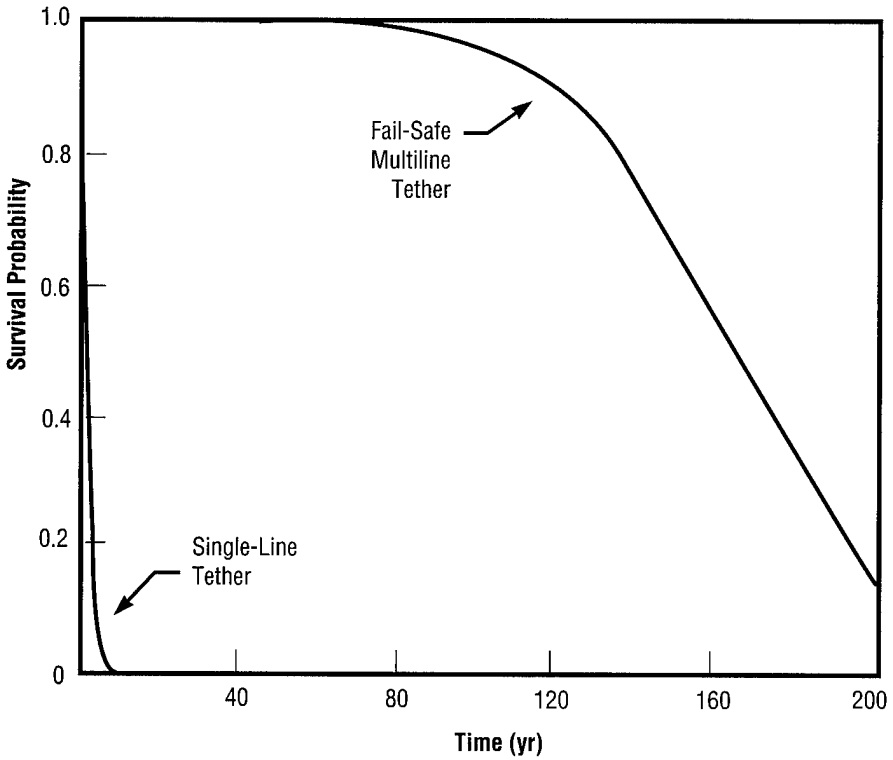

FIGURE 3.—Lifetime compensation of equal-weight, single-line and fail-safe, multiline tethers for a low-load mission.

Space Science

The Magnetosphere Imager Mission

C. Les Johnson/PS02
205–544–0614

One of the most important discoveries of the space age was that of the Van Allen radiation belts—vast clouds of intense radiation caused by the Earth and its rotating magnetic field being impacted by the supersonically expanding atmosphere of the Sun. After more than 30 years of spacecraft flights through this region, scientists now know that these radiation clouds contain electrical storms and disturbances that play important roles in the Earth's atmospheric processes. Through technology advances, pictures of this magnetospheric region can now be made, in a similar way to that of satellite photos of ordinary clouds commonly used for weather reports. Thus, NASA is poised to explore and expose the violent and variable region that surrounds our planet with entirely new types of satellite images.

For the past few years, MSFC has been studying the feasibility of flying a new generation of instruments aboard a small spacecraft to obtain such magnetospheric images. The Magnetosphere Imager mission was conceived by the NASA Office of Space Science and assigned to MSFC for further definition. The MSFC Magnetosphere Imager design team developed a mission concept to utilize a small, spin-stabilized spacecraft to carry a suite of four instruments into a high-elliptical Earth orbit for 2 years. The spacecraft will be launched by one of the new Med-Lite expendable launch vehicles and will fly over the Earth's poles to an apogee of 7 Earth radii. The mission instruments (listed in table 1) will obtain the first simultaneous global images of Earth's magnetospheric processes in multiple wavelengths of light and with energetic neutral atoms, as well as through active radio frequency sounding. In support of the technology required for the mission instruments, six advanced instrument research projects were completed in 1995 by universities, research laboratories, and industry. The results of the research were made available to NASA's Office of Space Science, Space Physics Division. Research topics are listed in table 2.

As a result of the MSFC engineering design study and the efforts of the Magnetosphere Imager science

TABLE 1.—*Strawman measurements and instrument complement for the Magnetosphere Imager mission.*

Instrument	Measurement
Hot-Plasma Imager	Energetic Neutral Hydrogen Atoms
Plasmasphere Imager	Solar Ultraviolet Light Scattered From Helium Ions at 304 Å
Far-Ultraviolet Imager	Magnetospheric Precipitation-Induced Far-Ultraviolet Light
Radio Sounder	Frequency-Swept Active Radio Frequency Sounding of the Magnetosphere

TABLE 2.—*Research for advanced technology Magnetosphere Imager instrumentation.*

Institution	Research Title
Boston University	Development and Evaluation of Multilayer Coatings for O^+ Imagers
Lockheed Palo Alto Research Laboratory	Surface Conversion Techniques for Low-Energy Neutral Atom Imagers
Lockheed Palo Alto Research Laboratory	Measurement of Precipitation-Induced Far-Ultraviolet Emissions and Geocoronal Lyman Alpha
Los Alamos National Laboratory	Ultraviolet Rejection for Low-Energy Neutral Atom Imaging
University of Iowa	Simulation of Radio Sounding in the Plasmasphere
University of Massachusetts at Lowell	Instrument Definition for a Radio Sounder for Global Magnetospheric Imaging

definition team, this exciting mission that will return never-before-seen or understood glimpses of near-Earth space appears to be both technically feasible and affordable. The estimated mission cost, not including launch, is approximately $70 million.

Hermann, M., and Johnson, L. August 1994. Inner-Magnetosphere Imager Solar Terrestrial Probe Class Mission Preliminary Design Study Report. NASA Technical Memorandum 108464.

Armstrong, T.P.; Gallagher, D.L.; and Johnson, C.L. October 1995. Magnetosphere Imager Science Definition Team—Executive Summary. NASA Reference Publication.

Sponsor: Office of Space Science

■■■■■

Passively Cooled Reconnaissance of the Interstellar Medium

Jonathan W. Campbell/PS02
205–544–7076

In the context of "faster, cheaper, better," this mission seeks to break new ground in the field of science. The interstellar medium has never before been directly investigated. By taking advantage of a satellite in Sun-synchronous orbit around the Earth and the Earth's orbit around the Sun, a spectrometer pointed outward could, in principle, sweep out the entire sky in just 6 months. Cheaper, gravity-gradient stabilization could be employed, and the satellite could be launched via a low-cost Pegasus-class bus.

The Passively Cooled Reconnaissance of the Interstellar Medium would survey the galaxy at infrared lines extremely difficult to see from the ground. These lines would provide valuable data on the characteristics of the interstellar medium. Densities, velocities, and temperatures as a function of position will allow tremendous insight into where new stars are forming and in the evolutionary processes at work in our galaxy. Ordinary telescopes operating in the visible cannot see the center of the galaxy because of intervening clouds, but this mission will enable scientists to see beyond the clouds to study the mysteries at the center.

In addition, a substantial technological benefit may be realized in the areas of passive cooling of satellites. Present technology uses large, heavy, bulky dewars to cool the temperature of the telescope down to acceptable cryogenic temperatures. These dewars are inherently expensive and costly. This program would employ an alternate approach in which a system of nested, conical Sun shields would provide the necessary cooling passively. Indeed, MSFC could become the center of expertise for passive cooling.

Sponsor: Advanced Systems and Payloads Office

■■■■■

Hard X-Ray and Gamma-Ray Imaging System

Jonathan W. Campbell/PS02
205–544–7076

The Hard X-Ray and Gamma-Ray Imaging System images the Sun at high photon energies. For example, solar flares occurring in the solar corona are highly transient events involving the release of tremendous amounts of energy. This energy takes many forms, including radiation across the electromagnetic spectrum, as well as high-energy protons and electrons. Hard x rays and gamma rays are part of this release and may be thought of as simply different colors of light invisible to the eye. Those high-energy photons do not reach the Earth since they are absorbed by the atmosphere. Imaging solar flares in these colors of photons should provide additional insight into the energy release and perhaps answer long-standing questions about the role of the Sun's magnetic field in storing energy. Solar flares can be potential threats to men working in orbit and can disrupt vital communications and navigation networks here on Earth. Understanding flares is the first step toward being able to predict them.

Hard x rays and gamma rays cannot be imaged as easily as the visible colors of light. The high-energy photons zip straight through conventional lenses and mirrors without being focused. For several years, MSFC has worked in developing new technology in the area of Fourier telescopes that employ fine grids and powerful computers to measure the Fourier components associated with hard x-ray and gamma-ray radiation. In addition, MSFC is a leader in the area of stabilized booms for space-based applications. Both of these technologies are critical to achieving an optimum, low-cost mission concept.

The hard x rays produced by the Sun are the same color as the x rays used by a dentist in looking at teeth. One potential spin-off benefit from this mission to the man on the street is in the area of nonintrusive medical imaging. This technology offers the capability of producing extremely high-resolution snapshots of the interior of the human body.

Sponsor: Center Director's Discretionary Fund

Space Transportation

MagLifter

Joe T. Howell/PS05
205–544–8491

Achieving an affordable and reliable launch infrastructure for low-cost, routine access to space is one of the enduring challenges of the space age. In a marketplace dominated by expendable launch vehicles grounded in the technology base of the 1950's and 1960's, diverse innovative approaches have been conceived since 1970 for reducing the cost per pound for transport to low-Earth orbit. For example, the space shuttle—a largely reusable vehicle—was developed in the 1970's with the goal of revolutionizing Earth-to-orbit transportation. Although the shuttle provides many important new capabilities, it did not significantly lower space launch costs. During the same period, a variety of other launch requirements (e.g., for vehicle research and development and microgravity experiments) have been met by relatively expensive, typically rocket-based solutions (e.g., rocket sleds and sounding rockets).

There are several basic strategies for cost reduction, including: (1) reducing the cost of hardware expended in launcher systems per pound of payload, (2) increasing the reusability per flight of highly reusable vehicles, and (3), for both of these, reducing the cost of launch operations. A variety of space launch concepts are still under study in this context, ranging from single-stage-to-orbit vehicles to "big, dumb boosters;" and from air-breathing hypersonic Earth-to-orbit vehicles like the National Aerospace Plane to advanced rocket concepts such as space nuclear thermal propulsion. Some exotic concepts involving "gun-type" systems have also been studied.

However, past analyses of launch systems involving electric propulsion have been largely limited to electromagnetic versions of "cannons," such as rail guns and coil guns. Despite significant theoretical advantages, these systems have had both technical and programmatic difficulties in maturing beyond research and development and prototype-level demonstrations.

A new approach, involving the use of superconducting, magnetically levitated ("maglev") and propelled vehicles, has been developed. Three configurations of the MagLifter concept shown in figures 4–6 combine the technology base of maglev systems being proposed and demonstrated for terrestrial applications with the best planned improvements in expendable launch and highly reusable vehicle systems. Together, the results suggest dramatic improvements in Earth-to-orbit costs may be possible. The MagLifter draws on a heritage of electromagnetic launch concepts and technical literature, but embodies several new technical characteristics which have not been thoroughly considered to date.

Sponsor: Office of Space Access and Technology

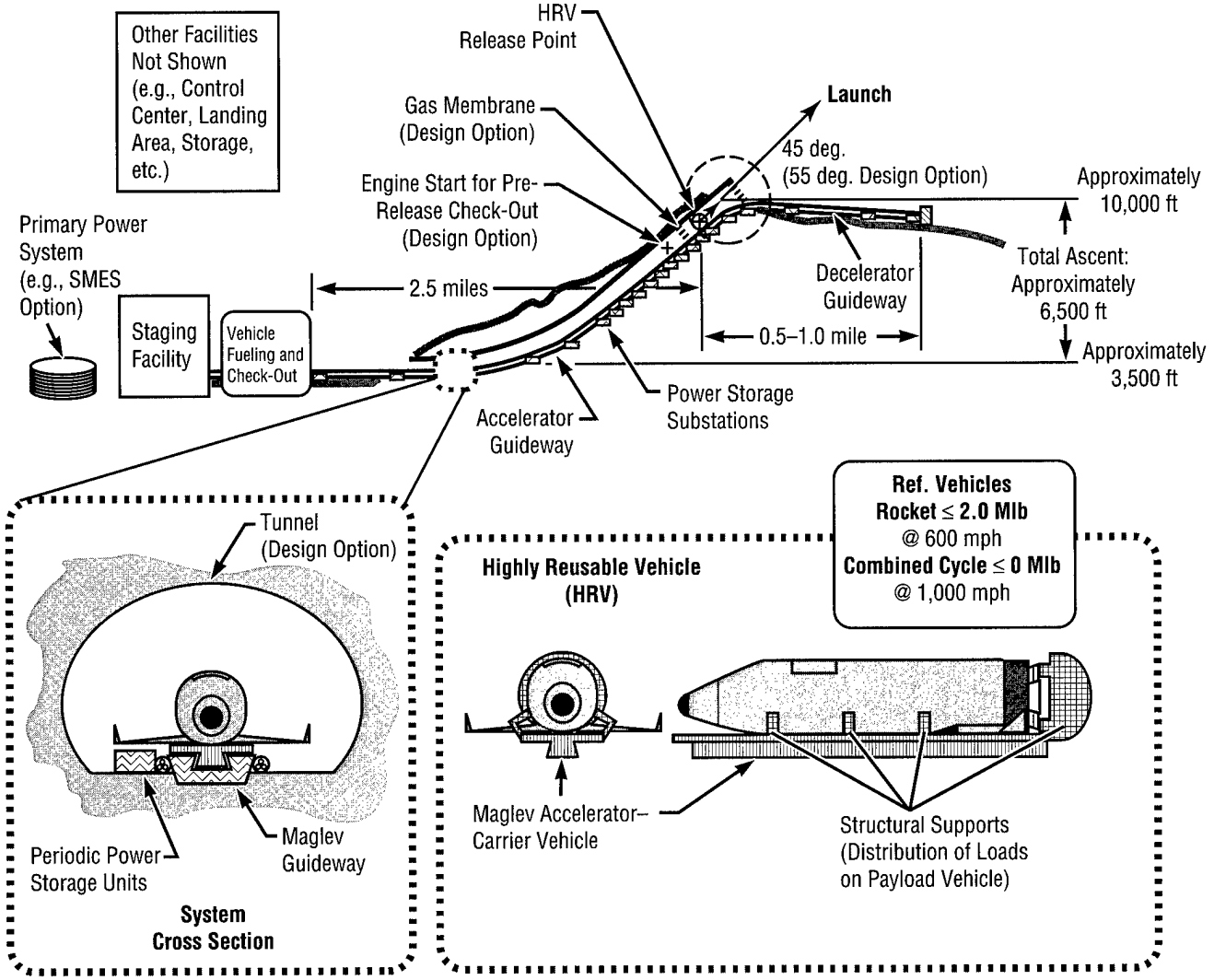

FIGURE 4.—MagLifter Space Launch System (configuration "i"); notional, full-scale system concept. This version of MagLifter is configured for a highly reusable vehicle that *does not* involve the use of aerodynamic lift during launch (i.e., a ballistic ascent trajectory).

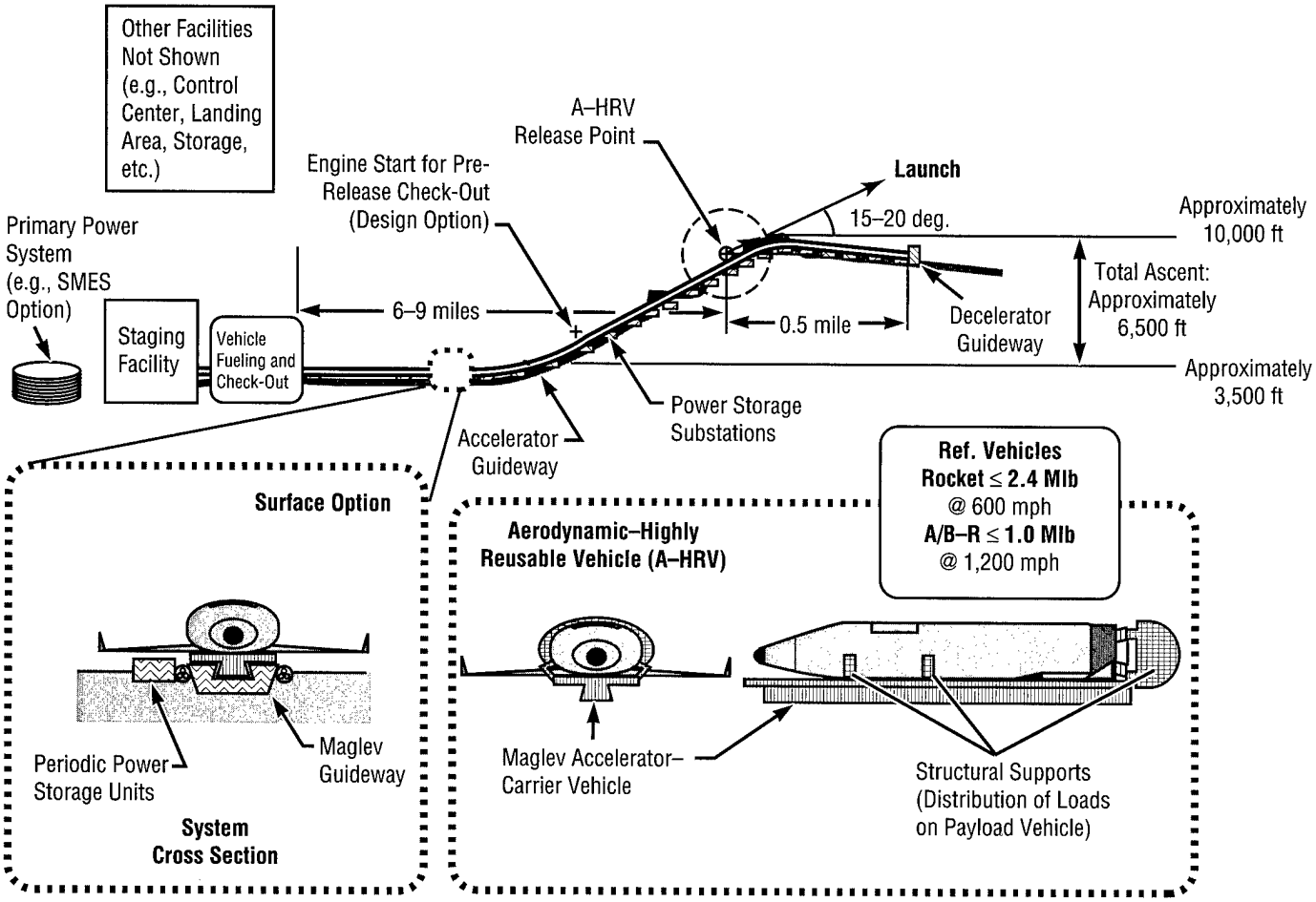

FIGURE 5.—MagLifter Space Launch System (configuration "j"); notional, full-scale system concept. This version of MagLifter is configured for a highly reusable vehicle that *does* involve the use of aerodynamic lift during launch.

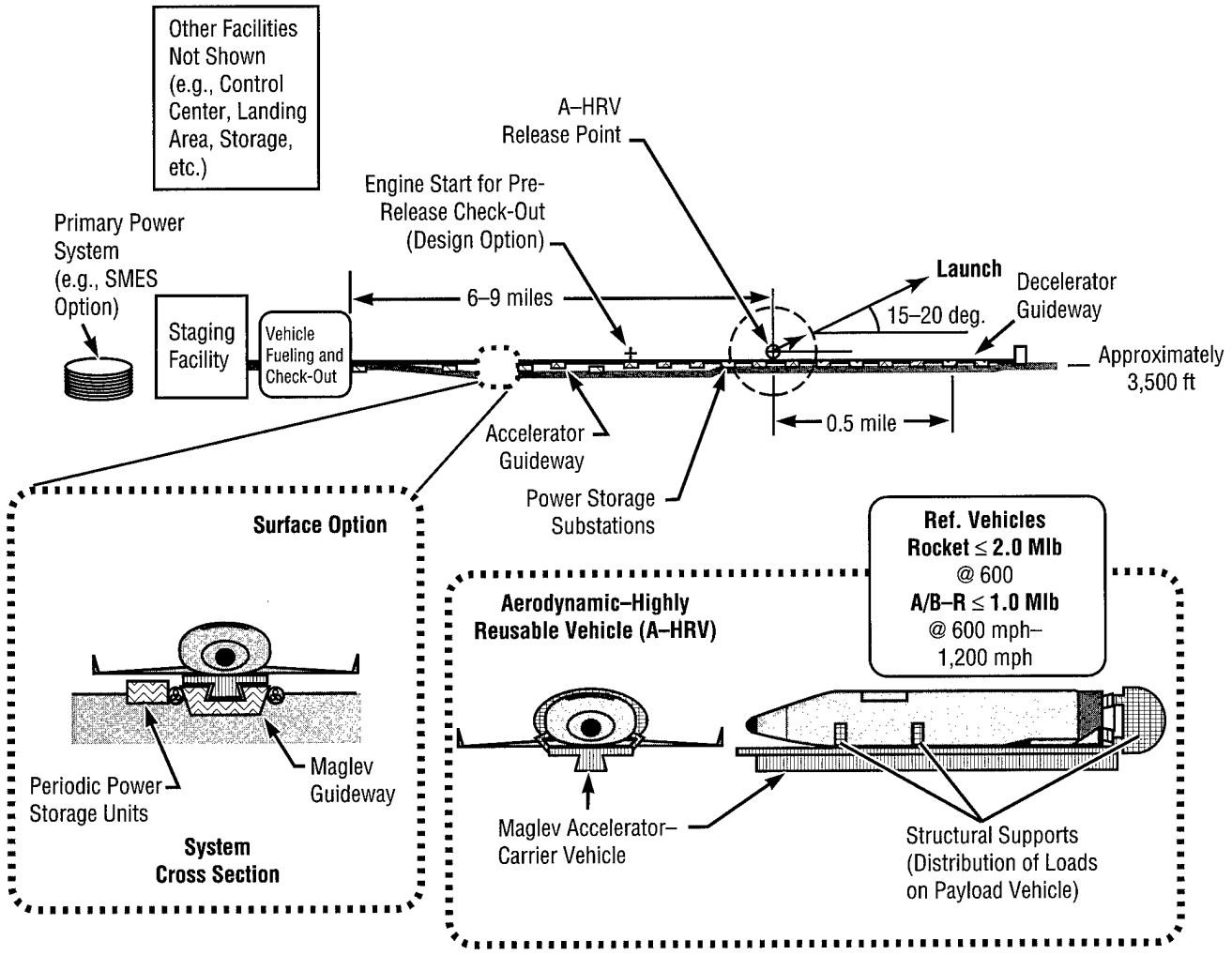

FIGURE 6.—MagLifter Space Launch System (configuration "k"); notional, full-scale system concept. This version of MagLifter is configured for a highly reusable vehicle that *does* involve the use of aerodynamic lift during launch *and runs horizontally*—0-degree inclination—at release of HRV

Solar Thermal Propulsion

Alan Adams/PS05
205–544–3607

Solar thermal propulsion is an advanced propulsion concept that utilizes concentrated solar energy to heat a propellant and thereby produce thrust. This propulsion concept will be used on an upper-stage vehicle with the main application being the transfer of payloads from low-Earth orbit to geostationary Earth orbit. The solar thermal propulsion concept is characterized as having low thrust (2 to 5 pounds force), high specific impulse (800 to 1,000 seconds), and is a much more efficient means of transporting payloads when compared to conventional chemical propulsion systems. Such efficiency will allow for the reduction of launch costs and for the increased competitiveness of the U.S. launch services industry.

MSFC has been involved with the design aspects and feasibility of solar thermal propulsion for the last few years. The initial involvement was a feasibility study conducted by MSFC's Program Development Directorate that provided the evidence that the concept offers sufficient performance gains over chemical propulsion systems, suggesting further detailed study was warranted.

Following that activity, MSFC has entered a cooperative agreement with a solar thermal consortium led by McDonnell Douglas. Part of NASA'S Aerospace Industry Technology Program effort, the Solar Thermal Upper-Stage Technology Demonstration Program, is a simulated integrated, systems-level ground test of a solar thermal propulsion system. MSFC is responsible for the testing of the liquid-hydrogen storage/feed system and the propulsion engine development. In the ground test program, the testing of the hydrogen storage/feed system will be performed at MSFC. These data will then be used as inputs to a test of the concentrator and engine, which will be performed at the Air Force Phillips Laboratory, Edwards Air Force Base. The concept to be tested utilizes an inflatable parabolic concentrator with foam rigidized support struts.

Key technologies associated with solar thermal propulsion include inflatable structures, engine design/fabrication, and pointing accuracy of the solar concentrators. In the solar thermal propulsion concepts being pursued by MSFC, the solar concentrators are inflatable structures made from a thin-film polyimide material, providing a lightweight structure for the vehicle and allowing greater payload capacity. The engine being designed and fabricated at MSFC is utilizing vacuum spray fabrication technologies.

Currently, MSFC is developing a flight experiment to demonstrate the key technologies mentioned above. The experiment will use a deployable Fresnel lens concentrator, an energy storage-type engine, and will be the first major milestone in the development of solar thermal propulsion. The experiment will not, however, perform an orbital transfer. At the successful conclusion of the experiment, a more ambitious flight will be performed, which will be more representative of a full-up upper stage, performing a low-Earth orbit to geostationary Earth orbit transfer. The flight date for the experiment is mid to late 1998. The likely launch vehicle for this flight experiment will be the Delta II launch vehicle.

Sponsor: Office of Space Access and Technology

Industry Involvement: McDonnell Douglas, United Applied Technologies, Thiokol Corporation

University Involvement: University of Alabama in Huntsville

Research

Virtual Keyboard for Hands-Free Operations

Jonnathan Kim/PD12
205–544–5387

The main objective of this research effort is to design an intelligent, hands-free, computer-input device for both space and commercial applications. The "virtual keyboard" can be used for future manned spacecraft or any environment that requires hands-free computer operations, e.g., a manufacturing environment. Another application, from which this idea was initially motivated, is in the area of providing an interface for the physically challenged: paraplegics, quadriplegics, and individuals with degenerative motor functions (fig. 7).

This project is currently being funded by the Center Director's Discretionary Fund, and the expected date of completion is December 1996. The first phase of research will investigate state-of-the-art technologies in eye tracking. During requirements definition, human factor issues related to perception, oculomotor capabilities, and learning will be carefully considered to help define verifiable system performance requirements. Thorough design analysis and human factor tests will be performed to determine an optimal configuration and design. During verification, the system will be tested to gauge the degree to which it satisfies the design requirement. Following verification, the system will be evaluated empirically with a variety of human subjects under various operational modes. Actual evaluation criteria and operational modes will be finalized during the experimental design, and will include such items as eye tracking and selection resolution, accuracy, and repeatability; required training/ learning time; fatigue effects; and environmental effects (e.g., ambient illumination and glare). The end product will be prototype hardware and software that demonstrate the feasibility of hands-free computer-input operations. In addition to the eye-tracking-driven interface, research will be performed to investigate the feasibility of using electroencephalogram data.

Sponsor: Center Director's Discretionary Fund

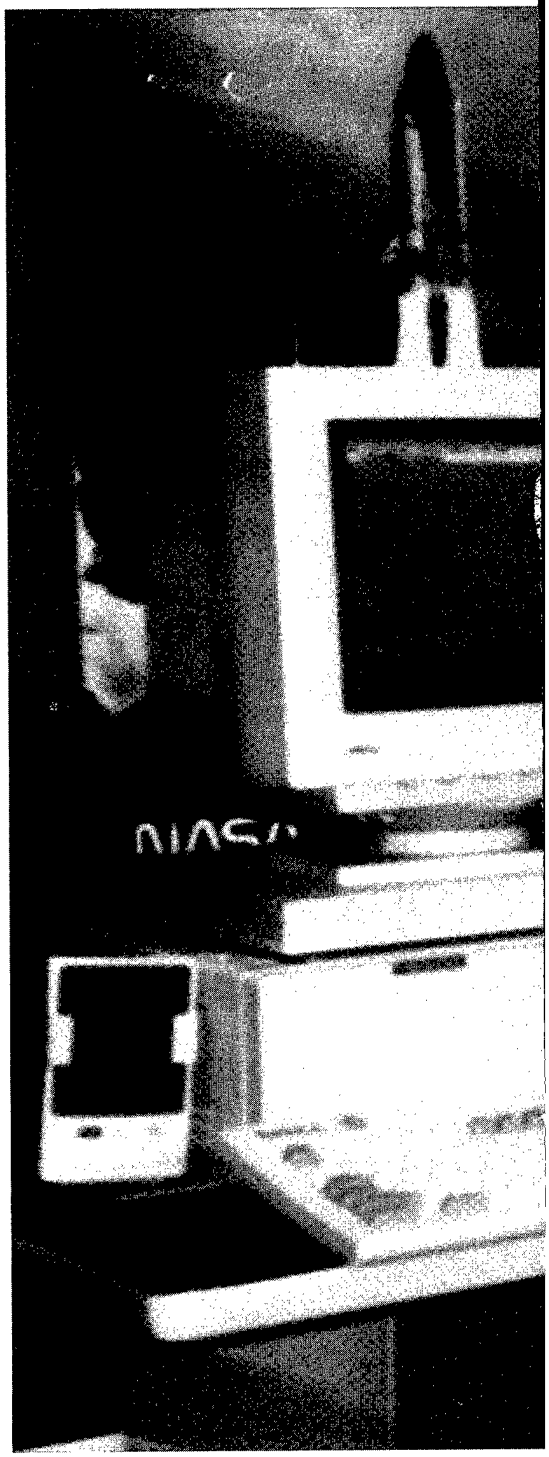

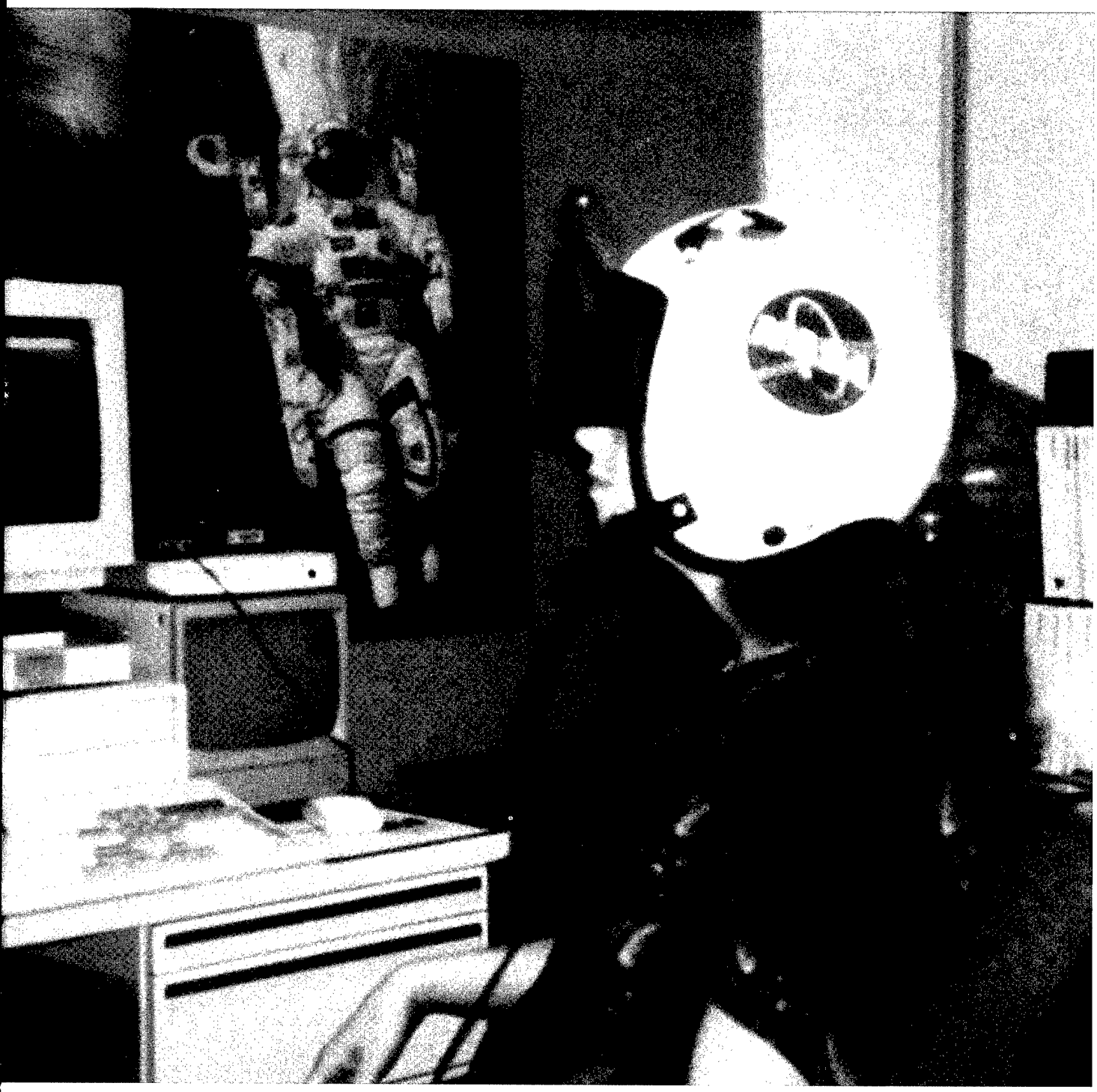

FIGURE 7.—Virtual keyboard.

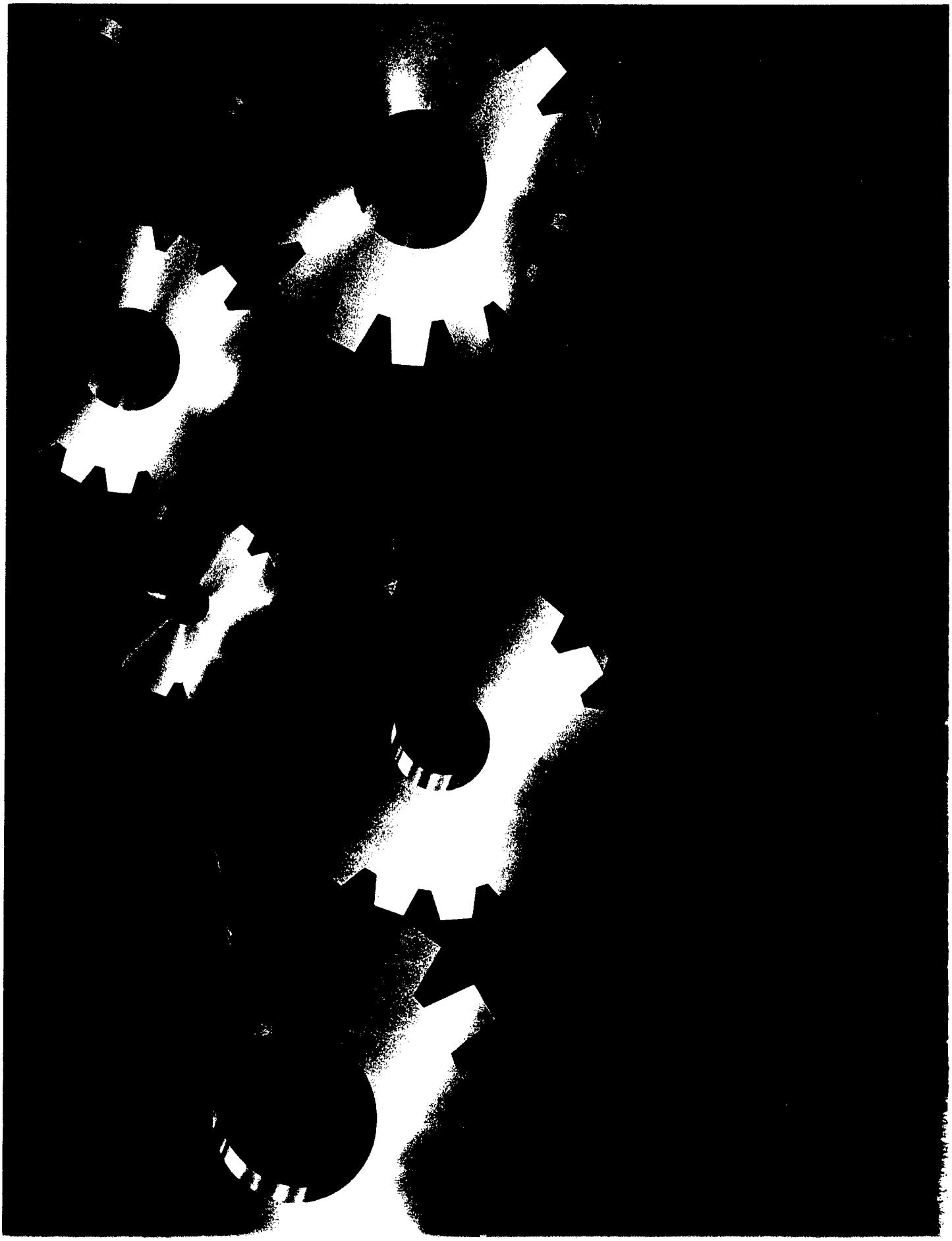

Research Programs

MSFC's primary research goal is to foster outstanding research in Earth system science, microgravity science, and physics and astronomy. This research falls within three of the five NASA Strategic Enterprises:

Research Area:	Enterprise:
Earth system science	Mission to Planet Earth
Microgravity science	Human Exploration and Development of Space (HEDS)
Physics and astronomy	Scientific Research

Microgravity science research concentrates on materials science and biotechnology. Special emphasis is placed on the growth and characterization of electronic and photonic materials using Spacelab furnace facilities, as well as the space growth and structure of protein crystals. Improved semiconductor single-crystal growth methods, such as the use of electromagnetic fields, are under development. Advances in x-ray optics are being utilized to enhance the onorbit characterization of protein crystals. Another area of research is in thin films for photonic applications.

Earth system science research focuses on the intricate workings of Earth as a system, with emphasis on the hydrology cycle. Research involves theoretical and experimental research on atmospheric and Earth system processes, environmental effects, and global change phenomena; it includes the development of innovative measurement systems and missions to advance associated scientific technical knowledge of planet Earth.

Physics and astronomy research focuses on astrophysics, space physics, and solar physics. The astrophysics program includes the continuation of the analysis of several exciting, unusual observations by the Burst and Transient Source Experiment (BATSE) on the Compton Gamma-Ray Observatory. Space physics activities involve the measurement and modeling of ion and plasma processes in the ionosphere and the magnetosphere, in addition to the development of laboratory and flight instruments. Solar physics research focuses on understanding the role of magnetic fields in solar processes.

MSFC is committed to communicating our science to the public more effectively and in enabling the productive use of science and technology in the public sector. Additional information is available on the WWW at http://wwwssl.msfc.nasa.gov/.

Gregory S. Wilson
Director
Space Sciences Laboratory

Microgravity Science

Electromagnetic Field Effects in Semiconductor Crystal Growth

Martin P. Volz/ES75
205–544–5078

Electromagnetic fields can interact with electrically conducting melts and substantially affect their fluid-flow processes. Indeed, the intriguing possibility exists of using these fields to control fluid flow in the melt during the solidification of semiconductor alloys. However, before such a possibility can be realized, it is essential to conduct a basic study of the fundamental interactions that electromagnetic fields can have on fluid-flow processes during semiconductor crystal growth. Recent work on this effort has focused on both constructing a model growth cell in which the basic flow processes can be experimentally observed and developing a theoretical framework that addresses the issues involved.

A new theoretical formulation of combined electromagnetohydrodynamics has been developed and shows the inconsistencies and shortcomings of the existing separate electrohydrodynamic and magnetohydrodynamic theories. The new model is for three-dimensional, unsteady, viscous fluid flows involving electrically charged particles and electric polarization and magnetization effects. All interaction between externally applied and internally induced electric and magnetic fields is incorporated into the model. An eigenvalue analysis of the governing system of nine nonlinear, coupled, differential equations has been performed. For certain combinations of material properties, it is possible to obtain complex conjugate eigenvalues, indicating that the hyperbolic-elliptic system could become inherently oscillatory. Future planned activities include numerical algorithm development and computer coding of the model.

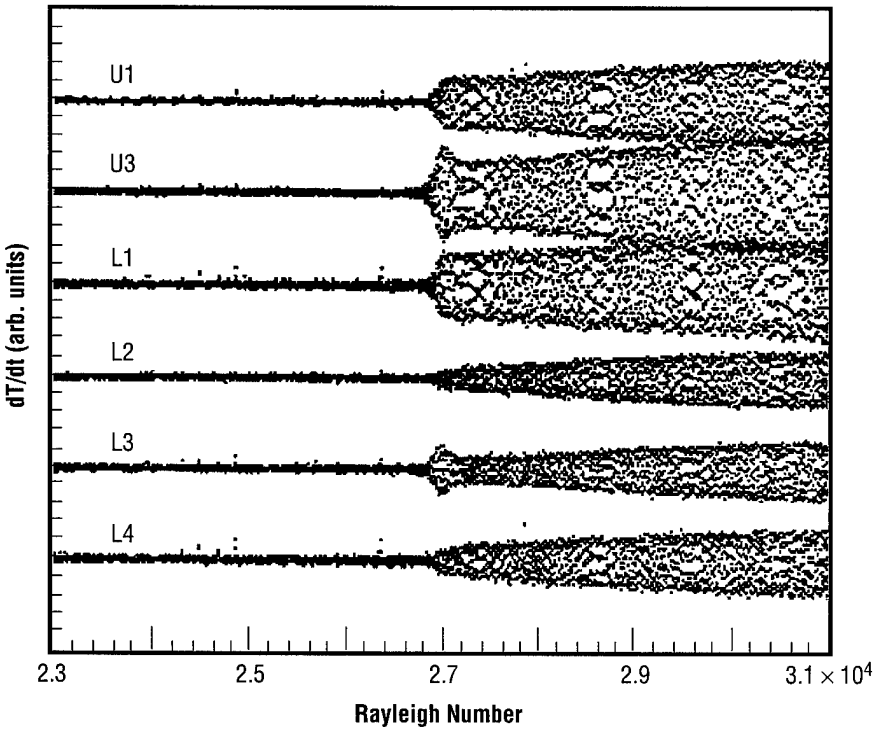

FIGURE 8.—Derivatives of thermistor signals versus Rayleigh number.

Experimentally, a cylindrical test cell was constructed and placed in the center of a rotating magnetic field. The cell contained liquid gallium. Thermistors were placed in the cell to record temperature changes, and researchers were to infer from them the nature of the fluid flow. The temperature difference between the top and bottom of the cell was slowly changed until transitions between fluid modes were observed. These transitions occurred at critical values of the Rayleigh number, a dimensionless number which is proportional to the temperature difference across the cell. A typical transition is shown in figure 8. The derivatives of the thermistor signals, designated "U1–L4," are plotted as a function of the Rayleigh number. The thermistor signals are vertically offset for clarity. When the Rayleigh number reaches 2.7×10^4, the flow transitions from being time-independent to time-dependent.

Critical Rayleigh numbers were measured as a function of rotating magnetic field strength, and several different fluid stability regimes were

identified. For weak rotating magnetic fields and small Rayleigh numbers, a regime was identified as having laminar flow. In that regime, the rotational fluid velocity depended on the magnetic field strength squared. The importance of this observation is that it indicates that a flow regime exists in which the benefits of a rotating magnetic field on the crystallization process are not compromised by time-dependent flow.

Dulikravich, G.S., and Lee, S. Electro-Magneto-Hydrodynamics: Part I—Introductory Concepts. Submitted to *International Journal of Nonlinear Mechanics*.

Mazuruk, K., and Volz, M.P. 1995. The Effect of a Rotating Magnetic Field on Fluid Flow in Crystal-Growth Configurations. Alabama Materials Research Conference, Birmingham, Alabama.

Volz, M.P., and Mazuruk, K. Flow Transitions in a Rotating Magnetic Field. Accepted for publication in *Experiments in Fluids*.

Sponsor: Office of Life and Microgravity Sciences and Applications

University Involvement: Pennsylvania State University

Magnetic-Damping Test of Convective Flows in Microgravity

Frank R. Szofran/ES75
205–544–7777

The fundamental objectives of this experiment are: (1) to test experimentally the validity of modeling predictions applicable to convective-flow magnetic damping in conductive melts as this applies to the directional solidification of metallic and semiconductor materials in the reduced-gravity levels available in low-Earth orbit; and (2) to assess the effectiveness of magnetic fields in reducing the fluid-flow occurrence in these materials during the space processing that results from density gradients (driven by either the residual steady-state acceleration or *g*-jitter) or surface-tension gradients (Marangoni flow).

During the past year, work has included Bridgman and floating-zone growth experiments, as well as numerical modeling of the Bridgman experiments. Ingots of gallium-doped germanium, germanium-silicon alloys (5-percent silicon), and indium antimonide-gallium antimonide (20-percent indium-antimonide) have been grown by the Bridgman method, while the floating-zone experiments were done with silicon samples.

For the gallium-doped germanium experiments (summarized in fig. 9, which shows data for the composition along the growth axes for four samples grown at different magnetic fields), convection is sufficiently vigorous to completely mix the melt at zero field. In the three nonzero fields, the data show that convection is reduced to the point that the compositions follow a diffusion-controlled curve for at least the first 30 percent of the length of the sample. At 5 Tesla, statistics show diffusion control over nearly the complete sample. These results confirmed the modeling prediction that an approximately 3-Tesla magnetic field would be required to achieve diffusion-controlled growth in the configuration that was used. The germanium-silicon alloy experiments showed that this alloy system is not gravitationally stable against convection as expected from a simple hard-sphere model of the melt, but that application of a magnetic field to the melt stabilizes it sufficiently to achieve diffusion-controlled growth. This is in contrast to indium antimonide-gallium antimonide, which exhibited complete mixing in the melt, even at a 5-Tesla applied magnetic field.

The silicon float-zone experiments were carried out in collaboration with the Kristallographisches Institut of the University at Freiburg, Germany, under a collaborative agreement with NASA. Using a mono-ellipsoid mirror furnace installed in a magnet in the MSFC Space Sciences Laboratory, 19 samples were grown and are being jointly analyzed by both university and MSFC researchers. These experiments extended to 3 Tesla the earlier experiments carried out at the university in their 0.5-Tesla magnet. By comparing these results with sounding rocket experiments carried out by the Kristallographisches Institut, the similarities and differences between reducing convection with an applied magnetic field versus reduced gravity have

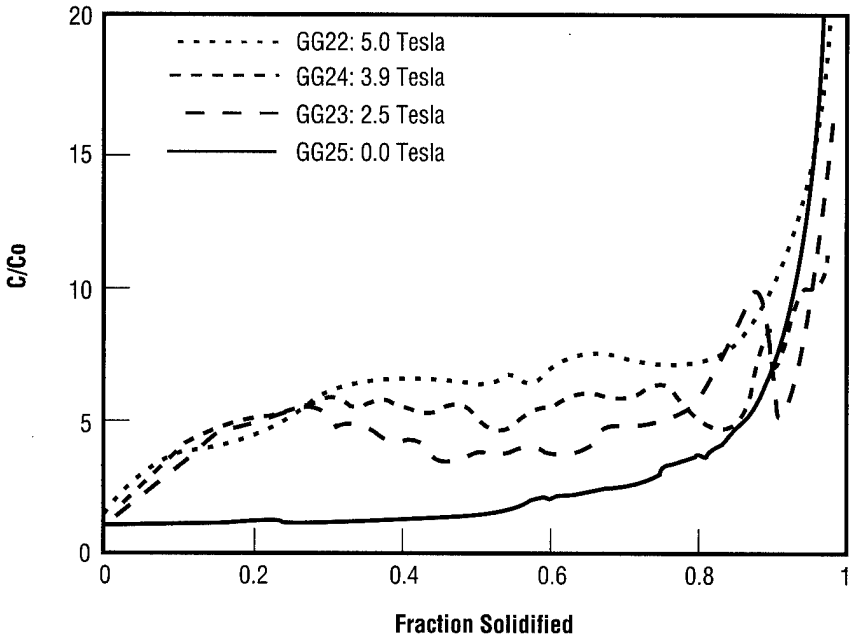

FIGURE 9.—Axial gallium concentration profiles versus field strength for Bridgman-grown germanium.

been elucidated. For samples grown in high-magnetic fields, both the Bridgman and floating-zone experiments provided some unexpected results. The magnetic field should reduce convection, and it does initially. However, findings from both types of experiments indicate that the effect of convective flow in the melt increases at some point during the growth (as is evident in fig. 9 for the gallium-doped germanium samples grown at 2.5 and 3.9 Tesla). One possible explanation for this is called "thermoelectromagnetic convection," which is driven by currents induced by variations in thermoelectric properties along the solidification interface, and known to exist under such conditions as in the liquid-metal cooling systems of nuclear reactors. Although such currents will exist without a magnetic field, they would not cause any motion of the melt unless there is a magnetic field present. Whether thermoelectromagnetic convection is significant or not is an important question that will be addressed in the coming year, because it will have a substantial impact on the design of a magnetically damped flight furnace now under consideration as a future module for the Space Station Furnace Facility.

The near-future plans in the modeling area include investigating the sensitivity of systems experiencing solutal forces to gravity parallel to the growth surface, continuing work on the modeling of magnetic and microgravity effects on thermosolutal convection, and simulating magnetic experiments of gallium-germanium and germanium-silicon now in progress.

Rolin, T.D., and Szofran, F.R. 1995. Determination of the Electrical Conductivity of Liquid $Ge_{0.95}Se_{0.05}$. *Journal of Crystal Growth*, 153, 6–10.

Szofran, F.R.; Volz, M.P.; Motakef, S.; and Lehoczky, S.L. Bridgman Growth of Germanium-Gallium Under Magnetic Fields to 5 Tesla. In preparation.

Cobb, S.D.; Rolin, T.D.; Volz, M.P.; Szofran, F.R.; and Lehoczky, S.L. Melt Resistivity and Magnetic Bridgman Growth of $In_{0.2}Ga_{0.8}Sb$. In preparation.

Cröll, A.; Szofran, F.R.; Dold, P.; Lichtensteiger, M.; Benz, K.W.; and Lehoczky; S.L. Floating-Zone Growth of Silicon Under Large Axial Magnetic Fields. In preparation.

Szofran, F.R.; Volz, M.P.; Cobb, S.D.; Lehoczky, S.L.; and Motakef, S. June 18–23, 1995. Bridgman Magnetic Field Growth of Dilute and Concentrated Semiconductors. Presented at the Eleventh International Conference on Crystal Growth, The Hague.

Cröll, A.; Szofran, F.R.; Dold, P.; Lichtensteiger, M.; Benz, K.W.; and Lehoczky, S.L. June 18–23, 1995. Floating-Zone Growth of Silicon Under Large Axial Magnetic Fields. Presented at the Eleventh International Conference on Crystal Growth, The Hague.

Sponsor: Office of Life and Microgravity Sciences and Applications

Industry Involvement: Computer-Aided Process Engineering, Inc.

High-Brilliance X-Ray Source for Protein Crystallography

Daniel C. Carter/ES76
205–544–5492

Protein crystallography is currently the most powerful method for determining the three-dimensional structures of proteins and other macromolecules. Determination of the three-dimensional structure of macromolecules is of fundamental importance in the area of molecular biology and has considerable potential for application in rational drug design and protein engineering. This method usually requires crystals that are relatively large and that possess a high degree of internal order.

Several microgravity experiments have successfully produced protein crystals that greatly exceed the quality of the best crystals obtained from ground experiments, allowing investigators to significantly improve the atomic structures of these proteins. However, many proteins of significant interest to the scientific community produce only small or weakly diffracting crystals, which, until recently, could only be analyzed using the high-energy radiation of Synchrotron facilities.

Advances in x-ray optics, particularly Kumakhov optics, have been designed and utilized by a team of scientists at MSFC, SUNY, and X-Ray Optical Systems, Inc., to produce new high-intensity x-ray sources. The project is outlined and proceeding in three stages. Initial tests of the stage II lens (fig. 10) conducted at MSFC's

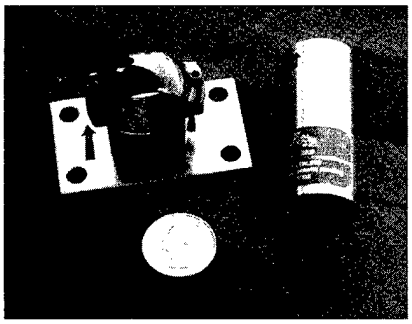

FIGURE 10.—Stage II lens and holder.

Laboratory for Structural Biology indicate that the brightness of the lens/x-ray source combinations is more than 160 times brighter than the conventional rotating anode generator. These systems will provide a tremendous improvement in the rate and quality of collected x-ray diffraction data, and smaller samples of more challenging protein structures may also be pursued. Low-power systems operating at 37 watts have been demonstrated to exceed the brightness of current rotating anode sources by a factor of 2. The low power requirements and high brilliance of this prototype system have important implications for developing an on-orbit x-ray diffraction facility. The numerous other applications for this technology include improved medical imaging.

Ullrich, J.B.; Ponomarev, I.Yu.; Gubarev, M.V.; Gao, N.; Xiao, Q.F.; and Gibson, W.M. 1994. Development of Monolithic Capillary Optics for X-Ray Diffraction Applications in X-Ray and Ultraviolet Detectors. Proceedings of the Society of Photo-optical Instrumentation Engineers, 2278:148–55.

MacDonald, C.A.; Abreu, C.C.; Budkov, S.; Chen, H.; Fu, X.; Gibson, W.M.; Kardiawarman, A.; Karnaukhov, A.; Ponomarev, I.Yu.; Rath, B.K.; Ullrich, J.B.; Vartanian, M.; and Xiao, Q.F. 1993. Quantitative Measurements of the Performance of Capillary X-Ray Optics in Multilayer and Grazing-Incidence X-Ray/Extreme-Ultraviolet Optics II. Proceedings of the Society of Photo-optical Instrumentation Engineers, 2011.

Ullrich, J.B.; Kovantsev, V.; and MacDonald, C.A. 1993. Measurements of Polycapillary X-Ray Optics. *Journal of Applied Physics*, 74:5, 933–39.

Ullrich, J.B.; Gibson, W.M.; Gubarev, M.V.; and MacDonald, C.A., 1994. Potential for Concentration of Synchrotron Beams With Capillary Optics. *Nuclear Instruments and Methods*, A347:401–6.

Gibson, W.M., and MacDonald, C.A. 1994. Polycapillary Kumakhov Optics: A Status Report in X-Ray and Ultraviolet Detectors. Proceedings of the Society of Photo-optical Instrumentation Engineers, 2278:156–67.

Wentink, R.; Carbone, J.; Aloise, D.; Gibson, W.M.; MacDonald, C.A.; Hanley, Q.E.; Fields, R.E.; and Denton, M.B. 1994. Charge-Injection Device Technology: An Imaging Solution for Photon- and Particle-Imaging Applications. Proceedings of the Society of Photo-optical Instrumentation Engineers, 2279.

Sponsor: Office of Life and Microgravity Sciences and Applications

Industry Involvement: X-Ray Optical Systems, Inc., Albany, New York

University Involvement: Dr. Walter Gibson, Center for X-Ray Optics, State University of New York at Albany

Protein Crystal-Growth Apparatus for Microgravity Facility Hardware

Daniel C. Carter/ES76
205–544–5492

A microgravity facility hardware for protein crystal growth has been designed by MSFC scientists and engineers based on a common ground-based method of growing protein crystals. The facility is unique in that it contains a disposable interface (or tray) with seven crystallization chambers (fig. 11) designed for improved logistics and handling. The hardware has unprecedented experimental capacity. Nine trays are housed in a cylinder with interlayered actuator assemblies, and six of the cylinders are contained within a one Single-Locker Thermal Enclosure System (fig. 12), offering a total of 378 individual experiments. Two or more of the enclosure units may be manifested per mission.

The facility hardware has flown successfully on STS–62, STS–67, and STS–73, and has produced important improvements in crystal perfection. Once in orbit, the hardware is activated by a simple clockwise rotation of the cam assembly. Notable successes include the production of crystals that allowed for the complete atomic structure and refinement of human antithrombin III by co-investigator Dr. Mark Wardell of

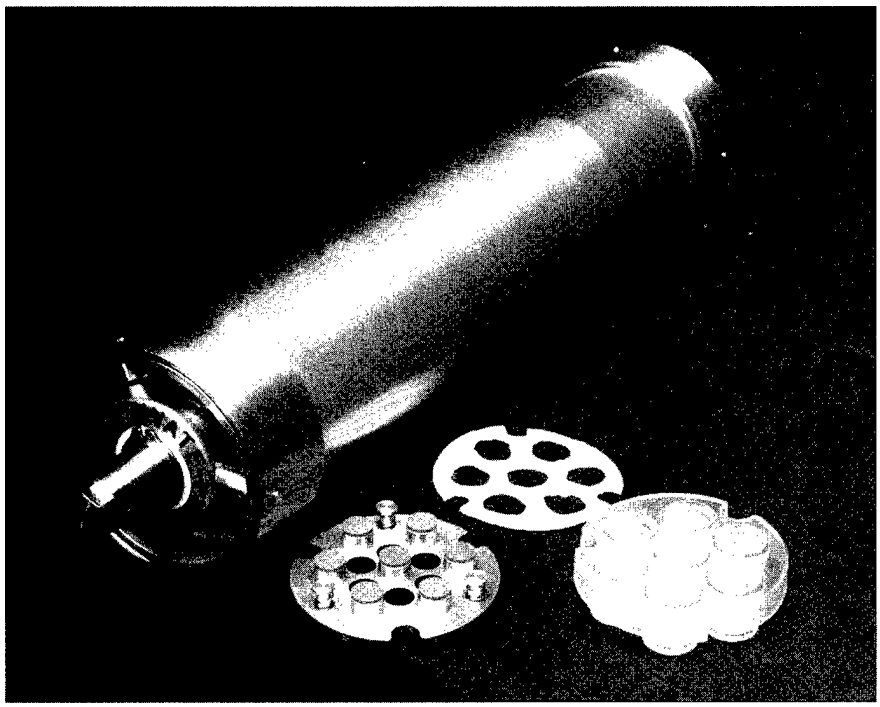

FIGURE 11.—Microgravity facility hardware for protein crystal growth, with disposable interface and seven crystallization chambers.

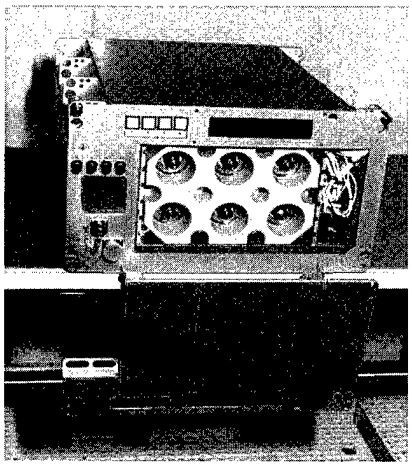

FIGURE 12.—Single-Locker Thermal Enclosure System with six cylinders.

Cambridge University. This protein, an important target for the development of improved therapeutics as anticoagulants for the prevention of blood clots, was manifested on all three flights. The U.S. Microgravity Laboratory 2 (STS–73), which launched in October, was notable in that it carried approximately 1,000 individual protein crystal-growth experiments containing 12 different proteins from a total of eight academic, government, and industrial co-investigators.

Projects have included important research involving the human immunodeficiency virus (HIV–1), the human cytomegalo virus, heart disease, and drug efficacy and delivery. The total number of individual experiments flown in the crystal-growth apparatus during 1995 exceeded the total number of experiments flown during the previous decade. The protein crystal-growth apparatus for microgravity is operated as a government facility and access is openly available to the general scientific community.

Lim, K.; Ho, J.X.; Wright, B.S.; Twigg, P.D.; Miller, T.; Chapman, J.; Keeling, K.; and Carter, D.C. Analysis and Crystallographic Refinement of Hen Egg-White Lysozyme at 1.4 Angstrom From Crystals Produced in Microgravity. Submitted for publication.

Sponsor: Office of Life and Microgravity Sciences and Applications

Industry Involvement: Monsanto Searle, DuPont Merck, Eli Lilly & Company

University Involvement: Department of Haematology, Cambridge University, United Kingdom; Universite Catholique de Louvain, Belgium; University of Georgia; University of Pittsburgh; Virginia Commonwealth University; McMaster University, Canada; University of Colorado; University of Groningen, The Netherlands

Phase-Shifting Interferometric Analysis of Protein Crystal-Growth Boundaries and Convective Flows

William K. Witherow/ES76
205–544–7811

The objective of the proposed study is to obtain experimental evidence for several characteristics of a crystallizing protein solution and model their effects on the crystal-growth process. The characteristics to be studied include the presence of concentration gradients during the crystal growth, the extent of the boundary layer from the crystal face, and the effect of buoyancy-driven convection on the growth. Phase-shifting interferometry can provide significant insight into this issue, and will produce a visual confirmation of the concentration profile at the boundary layer and concentration values within the depletion region. Phase-shifting interferometry has the potential to offer a direct visualization of convective flows within proteinic crystallizing solutions.

Protein crystals are grown to determine the three-dimensional structure of proteins. By utilizing x-ray or neutron diffraction, the collected information allows the direct identification of macromolecule active sites, their conformation, and the sequence of the amino acids. Sections of very large assemblies of proteins, such as structural proteins or viruses, can also be crystallized. Crystallization is therefore the starting point of any study aimed at the

development of new drugs and the understanding of viral diseases. Crystallization techniques for proteins are now well known, but a biophysical understanding of the growth mechanisms is still underdeveloped. This aspect of protein research needs to be expanded, as the proteins being studied are more complex and their purification more costly.

Since the beginning of the 1980's, tens of proteins have been crystallized in microgravity. Microgravity-grown crystals of several proteins were found to be either larger or diffracted with higher resolution than ones previously grown on the ground. These results seem to demonstrate that a reduction of gravity affects the interfacial growth mechanisms that are directly dependent upon the mass-transport regime. Convection is known to play a significant role in the growth kinetics of inorganic crystals, but its importance is still debated in relation to the crystallization of biological macromolecules. There is little doubt about the existence of convective flows in proteinic solutions, but the flow rates they generate close to the crystal/solution interface and their effect on growth kinetics have not been quantified experimentally. The phase-shifting interferometry technique will allow researchers to determine these values and will provide direct comparison between solutal flows in crystallizing solutions under various levels of gravity. An examination of the flows in the fluid and their correlation with crystal growth will strongly depict the role of microgravity in protein crystal growth.

Mach-Zehnder and reflection interferometry, with a magnification of up to 1,000×, will be used to examine growing protein crystals. Phase shifting will be accomplished using an electro-optic phase modulator or a piezo-electric mirror. Abel inverse transforms will be used on the resulting phase maps to provide planar phase information.

Equipment is on order to construct the phase-shifting mechanisms required for the optical systems. Protein crystal-growth material will be provided by MSFC's Biophysics Branch Center.

This study will provide new techniques for viewing protein crystals as they grow. Miniaturization of the optical system could lead to shuttle or space station experiments in microgravity.

Sponsor: Office of Life and Microgravity Sciences and Applications

Diode-Laser Holographic-Imaging System Applied to the Study of Fluids in Microgravity

William K. Witherow/ES76
205–544–7811

Holography is an important research method because it records an image of the entire volume of a test cell at a given instant in time. When a hologram is constructed, it records the wavefront coming from the test cell; when the hologram is reconstructed, the same wavefront is reproduced. The reconstructed wavefront can be analyzed by the same optical techniques that could have been used on the original test cell.

This capability is important in many areas of research, including solution crystal growth, fluid physics, and particle phenomena. As an example, quantitative studies of transparent dispersion growth require diameter measurements from numerous microscopic droplets at a given instant in order to produce statistically significant results. Typically, the droplets will be undergoing changes in position or size as the experiment progresses. Accurate measurement of the entire population of droplets is impossible by normal techniques. However, by recording a hologram of the experiment, the entire test-cell volume is stored. The entire test cell from the reconstructed hologram can be investigated by microscopy to measure all of the droplets.

The primary objective of the proposed research is the development and testing of a compact, state-of-the-art, modular, holographic-imaging system based on diode-laser technology, incorporating micro-optics in order to record full three-dimensional images of the test cell. The apparatus has been designed to be compatible with a variety of test-cell modules. The device is suited to applications in ground-based laboratories, as well as reduced-gravity environments, e.g., the space shuttle, the KC–135 aircraft, and sounding rockets.

A second objective of the research is to develop a compact apparatus designed for microgravity fluid-physics studies. This fluids module will be designed to plug in to the imaging system, and will be used in order to verify that system's functionality. Several fluid-handling functions will be incorporated, including the ability to (1) produce well-defined dispersions having user-specified characteristics, (2) deploy numerous small droplets of selected volumes, and (3) deliver selected volumes of fluid.

An initial breadboard system has been constructed to test the capabilities of the diode laser to construct holograms. In-line holograms have been made of static glass beads (approximately 200 meters in diameter) suspended in water and of calibration test patterns. Side-band holograms of melting ice in water have also been made. The capabilities of the initial system are being evaluated. A fluids-processing module was developed for the KC–135 flight with heating and mixing capabilities.

A miniaturized holographic system will be designed based on current optics technology. An optics breadboard table, on which the system will be constructed with miniaturized optical components, is the same size as a shuttle locker. Once constructed, the system will be tested and refined, and a variety of experiments will be performed to demonstrate its capabilities. The holographic system and the microgravity fluids module will be combined and tested on the KC–135.

Sponsor: Center Director's Discretionary Fund

Investigation of Local Effects on Microstructure Evolution

Donald O. Frazier/ES01
205–544–7825

The principal reason for processing materials in the microgravity environment is to obtain improved material properties. These properties are generally related to the purity and microstructural morphology of the bulk material. Results from early space-processed materials showed the inadequacy of the then-current models for predicting microstructure. Of the many parameters that influence development of microstructure, this effort concentrates on the diffusive mass transport between droplets in a two-phase system. Of particular interest is the local environment around a growing or shrinking droplet (the number and spacing between droplets in the immediate neighborhood of a given droplet). The primary goal of this work is to improve understanding of microstructure evolution in solidifying materials. The approach uses data from experiments on transparent materials to develop better predictive computer models.

The effort, to date, has resulted in experimental observation of diffusional coarsening among a finite cluster of precipitates forming spherical caps on the wall of a thin cell in a liquid-liquid system using a holographic technique. Numerical modeling of the process using the multipole expansion method and the assumption of two-dimensional diffusion fields has yielded good

agreement with experimentation. Both monopole and dipole approximations closely follow the experimentally observed scaling laws characteristic for mixed-dimensional coarsening, i.e., three-dimensional droplets and two-dimensional diffusion fields. N^{-43} and R^4 varied linearly with time, where N is the number of droplets in the experimental field of view, and R is the average droplet radius.

Experimental observations of dynamic local behaviors within the context of a particle ensemble are accessible by optical techniques, including holography. The evolution of individual droplets in two- and three-dimensional diffusion fields is under study. Mixed dimensional systems have droplets tethered by the cell surfaces, and collection of a considerable amount of ground-based data, avoiding sedimentation, is possible. The more difficult unit-gravity experiment is the three-dimensional case, in which sedimentation is also a problem, as well as buoyancy-driven convection. A flight experiment for this case is under consideration.

The research team has developed a multipole representation of sources and sinks to represent interacting droplets. It has been noted that screening effects occur that are analogous to the Debye-Huckle theory of ionic solutions in which potential sinks and sources are not uniformly distributed. Measurements of droplet-size distribution and droplet location for a larger area of the experiment test cell are in progress using holograms taken during the experiment. Using holography eliminates questions about whether experimental conditions were consistent from experiment to experiment. Data will elucidate the effect of screening length on the diffusive growth rates. Experiments using a limited number of tethered droplets are underway. Measurements of growth rates at different temperatures, and hence different density gradients, will clarify the effect of convection on the ripening process.

A better understanding of the parameters affecting development of the microstructure should lead to improved processes to form industrially important materials with enhanced properties. Properties such as conductivity, structural integrity, and homogeneity are all influenced by microstructure. The team has shown that local effects—enhanced by holographic techniques—deviate significantly from global behavior predictable by Lifshitz, Slyozov, and Wagner. These deviations can be important in predicting material microstructure.

Rogers, J.R.; Frazier, D.O.; Downey, J.P.; Witherow, W.K.; Facemire, B.R.; Fradkov, V.E.; Mani, S.S.; and Glicksman, M.E. 1994. Coarsening of Three-Dimensional Droplets by Two-Dimensional Diffusion: Part I, Experiment. *Journal of Electronic Materials*, 23(10):999–1,006.

Fradkov, V.E.; Mani, S.S.; Glicksman, M.E.; Rogers, J.R.; Downey, J.P.; Witherow, W.K.; Facemire, B.R.; and Frazier, D.O. 1994. Coarsening of Three-Dimensional Droplets by Two-Dimensional Diffusion: Part II, Theory. *Journal of Electronic Materials*, 23(10): 1007–13.

Sponsor: NASA Office of Life and Microgravity Sciences and Applications

Industry Involvement: Rensselaer Polytechnic Institute, Troy, New York

Polydiacetylene Thin Films for Photonic Applications

Donald O. Frazier/ES01
205–544–7825

The goal of this work is to study the process of photodepositing polydiacetylene films onto transparent substrates from monomer solutions by irradiation with ultraviolet light. The process is a novel technique for the formation of thin amorphous films useful in nonlinear optical devices. Further, the process involves gravitational effects during photopolymerization—heretofore unreported in the literature. This work represents the extension of an earlier funded Research and Technology Operating Plan.

Polydiacetylenes are an extremely promising class of polymers for such photonic applications as wave-guiding and nonlinear optics.[1,2] Because of their highly conjugated electronic structures, they can have large, nonlinear optical coefficients with very fast response times, rendering them useful for applications such as ultra-fast, all-optical switching. Researchers have continued, through various discretionary funding sources, to conduct ground-based research on polydiacetylenes, as well as other organic and polymeric nonlinear optical materials. As a result, a simple, novel technique for the formation of thin amorphous films of a polydiacetylene (PDAMNA) derived from 2-methyl-4-nitroaniline was discovered and developed here at MSFC (patent pending). [3,4]

It is well known that such gravitational effects as buoyancy-driven convection can affect solution processes.[5] Evidence of this is seen in the photodeposition of PDAMNA thin films from solution: films grown in one-gravity contain small (submicron) solid particles embedded throughout them. These particles consist of precipitated polymer that forms in the bulk solution as polymer chains grow and eventually exceed their solubility. Thermal convection, induced by uneven heat generation in the solution from the ultraviolet radiation, transports the particles to the surface of the growing film, where they become embedded. These particles are defects that can scatter light, thereby lowering the optical quality of the films.

The objective of this work is to study photodepositing polydiacetylene films onto transparent substrates and the accompanying gravitational influences on film quality and morphology. By irradiating only part of the substrate with ultraviolet light, films can be obtained in desired patterns; a laser can even be used to form polymeric circuits. By varying the orientation of the growth chamber with respect to gravity to minimize convection, the concentration of particles in the films can be reduced but not eliminated. Additionally, there is some evidence to suggest that convection can have a detrimental effect on molecular orientation in thin films. This is important because well-ordered films are capable of significantly greater optical nonlinearities than poorly ordered films. The turbulent molecular motions that take place during convection can cause the growing polymer chains to become entangled and matted around each other, thus disrupting any natural ordering that might otherwise occur. Researchers assess that a convection model for the most gravitationally stable orientation in one-gravity is one of an unstable layer atop a stable layer, with penetrative convection. An experiment has been scheduled to fly on CONCAP IV [CONsortium Complex Autonomous Payload] aboard STS–69 (Fall 1995) to photodeposit PDAMNA thin films.

Researchers have been investigating the use of liquid crystal moieties chemically incorporated into the structure of PDAMNA to aid in inducing self-alignment of the polymer chains,[6] and have recently synthesized a modification of the diacetylene monomer that appears to exhibit the desired liquid crystalline behavior. Pre-ordered substrates are being used as templates upon which to carry out photodeposition in hopes of achieving quasiepitaxial film growth.

The reduced convection environment of microgravity could be a significant asset to achieving molecular orientation in these films. Further, scattering losses in these promising nonlinear optical films could be markedly minimized, leading to benchmark devices. Among the most important assets to this research are the discoveries of a new process for depositing thin films with good optical quality, and a heretofore unexplored mechanism leading to convection affecting thin-film growth.

Photopolymerization in solution seems to be a gravitationally sensitive

process. Observed variations in film quality due to reaction-cell orientations relative to the gravity vector raise some interesting opportunities for microgravity research. Fundamental science questions will be answered through microgravity processing, with probable technological advances through benchmark device fabrication on orbit.

[1]*Nonlinear Optical Properties of Organic Molecules and Crystals*, Vol. 2. 1987. Chemla, D.S., and Zyss, J., eds. Academic Press: Orlando, Florida.

[2]Prasad, P.N., and Williams, D.J. 1991. *Introduction to Nonlinear Optical Effects in Molecules and Polymers.* John Wiley and Sons, Inc.: New York.

[3]Paley, M.S.; Frazier, D.O.; Abdeldeyem, H.; and McManus, S.P. 1994. *Chemistry in Materials,* 6(12):2,213.

[4]Paley, M.S.; Frazier, D.O.; Abdeldeyem, H.; Armstrong, S.; and McManus, S.P. 1995. *Journal of the American Chemical Society,* 117(17):4,775.

[5]*Fluid Sciences and Materials Science in Space.* 1987. Waler, H.U., ed. Springer-Verlag: New York.

[6]*Side-Chain Liquid Crystal Polymers.* 1989. McArdle, C.B., ed. Chapman and Hall: New York.

Sponsor: Center Director's Discretionary Fund; Office of Space Applications and Technology

Industry Involvement: Westinghouse Corporation, Optron Systems

University Involvement: University of Alabama in Huntsville, Huntsville, Alabama; Alabama A&M University, Huntsville, Alabama; University of New Mexico, Highlands, Las Vegas, New Mexico; University of Puerto Rico at Mayaguez, Mayaguez, Puerto Rico; Spelman College, Atlanta, Georgia; Fisk University, Nashville, Tennessee; University of Michigan, Ann Arbor, Michigan

Prediction of Nonlinear Optical Properties of Organic Materials

Craig E. Moore/ES75
205–544–7585

To allow screening of potential nonlinear optical organic compounds, researchers have developed a procedure to predict second- and third-order polarizabilities of organic materials that, within families of compounds, is accurate within 25 percent of the experimental values. This will facilitate nonlinear optical research by limited synthesis of new compounds to those most likely to exhibit appropriate properties. The procedure is as follows:

(a) Using a semi-empirical Hamiltonian (AM1), the polarization of the molecule is calculated in the presence of 252 static fields. AM1 has been chosen because it has a more realistic treatment of the nitro groups in aromatic molecules than other semi-empirical Hamiltonians, such as MNDO. The MOPAC program has been modified to perform these calculations.

(b) The polarization versus static-field information is processed by the HYPER program, developed in-house to generate all required tensor elements using polynomial fits. The polynomial fits are performed from orders 4 to 18, and the numerical uncertainty of the values obtained is used as a measure of the error of the prediction. The advantages of the HYPER program over the procedure implemented in MOPAC

are twofold: it estimates the effect of numerical instabilities in the data and calculates terms related through Kleinman symmetry independently, so that adherence to this property may be evaluated.

(c) Two major modifications in the method of calculating hyperpolarizabilities were recently incorporated in the MOPAC program. First, the placement of electric "sparkles" to generate the static fields used by MOPAC has been increased in strength and placed 100 times farther from the molecule. Although the molecules experience the same field strength, the field is more homogeneous, allowing for greater numerical stability in the calculations. It also allows one to conduct calculations on much larger molecules such as C84 and other fullerenes. Secondly, calculations involving more fields have given results where Kleinman symmetry is obeyed for even the smallest elements. While this has little effect in the estimations of molecular beta or gamma, it proves the self-consistency and reliability of the method.

(d) For third-order polarizabilities, a term approximating core effects is added, based on the number and type of atoms present. These core corrections were obtained from empirical fits using published experimental values.

(e) In order to allow comparison of predictions with experimental values, adjustments are made to dynamic fields. In the case of second-order polarizabilities, a "correction equation" has been developed based on p-nitroanaline published measurements. In the case of third-order polarizabilities, the correction used is based on the two-level approximation (ground and one excited state).

(f) Finally, the values are adjusted to account for intermolecular effects—solvent effects, in particular. For second-order polarizabilities, scientists obtained two empirical corrections as a function of the refractive index and the dielectric constant of the solvent based on p-nitroaniline data. For third-order polarizabilities, researchers have used empirical data on benzene.

Although the procedure, as it is, has been proven useful for materials scientists, from a scientific point of view, parts (d) and (e) (i.e., accounting for dispersion and intermolecular effects) need further work. Researchers are currently working on developing a correction for dynamic fields based on the two-level approximation.

Sponsor: Office of Life and Microgravity Sciences and Applications

Earth System Science

Numerical Modeling of Nonlinear Baroclinic Fluid Systems

Timothy L. Miller/ES42
205–922-5882

In developing a comprehension of the processes that affect global change on Earth, a component that presents one of the greatest challenges is that of the fluid system composed of the atmosphere and oceans. Clearly, a broader understanding of this system is an important one, since the atmosphere is the fluid system in which we live—the system that supplies the land with fresh water and shields life from harmful solar radiation. The oceans interact with the atmosphere through exchanges of heat, water, and momentum and provide a very large "thermal mass" for the system. Due to the complex nature of this system and the difficulty in obtaining sufficient observational data on it, accurately predicting its behavior for all but very short time periods remains an elusive goal. The aim of this research is to develop a better understanding of the Earth system through the use of various computer models to allow the study of the atmosphere, as well as the complicated behavior of a rather simple fluid system driven by horizontal temperature gradients and influenced by rotation.

One means of investigating the behavior of the Earth's atmosphere and oceans is to conduct laboratory experiments in cylindrical and spherical containers where a fluid such as water is differentially heated and rotated. Depending upon the strength of the differential heating and the rate of rotation, the flow may be very simple—steady in time and axisymmetric in structure. For other values of the heating and rotation, the flow may be made of steady, regular waves, or it may be quite irregular and chaotic. Such experiments have been conducted in laboratories, both at MSFC and elsewhere, resulting in a numerical model developed at MSFC that tests our ability to predict flow types and to assist in comprehending such processes as heat and momentum transport. Additionally, studies are being performed to help design space-flight experiments using the geophysical fluid-flow cell apparatus.

The Geophysical Fluid-Flow Simulator enables scientists to experiment with both spherical or cylindrical flows. Flow analysis proceeds in several steps: calculation of the axisymmetric flow (that which would be seen if no variations in longitude are allowed); calculation of the linear stability of that flow to three-dimensional wave perturbations; calculation of the wave amplitude where interaction between the wave and the longitudinal mean flow is allowed; and the calculation of the fully nonlinear flow with full interaction between all components of the flow. The extent to which each of these steps can be directly applied to the actual flows depends upon the nonlinearity of the flow, which, in turn, depends upon the experimental parameters. For highly nonlinear flows, a time series of images of the predicted flow are produced; the images are shown in computer animations to illustrate the interactions between various types of structures in the flow.

Recent work has placed emphasis on vacillatory flow in the baroclinic annulus experiments. The flow occurring in the gap between two concentric, co-rotating cylinders that are differentially heated is computed with high resolution and for (typically) several tens of rotational periods. For certain combinations of rotation rates and temperature differences, the resulting flow is three-dimensional and undergoes a periodic oscillation in the amplitude of the "wave" part of the structure. Agreement between the computer simulations and previous laboratory experiments is very good. The computer calculations allow the investigation of more cases than has been done experimentally. This work has resulted in the demonstration that a numerical model can be used to identify deterministically predictable regions in parameter space, as opposed to regions in which the result is highly sensitive to numerical and physical parameters. An investigation into the mechanics of the various flow regimes is continuing.

Lu, H.-I.; Miller, T.L.; and Butler, K.A. 1994. A Numerical Study of Wave-Number Selection in the Baroclinic Annulus Flow System. *Geophysical and Astrophysical Fluid Dynamics*, 75:1–19.

Sponsor: Office of Mission to Planet Earth

Global Modeling of Surface Boundary Forcing

Daniel E. Fitzjarrald/ES42
205–544–1151

Franklin R. Robertson/ES42
205–922–5836

From a climate dynamics perspective, water-related processes are the key links between ocean, atmosphere, and land biosphere components. Thus, in order to develop a predictive capability for anticipating variability or change in climate, either locally or in a global sense, an improved physical basis for linking the hydrologic and energy cycles in climate models has high priority. MSFC is continuing its joint investigation with Pennsylvania State University and the National Center for Atmospheric Research in using the GENESIS Earth System model to study short-term climate variability. The team has approached this problem on two fronts: (1) using existing data sets emerging from the Pathfinder effort to critique and validate the hydrologic cycle of GENESIS model versions, and (2) performing sensitivity experiments to have a better understanding of the linkages between ocean, atmosphere, and land biosphere subsystems, particularly with respect to replicating recent short-term climate anomalies, such as El Niño/Southern Oscillation events.

The effort's experimental strategy has initially involved a series of 10-year model integrations based on the Department of Energy's Atmospheric Model Intercomparison Project format. This involves specifying observed sea-surface temperature values as lower boundary forcing and performing an additional control integration forced with seasonally varying sea-surface temperatures. Initial experiments were done at R12 (5.0 by 7.0 degrees) horizontal spatial resolution; the more recent model version, GENESIS 2.0, uses T31 (3.75 by 3.75 degrees). Results to date have clarified the nature of the predictability problem for interannual climate variations: (1) tropical sea-surface temperature forcing has a robust quasilinear response in the vicinity of the heating (rainfall, divergent circulations, and radiative anomalies associated with the 1982 to 1983 and 1986 to 1987 El Niño/Southern Oscillation events are captured reasonably well); (2) far-field, middle-latitude response is characterized by a much lower signal-to-noise ratio, due in large measure to the natural variability inherent in higher latitude baroclinic flow; and (3) warm-season, middle-latitude anomalies, such as the 1988 drought over the United States in early summer, show signs of significant predictability.

Our most important and recent result from GENESIS 2.0 comparing 1985 to 1989 gives evidence of positive water-vapor feedback averaged over the tropical oceans (30 °N to 30 °S) in association with elevated sea-surface temperatures.
Figure 13 shows two curves depicting the outgoing longwave radiation at the top of the Earth's atmosphere for this region. The solid curve is the value measured by the Earth Radiation Budget Satellite and includes a mixture of radiative effects from moisture and temperature anomalies. We have few good direct measurements of water vapor, but we can calculate the effects of sea-surface atmospheric temperature variations on the radiation quite well (dotted line). The difference in these two curves is the effect that changes in water vapor have on the longwave radiation leaving the planet. Analysis has shown that for an increase in 1 Kelvin in sea-surface temperature, the water-vapor trapping of terrestrial radiation increases by about 2 watts per square meter. A similar result has been found for the GENESIS model. This kind of study is helping us understand the role that deep tropical convection might play in future climate change through its effect on the atmospheric water-vapor field.

Recent availability of the International Satellite Land Surface Climatology Project data set, observed precipitation, and satellite estimates of surface-incident solar radiation (plus other data) now permit the global diagnosis of a soil-moisture time series with reasonably accurate observational constraints. Scientists have begun an integration in which the observed precipitation and incident solar radiation are used in lieu of the corresponding GENESIS fields to force the model land-surface package, thus synthesizing an "observed" soil-moisture field analogous to the observed sea-surface temperatures.

For the longer term, the research team plans to test a coupled modeling system involving GENESIS and nested regional models having land surface and hydrologic components. This coupled, nested system will be evaluated for its ability to translate anomalous sea-surface temperatures

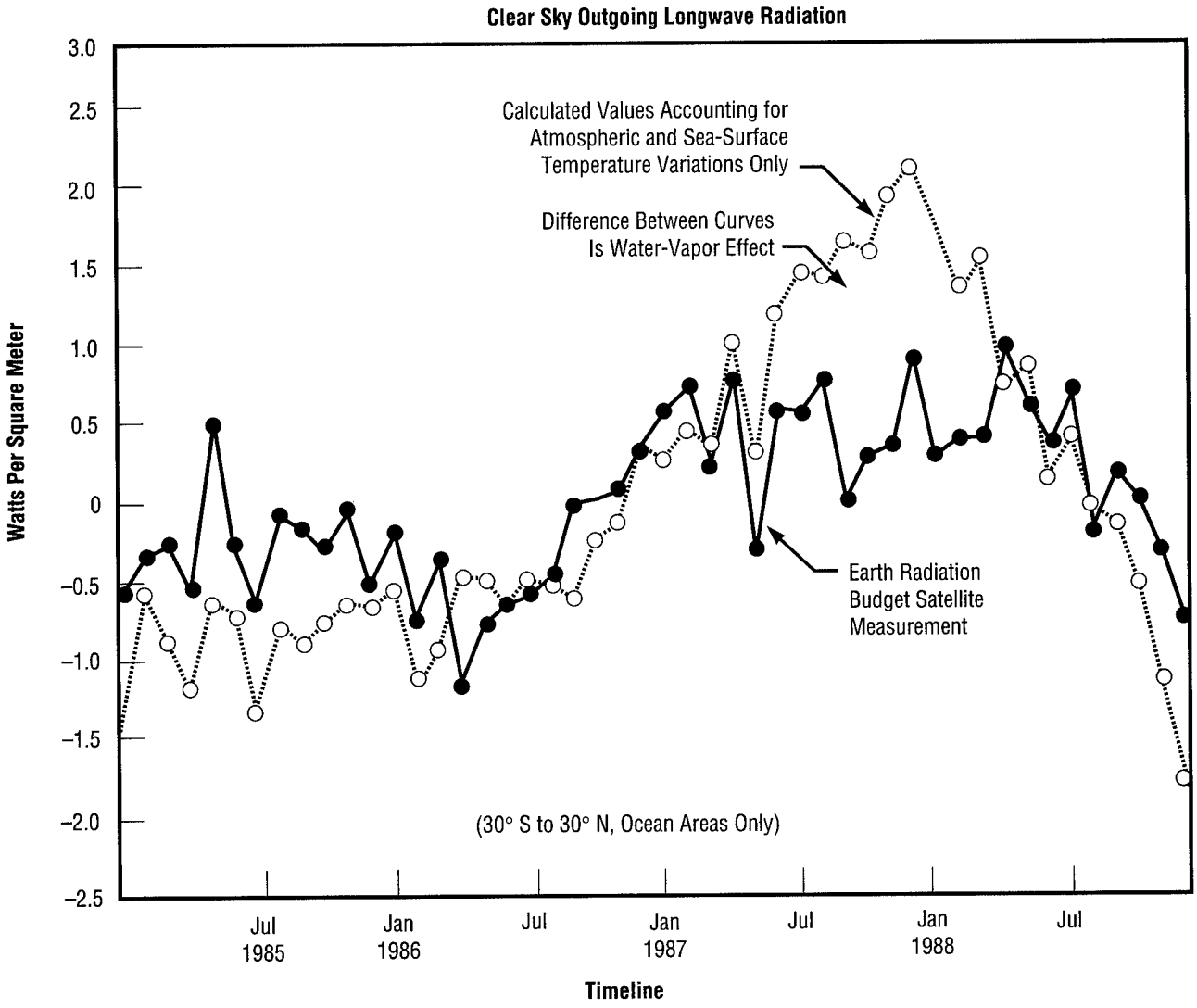

FIGURE 13.—Earth radiation satellite diagnostics of positive water-vapor feedback.

and land-surface forcing into regional and local hydrologic changes. Collectively, these findings will illustrate the mechanisms by which hydrology, radiation, and dynamics are involved in climate variability.

Sponsor: Office of Mission to Planet Earth

University Involvement:
Pennsylvania State University

Other Involvement: National Center for Atmospheric Research

Global Multiphase Water Analysis

Franklin R. Robertson/ES42
205–922-5836

The atmospheric hydrologic cycle is fundamental to the character of Earth's climate. While the distribution and variability of rainfall obviously affect human activities, even the distribution of clouds and water vapor are intimately connected to climate and its associated human impacts. Unfortunately, accurate water budgets are currently lacking because of the considerable uncertainties associated with cloud climatologies, water-vapor measurements, and vertical motion fields. Current four-dimensional data analysis models have yet to incorporate sufficiently accurate representations of moist physics required to adequately couple radiation, dynamics, and cloud production. Researchers have been developing an integrated analysis of vapor, cloudiness, and precipitation (2.5-degree spatial resolution, ±70.00 degrees latitude, daily and longer time scales) over various time periods that coincide with major field-study campaigns (Tropical Ocean Global Atmosphere-Coupled Ocean Atmosphere Response Experiment) and algorithm test-bed development (1987–88 NASA/National Oceanic and Atmospheric Administration Pathfinder Period).

A unique aspect of this study is a semiprognostic approach whereby parameterized bulk microphysics and convective processes are used along with the observational constraints to drive conservation equations for water vapor, cloud liquid and ice, and precipitation. Only moisture fields are prognosed, with the temperature, horizontal wind, and vertical motion being taken from the European Center for Medium-range Weather Forecasting's gridded analyses. Employed are wind and temperature fields from global gridded analyses and water vapor from the Special Sensor Microwave/Imager to constrain vapor and condensate budgets. Researchers analyze the resulting three-dimensional fields of moisture variables and examine the ice budgets for consistency with observations of cloudiness. This methodology has led to an analysis of atmospheric water substance that is consistent with satellite observations—the best estimates of water transport by wind—and simple but physically based representations of cloud microphysical processes.

During the past year, researchers have been able to evaluate the quality of the synthesized fields by comparing them to several independent satellite data sets: (1) synthetic 6.7-micron channel imagery constructed from analyzed thermodynamic fields versus HIRS CH12 and Geostationary Operational Environmental Satellite 6.7 channel data, (2) cold cloud top-frequency statistics of synthesized clouds versus those detected by HIRS, and (3) the horizontal structure of diagnosed precipitating ice against that derived from the Special Sensor Microwave/Imager and MSU. The role of kinematic transport on large-scale cloud distributions associated with baroclinic events in middle latitudes versus convective outflows has been examined.

This project's analysis technique is expected to contribute significantly to understanding the processes that maintain the observed atmospheric distribution of clouds, water vapor, and precipitation. It is also serving as a test-bed for physics process subroutines models that will be incorporated into improved global climate models.

Sponsor: Office of Mission to Planet Earth

Astrophysics

The Third Burst and Transient Source Experiment Catalog of Gamma-Ray Bursts

Charles A. Meegan/ES84
205–544–7694

The Burst and Transient Source Experiment, developed and managed at MSFC, is one of four gamma-ray instruments in the Compton Gamma-Ray Observatory, which was launched in April 1991. The primary objective of the experiment is to gather information on gamma-ray bursts—brief, intense flashes of gamma radiation—from unknown celestial sources. The experiment instrument remains the most sensitive tool ever deployed for studying these events.

Early program results[1] showed that the bursts observed were uniformly distributed in angular position on the sky, but that there were far fewer faint bursts than would be expected if the sources were uniformly distributed in space. No known celestial objects in our galaxy have such a spatial distribution, leading most researchers to the conclusion that the burst sources must be in distant galaxies. (See the following article for implications of this hypothesis.) If this turns out to be the case, then gamma-ray bursts must be the most luminous events in the Universe. Others believe that an extended halo of sources around our own galaxy can fit the data, with much lower energy requirements. The nature of gamma-ray bursts is currently hotly debated, but poorly understood.

The experiment team has recently completed a catalog of 1,123 gamma-ray bursts observed up to September 19, 1994. The catalog (referred to as the "3B" catalog) is the largest catalog of its kind, improves upon two previous releases of experimental data, and is now publicly available from the Compton Observatory Science Support Center at Goddard Space Flight Center. The World-Wide Web address is http://cossc.gsfc.nasa.gov/cossc/cossc.html. These data will be studied by astrophysicists around the world for clues to the origin of gamma-ray bursts.

A major effort in generating the 3B catalog has been directed toward improving the accuracy of the angular positions. Previously, the systematic errors in locations were about 4 degrees. Improvements in the location algorithm have now reduced this error to about 1.6 degrees. All of the previously cataloged bursts have had their locations recomputed for the 3B catalog. The accuracy of the locations is important in exploring the possibility that more than one burst may be coming from a single source. The existence of such repetitions is currently a controversial issue.

The distribution on the sky of the 1,123 bursts of the 3B catalog is shown in figure 14. The sky is shown in galactic coordinates, with the galactic plane along the equator and the galactic center in the center of the plot. Galactic objects generally show a concentration toward the equator or center. Within the statistical uncertainty, the gamma-ray bursts are distributed isotropically.

The distribution in peak intensity is shown in figure 15. The peak intensity is the peak photon flux in a 1,024-millisecond interval as measured at the detector. In general, the peak intensity distribution is a convolution of the

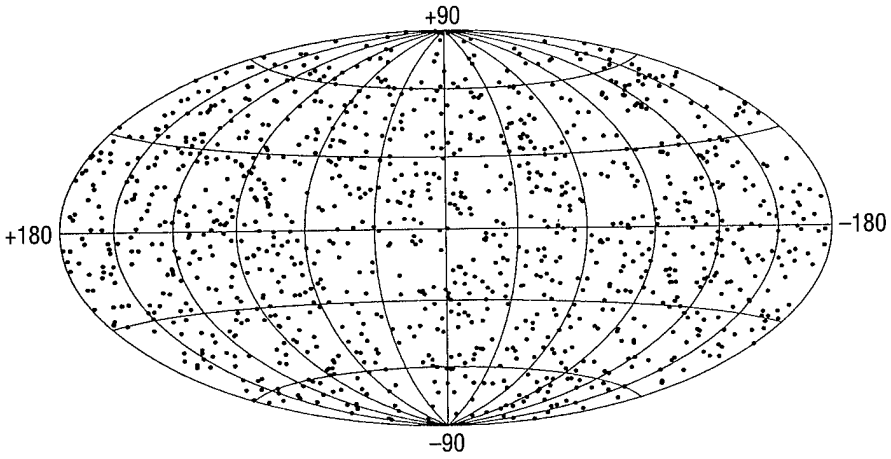

FIGURE 14.—The locations, in galactic coordinates, of 1,123 gamma-ray bursts in the 3B catalog. The bursts are isotropic to within the statistical uncertainty.

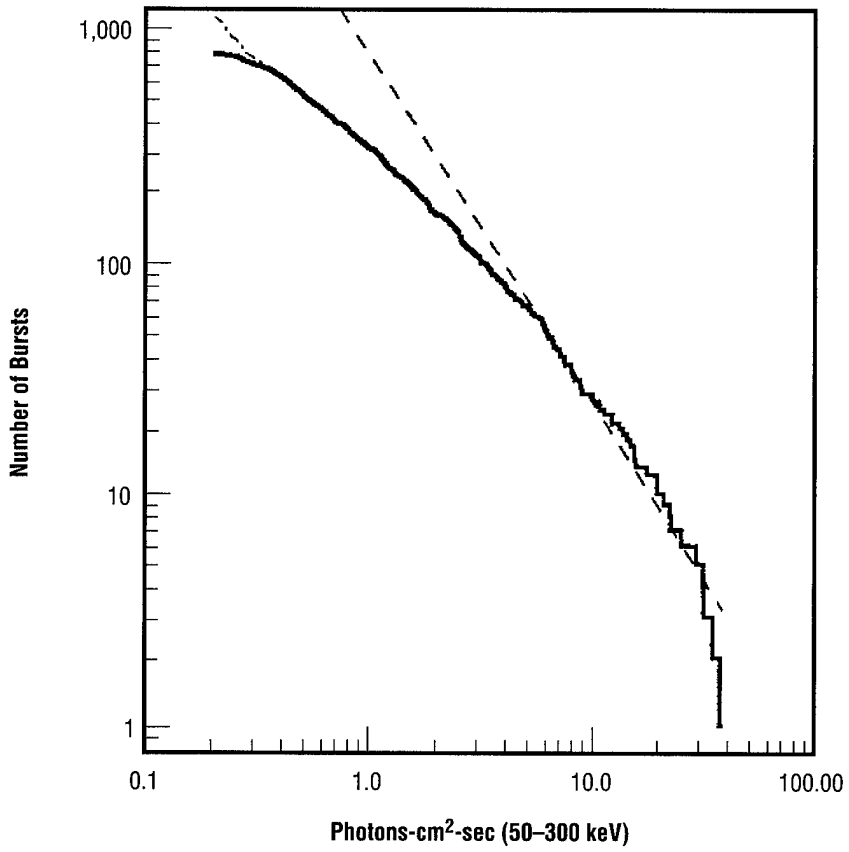

FIGURE 15.—The intensity distribution of gamma-ray bursts. The dashed line is the –3/2 power law expected for a spatially uniform distribution of sources.

intrinsic luminosity distribution with the distribution in distance. However, if the sources are uniformly distributed in space, then the brightness distribution will follow a –3/2 power law for any luminosity distribution. The data clearly show a deviation from the –3/2 power law (the dashed line in fig. 15). A number of studies have shown that the shape of this distribution is consistent with the sources being at cosmological distances where red-shift effects cause the deviation from the –3/2 curve.

The location and brightness distributions provide the most direct evidence on the spatial distribution of gamma-ray burst sources. The third Burst and Transient Source Experiment Catalog of gamma-ray bursts will be crucial in finally understanding these enigmatic events.

[1]Meegan et al., 1992. *Nature*, 355:143–5.

Sponsor: Office of Space Science

Gamma-Ray Bursts as a Tool for Cosmology

John M. Horack/ES84
205–544–1872

Gamma-ray bursts are brief, intense, and complex flashes of gamma-ray energy that emanate from seemingly random point-like locations on the sky at unpredictable times. Until recently, the accepted theory of the origin of bursts involved the production of gamma-ray energy in or near the powerful magnetic fields of neutron stars. The launch of the Burst and Transient Source Experiment, with its ability to localize each detected burst to a restricted region of the sky, was expected to produce a map of the positions of these bursts, revealing the band of the Milky Way.

Contrary to expected results, however, the ensemble of positions for over 1,100 bursts detected to date is isotropic (fig. 14 of preceding article). The burst experiment has also shown that the radial distribution of bursts is inhomogeneous: beyond some unknown distance, the number density of burst sources decreases below the value observed locally in space. This behavior is signaled by the comparative deficit of faint bursts in the data, displayed graphically by the failure of the brightness distribution to continue along the indicated –3/2 line (indicative of homogeneity), instead falling far below the line at low brightnesses (fig. 15 of the preceding article). We appear to be at the center of a confined, spherical distribution of burst sources—a situation found in observing no other set of galactic objects.

Most scientists now believe that this combination of angular isotropy and spatial inhomogeneity is explained by a population of bursts not in our own galaxy, but at cosmological distances near the edge of the observable Universe. The isotropy of the bursts in this model is a natural consequence of the Universe looking the same in all directions on large scales. The deviation of the brightness distribution from the –3/2 line is caused by cosmological effects related to the known expansion of the Universe, specifically red-shifting of the burst spectrum and time-dilation of both the apparent rate of photon emission and the time between burst events. If the cosmological model is correct, the bursts' tremendous distances require them to be among the most energetic objects in the Universe, releasing in just 10 seconds perhaps as much energy as the Sun emits in its total lifetime.

Bursts at cosmological distances not only offer the possibility of serving as interesting physics laboratories in their own right, but may help us learn how the Universe is put together. The manner in which the brightness distribution deviates from the –3/2 line in the cosmological burst scenario is, in part, dependent on the values of two important cosmological numbers: σ_o, the "density parameter," which describes how much material is contained in the Universe, and q_o, the "deceleration parameter," which describes how fast the expansion rate of the Universe is changing with time.

The numerical values for these parameters are unknown, yet they have already determined the eventual fate of the Universe. Will the Universe continue to expand forever? Will the Universe eventually stop expanding, begin to contract, and eventually end with a "big crunch?" What is the geometry of the Universe, "open" or "closed?" Each of these questions could be answered precisely, provided one had a reliable, accurate measure of the values of σ_o and q_o.

In addition to the values of σ_o and q_o, the shape of the burst-brightness distribution also depends on how far out into the Universe researchers can detect bursts, the relative frequency and energy output of bursts in the early Universe compared to today, and the exact shape of the gamma-ray bursts' individual spectra. Each of these can be measured or estimated to varying degrees of uncertainty.

By comparing the shape of the observed brightness distribution to that of a model distribution that incorporates specific values of σ_o, q_o, and other parameters, researchers can assess the consistency between a given model of the Universe and the observed gamma-ray burst distribution. In this way, one can learn what possible constructions of the Universe may be valid and, equally important, what ones may be invalid. Further information can be obtained by combining results with independent measurements of other cosmological objects using such experiments as the Hubble Space Telescope.

Indeed, the use of gamma-ray bursts as a tool in cosmology is an illustration of the serendipitous nature of the scientific enterprise. The Burst and Transient Source Experiment was built to confirm the belief that bursts were mildly energetic releases of energy occurring in our own Milky Way Galaxy. Instead, the experiment has revealed the possibility that bursts are among the most distant and energetic objects in the cosmos. As such, they offer the possibility of serving as an excellent new tool to explore the structure, dynamics, and eventual fate of the Universe.

Sponsor: Office of Space Science

Measurements With a Superconducting Magnet Spectrometer

Thomas A. Parnell/ES84
205–544–7690

James H. Derrickson/ES84
205–544–7698

A recently constructed superconducting magnet spectrometer will measure the composition and spectra of cosmic rays over 3 orders of magnitude in energy from a few billion electron volts to approximately 1 tera-electron volt. This measurement will overlap the prior data below 100 billion electron volts and extend upward to the high-energy data measured by the Japanese/American Cooperative Emulsion Experiment. (This experiment is part of a continuing collaborative effort with Japanese and American universities.) Additionally, the magnet spectrometer will analyze secondary charged particles emerging from the cosmic-ray interactions with targets in the instrument in an energy regime where a nuclear phase change in matter is predicted to occur. With a magnetic field of 1.2 Tesla and a position resolution of less than 2 micrometers in the emulsion chamber, the primary spectra of heavy nuclei can be measured to approximately 1 tera-electron volt, and nuclear interactions can be studied up to approximately 10 tera-electron volts.

The magnet spectrometer target contains lead plates and passive detectors, consisting of thin sheets of CR39 track detectors, emulsion plates, and spacers designed to measure the momenta of the cosmic-ray primaries to approximately 1 tera-electron volt. Also, a systematic study of the interaction characteristics of energetic cosmic-ray nuclei permits a re-examination of the "standard" nuclear interaction model, since occasional unexplained "exotic" events have been observed at high energies. Those events have an excess ("Chirons") or deficiency ("Centauros") of neutral particles compared to the charged particles produced in the interactions. With emulsion chambers in a balloon-borne superconducting magnet, more definitive measurements of the charged secondary particles produced in nuclear interactions will be made in order to test new theoretical interaction models and compare the data to the standard models currently in use.

The subject experiments are expected to bridge the existing low- and high-energy spectral data for the cosmic-ray elements carbon through iron, and allow data from several previous experiments to be cross-calibrated. This would extend the confirmed cosmic-ray energy spectra over many decades in energy, enabling a better comparison with predictions of supernova remnant acceleration models of cosmic rays.

The balloon flight instrument contains two 50- (width) by 50- (length) by 40-centimeter (height) emulsion chambers that include two special target sections (fig. 16). One target section is a stack of magnet-interaction chambers that consist of lead and emulsion plates, as well as CR39 track detectors separated by low-density spacers. The other target section contains a "beam tracker" of CR39 plates with spacers on top of a single magnet-interaction target module. Both stacks have an "ionization calorimeter" on the bottom that provides data on high-energy, primary cosmic rays above 500 billion electron volts by measuring the electromagnetic cascade energy of each event. The beam tracker determines the charges and momenta of the primary cosmic-ray nuclei by the CR39 etch-pit method and track curvature, respectively. The magnet-interaction section detects interactions in lead targets and enables measurements with emulsion plates of production angles and momenta of most of the secondary charged particles. The ionization calorimeter has x-ray films and emulsion plates with 8 radiation lengths of lead to generate electromagnetic (gamma-ray/electron) showers, which will provide individual cascade/shower energy measurements.

The balloon-borne magnet spectrometer experiment is shown schematically in figure 16. The solenoid magnet has an open bore of 85 (depth) by 180 centimeters (length). The magnet structure has a low mass thickness, reducing the cosmic-ray event loss due to nuclear fragmentation. It operates at a maximum field strength of 1.2 Tesla in the persistent current mode with 520 amperes. The emulsion chamber boxes are supported by a shaft arrangement that penetrates the magnet's open bore (fig. 17) and is fastened to horizontal support bars on the gondola (shown in figs. 16 and 17). The magnet alone weighs 450 kilograms with a 10-day liquid-helium supply (250-liter cryostat).

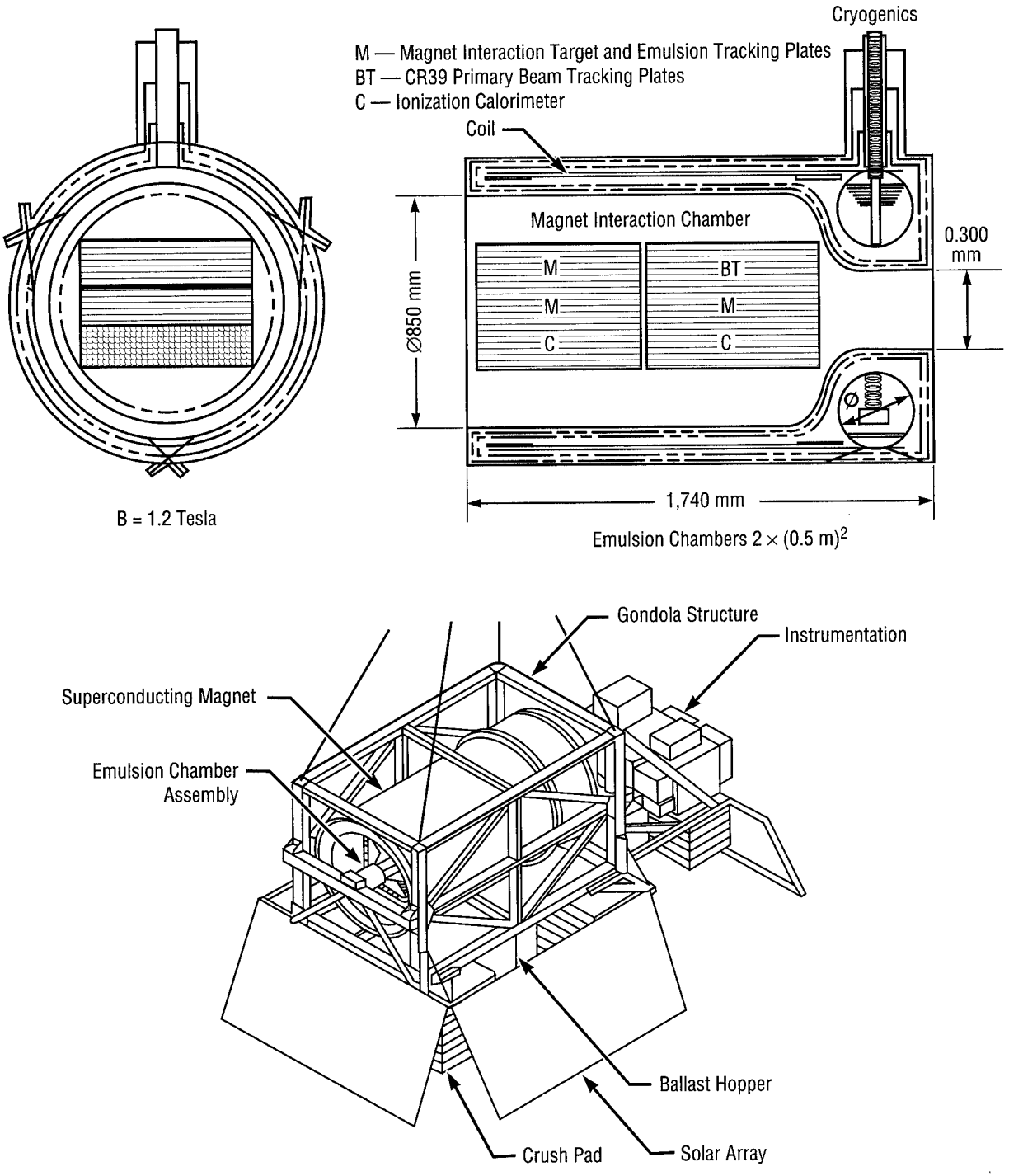

FIGURE 16.—The configuration of the gondola, superconducting magnet, and the emulsion chambers for a Japanese/American Cooperative Emulsion Experiment flight, the Super-JACEE. The weight of the scientific apparatus is 1,400 kilograms.

The magnet system with gondola, emulsion chambers, flight monitor and control system, and ground-support equipment has been assembled at MSFC. The first test-flight experiment on a high-altitude balloon was successfully conducted from Fort Sumner, New Mexico, on September 27, 1995, gathering data for a period of approximately 20 hours. At least one long-duration balloon flight (of approximately 10 days) is planned, followed by 3 years of data analysis.

Parnell, T.A. 1989. American Institute of Physics Conference Proceedings. American Institute of Physics. New York, 203:56–75.

Asakimori, K., et al. 1991. Proceedings of the Twenty-Second International Cosmic-Ray Conference. Dublin, 2:567–70.

Mito, T., et al. 1989. Institute of Electrical and Electronics Engineer Magnetics, 25:2, 1,663.

Yamamoto, A., et al. 1989. Institute of Electrical and Electronics Engineer Magnetics, 24:2, 11,421

University Involvement: University of Alabama in Huntsville, Louisiana State University, University of Washington (Seattle), Institute of Nuclear Physics (Krakow), Institute for Cosmic-Ray Research, University of Tokyo, Hiroshima University, Kobe University, Kobe Women's Junior College, Kochi University, National Laboratory for High-Energy Physics (KEK), Okayama University of Science, Tezukayama University, Waseda University

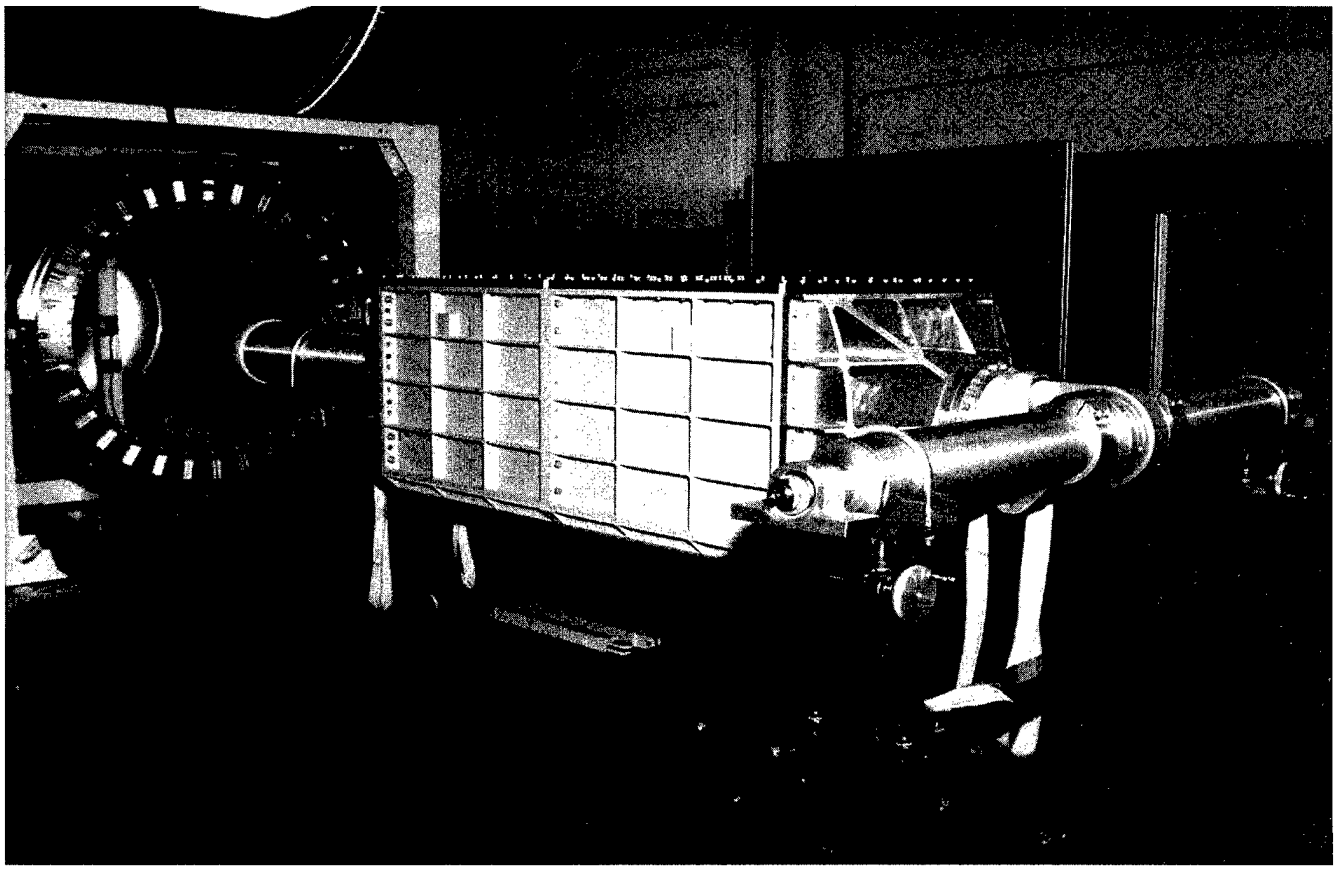

FIGURE 17.—Emulsion chamber assembly ready for insertion into the open bore of the superconducting magnet.

Solar Physics

Newly Discovered Flows on the Sun's Surface

David H. Hathaway/ES82
205–544–7610

An image-processing technique applied to solar Doppler velocity data from the Global Oscillations Network Group prototype instrument has enabled scientists to measure, with far better accuracy, the flow patterns on the surface of the Sun. These flows include a well-known east-west flow (differential rotation), a north-south meridional flow, and a cellular convective pattern in which the solar gases rise up from the interior, spread out across the surface, and sink inward around the edges of the cells. The meridional flow and the largest of the cellular flows have been particularly difficult to measure in the past. Both of these flows are now measured with enough accuracy to reveal unexpected details in their motions.

Solar astronomers have recognized that the Sun's magnetic field often exhibits a large cellular pattern with sunspots forming where the magnetic field becomes concentrated. The existence of a "giant-cell" convection pattern was suggested more than 30 years ago to explain these observations. However, all efforts to measure such flows have been unsuccessful or inconclusive. If such flows exist, it might be easier to predict the formation and evolution of sunspots and any associated activity such as flares or coronal mass ejections. The importance of predicting solar activity for planning space missions, for communications, and even for managing electrical power distribution grids, makes the search for giant cells an important ongoing effort within the solar physics community.

At least two instruments for measuring flow patterns on the Sun have recently been developed. (1) The Global Oscillations Network Group project has established a ground-based network of telescopes. This project deployed its instruments at six sites around the world in 1995. It has operated a prototype instrument in Tucson, Arizona, since mid-1992. The instrument has good spatial resolution but is hampered by the Earth's atmosphere. (2) The Solar Oscillations Investigation-Michelson Doppler Imager team has developed a space-based telescope for the Solar and Heliospheric Observatory mission, which was launched by an Atlas 2AS in December of 1995. The spacecraft will orbit a point in space a million miles from the Earth in the Sun's direction where the Earth's and the Sun's gravitational pull are equal. Both of these instruments work on the same principal, but the Solar Oscillations Investigation instrument will have much better spatial resolution and will not be influenced by the Earth's atmosphere.

Data from the Global Oscillations Network Group prototype instrument was analyzed using an image-processing technique developed by the author. This technique extracts each component of the flow and accounts for the complete velocity signal. The results of the analysis indicate the presence of a weak meridional flow that fluctuates from about 20 meters per second (40 miles per hour) to more than 50 meters per second (100 miles per hour) over the course of several months. The results also indicate the presence of a large cellular pattern like that expected for the giant cells.

Prior to this work, a meridional flow was known to carry magnetic field elements from the equatorial regions toward the poles. The precise structure of this flow and any variations with time were difficult to measure because of its relative weakness (the differential rotation produces east-west flows of about 200 meters per second or 400 miles per hour, and the small cellular pattern called "supergranulation" has flow speeds of about 500 meters per second or 1,000 miles per hour). The analysis of the Global Oscillations Network Group prototype data reveals both spatial structure and variations in time, as shown in figure 18. In late 1992, the meridional flow was poleward and less than about 30 meters per second. It increased to more than 50 meters per second in 1993 and then dropped to 20 meters per second in 1994 and 1995. Computer models for the transport of magnetic field elements across the solar surface had previously indicated that such changes might occur, and now these observations confirm that the Sun's meridional flow does change over fairly short time intervals.

The giant-cell convection pattern is also difficult to measure because of its relative weakness. The pattern is extracted by determining the full spectrum of the cellular convective motions and then extracting only the largest of these components. The resulting flow pattern for June 24, 1995, has all of the characteristics expected of giant-cell convection. Analysis of additional data in the days preceding and following

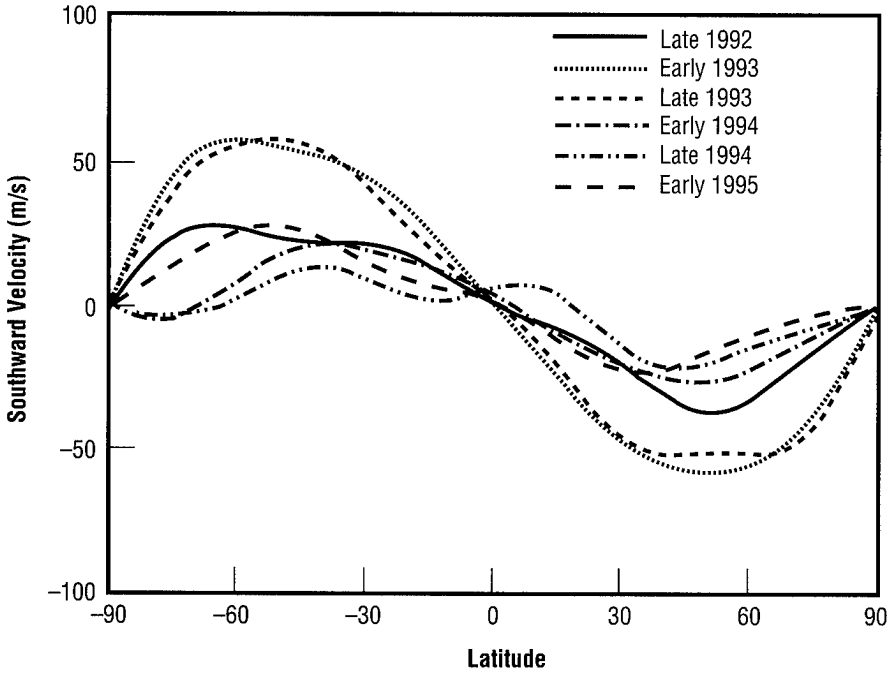

FIGURE 18.—The Sun's meridional flow velocity at 6-month intervals.

this shows that the flow pattern persists from day to day and rotates at about the same rate as the magnetic field pattern. These flows are also fairly weak, less than about 20 meters per second or 40 miles per hour, but they persist for days and probably even weeks or longer. The long lifetimes of these flows are important in organizing the large-scale magnetic field patterns.

Future work with data from both the Global Oscillations Network Group and Solar Oscillations Investigation instruments should produce additional information about these flows and about how they influence the Sun's magnetic field. These flows may also contain important information about the dynamics of the Sun's convection zone and the source of the 11-year sunspot cycle. With greater understanding of these flows, researchers may someday be able to predict the emergence of sunspots and the occurrence of solar activity that influences the near-Earth environment.

Hathaway, D.H. 1992. Spherical Harmonic Analysis of Steady Photospheric Flows II. *Solar Physics*, 137:15–32.

Hathaway, D.H. 1996. Doppler Measurements of the Sun's Meridional Flow. *Astrophysical Journal*, in press.

Sponsor: Office of Space Science

Heating Magnetic Structures in the Solar Corona

Jason G. Porter/ES82
205–544–7607

One of the main problems of solar physics is describing the processes that heat the Sun's extended outer atmosphere, the solar corona. During the past year, a group of solar astrophysicists from MSFC and the University of Tokyo have been using data from the MSFC vector magnetograph, together with data from the soft x-ray telescope on the Japanese Yohkoh satellite, to determine the causes of some of the variations in the heating rate between different magnetic structures in the corona. These structures take the form of loops arching up into the corona, following the magnetic lines of force between areas of opposite polarity in the photosphere (the "footpoints" of the loops). The team has found an apparent example of the energy transfer from active low-lying loops into higher, more-extended loops. These observations suggest that the coronal heating energy from the compact low-loop site is injected into the neighboring loops as waves that dissipate in the body of the high loops, rather than in the form of coronal plasma or energetic particles.

In figure 19, a Yohkoh soft x-ray telescope image is superposed on black and white contours, enclosing areas of positive and negative flux in the MSFC magnetogram. The main features in the x-ray image are: (area 1) a bright region along the northern portion of the main neutral line between positive and negative

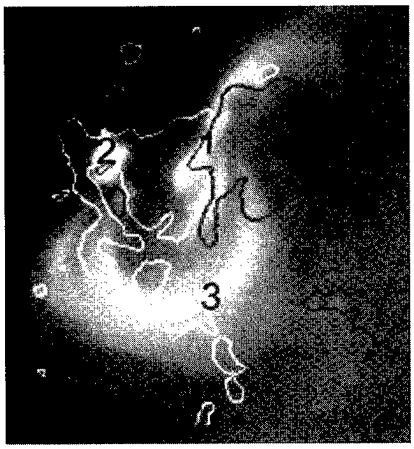

FIGURE 19.—Soft x-ray image superposed on contours of magnetic field strength.

areas; (area 2) a compact bright region spanning a secondary neutral line north of an island of included positive polarity within the main negative polarity region; and (area 3) several high, bright loops having one end rooted in the main patch of positive polarity, with the other lying in negative polarity near the included positive island. This image is the earliest obtained of the x-ray brightening in area 2, associated with the beginning of an Hα subflare. However, the high loops in area 3 showed enhanced emission for more than an hour prior to the start of the subflare, and continued to do so for more than an hour after it ended, with no evidence of the enhancement evolving to higher loops during this time. This argues against heating of the high loops by a flare-like internal release of energy triggered by the subflare near their footpoints.

Figure 20 shows more detail from the magnetogram of the region.

Comparison with figure 19 shows that the west end of the enhanced loops lies in a broad region of moderately high positive field strength, on the order of 500 Gauss, lying between the two main positive flux concentrations. The east end is rooted in negative flux near the island of positive flux. One might ask why should these particular loops, out of all the magnetic loops filling space in and about the active region, show enhanced x-ray emission? A plausible answer is that some special activity near their feet drives enhanced coronal heating in only these loops. The obvious candidate for the seat of this localized anomalous activity is the east-end island of reversed polarity.

A sequence of x-ray images (taken after the one shown in fig. 19) shows smaller brightenings in area 2 (microflares). The high loops of area 3 also fluctuate in brightness throughout this time. Throughout the sequence, there is a clear emission gap separating the subflaring/microflaring low loops rooted in the included polarity island and the associated high loops rooted nearby. This gap shows there is no direct transfer or generation of energetic particles and hot coronal plasma at an interface between the low loops and the feet of the high loops (the mechanism suggested for most reported observations of energy transfer between structures during flares). Instead, the microflares may generate waves that propagate into and dissipate along the nearby high loops. The fact that these microflares have little signature themselves in soft x-ray telescope observations can be accounted for by another recent analysis showing that the emission from small microflares is cooler than that from large microflares and subflares,[1] i.e., the heating leading to the continuously enhanced emission from the high loops may be maintained via a series of small events whose energy first goes preferentially into motion, generating waves, rather than directly heating plasma to coronal temperatures.

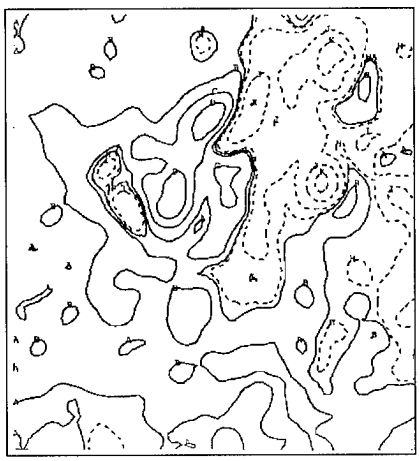

FIGURE 20.—Detailed magnetogram.

[1]Porter, J.G.; Fontenla, J.M.; and Simnett, G.M. 1995. *Astrophysical Journal*, 438, 472.

Sponsor: Office of Space Science

Solar Magnetic Fields

Mona J. Hagyard/ES82
205–544–7612

The interaction of magnetic fields and plasmas is the root cause of the dynamic, high-energy phenomena of flares, mass ejections, and eruptive filaments observed on the Sun. Thus, in current solar research, extensive observational studies are carried out to develop an understanding of just how the solar magnetic field plays this key role in solar activity. MSFC has a unique instrument for observing the Sun's magnetic field, the MSFC solar vector magnetograph; information derived from observations with it has made significant contributions to an understanding of solar activity. In particular, this instrument permits observations of the transverse component of magnetic fields from which calculations of important solar parameters such as electric currents and magnetic shear can be made; these parameters cannot be obtained from conventional solar magnetographs. Research at MSFC has shown significant correlations of these parameters with the occurrence of major solar flares. Therefore, the MSFC research shows promise in developing techniques to predict major flares. Such predictions will be necessary as the Agency enters the era of the space station, lunar bases, and planetary exploration when people in space will be susceptible to the harmful effects of energetic particles and radiation produced by solar flares.

Over the past year, MSFC's observational program has been reduced since the Sun's cycle of activity is near its minimum phase, during which there is little flare activity. Consequently, more emphasis has been given to analyses of archived data, development of unique data analysis methods and new theoretical models, and instrument development.

Data Analysis and Modeling

Recent accomplishments include new data analysis methods to calibrate vector magnetograph data more accurately, to resolve the ambiguity in the measured azimuth of the transverse field, and to describe more accurately the nonpotential state of magnetic fields. A new theory was developed to extrapolate potential fields for a finite field of view using all three components of the photospheric field. Research carried out recently includes a study of magnetic shear in C-class flares, an analysis of the morphology and evolution of the June 1991 active region that produced some of the most intense solar flares of cycle 22, a study of subflares and surges associated with parasitic polarities, a description of magnetic complexity in terms of fractal dimensions, an analysis of electric currents in active regions, and a study of correlations of magnetic shear with enhanced heating observed in Yohkoh soft x-ray images. Numerous collaborations with scientists from other institutions were also initiated and have resulted in journal publications.

The Experimental Vector Magnetograph

The Experimental Vector Magnetograph represents a state-of-the-art vector magnetograph that will permit measurements of the solar magnetic field with the highest accuracy that modern technology allows. During the past year, the image stabilizer was installed and tested, and modifications of its control software were made to enhance its performance. Magnification optics were designed, fabricated, and installed, permitting tests of the passband variation of the Fabry-Perot spectral filter as a function of angle. Also, a new computer system was installed to handle the large arrays of data from the Experimental Vector Magnetograph, with software being developed to perform the data analysis with this computer.

Moore, R.; Porter, J.; Roumeliotis, G.; Tsuneta, S.; Shimizu, T.; Sturrock, P.; and Acton, L. 1994. Observations of Enhanced Coronal Heating in Sheared Magnetic Fields. *New Look at the Sun With Emphasis on Advanced Observations of Coronal Dynamics and Flares*. Enome, S., and Hirayama, T., eds. Nobeyama Radio Observatory Report, 360:89.

Gary, G.A., and Démoulin, P. Reduction, Analysis, and Properties of Electric Current Systems in Solar Active Regions. *Astrophysical Journal*, 445:92.

Hagyard, M.J., and Kineke, J.I. 1995. Improved Method for Calibrating Filter Vector Magnetographs. *Solar Physics*, 158:11.

Sponsor: NASA Office of Space Science

The Fine-Scale Structure of the Interplanetary Magnetic Field

Steven T. Suess/ES82
205–544–7611

The interplanetary magnetic field is the magnetic field carried away from the Sun by the solar wind. The Sun rotates as the solar wind carries magnetic flux away from the Sun, so that the footpoint of each magnetic field line is twisted around in the direction of solar rotation. The resulting spiral magnetic field, an Archimedian spiral, was predicted long ago by Parker.[1] Superimposed on the average interplanetary magnetic field spiral is a fluctuating component, which has been examined using Ulysses data.

To study the fluctuating component requires a timing mark—something in the interplanetary magnetic field that can be identified and followed from one location to another. The only such feature is the surface across which the direction of the field changes. This is a continuous surface dividing the magnetic north of the Sun's field from the magnetic south. Over the 11-year sunspot cycle, the Sun's magnetic dipole is sometimes tilted by up to 90 degrees away from the rotation axis, and the surface dividing these two magnetic hemispheres—known as the "heliospheric current sheet" because it contains a large-scale electrical current—is similarly tilted. This sheet can be used as a timing mark both to study and to depict the magnetic field's fluctuating component. The average heliospheric current-sheet location just follows the Archimedian spiral of the average interplanetary magnetic field.

Solar wind plasma data, collected by an instrument on Ulysses,[2] were analyzed to determine the character of the fluctuating velocity vector in the vicinity of the heliospheric current sheet. A simple model was then developed to compute how the fluctuating velocity would deform the sheet as the magnetic field is carried away from the Sun by the solar wind.

Results have shown how the interplanetary magnetic field is distorted by the solar wind: the fluctuating magnetic field predicted using a simple model was like that which was observed. This straightforward explanation has largely replaced more complex explanations involving fine structure in the solar corona and waves on the heliospheric current sheet. Figure 21 provides a calculation of the fluctuating sheet made using data from the Ulysses solar wind plasma instrument. The eddies in the solar

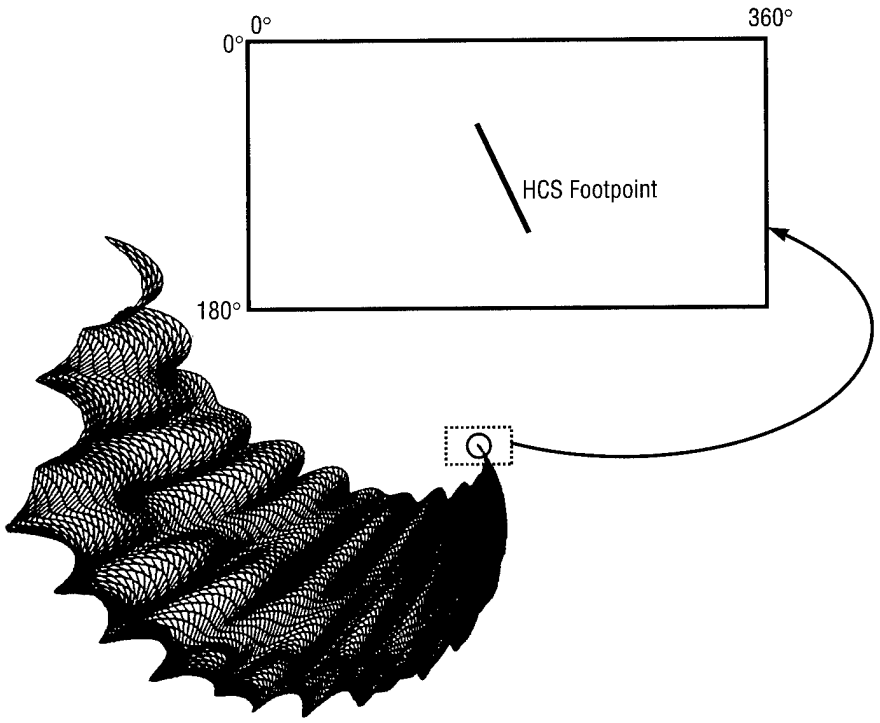

FIGURE 21.—A local section of the heliospheric current sheet centered on the equator, inclined at 70 degrees to the equator, extending over 10 degrees in longitude and 27.5 degrees in latitude. The section shown is between the Sun and 2.0 astronomical units. A projection of the footpoint of this section onto the Sun, in Carrington coordinates, is shown above. The topology of the sheet has been computed in this case for a fluctuating radial-velocity amplitude of ±25 kilometers per second and transverse amplitude one-seventh as large.

wind move the sheet around so that its smoothly inclined section (shown near the Sun as a straight line) becomes the highly "ruffled" surface at 2.0 astronomical units (twice the distance from the Sun as the Earth's orbit).

[1]Parker, E.N. 1963. *Interplanetary Dynamical Processes*. Wiley-Interscience: New York.

[2]Suess, S.T. 1995. Solar Wind Eddies and the Heliospheric Current Sheet. *Journal of Geophysics Resources*, 100, 12, 261–12, 273.

Sponsor: NASA Headquarters Program Office; Ulysses Project/ Missions Operations and Data Analysis, Space Plasma Physics Division

Three-Dimensional Magnetic Field-Line Topology in the Outer Heliosphere

Steven T. Suess/ES82
205–544–7611

Voyagers 1 and 2 (V1 and V2) are rapidly approaching the interface between the solar wind and the plasma in the local interstellar medium. The most accurate estimates today place this encounter as taking place starting almost immediately and lasting until around the year 2010.[1] After that time, the two spacecraft will be entirely in the local instellar medium. During the encounter, Voyagers 1 and 2 will be crossing a region of space known as the heliosheath—a region still within the heliosphere (its volume dominated by solar wind plasma).

The heliosheath solar wind has been slowed as it passes through the "termination shock" and has turned to begin flowing parallel to the wind in the local interstellar medium and down the heliotail. The interaction between the interstellar wind and the solar wind is illustrated in figure 22

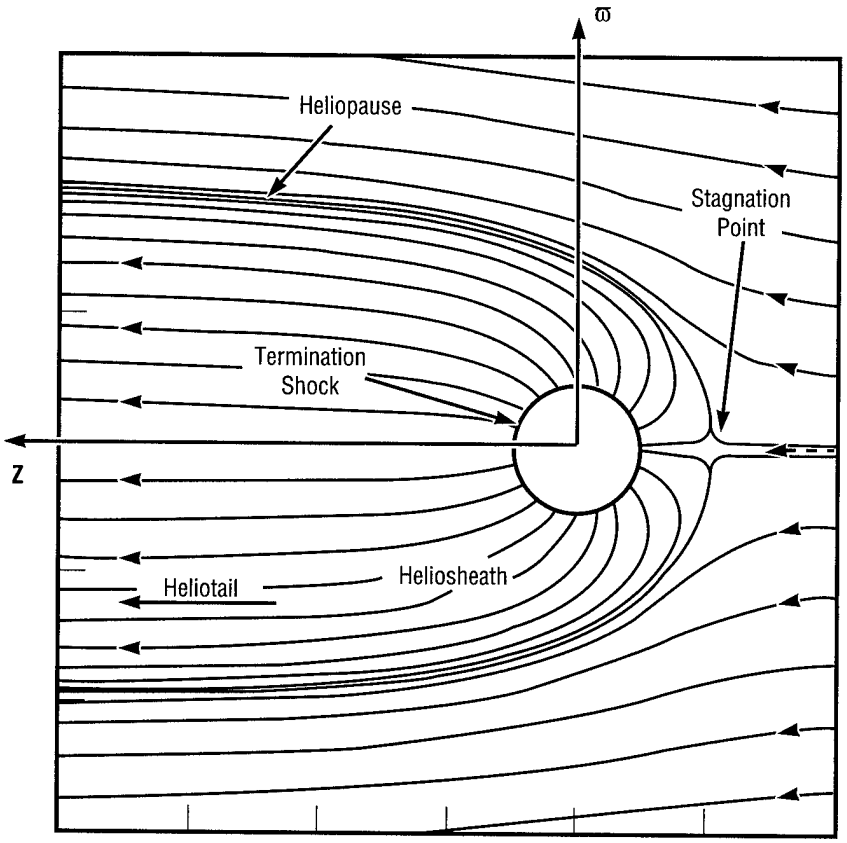

FIGURE 22.—Interaction between the local interstellar medium wind and the solar wind.

(labels indicate the various volumes just described); Voyagers 1 and 2 are traveling in the upstream direction, to the right. To characterize the scale in this figure, the radius of the termination shock is probably about 75 astronomical units (one unit is the average distance from the Sun to the Earth). All of the planets lie inside 50 astronomical units and inside the present locations of Voyagers 1 and 2.

While in the heliosheath, the Voyagers will perform several measurements. One of the most important of these is the determination of the topology of the magnetic field lines. Because the spacecraft will only measure the vector magnetic field direction and amplitude along the path of their orbits, the interpretation of the results will depend on having a model in hand for comparison. Over the past year, MSFC researchers have completed the first and only such model, successfully computing the topology of magnetic field lines in the heliosheath and the imprint of the solar magnetic cycle on this topology.[2] Figure 23 provides the topology of the magnetic field lines. (The sphere in the figure is the termination shock shown in fig. 22.) Several sample field lines in the northern hemisphere have been selected for the purpose of this illustration, and only some of the physical parameters have been chosen to illustrate the overall topology without unnecessary complexity. The varying of the interplanetary spiral magnetic field (an Archimedian spiral) out through the termination shock and into the heliosheath had not been previously visualized. The looping spirals are advected either north or south, depending on whether they lie in the northern or southern hemisphere of the Sun (fig. 23). Only loops in the northern hemisphere are shown—with a mirror reflection of the loops existing in the southern hemisphere. This splitting is a consequence of the interaction between the solar wind and the local interstellar medium being a type of stagnation point flow (fig. 22), with the splitting occurring in the vicinity of the stagnation point. As the magnetic loops are carried back into the heliotail, they form two lobes in the northern and southern portions of the heliotail.

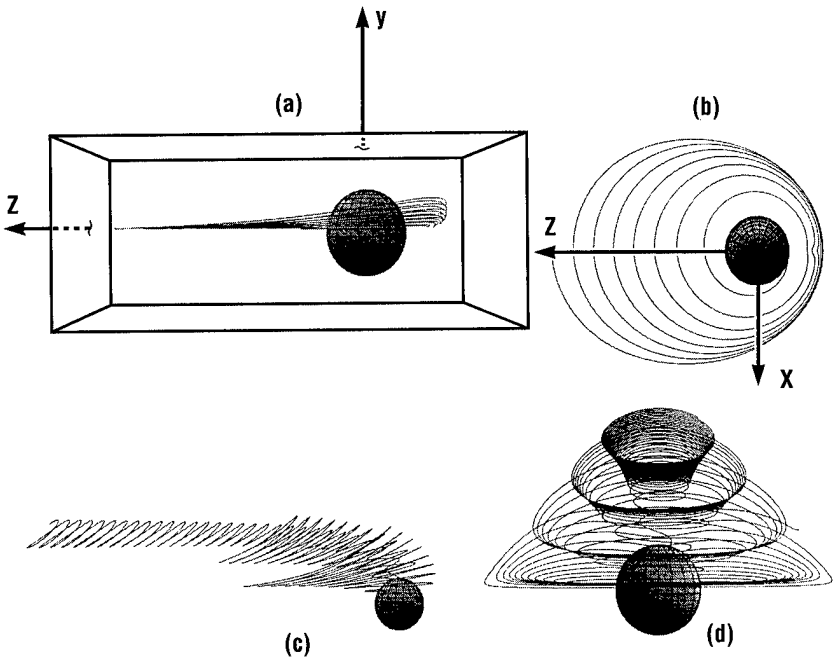

FIGURE 23.—Topology of magnetic field lines.

Model calculation (illustrated in fig. 23), when compared with the observational results from Voyagers 1 and 2 as they cross the upstream heliosheath, will be used to determine the appropriate physical parameters for the heliosphere—the interstellar medium system. The magnetic field model itself will then become a quantitative tool for evaluating the entry of galactic cosmic rays into the heliosphere.

[1]Gurnett, D.A.; Kurth, W.S.; Allendorf, S.C.; and Poynter, R.L. 1993. Radio Emission From the Heliopause Triggered by an Interplanetary Shock. *Science*, 262:199–203.

[2]Nerney, S.F.; Suess, S.T.; and Schmahl, E.J. 1995. Flow Downstream of the Heliospheric Terminal Shock: Magnetic Field-Line Topology and Solar Cycle Imprint. *Journal of Geophysical Resources*, 100:A3, 3,463–71.

Sponsor: NASA Headquarters Program Office; Dr. V. Jones/Cosmic and Heliospheric Physics Branch, Space Plasma Physics Division

Solar Flares

Ronald L. Moore/ES82
205–544–7613

A solar flare is an explosion in a strongly magnetic region of the solar atmosphere—a violent burst of bulk mass motion, plasma particle energization, and radiation. Large solar flares are the greatest explosions in the solar system, blasting out through the solar wind, disrupting the magnetospheres of planets, and sweeping to the outer reaches of the heliosphere. From the observed strength and sheared structure of the magnetic field at flare sites, it is quite certain that the energy released in flares comes from the magnetic field, i.e., that flares are magnetic explosions. The basic questions posed by flares are: how does the magnetic field explode and how does the explosion produce the observed massive energization of electrons and ions to hard x-ray energies and beyond?

Flares often occur in complex magnetic field configurations made up of multiple impacted bipoles, each with its own polarity inversion. In these cases, the coronal loops and chromospheric ribbons that brighten in the flare have a correspondingly complex morphology. However, in some flares practically all of the energy release occurs within a magnetic field that bridges only a single inversion line, so that the arrangement of loops and ribbons is simpler: a single arcade of coronal flare loops bridges the single inversion line and is rooted in a pair of flare ribbons that bracket this inversion line. This general class of single-bipole flares includes a subclass known as "two-ribbon eruptive flares;" the largest and most powerful flares are usually of this type.

Solar scientists at MSFC recently proposed that the bulk dissipation of the magnetic field required for the electron energization for the hard x-ray emission in the explosive phase of flares occurs in a "fat current sheet"—a wall of cascading magneto-hydrodynamic turbulence sustained by highly disordered, driven reconnection of opposing magnetic fields impacting at a turbulent boundary layer.[1] In two-ribbon eruptive flares, this turbulent reconnection wall develops at the usual reconnection site in the standard model for these flares; i.e., the reconnection wall stands in the vertical magnetic rent made by the eruption of the sheared core of the preflare closed bipolar field.

During the past year, MSFC solar scientists, in collaboration with solar scientists at Goddard Space Flight Center, used the well-observed great two-ribbon eruptive flare of April 24–25, 1984, to assess the feasibility of both the standard model for the overall three-dimensional form and action of the magnetic field, as well as the turbulent reconnection wall within it.[2] The observed aspects of this flare that were used included the preflare photospheric vector magnetic field (observed with the MSFC vector magnetograph); the occurrence of a flare spray and the size, form, and spreading of the chromospheric flare ribbons (fig. 24); and the rate of production of hard x rays in the explosive phase of the flare (observed by Goddard's hard x-ray burst spectrometer on the Solar Maximum Mission). Researchers found that: (1) the morphology of this flare closely

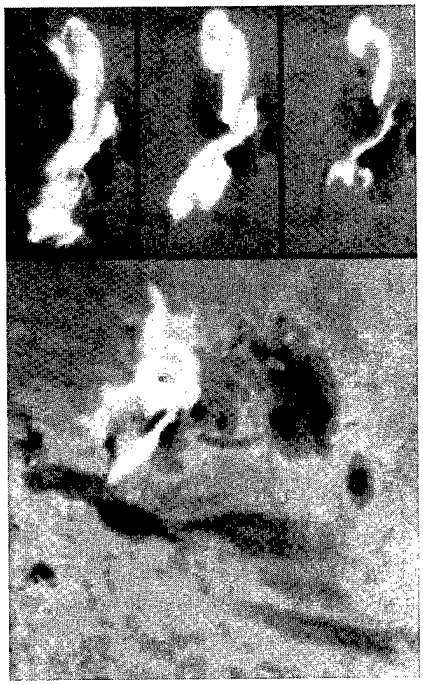

FIGURE 24.—Spreading of chromospheric flare ribbons.

matched that of the standard model; (2) the preflare sheared-core field had enough stored magnetic energy to power the flare; (3) the model turbulent wall required to achieve the flare's peak dissipative power easily fit within the flaring magnetic field; (4) this wall was thick enough to have turbulent eddies large enough (diameters on the order of 10^8 centimeters) to produce the energy-release fragments (of order 10^{26} ergs) typically observed in the explosive phase of flares; and (5) the aspect ratio of the reconnection wall was in the 0.1-to-1 range predicted by Parker.[3] In view of these observations, researchers therefore concluded that the viability of their version of the standard model (i.e., having the magnetic field dissipation occur in a turbulent reconnection wall) is well confirmed by this typical great two-ribbon flare.

[1]LaRosa, T.N., and Moore, R.L. 1993. A Mechanism for Bulk Energization in the Impulsive Phase of Solar flares: Magnetohydrodynamic Turbulent Cascade. *Astrophysical Journal*, 418, 912.

[2]Moore, R.L.; LaRosa, T.N.; and Orwig, L.E. 1995. The Wall of Reconnection-Driven Magnetohydrodynamic Turbulence in a Large Solar Flare. *Astrophysical Journal*, 438, 985.

[3]Parker, E.N. 1973. The Reconnection Rate of Magnetic Fields. *Astrophysical Journal*, 180, 247.

Sponsor: Office of Space Science

Three-Dimensional Rendering and Image Analysis of Coronal Loops

G. Allen Gary/ES82
205–544–7609

In MSFC's Solar Physics Branch, research is conducted on solar magnetic fields and their physical associations and effects in the photosphere, corona, and interplanetary medium. Extensive efforts have been carried out in relating the MSFC vector magnetograms to flare theories. This research is extremely useful in that it describes the observed coronal magnetic structures in the solar atmosphere in relation to the observed photospheric magnetic field on the solar surface. The photospheric field is derived from the unique MSFC solar vector magnetograms. Using these data and observed x-ray images of the Sun, researchers are developing general data-analysis tools to be used to analyze soft x-ray images. The research objective is to be able to define the available free energy via the three-dimensional magnetic- and electric-current morphology transversing through the solar atmosphere.

The research includes the development of software that will display pseudo soft x-ray images given magnetic field lines, density, and temperature. The development process is as independent of specific models as possible to allow for many models in the final version. Crucial is the ability to provide an efficient computer algorithm that renders a three-dimensional volume into a two-dimensional image with

adequate quality compatible for analysis and comparison with observations (e.g., from the soft x-ray telescope/Yohkoh). The code will provide a systematic comparison between (1) observed coronal flux tubes and models and (2) coronal flux tubes and their photospheric footpoints. Using existing codes and scaling laws to determine the coronal density and temperatures, and an instrument response code, one can theoretically determine the observed emission characteristics for each volume cell (voxel). Given this and some magnetic-field configuration (e.g., from a potential field or force-free field), the problem is one of integrating along the line of sight and displaying the resulting image. This problem is being addressed. A reasonable volume could have a million voxels, and an associated brightness must be calculated at each cube. Here, efficiency is the key point for the extensive volume-rendering programs. Having the brightness values, the code must integrate the semitransparent solar plasma and display the results in various graphic formats. This analysis package is of paramount importance in the research. The backward interpretation can begin—that is, having a two-dimensional image, the three-dimensional configuration can be inferred, and further studies of coronal temperatures, emission characteristics, field modeling, footpoint, and photospheric correspondence will proceed.

The description of the coronal magnetic field is a key component in understanding solar activity. Hence, this topic is in direct support of flight- and ground-based vector magnetograph programs which are specific NASA programs and a focus of the activities of the MSFC Solar Science Branch. The results are of particular significance to the mechanisms of solar variability and spaceborne magnetograph programs aimed at understanding the physical cause of variations in and from the Sun. The free magnetic energy that drives much of the variation is directly connected to the magnitude of the electric currents and heating in the solar atmosphere. To understand the dynamics of the x-ray imagery (e.g., from Yohkoh), one needs also to understand the electric currents (the source of energy) and the coronal configuration. The general analysis of the magnetic structures and their associated electric-current systems will discriminate between contending theoretical models. There is clearly a need for this analysis, as it relates to observations and reduced and analyzed data from the MSFC vector magnetograph and the development of the next-generation solar-orbiting instruments.

The research program is developing a formal basis for deriving and investigating solar magnetic structures and obtaining a better physical understanding of these results. MSFC magnetograms will be analyzed extensively to characterize the photospheric magnetic fields. The specific strength of this research is that the scientific investigation continues a strong program by the Solar Physics Branch in the area of magnetic field analysis. These studies are of the highest scientific merit to solar physics and are fundamentally important to the NASA Space Physics Program. The objectives are assured through a thorough technical approach. The relevance of the work lies in the deeper understanding it will provide of the processes underlying the observed structure of solar active regions, which are the main contributors to solar variability in ultraviolet and x rays.

Gary, G.A., and Démoulin, P. 1995. Reduction, Analysis, and Properties of Electric Current Systems in Solar Active Regions. *Astrophysics Journal*, 445:982.

Gary, G.A., and Rabin, D. 1995. Line-of-Sight Magnetic Flux Imbalances Caused by Electric Currents. *Solar Physics*, 157:185.

Gary, G.A., and Hagyard, M.J. 1990. Transformation of Vector Magnetograms and the Problems Associated With the Effects of Perspective and the Azimuthal Ambiguity. *Solar Physics*, 126:21.

Gary, G.A. 1990. Mathematical Basis for the Extrapolation of Solar Nonlinear Force-Free Magnetic Fields. *Memorie della Societa Astronomica Italian*, 61:457.

Gary, G.A. 1991. Numerical Modeling Techniques for Extrapolating Solar Vector Magnetic Fields From the Photosphere. *Direct and Inverse Boundary Value Problems*. (New York: Peter Lang), 67.

Gary, G.A., and Musielak, Z.E. 1992. A Regularization Method for Extrapolation of Solar Potential Magnetic Fields. *Astrophysical Journal*, 392:272.

Sponsor: NASA Office of Space Science

Space Physics

Particle Transport From the Magnetosphere's Low-Latitude Boundary Layer

Barbara L. Giles/ES83
205–544–7637

The interaction between solar and terrestrial magnetospheric plasmas takes place through a diffuse boundary layer across which properties of the two plasma regimes gradually merge. Several modeling studies have addressed the question of the relative contribution, throughout the magnetosphere, of the solar wind particles able to penetrate the Earth's magnetic protective layers relative to those magnetospheric particles that originate in the ionosphere. For example, Delcourt et al[1]. examined dayside magnetopause entry points for solar wind protons and traced their dayside-to-nightside transport over the polar cap. This study found an inward limit of solar wind plasma penetration as a direct consequence of the field-line topology.

Here we examine the questions of whether solar wind and ionospheric plasma of the low-latitude boundary layer, streaming tailward, can play a significant role in the transport of plasma from the magnetosheath to the central plasma sheet.

This survey considers particle behavior in Tsyganenko and Modified Volland fields. Two broad classes of particles are included, representing solar plasma and ionospheric plasma as separate ranges of initial velocities (in the plasma convection frame). During steady conditions, solar and ionospheric populations convected into the low-latitude boundary layer exhibit the behaviors discussed below.

Precipitation along magnetic field lines into the ionosphere are found to be associated with large initial ratios of parallel-to-perpendicular particle velocity, but also occur after evolution of a trajectory in which large magnetic-moment decrease or parallel acceleration occurs. Ionospheric protons, because of their smaller initial parallel velocities, are less likely to be precipitated than solar protons.

Plasma escape downstream in the magnetotail occurs mainly in the outer layers of the low-latitude boundary layer, and occurs further inward along the dusk flank than for the dawn flank, largely because of the asymmetric effects of gradient and curvature drifts.

Plasma trapping and transport to the inner magnetosphere occurs for both solar wind and ionospheric populations, and many particles enter long-term convection trapping. Trapping appears as prolonged bouncing motions during convection along the magnetopause, during which the particles lose energy steadily, prior to ultimate escape. Particles with larger magnetic moments drift more rapidly inward along the dawn flank and outward along the dusk flank. Those drifting sufficiently inward are returned earthward through the plasma sheet, generally gaining significant energy during that phase of their motion. Some particles enter closed convection paths that have the potential for long-term trapping in the convection cell vortices. Bounce phase variations lead to considerable aperiodicity in these trajectories, even though they may be closed in a larger sense.

Energization to ring-current energies occurs for some protons originating in the low-latitude boundary layer—mainly those protons that begin earthward convection sufficiently duskward within the plasma sheet or that gain sufficient magnetic moment in their earthward transit. Particles that begin earthward convection sufficiently duskward within the plasma sheet or that gain sufficient magnetic moment in their earthward transit travel generally duskward and reach very high energies (10's of kiloelectron volts) in the inner magnetosphere, forming a ring-current contribution.

In summary, the low-latitude boundary layer is found to be a more effective source of solar plasma to the plasma sheet than the high-latitude plasma mantle. Ionospheric plasma convected into the low-latitude region is also delivered in part to the plasma sheet, where it is energized.

[1]Delcourt, D.C.; Moore, T.E.; Sauvaud, J.A.; and Chappell, C.R. 1992. Nonadiabatic Transport Features in the Outer Cusp Region. *Journal of Geophysical Research,* 97:16, 883.

[2]Moore, T.E.; Giles, B.L.; and Delcourt, D.C. 1994. Particle Transport From the Low-Latitude Boundary Layer. *EOS Transactions*, American Geophysical Union.

Sponsor: Office of Space Science and Applications

MSFC Thermal Plasma Instrumentation Probing the Topside, Cleft Ionosphere

Craig J. Pollock/ES83
205–544–7638

Mission and Science Objectives

The Sounding of the Cleft Ion-Fountain Energization Region was a scientific sounding rocket mission conceived to study the prolific outflow of plasma known to emanate from the high-latitude dayside auroral zone. Scientists have known for nearly 10 years that on the order of 10^6 grams per hour of oxygen ions and other ions flow outward from this region of the globe into deeper space. The plasma eventually either becomes entrained in the large-scale magnetospheric convection pattern or escapes the influence of Earth altogether. While the implications of this outflow for the Earth's lower atmosphere or the interplanetary medium and beyond are probably inconsequential (even over long time scales), the same cannot be said regarding their effect on the near-Earth space environment, which may be profoundly influenced by the resultant mass-loading by entrained outflowing plasma. For this reason, the nature and cause of the subject plasma outflow is of great interest to space scientists.

The spacecraft for the Sounding of the Cleft Ion-Fountain Energization Region mission, a Black Brant XII sounding rocket, was optimized to achieve maximum altitude within the geomagnetic cleft region, which generally extends several hours to either side of local magnetic noon in the high-latitude ionosphere and magnetosphere. The scientific payload consisted of alternating-current and direct-current electric-field antenna/receiver sets provided by Cornell University and the University of Bergen (Norway), energetic charged-particle spectrometers provided by the University of New Hampshire, a thermal ion-mass spectrometer (the Scanning Thermal Ion-Composition Spectrometer) provided by MSFC with participation from the University of Texas at Dallas, and the first truly differential and directional thermal electron spectrometer (the Thermal Electron Capped-Hemisphere Spectrometer) ever to be flown in space, which was provided by MSFC with participation from the University of Alabama in Huntsville. Geophysical ground observations were provided on Svalbard, under the vehicle trajectory, by the University of Alaska, the University of Oslo, and University Courses on Svalbard. Ground-based radar diagnostics were provided by the European Incoherent Scatter Radar Facility at Tromso, Norway.

The scientific objective of the mission was to determine why such profuse flows of heavy ionospheric ions emanate from the target region, in spite of the fact that these ions should be strongly gravitationally bound to the Earth. Escape requires energization to roughly 100 times their thermal energy, and—while a number of available energy sources have been identified—the ejection mechanism has not been determined to this point.

MSFC Instrumentation

The Scanning Thermal Ion-Composition Spectrometer was programmed to provide the three-dimensional phase space distribution of hydrogen, helium, and oxygen ions in the energy per charge range from 0.1 to 20 volts. This instrument has flown earlier on several rockets, including members of the highly successful Argon Release for Controlled Studies sounding rocket and the TOPside Probe of the Auroral Zone series.

The Thermal Electron Capped-Hemisphere Spectrometer is a new instrument, developed at MSFC to address the challenging electron energy regime below 5 electron volts. For this instrument, the capped-hemisphere concept of Carlson et al. was brought forth, adding the primary innovation of miniaturizing the sensor to account for the small-scale gyration executed by the target electrons in the Earth's geomagnetic field. The radius of the trajectory curvature of a selected electron within the spectrometer's electrostatic analyzer is only 0.6 centimeter. The instrument was programmed to sweep electron energies from 0.3 up to 60 electron volts, spending most of its time at energies less than 4 electron volts.

Flight Overview

The Sounding of the Cleft Ion-Fountain Energization Region rocket was launched into the pre-noon auroral zone from the Andoya rocket range on the northwestern Norwegian coast, climbed to an apogee of 1,480 kilometers (a NASA sounding rocket record) above the Svalbard Archipelago, and fell to the Earth approximately 750 kilometers short of the geographic North Pole, after 22 minutes of flight. All instrumentation and payload subsystems performed flawlessly

throughout the flight. The geophysical target was hit squarely, and a high-quality data set was obtained. Several energetic electron-precipitation events (auroral arcs) were encountered, beginning near apogee and extending into the down leg.

Thermal Plasma Results

Figure 25(a) shows a color-coded display, in energy-time spectrogram format, of the $\log_{10}$ of Thermal Electron Capped-Hemisphere Spectrometer count rates (proportional to electron-energy flux) from one of eight detector channels, in the energy range of 0.3 to 4 electron volts. During the up leg, the energy of peak flux increased from less than 1 to near 2 electron volts, due to an increasingly positive spacecraft potential as the spacecraft moved into regions of lower electron density under solar extreme-ultraviolet photon bombardment. Near 700 seconds flight time, the nature of the measured electron distributions changed as the payload flew into the dayside auroral zone. Intermittent bursts of superthermal electrons observed in the data are seen to correlate with energetic electron precipitation (kiloelectron volts) observed by the University of New Hampshire's energetic particle spectrometers. As the payload proceeded further northward, the thermal electron core became more steady, with peak flux remaining consistently near 1 electron volt.

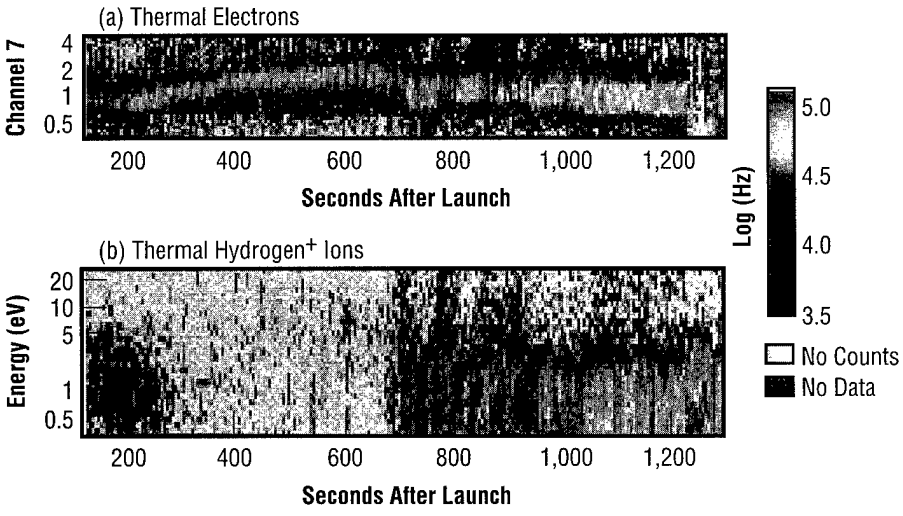

FIGURE 25.—Energy versus time color spectrograms of: (a) thermal electrons observed by the Thermal Electron Capped-Hemisphere Spectrometer; (b) thermal hydrogen ions observed by the Scanning Thermal Ion-Composition Spectrometer during the sounding-rocket flight into the topside, ionospheric cleft on January 25, 1995.

Figure 25(b) shows hydrogen-ion count rates obtained with the Scanning Thermal Ion-Composition Spectrometer in energy-time spectrogram format, similar to that presented in figure 25(a). Here, the energy per charge range extends from 0.25 to 25 volts. The thermal core of hydrogen ions appeared in this data set early on the up leg, but then disappeared out of view due to the repulsive effect of growing positive spacecraft potential. However, at the low-latitude edge of the cleft, ion count rates suddenly returned and heated populations of ionospheric ions were observed, e.g., near 800 seconds after launch. These hydrogen ions and concurrently observed oxygen ions are likely to be flowing outward in response to the local heating, but the full three-dimensional analysis required to confirm this has not yet been completed. Note that between 1,250 and 1,325 seconds after launch, the energy at peak flux of hydrogen ions increased from near 1 to several electron volts. This interval corresponds to an interval illustrated in figure 25(a), where electron counts dropped out. The combined signature is consistent with an increase in negative spacecraft floating potential to nearly 2 volts. The reason for this excursion is unknown at this time, but must be due to variation of in situ plasma properties as the payload drops back through the f-region ionosphere (which will be the subject of future study).

Future Work

The thermal data sets collected will offer a unique view of the topside, cleft ionosphere. Full three-dimensional analysis of these data will permit the evaluation of ion outflows and electron currents or pressure

gradients that may be responsible for driving the flows.

The Sounding of the Cleft Ion-Fountain Energization Region thermal electron and ion data sets are the only complete thermal plasma measurements that have ever been obtained in the Earth's ionosphere. Until now, no capability (other than the Thermal Electron Capped-Hemisphere Spectrometer) is known to exist for measuring the differential/directional, ionospheric, electron-distribution function in the energy ranges below 1 electron volt. Coupled to the thermal ion data, an opportunity exists for the first time to fully address the question of spacecraft charge state and the direct measurement of in situ electric current, including all charge carriers.

Sponsor: Office of Space Science

University Involvement: Cornell University, University of Bergen (Norway), University of New Hampshire, University of Alabama in Huntsville, University of Texas in Dallas, University of Alaska, University of Oslo (Norway), University Courses on Svalbard

Other Involvement: European Incoherent Scatter Radar Facility, Tromso, Norway

Cold Plasma in the Earth's Magnetosphere

Dennis L. Gallagher/ES83
205–544–7587

Dominated by the terrestrial magnetic field and largely excluding the solar wind, the magnetosphere is a vast region surrounding the Earth in which populations of hot and cold ionized gases or plasmas carry mass away from the upper atmosphere and carry energy back. The processes of energy and particle transport ultimately lead to solar heating and convection in the Earth's ionosphere. One element of such processes studied in MSFC's Space Plasma Physics Branch is the population of cold plasmas that originate in the ionosphere. These cold plasmas include singly ionized hydrogen, helium, oxygen, and molecular ions, and doubly ionized helium and oxygen.

Cold plasmas dominate other hotter plasmas in the inner magnetosphere by their number and mass. Further, they directly influence many of the dynamic processes important in this environment. Energy carried by waves inward toward the Earth can be excluded from, or admitted to, low altitudes as a result of the density and composition of cold plasmas. Energetic particles trapped in the Earth's magnetic field can be released into the ionosphere or allowed to escape out into the magnetosphere through interactions with cold plasmas.

Although the ultimate goal of researchers is to develop a theoretical understanding of the many processes important in the magnetosphere, the path to this understanding is through measuring the properties of plasmas and assembling these many thousands of measurements into coherent pictures of our local space environment. The development of empirical, or data-based, models of our terrestrial cold plasma environment is an important part of the activities leading to accomplishing the overall goal.

Many measurements of plasma density, composition, and temperature have been made by MSFC and other researchers in the inner magnetosphere over the more than 30 years of instrumented spacecraft operations in orbit about the Earth. MSFC researchers have used measurements from the Retarding Ion Mass Spectrometer onboard the Dynamics Explorer 1 spacecraft to characterize cold plasmas near the Earth. Descriptions of such measurements have been organized by space weather conditions and position in space to allow for the development of mathematical equations that can be used to represent conditions in the space environment. These mathematical descriptions, or empirical models, have now been combined with similar models produced by other researchers for complementary conditions and locations to synthesize a more complete global model of cold plasma density. (Figure 26 is a graphical presentation of plasma density as a function of position corresponding to steady, moderately active space weather conditions. Density is coded in gray-scale intensity, with the lightest shading corresponding to the highest densities.) New to this type of model development is the incorporation of high-latitude and

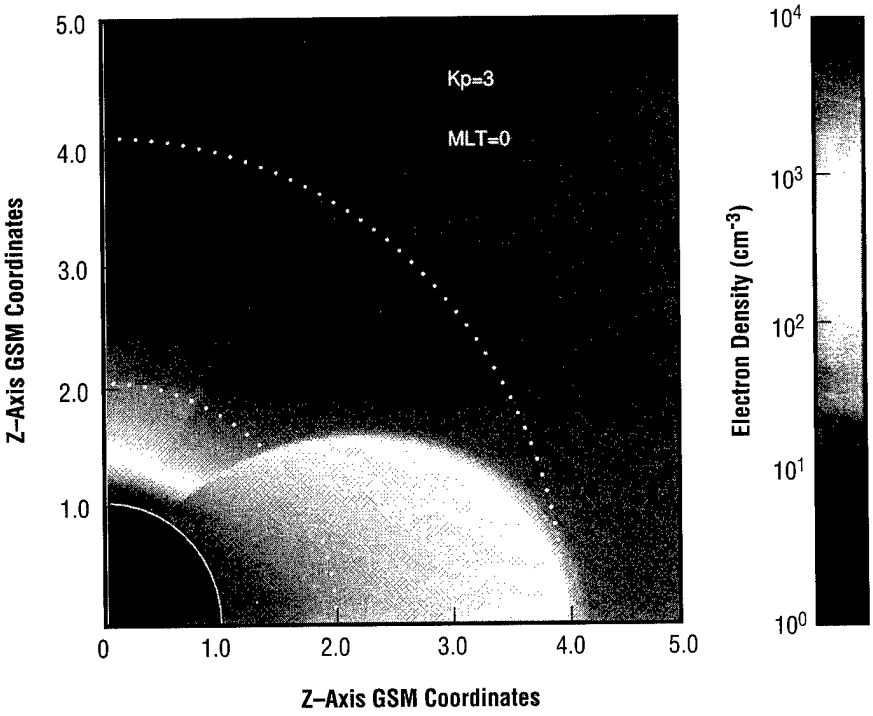

FIGURE 26.—Plasma density as a function of position.

low-altitude plasma densities. At low altitude, the new empirical model is joined to the International Reference Ionosphere model, which is itself a global, empirical model of densities, composition, and temperature in the ionosphere that has been developed as an international cooperative effort.

As discussed earlier, the development of a global, empirical model of cold plasma densities in near-Earth space is a key step in the search for a deeper understanding of the physical processes important in the transport of the Sun's energy to the Earth. Empirical models, such as what is being developed, are used to guide and test theories for how nature works in this region. Computer simulations of space plasma processes also benefit from the use of empirical models by allowing researchers to employ realistic descriptions of the space environment, which greatly improve the accuracy of their predictions for conditions in space.

Beyond the purely scientific applications, however, there are many practical applications of these empirical modeling results. Critical to the success of modern telecommunication and research satellites is the ability to reliably predict the conditions in space in which satellites will operate. Ionizing radiation can penetrate sensitive electronic components, either causing damage or disrupting onboard computers. Satellites designed with electrically insulating surfaces are susceptible to high-voltage charging in space plasmas. Voltages can easily become high enough to break down insulators, causing electric discharging and physical damage to the spacecraft. Low cold plasma densities tend to allow spacecraft charging, while high cold plasma densities tend to reduce the severity of ionizing radiation populations.

Accurate representations of cold plasma densities also play a role in designing better radio communication, such as through the global positioning system. This system, which can be used on aircraft, boats, and cars, is a system of satellites in orbit around the Earth that broadcast radio signals used to accurately determine the position of receiving stations on the surface of the Earth. These satellite receivers are even small enough for individuals to carry and operate off of batteries. Variations in cold plasma density act as noise to these navigational signals, which reduces the accuracy in determining receiver position. Accurate modeling of cold plasma densities can be used to predict global positioning system-receiver accuracy and possibly improve future designs.

More than 30 years of spacecraft observations of the Earth's natural space environment has led to the development of empirical models of a variety of regions and plasma populations. Research in the Space Plasma Physics Branch has resulted in the synthesis of a global, empirical model of near-Earth cold plasma densities. The steady-state descriptions given by this modeling provide density as a function of position, solar luminosity, and local space weather conditions. Modeling results will be used to better understand the volatile

processes going on in space plasmas and to better design and operate manmade systems in space.

Gallagher, D.L.; Craven, P.D.; and Comfort, R.H. 1988. An Empirical Model of the Earth's Plasmasphere. *Advances in Space Research*, 8, 15.

Gallagher, D.L.; Craven, P.D.; Comfort, R.H.; and Moore, T.E. 1995. On the Azimuthal Variation of Core Plasma in the Equatorial Magnetosphere. *Journal of Geophysical Research*, in press.

Gallagher, D.L.; Craven, P.D.; and Comfort, R.H. July 2–14, 1995. Modeling of the Earth's Plasmasphere. Abstracts for the International Union of Geodesy and Geophysics, Twenty-First General Assembly, Boulder, Colorado.

Sponsor: Office of Space Science

University Involvement: University of Alabama in Huntsville

The Dusty Plasma Experiment

James F. Spann/ES83
205–544–5339

Much the same way dust collects on computer monitors so too does dust respond in space. The electrical forces resulting from a charge on a grain of dust will often be stronger than its gravitational force (weight) and will frequently dominate the interaction within a cloud of dust grains. In a space environment, charged electrons and ions interact with dust grains, resulting in the formation of what is called a "dusty plasma." Dusty plasmas are found in most regions of space. Because of this, charged dust plays a role in understanding space dynamics.[1]

The size of spaceborne dust grains can range from 0.1 micron to greater than 1 millimeter in size. The regions of space in which charged dust grains manifest themselves include the Earth's atmosphere, where naturally occurring and manmade aerosols and particles play a significant role in the Earth's energy balance and atmospheric chemistry; high-altitude clouds, where charged ice dust influences radar signals; and the magnetosphere, where they interact with such objects as spacecraft and meteorites and influence the observed plasma and optical signatures. Charged dust particles in the planetary rings of Saturn and Uranus affect the diameter and structure of the rings. Dust particles have been found in the magnetosphere of Mars, comet tails, and in the interstellar medium where they are responsible for the conversion of a significant fraction of the ultraviolet and visible energy to infrared radiation.

The principal charging mechanisms of dust particles in space are known to be photo-ionization, due to incident ultraviolet light; secondary electron emission, due to collisions with energetic ions and electrons; and absorption of charged particles, due to collisions with thermalized ions and electrons. Because dust is an integral component of the Earth's and other planetary systems, understanding the charging of particles in a space environment is key to understanding observed phenomena.

A laboratory experiment called the dusty plasma experiment has been set up at MSFC in which a single micron-sized charged dust grain is studied at a time. The objective of the research is to experimentally study the interaction of micron-sized particles with electron beams and ultraviolet light. This is done to simulate space-like conditions that affect the charge of a dust grain. Specifically, the experiment will investigate under what conditions and to what extent particles of various compositions and sizes become charged, or discharged, while exposed to an electron beam and ultraviolet radiation environment. The emphasis will be the study of the two charging mechanisms: secondary emission of electrons and photo-ionization.

This experiment is unique in that a single charged dust grain will be studied at a time under stable conditions. Typically, charged dust experiments have employed techniques which study either a cloud of dust grains or individual grains as they pass by. This experiment will use an electrodynamic balance that will

cause a charged dust grain to be stably suspended in an alternating electric field. (Figure 27 is a schematic of an electrodynamic balance.) Once a dust grain of known composition is trapped, its weight (due to gravity) is

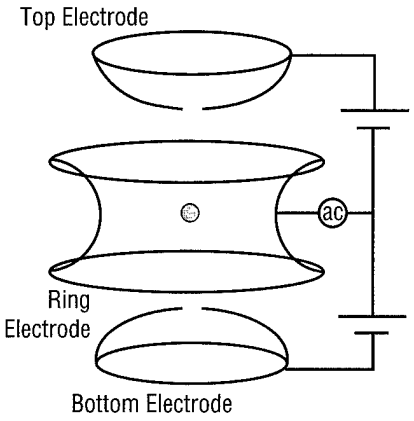

FIGURE 27.—A schematic illustration of an electrodynamic balance where the charge-to-mass ratio of a particle is directly measured. A charged particle will be stably bound in the center of the electrodes, and its weight under gravity will be balanced by a constant electric field.

balanced with a constant offset electric field. In this way, the charge-to-mass ratio of the grain is directly measured. Using light-scattering techniques and viscous drag measurements, the dust grain size and, consequently, its mass is determined. Therefore, the charge of an individual dust grain is measured. The electrodynamic balance is housed in a vacuum chamber and evacuated to pressures less than 10^{-5} torr once a dust grain is trapped. The charge of a dust grain will be measured under various space-like conditions as it responds to different energies and fluxes of incident electron beams and ultraviolet light.

The goal of the dusty plasma experiment is to measure the response of an individual dust grain to various space-like environments. In so doing, a better understanding of the fundamental charging mechanisms and of the observed and modeled phenomena of dusty plasmas will be obtained. See figure 28.

Goertz, C.K. 1989. Dusty plasmas in the Solar System. *Rev. Geophys.*, 27, 271.

Sponsor: Center Director's Discretionary Fund

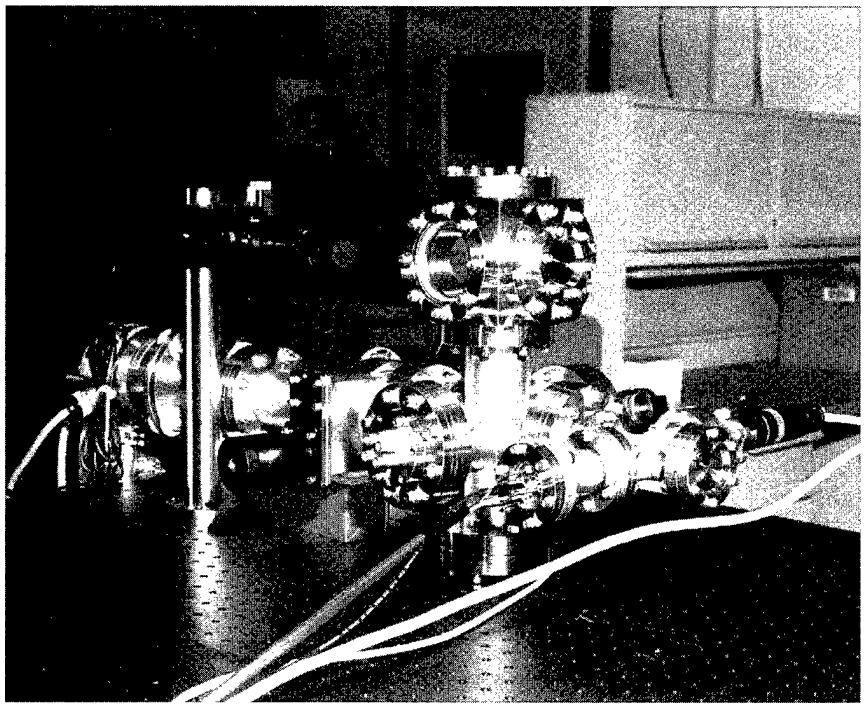

FIGURE 28.—The experimental apparatus for the dusty plasma experiment showing the vacuum chamber. The turbomolecular vacuum pump, used to evacuate the chamber, and the helium-neon laser, used to illuminate the dust grain, are shown in the background. The cube with viewports houses the electrodynamic balance.

Quantitative Determination of the Rate of Hydrogen-Ion Heating by an Argon-Ion Beam

Michael O. Chandler/ES83
205–544–7645

The Argon Release for Controlled Studies sounding rocket was launched from the Poker Flat Research Range on February 23, 1990, carrying a complement of scientific instruments designed to study the near-Earth plasma environment. Among the instruments in the payload was the superthermal ion-mass spectrometer, which was designed and built by MSFC. One of the goals of this flight was to study the interaction of an artificially produced argon-ion beam with the naturally occurring plasma. Argon-ion beams of 100 to 200 electron volts were ejected from a daughter payload, while the naturally occurring ions were observed on the main payload using the superthermal spectrometer. The interaction of the beam and the background plasma generated plasma waves (specifically lower hybrid waves), which, in turn, preferentially heated the ambient hydrogen ions. A previously published study[1] showed that the heating was also restricted to directions perpendicular to the magnetic field, resulting in hydrogen ions that possessed distinctly different characteristic temperatures when viewed in directions parallel and perpendicular to the magnetic field.

A further investigation of these data was initiated in an effort to determine the local heating rate for the hydrogen ions as a result of the beam-plasma interaction. The approach was to model the natural cooling of hydrogen ions to the background-neutral atmosphere and assume that these two species were in local thermodynamic equilibrium, i.e., that their total cooling rate was equal to their total heating rate. Thus, calculating the total cooling rate from the model also provided the total heating rate. For the beam-heated hydrogen ions (i.e., the ones observed perpendicular to the magnetic field), the total heating was a combination of the beam heating and any naturally occurring ion heating that was present. Given this, the temperature observed in the direction parallel to the magnetic field was assumed to provide a measure of the undisturbed plasma—the hydrogen ions unaffected by the argon-ion beam. Therefore, the normal daytime heating of the ions which took place in the absence of any beams could be equated to the total cooling rate of the parallel ions. Finally, the heating due to the beam-plasma interaction was taken to be equivalent to the total cooling rate of the perpendicular ions (equal to their total heating rate) less the total cooling rate of the parallel ions (equal to the normal daytime heating rate).

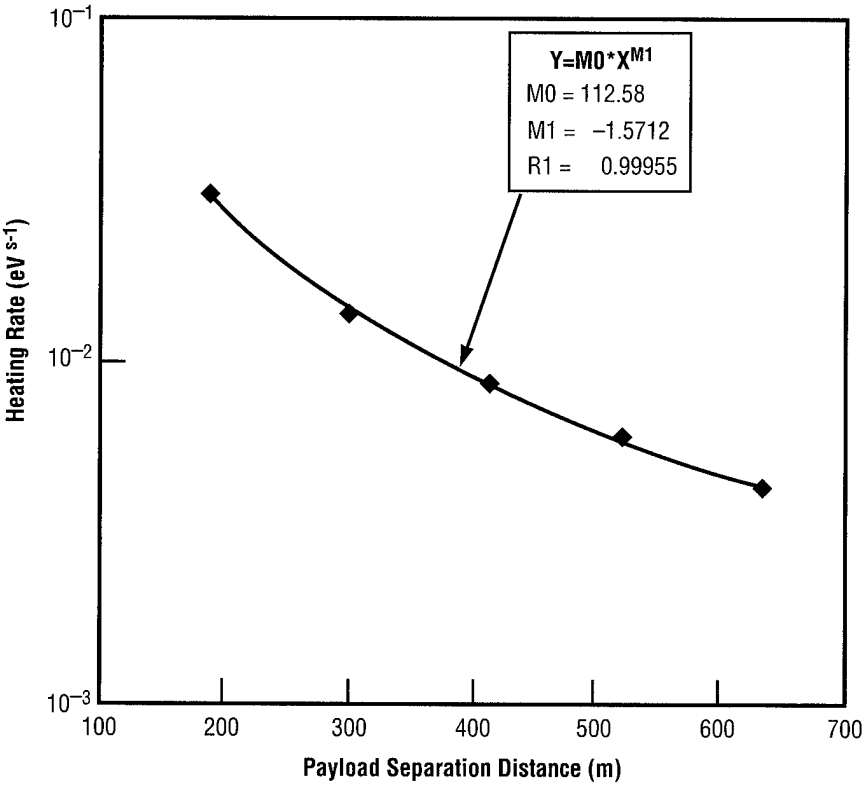

FIGURE 29.—The beam heating rate/ion as a function of the distance between the payloads.

The findings of this study not only give a quantitative measure of the beam heating, but also show the variation of this heating with the changing distance between the mother and daughter payloads (i.e., between the beam origin and the superthermal ion-mass spectrometer). Figure 29 illustrates this variation and includes an approximation to the data in the form of a power-law function. The result is that for the Argon Release Controlled Studies sounding rocket geometry, the rate of ambient ion-beam heating decreased as the 3/2 power of the separation distance. This fact can now be applied to the observed wave data and to plasma theory to determine the mechanism for transfer of energy from the beam to the hydrogen ions. Similar heating is observed to occur naturally in regions of the near-Earth plasma environment and upper atmosphere near the latitudes associated with the aurora.

Pollock, C.J.; Chandler, M.O.; Moore, T.E.; Arnoldy, R.L.; Kintner, P.M.; Chesney, S.; and Cahill, L.J., Jr. 1995. Preferential Heating of Light Ions During an Ionospheric Argon Ion Injection Experiment. *Journal of Geophysical Research*, 100:14, 557.

Sponsor: Office of Space Science

University Involvement: University of New Hampshire, Cornell University, University of Minnesota

Helium- to Hydrogen-Ion Ratios in the Inner Magnetosphere

Paul D. Craven/ES83
205–544–7639

The solar extreme-ultraviolet radiation at 304 angstroms, which is resonantly scattered from helium ions has been proposed as a possible candidate for imaging of the magnetosphere.[1] The spatial distribution of the helium-ion density in the magnetosphere determines the amount of scattered 304-angstrom energy that reaches the detector from an element of solid angle along a given line of sight. The energy reaching the detector is the sum of all the sources in the line of sight, so that some a priori knowledge of the average spatial and temporal distribution of the helium ions would be helpful in deconvolving the images of the magnetosphere. Models that have been used to simulate a magnetosphere image from helium ions have approximated the spatial distribution by assuming a constant helium-ion density above some base altitude on a given L shell [2] or, alternatively, a constant helium ion-to-total density ratio.[3] Total density in the magnetosphere is assumed to be represented by hydrogen ions. The behavior of the helium-to-hydrogen-ion ratio will be important in creating models of the ion composition of the inner magnetosphere, in understanding the physics of the light ions, and in interpreting images of the magnetosphere obtained using the scattered 304-angstrom radiation.

With several years of data from the Retarding Ion Mass Spectrometer on the Dynamics Explorer 1 now available, covering both high and low solar activity, it seems an advantageous time to examine the helium-to-hydrogen-ion density ratio in more detail and, in particular, to examine how this ratio varies in the plasmasphere. The data cover the declining phases of the solar cycle from near maximum to minimum, all seasons, and most local times. The same instrument is used for both phases of the solar cycle so that it is possible to follow changes in the ratio with the solar cycle with no instrument cross calibrations. Densities are derived from each sample using the method described by Comfort et al., 1982,[4] which requires that the ion-distribution function be near Maxwellian. Derived density values are confined mostly to the plasmasphere as a result of this restriction. The data were taken between October 7, 1981, and December 31, 1984, and the full data set is plotted in figure 30, in which gray represents data taken during high solar activity ($P > 150$) and black represents data taken during low solar activity ($P < 150$).

A preliminary examination of the data indicated that the ratio varied most with radial distance, r, and secondly with solar activity, P. The dependence on season, local time, geomagnetic activity, and latitude appeared to be much weaker than with r or with P. However, the spread of the ratios is large, due in part to the variation with r and P. In order to see the weaker dependencies and to model the behavior of the ratio, the helium-to-hydrogen-ion density ratios were detrended on r and P by assuming that the ratio is separable into products of

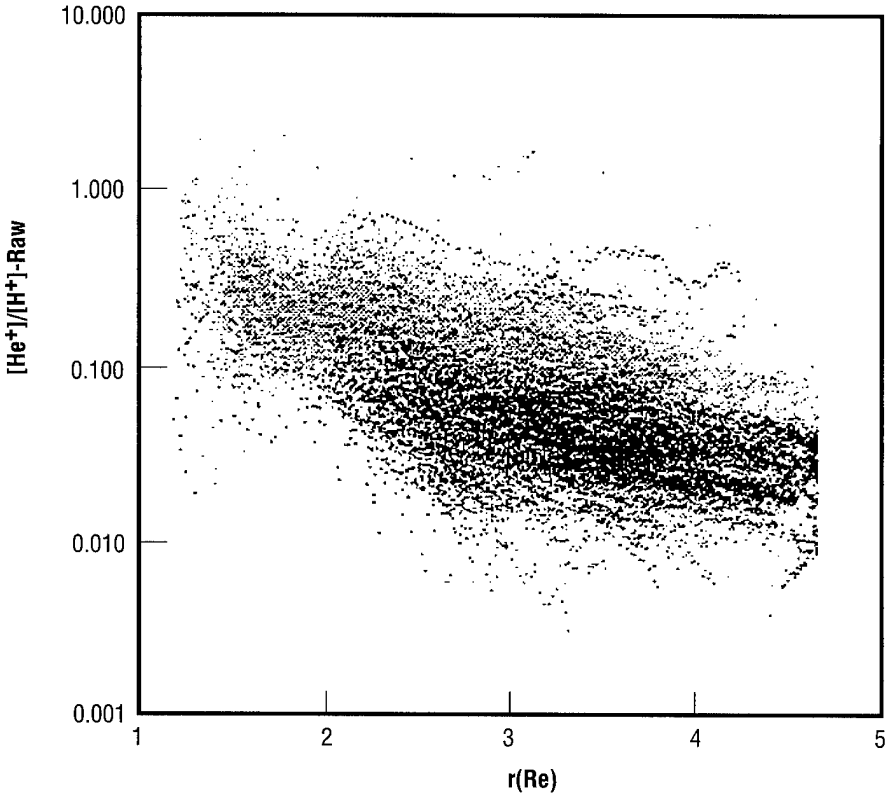

FIGURE 30.—Full data set taken between October 7, 1981, to December 31, 1984.

functions of each independent variable, i.e.:

$$R(r, P, Kp, ...) = f(r)g(P)h(Kp).... \quad (1)$$

This treatment assumes that the independent variables are not correlated. The total data set is first fit to an analytical function of r, $f(r)$. The data are then detrended on r by dividing each data point by the value of the function $f(r)$. An analytical function of P, $g(P)$ was then fit to the ratios which have been detrended in r. The measurements were then detrended in P and the r dependence fit again using the same functional form for $f(r)$ as before. The dependence on both r and P, i.e., $f(r)g(P)$, was then removed from each data point in the original data set. The data, adjusted for both the r and the P dependence, are then given by:

$$R_d = h(Kp)... = R/Cf(r)g(P) \quad (2)$$

where C is a normalizing constant defined so that the average value of $\langle R_d \rangle = 1.0$.

Two very basic characteristics of the ratio of helium-to-hydrogen-ion densities in the plasmasphere are apparent in this study. One is that the ratio decreases with r in the plasmasphere, and the other is the strong dependence of the density ratio on solar activity. Histograms of the ratio for the Dynamics Explorer 1/ Retarding Ion Mass Spectrometer data for low and high solar activity show a dramatic difference in the distribution of the samples, which emphasizes the importance of the solar input. For high solar activity, the histogram (after adjusting for the r dependence) is a broad distribution of values with an overall mean ratio of 0.25 (fig. 31). For low solar activity, there is a narrow distribution (fig. 32); the mean-adjusted ratio of which is 0.10. These values agree with previously published results from other satellites; their importance lies in the fact that they represent different phases of the solar cycle but are measured by the same instrument. These data are qualitatively consistent with a model of the plasmasphere developed, and being updated, by researchers (principally P.G. Richards) now at the University of Alabama in Huntsville. Results from this model indicate that the ratio increases with increasing solar activity[5] and decreases with increasing radial distance.

The importance of being able to accurately model helium-to-hydrogen-ion density ratio in the plasmasphere should not be overlooked. In order for images at 304 angstroms to represent the plasma density and not just helium ions in the plasmasphere, the relation between helium-ion density and the total density must be known. The data

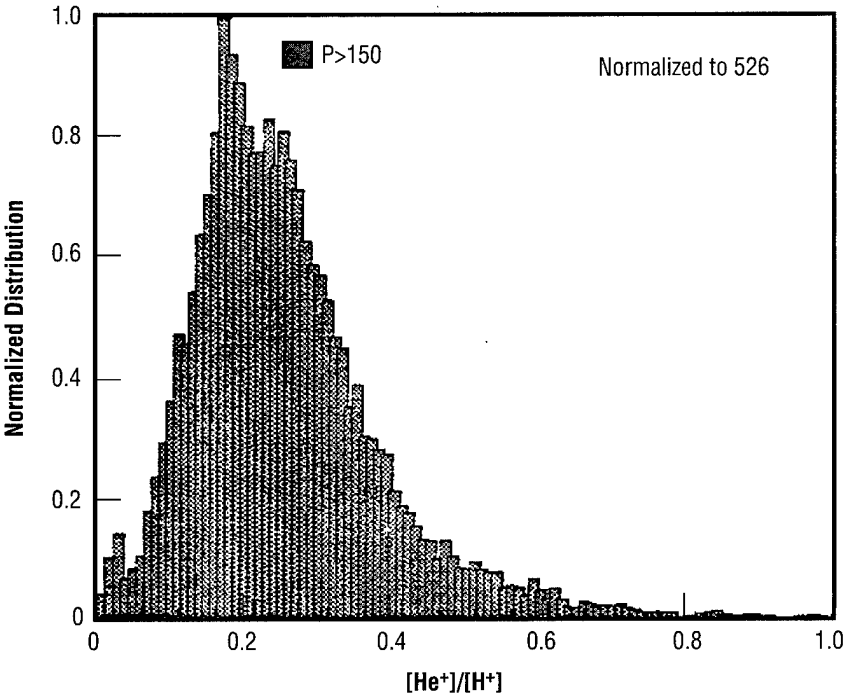

FIGURE 31.—Histogram of ratios for high solar activity.

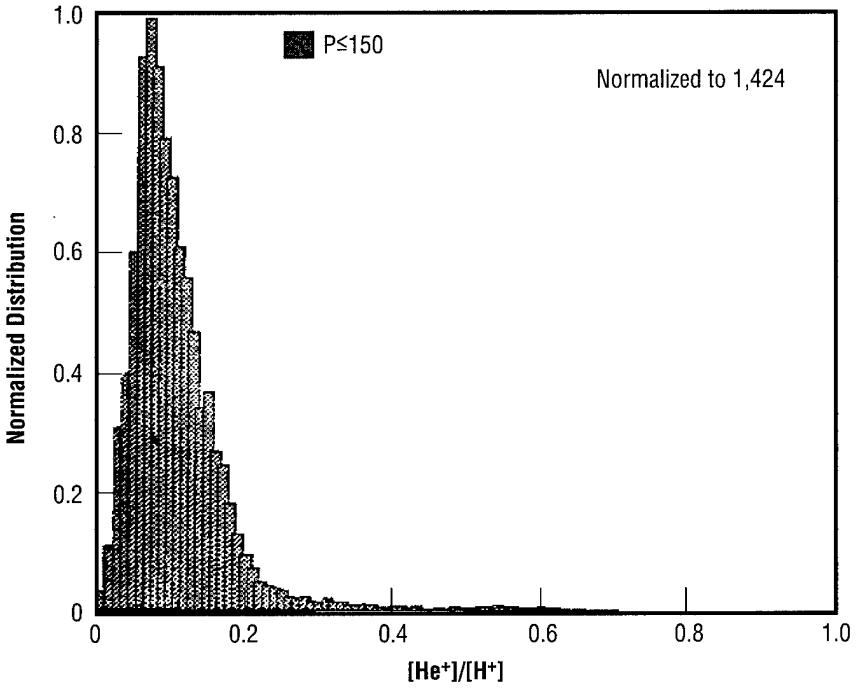

FIGURE 32.—Histogram of ratios for low solar activity.

presented here suggest that the relationship can be represented by equation (1). In order to correctly deconvolve images of helium-ion-scattered, 304-angstrom light, or to represent the results as total density, this relationship must be taken into account.

MSFC has found through a statistical study that the helium- and hydrogen-ion ratio varies with geocentric distance (or altitude) and that its variation in the plasmasphere, before any corrections are made, is about an order of magnitude from about 1 Earth radius to 4.5 Earth radii, decreasing with increasing geocentric distance. The ratio varies significantly with the solar cycle, being greater for higher activity than for low. The ratio has no apparent dependence on geomagnetic activity and is weakly dependent on the day of year, local time, and latitude after adjustments have been made for the distance and solar activity dependence. More detailed study is needed to understand the remaining spread in the data for any of the given variables. Such studies will need to consider geomagnetic activity history, ion temperatures, and production of helium and hydrogen ions in the ionosphere, among other things. Missions that image the magnetosphere will need to use models of the helium-ion distribution to help interpret the images, and MSFC provides a data-based model.

[1]Johnson, C.Y.; Young, J.M.; and Holmes, J.C. 1971. Magnetoglow—A New Geophysical Resource. *Science*, 171, 379.

[2]Meier, R.R., and Weller, C.S. 1972. Extreme-Ultraviolet Resonance Radiation From Helium Atoms and

Ions in the Geocorona. *Journal of Geophysical Research*, 77, 1, 190.

[3]Meier, R.R. 1991. Ultraviolet Spectroscopy and Remote Sensing of the Upper Atmosphere. *Space Science Reviews*, 59, 1.

[4]Comfort, R.H.; Baugher, C.R.; and Chappell, C.R. 1982. Use of the Thin-Sheath Approximation for Obtaining Ion Temperatures From the ISEE 1 Limited Aperture RPA. *Journal of Geophysical Research*, 87, 5, 109.

[5]Newberry, I.T.; Comfort, R.H.; Richards, P.G.; and Chappell, C.R. 1989. Thermal Helium Ions in the Plasmasphere: Comparison of Observations With Numerical Calculations. *Journal of Geophysical Research*, 94, 15, 265.

[6]Young, D.T.; Balsiger, H.; and Geiss, J. 1982. Correlations of Magnetospheric Ion Composition With Geomagnetic and Solar Activity. *Journal of Geophysical Research*, 87, 9,077.

Sponsor: Office of Space Science

Industry/University Involvement: R.H. Comfort, Research Scientist, University of Alabama in Huntsville/ Center for Space Plasma and Aeronomy Research

Plasma Tornadoes

Thomas E. Moore/ES83
205–544–7633

A sounding rocket that flew over a bright Alaskan aurora has observed what appear to be supersonic plasma tornadoes in space. Not just a single twister, but as many as 16 rows of individual vortexes were traversed as the payload flew poleward across the aurora. Plasma wind velocities inside the row of tornadoes reached as high as 3,000 meters per second (6,500 miles per hour), at an altitude of about 500 to 550 kilometers, equal to the highest space shuttle orbits. At that altitude, the sound speed in the plasma is approximately 1,500 meters per second, making these twisters supersonic.

Development of the instrumented payload and analysis of the data were carried out by researchers at Cornell University, the University of New Hampshire, and MSFC, each of whom contributed to the plasma or field instrumentation. An understanding of the data has come from a lengthy analysis, which was complicated by the spin and "coning," or precession, of the payload as it sailed through space over the aurora.

Apparent tornadic flows in auroras have been previously reported by ground observers and recorded through low-light level television imagery of auroral dynamics by cameras on the ground. To see the vortex-like motions, it is best to view the aurora nearly overhead but slightly toward the equator so as to view directly along the local magnetic field lines. Fluctuations in the brightness of the auroral light display are then seen to move in a circular fashion around bright spots in the aurora that appear as bright rays from more oblique perspectives. The location and spin rate of the vortexes are usually highly variable, though often well-organized into an extended bright row that has a drapery-like appearance.

The rocket observations are the first to indicate that the apparent vortical motions in the television imagery are real plasma flows. Previous rocket payloads have provided ample evidence of strong and highly variable plasma winds that can be observed directly as motions of the plasma relative to the rocket payload, or as variations of the electric field in the region around the payload, sensed by sensitive antennas deployed from the payload. All plasma winds in magnetic fields can be sensed this way because they produce a characteristic electric field. A vortical pattern of the variations has not previously been discovered in plasma flow or electric field data.

The vortical motions are perhaps best visualized by means of a plot of the horizontal wind vector as a function of position along the rocket ground track, as shown in figure 33. The region including the aurora spans three panels in this figure, which should be read from left to right and top to bottom. Before the payload enters the auroral region, the flow is relatively slow and directed generally equatorward (a headwind for the rocket). Entry into the aurora is marked by a large increase in the plasma flow vector, followed immediately by rotation of the plasma wind vector to the left (as seen in this view from above). The rate

of rotation is irregular, but the sense of rotation is evidently monotonic.

Strong plasma heating is associated with the region of aurora and intense vorticity. All observed ion species were heated by a factor of approximately two in absolute temperature in the event shown in figure 33. Figure 34 shows the time series of measured plasma temperature for this event, indicating the auroral heating that was present. At present, it is not clear how the heating and the vortical motion are coupled. The high-speed plasma winds themselves are a possible source of heating, since the plasma probably flows through a permeating gas that is relatively stationary. The frictional interaction between the two is sufficient to produce significant heating of the heavier plasma ions. However, the observed heating of the heavier species is somewhat larger than can be accounted for by friction, and the heating of the light species is far in excess of that which can be produced by friction. Therefore, it is likely that the heating is enhanced by the highly structured vortical flows in some way, perhaps through the dissipation of the vorticity into turbulence that heats the plasma.

Auroral tornadoes probably have an origin very different from that of ground-level tornadoes, which get their energy from enhanced vertical motions of the atmosphere, driven by the release of latent heat during the condensation of water vapor, combined with the rotation of the Earth. In space, the vortexes are likely to "spin off" from jet stream-like channels of supersonic plasma flow that are driven by a direct coupling between the auroral plasma and the solar wind, which passes the Earth at speeds up to 400,000 meters per second (1,000,000 miles per hour). The Earth's magnetic field transmits the solar wind motion and energy to the aurora, creating a region of intense shear that leads to development of multiple vortexes. The plasma heating is probably a by-product of the process rather than a driver of it, as in the case of tropospheric tornadoes.

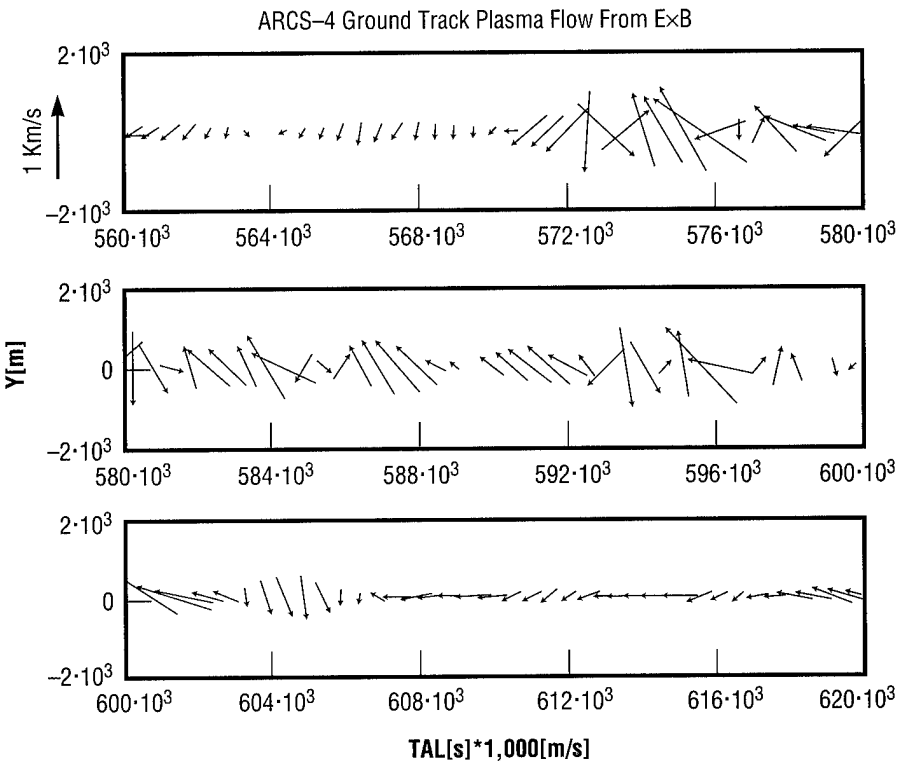

FIGURE 33.—Ground track display of the horizontal plasma-velocity vectors recorded at 0.5-second intervals over an auroral display. The ground track proceeds from left to right and top to bottom through the three panels of the figure, as the payload moves poleward across the aurora.

Moore, T.E.; Chandler, M.O.; Pollock, C.J.; Reasoner, D.L.; Arnoldy, R.L.; Austin, B.; Kintner, P.M.; Bonnell, J. 1996. Plasma Heating and Flow in an Auroral Arc. *Journal of Geophysical Research*, 101, in press.

Pollock, C.J.; Chandler, M.O.; Moore, T.E.; Arnoldy, R.L.; Kintner, P.M.; Chesney, S.; and Cahill, L.J., Jr. 1995. Preferential Heating of Light Ions During an Ionospheric Argon-Ion Injection Experiment. *Journal of Geophysical Research*, 100:15,477.

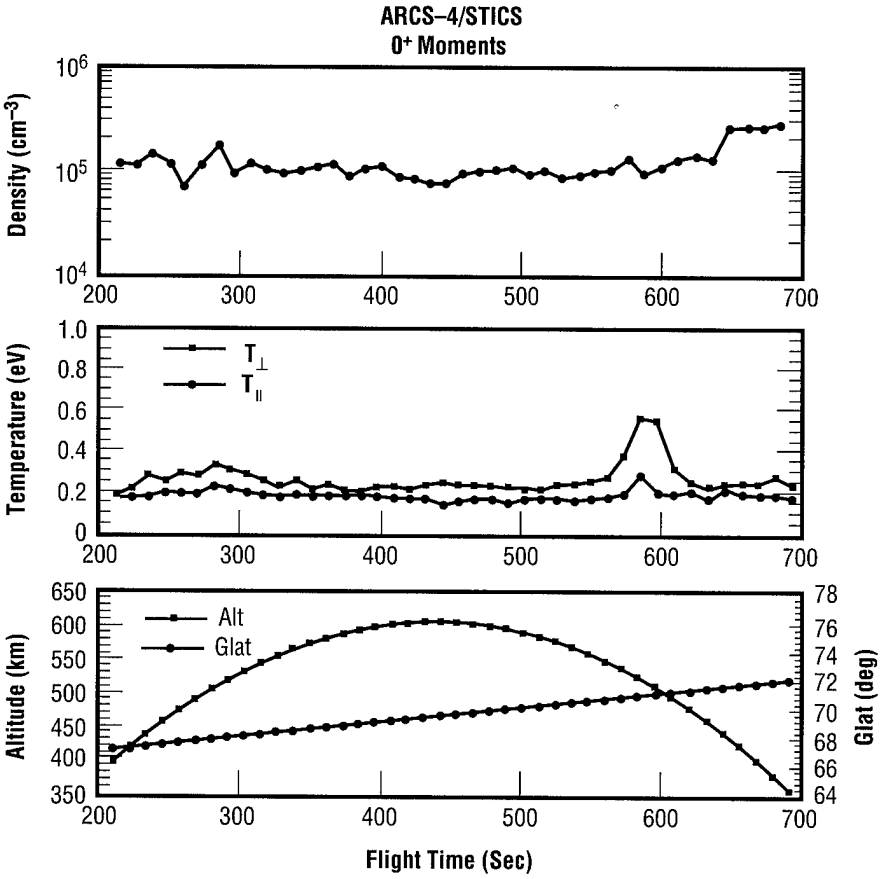

FIGURE 34.—Temperatures of the oxygen ions as a function of flight time and ground track position over an auroral display.

Sponsor: Office of Space Science

University Involvement: Cornell University, University of New Hampshire

Absolute Sensitivity Measurement for the Thermal Ion Dynamics Experiment

Victoria N. Coffey/ES83
205–544–7635

Space plasma can be described to a surprisingly adequate extent for many purposes by simply specifying the moments of the velocity distribution function, $f(v)$. For this to be accomplished, the instrument's geometric factor, or absolute sensitivity, has to be measured before flight. With the knowledge of the instrument's raw count rate in a certain state and the energy-dependent geometric factor, information about the plasma can be obtained by calculating the density, velocity, and temperature.

Previous experience shows, however, that the range of geometric factors previously considered adequate are actually inadequate when a space plasma instrument is carried into regions of very low plasma density. Also, positive floating potentials of spacecraft exposed to sunlight and low density plasmas make low energy plasma observations all but impossible by excluding low energy ions from the spacecraft, exacerbating the sensitivity problem.[2] Resulting from these circumstances, a fundamental design goal of the Thermal Ion Dynamics Experiment has been to achieve a geometric factor much greater than that of previous instruments.

The Thermal Ion Dynamics Experiment is a space plasma flight instrument that will be carried on the

POLAR spacecraft for the Global Geospace Mission, and was developed to make three-dimensional plasma composition measurements capable of tracking the circulation of low energy (0 to 500 electron volts) ions through the polar magnetosphere.[2] Its final testing and calibration before flight was conducted early this summer in the Low Energy Electron and Ion Facility, with one of the main objectives being to measure the geometric factor of the instrument.

The Thermal Ion Dynamics Experiment

The Thermal Ion Dynamics Experiment will provide low energy measurements that are differential in energy and direction as well as mass, with range and resolution adequate for the full characterization of velocity distribution features known to exist in the low energy plasma populations.[2] Two of its design characteristics, its methods of energy and mass analysis, allow for a large geometric factor necessary to obtain these velocity distributions.

To be detected, ions will enter one of seven polar angle apertures and pass through a collimator, an energy analyzer, and then a mass analyzer. An electrostatic mirror combined with a retarding potential analyzer provides the differential energy analysis. Ions that are too energetic pass through the mirror and are lost, while those of insufficient energy are reflected by the retarding potential analyzer. This electrostatic element combination forms the energy bandpass, which can be adjusted in width by selection of the potential bias ratios. The mirror, which plays a major role in the achievement of the large Thermal Ion Dynamics Experiment geometric factor, is of a quasiparabolic shape and translates a large collection area and small solid angle to a small collection area/large solid angle at the entrance to the mass analysis section.[2]

Coupled with each energy analyzer system is a time-of-flight system for mass analysis. After the ions exit the energy analyzer section, they are accelerated through an ultraviolet rejection section and then pass through a carbon foil, where a secondary election is collected at a microchannel plate, initiating the "start" pulse. The ions continue through the time-of-flight region and arrive at a microchannel plate where the "stop" pulse is generated. The delay between the start and stop signals is inversely proportional to the velocity at a known energy/charge and can be converted to a mass/charge. Unlike other magnetic mass analysis systems, the time-of-flight technique permits the use of a large entrance aperture, since no object slit is required to form a mass spectrum image. The large pre-acceleration potential also allows usage of a very large angular acceptance aperture, so that very large geometric factors become possible.[2]

Low-Energy Electron and Ion Facility

The instrument's geometric factor and other response characteristics were tested and calibrated in the Low Energy Electron and Ion Facility. This laboratory system, which has been used for several flight programs, was designed for testing and calibration of low energy particle detectors over a range of particle energy, mass, flux, and angular acceptance. It features a large vacuum chamber, a patented ion source designed to produce low energy ion beams with a large area, beam-imaging diagnostics, and a rotation table that enables motor-driven positioning of the instrument relative to the particle beam. The flight instrument can be placed on the turntable fixture so that the instrument can be tilted ±90 degrees and rotated ±180 degrees relative to the ion source. National Instrument's data acquisition and control software, LabVIEW, was used to link the computers and control the laboratory devices to make efficient use of a flight instrument's testing and calibration time.

Calculating and Measuring the Absolute Sensitivity of an Instrument

The geometric factor is the relation between the number of particles, C (particles/second), transmitted by the instrument in a known sensitive state and the differential directional flux, or intensity, at the instrument aperture, j, (particles per square centimeter per second per electron volt per steradian).

$$C = G * j$$

The symbol for the geometric factor in this relation is G, and it is the product of the integral factors, dA, $d\Omega$, and dE. The effective area, dA, is the measure of the effective area that the instrument presents to the exterior environment; $d\Omega$ is the effective solid angle response width; and dE is the effective energy response width. To make this measurement in the laboratory, it is important to expose the instrument to a monoenergetic and unidirectional beam of known intensity and purified composition.

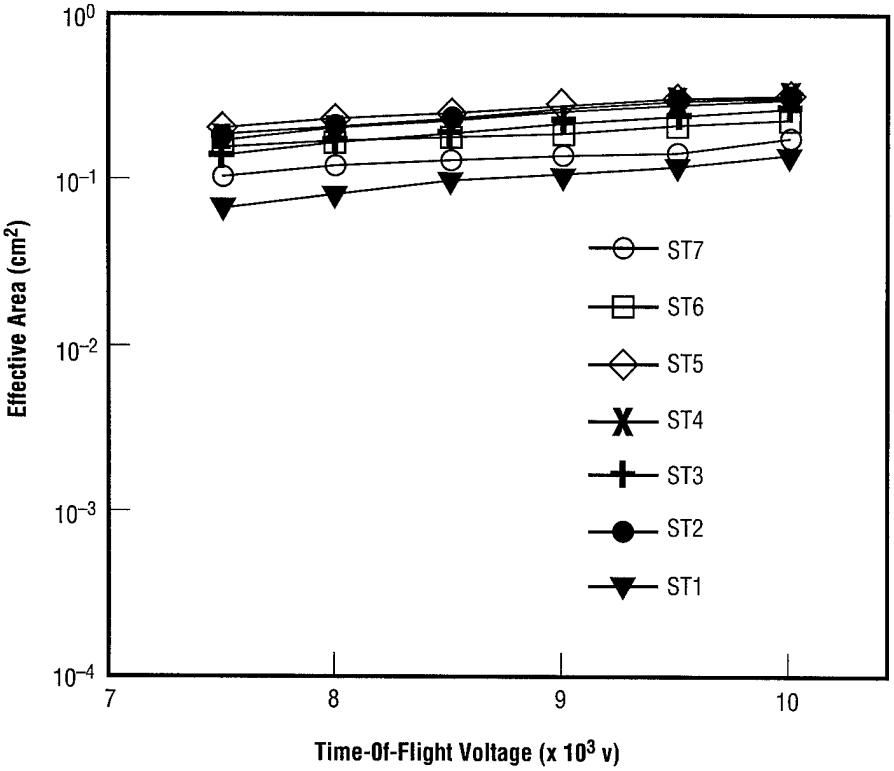

FIGURE 35.—Thermal Ion Dynamics Experiment final calibration: June 16, 1995. Sensitivity to ions derived from an H_2 bleed.

The effective area (fig. 35) is shown for the seven "start" signals as a function of the instrument's time-of-flight voltage. These numbers multiplied by the energy response width and the solid angle response width will give the geometric factor of the instrument. During calibration, the Thermal Ion Dynamics Experiment geometric factor was measured to be at least 10 times larger than previous flight instrument testings in our laboratory.

Biddle, A.P., and Reynolds, J.M. 1985. An Integrated Development Facility for the Calibration of Low Energy Charge Particle Flight Instrumentation.

The Thermal Ion Dynamics Experiment and Plasma Source Instrument. 1995. *Space Science Reviews*, 71:408–58.

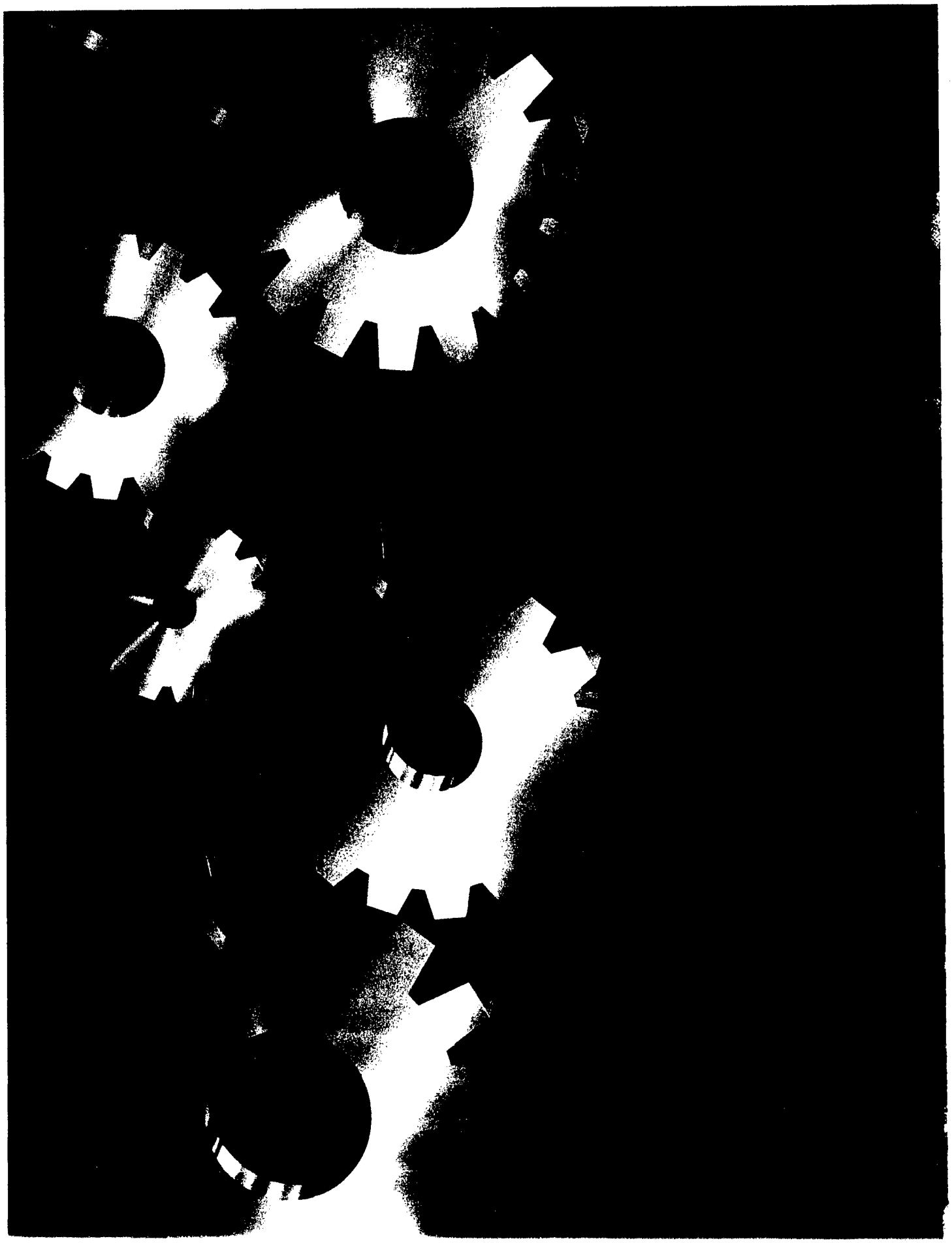

Technology Programs

MSFC's primary goal is to be the world's leader in the technology development and program activities related to space transportation and microgravity science. To efficiently support the "NASA Team," MSFC clearly must excel technically in these areas, as well as provide unique support in areas led by other Centers. Each NASA center must focus and direct its efforts primarily on the areas assigned. Only in this way can this team enable success in the three key NASA missions:

- To advance and communicate scientific knowledge and understanding of Earth, the environment of space, the solar system, and the Universe;
- To explore, use, and enable the development of space for human enterprise; and
- To research, develop, verify, and transfer advanced aeronautics, space, and related technologies.

Space transportation, which includes propulsion, avionics, and other topics, is one which really must be considered the foundation of all other space endeavors. Without it, there will be no space travel. We must provide the Nation with cost-effective, efficient means to go to space. We at MSFC are dedicated to providing this capability to the Agency and the Nation.

The following articles are some selected topics describing a broad spectrum of these technology activities (evolutionary and revolutionary) ongoing at MSFC which hold promise of providing the space transportation and microgravity science capabilities of the future.

James M. McMillion
Director
Science and Engineering

Propulsion and Fluid Management

Low-Cost Turbomachinery Technology

Matthew W. Marsh/EP32
205–544–1773

Typically, turbomachinery used in liquid rocket engines is composed of complex geometries made from high strength-to-weight super alloys. These high-performance machines usually have long design and fabrication cycle times—on the order of 3 to 5 years. Such factors increase development time and result in high costs.

A simple, low-cost turbopump was designed in-house to demonstrate the ability to reduce the overall cost and life-cycle time of turbomachinery. The subject turbopump design, SIMPLEX, has been engineered to provide a discharge pressure of 1,500 pounds per square inch absolute of liquid oxygen at 90 pounds mass per second, as shown in figure 36. This size range would be capable of supporting a 40,000-pound-thrust hybrid motor. The SIMPLEX turbopump will be powered by gaseous nitrogen or gaseous oxygen, eliminating the need for an interpropellant seal required to separate the fuel-rich turbine gases from liquid oxygen, and resulting in a simplified design. Materials used in the turbine flow paths will utilize existing characterized metals at 800 degrees Rankine that are compatible with a warm oxygen environment. The goal for this effort

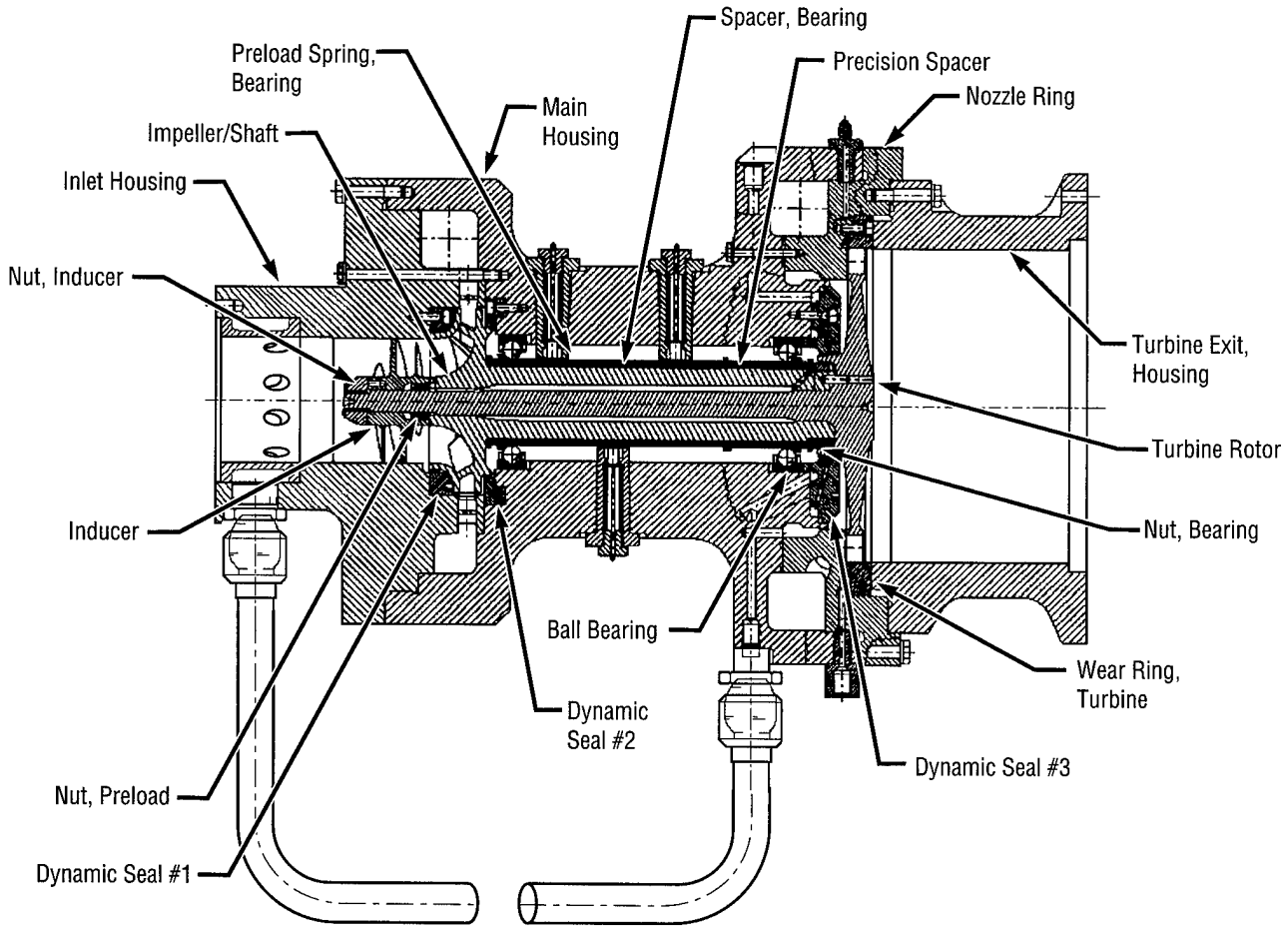

FIGURE 36.—SIMPLEX turbopump cross section.

was to reduce the design and fabrication cycle by a factor of 2.5 (18 months). The cost goal for the first unit fabrication and assembly was $130,000, which represented a reduction factor of 10 when compared to similar turbopumps.

The design and analysis were completed in less than a year, and the detailed analysis process itself was completed by a multidisciplined, concurrent engineering team. Manpower, schedule, and cost data were tracked during the process for comparison to the initial goal. The SIMPLEX hardware has been assembled. Three test series are planned over the following 8 months. Overall design, fabrication, and assembly were completed in 27 months—a reduction in cycle time by a factor of 1.7. Actual unit cost of the first assembly hardware was $205,000 (a reduction factor of 6). Total program cost was only $315,000, as compared to $500,000, the original cost goal (a savings of 37 percent). Although unit cost and schedule goals were not achieved, substantial improvements have been demonstrated. The SIMPLEX turbopump is currently in testing at MSFC.

The in-house design demonstrated the capability of developing a low-cost liquid-oxygen turbopump via an improved design and fabrication process. The prototype will also demonstrate a liquid-oxygen pump driven by an oxidizer-rich turbine gas. The increased ability to estimate rocket engine turbomachinery costs has been another benefit.

Marsh, M.; Cowan, P.; Forbes, J.; and Van Hooser, K. May 17–19, 1994. SIMPLEX Turbopump Design. Presented at the 1994 Conference on Advanced Earth-to-Orbit Propulsion Technology, MSFC.

Sponsor: Office of Advanced Concepts and Technology, Earth-to-Orbit, Reusable Launch Vehicle

Low-Cost Combustion Devices Component Design Verification

David L. Sparks/EP33
205–544–7111

A test program designed to evaluate the performance of ultra-low-cost combustion chambers and injectors is continuing at MSFC. Future combustion devices manufactured using the techniques demonstrated during this program can result in thrust chamber assemblies costing a fraction of previous designs.

Private industry approached NASA/MSFC's Propulsion Laboratory looking for innovative ways to reduce future propulsion system costs. Historically, the thrust chamber, nozzle, and injector (known as the thrust chamber assembly) represent 37 percent of total engine unit cost. Several different design approaches were evaluated as a means of reducing this ratio. The two approaches selected as having the highest potential for cost savings were a film-cooled ablative combustion chamber and a simplified design concept for impinging injectors. Both of these concepts would be brought together for unified testing in the breadboard "Fastrak" engine.

In-house engineering and manufacturing resources were used to produce the critical parts for the Fastrak engine. MSFC personnel designed and fabricated ablative-type combustion chamber liners for use in hardware specifically modified for this test program. A like-on-like, monolithic injector face was also designed and manufactured to operate

with the selected propellant combination.

Hot-fire testing of the engine began in September 1994 (fig. 37) to evaluate interaction of the two design approaches in a combustion environment using liquid oxygen and kerosene propellants. Two primary objectives of the test program include demonstrating the durability of ablative thrust chambers and monitoring the effects of film cooling on erosion rates. The latter objective is critical because of the potential for performance degradation due to throat erosion during engine operation. Injector efficiency and wall compatibility are also being evaluated to ensure performance goals are achieved.

Twenty tests have been conducted at chamber pressures up to 500 pounds per square inch absolute, with durations to 60 seconds. To date, erosion rates in the throat region (the area of greatest concern) have been insignificant (with film-cooling levels of 10 to 13 percent), and injector efficiency is approximately 94 percent. The remaining tests will focus on lower film coolant flow rates and very

FIGURE 37.—Fastrak fire testing.

long duration firings (up to 250 seconds) to establish chamber liner longevity.

The early successes of the Fastrak program prompted the next step in the evolution of this technology. A new, much larger, thrust chamber assembly was designed and built at MSFC this year. Aptly named "Fastrak II," it incorporates the same design philosophy as its breadboard predecessor, but creates a flight-type thrust chamber assembly (fig. 38). Fastrak II was designed to produce 40,000 pounds of thrust at altitude and operate with the same propellant combination as Fastrak. Advanced composite material manufacturing techniques used by MSFC's Materials and Processes Laboratory and its contractor were used to construct the integral thrust chamber/nozzle assembly. This time, the liner uses a thin, lightweight carbon filament wrap on the exterior as a structural close-out of the pressure vessel. The Fastrak II injector design reduces to just five the hundreds of parts usually required for injectors. In-house conventional machining was used to produce the five-piece design. The Fastrak II thrust chamber assembly is 82 inches tall and 46 inches in diameter. It will be tested in test stand 116 beginning in September 1995. Data gathered from both of these test articles are considered essential to the successful development of the low-cost propulsion system for the Orbital Sciences Corporation X–34/OV–1, for which MSFC has design and test responsibilities.

Sponsor: Office of Space Access and Technology

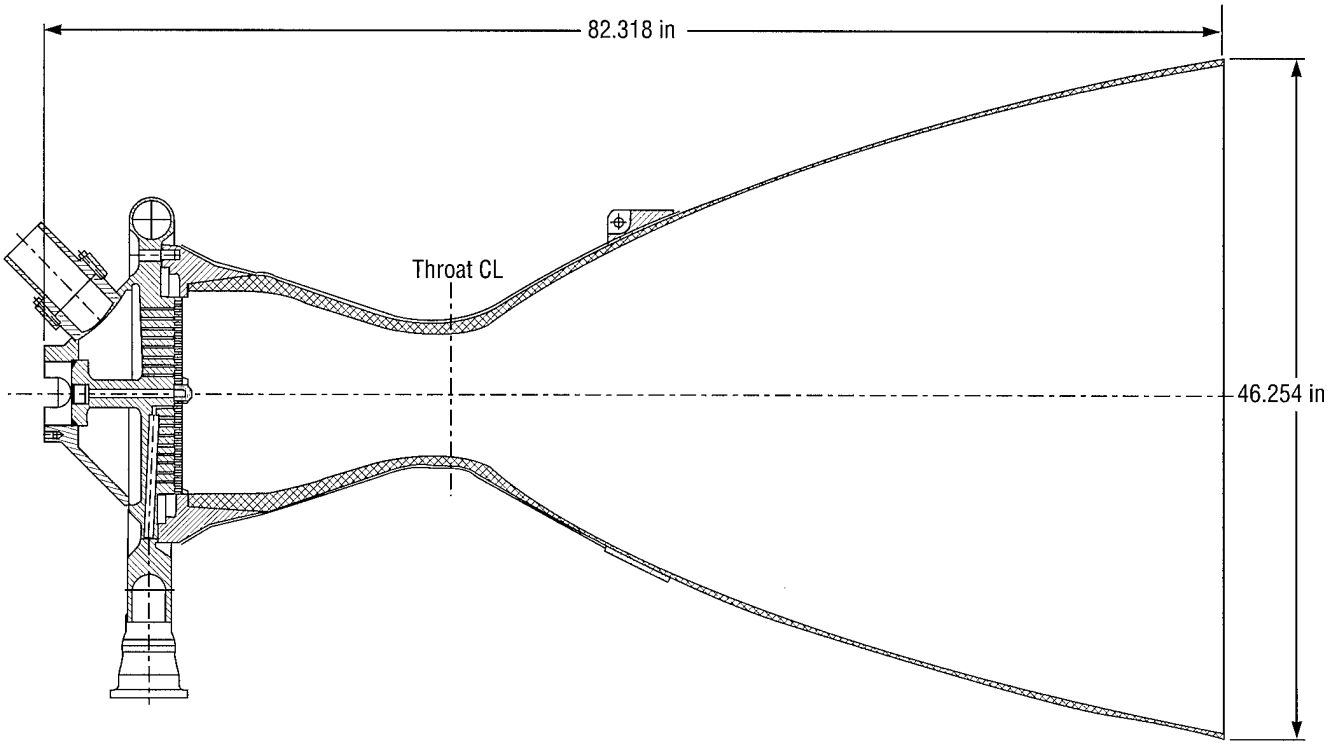

FIGURE 38.—Fastrak II cross section.

Magnetically Actuated Propellant Orientation

George Schmidt/EP25
205–544–6055

In a low-gravity environment, acquisition of vapor-free propellant is complicated by the indeterminate location of bulk liquid with respect to the tank outlet. Proper design of engine feed or propellant transfer systems requires methods to control liquid orientation and an understanding of fluid motion in response to disturbances and imposed accelerations. Traditional approaches for controlling and positioning cryogenic liquids, such as periodic thruster firings and capillary retention devices, exhibit several drawbacks that could be mitigated by employing systems that exploit the inherent paramagnetism of liquid oxygen and diamagnetism of liquid hydrogen. With the advent of lightweight, high-temperature superconductors and high-flux-density, rare-Earth magnets, the use of magnetic fields to control large fluid quantities in microgravity appears feasible, and could enable low-gravity settling, venting, fill, and acquisition without the need for capillary retention systems or propulsive firings. Some of these potential applications are shown in figure 39.

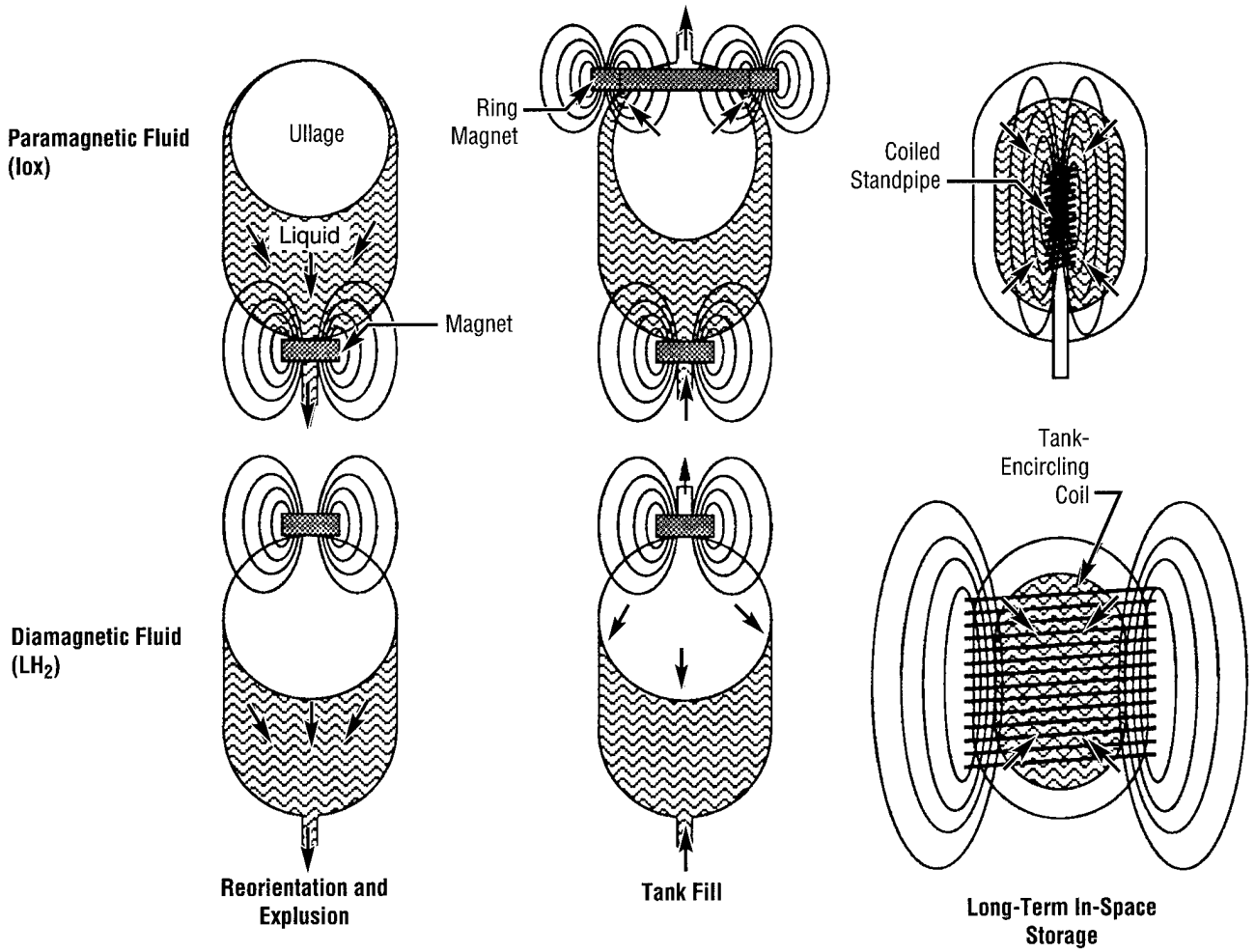

FIGURE 39.—Potential applications of using magnetic fields to control large fluid quantities in microgravity.

This project is currently evaluating the feasibility and practicality of magnetically actuated propellant orientation for spacecraft applications. The scope has been restricted to liquid oxygen primarily because: (1) its control offers the nearest-term application of magnetically actuated propellant orientation technology, (2) the magnetic properties of paramagnetic fluids are well known, and (3) liquid-oxygen behavior has been tested before in low-gravity on a laboratory scale. One of the primary objectives is to determine the range of magnetic field strengths required to perform reorientation and maintain liquid orientation during tank fill and expulsion. This range will provide a basis for evaluating whether these magnetic field requirements fall within the capabilities of current or anticipated superconducting magnet technology.

The project involves low-gravity experiments utilizing the KC–135 aircraft. All experiments employ the subscale hardware shown in figure 40 and a noncryogenic ferrofluid that simulates the paramagnetic behavior of liquid oxygen. The ferrofluid is a commercially available, kerosene-based solution containing a suspension of extremely fine ferrous particles. Several properties of this fluid (i.e., particle density, viscosity, and surface

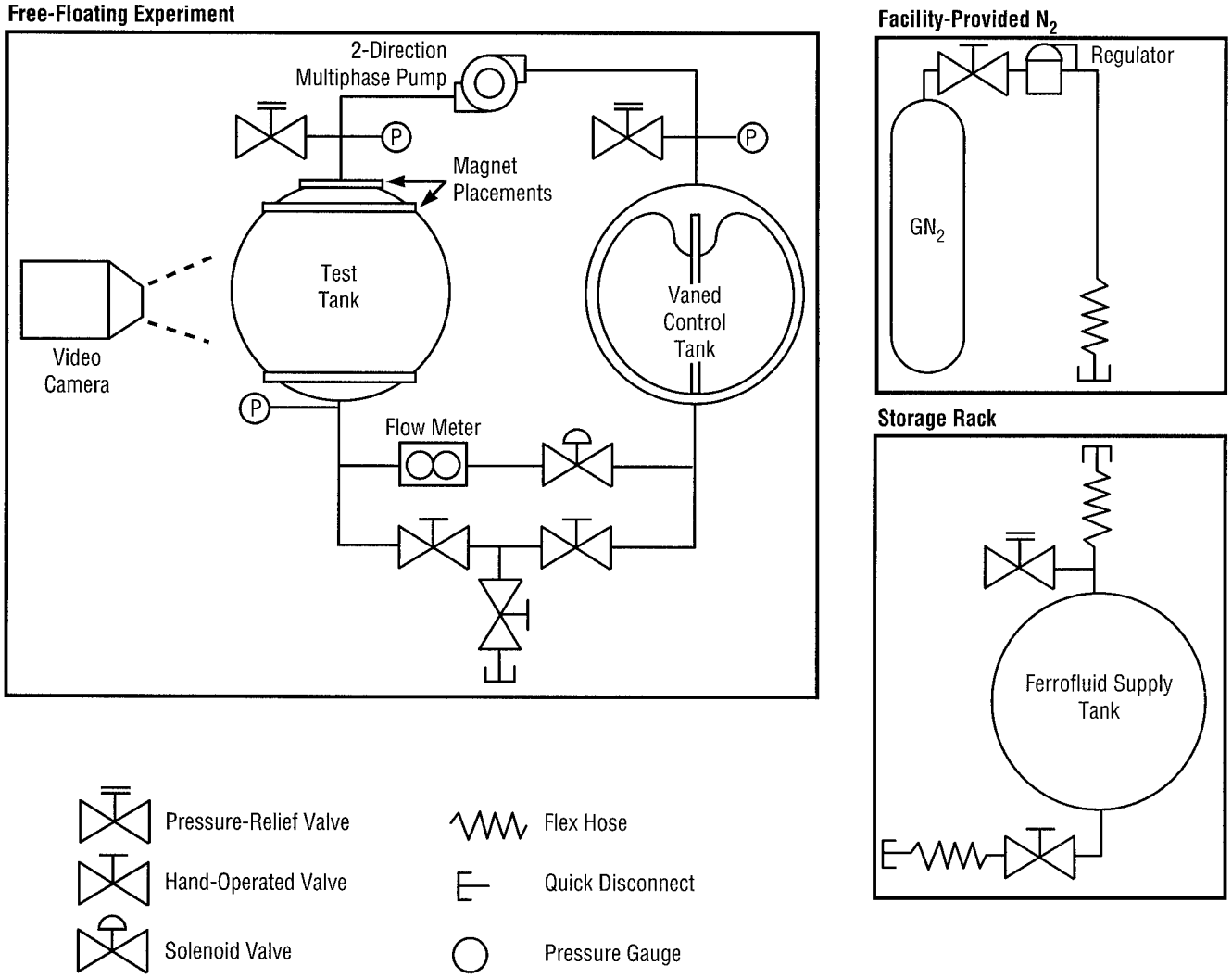

FIGURE 40.—Subscale hardware to be used in KC–135 experiments.

tension), along with tank diameter, flow rates, and magnetic field intensities, are being scaled to model liquid-oxygen behavior in a spacecraft-type application. Design and assembly of the test article is completed, and the facility flew aboard the KC–135 in September 1995. Two other series of tests will be conducted in April and June of 1996.

Scaling analyses have shown that magnets in the size range of 1 to 10 Tesla should be adequate for propellant reorientation in a full-scale liquid-oxygen application. These results, however, are rather limited since the fields can typically assume very complicated geometries, which are difficult to characterize in terms of dimensionless groupings. Consequently, another aspect of this activity is focused on modifying an existing computational fluid dynamic to include the body and surface forces arising from the interactions between the fluid and magnetic field. This will provide a more rigorous means of assessing fluid behavior and will enable the modeling of more complicated field geometries and advanced concepts, e.g., liquid hydrogen. Videotaped recordings of fluid motions taken from the low-gravity tests will be used to validate the revised computational fluid dynamics model.

Sponsor: Center Director's Discretionary Fund

Main and Preburner Injector Technology

John Hutt/EP13
205–544–7125

MSFC is currently conducting combustion research of injector elements using small windowed combustors. The objectives of this testing—which will be accomplished with a combination of advanced laser diagnostics and traditional engineering measurements—are to provide data that can be used to design liquid-propellant rocket injectors for optimum operation with respect to performance, heat transfer, combustion stability, and materials compatibility. The foundation of the laser measurements will be based on data sets of temperature, chemical species, velocity field, and liquid droplet distribution through the application of Raman spectroscopy, laser Doppler velocimetry, and phase Doppler particle analysis.

A test rig has been delivered to MSFC currently configured to test an Aerojet unielement combustor (fig. 41). Tests began October 15, 1995, with the initial test series to study the performance of a swirl coaxial injector element designed for use in a liquid-oxygen/gaseous-hydrogen oxidizer-rich preburner for application to the reusable launch vehicle engine concepts. The Aerojet combustor is designed to operate at pressures up to 10,300 kiloPascals (1,500 pounds per square inch).

In parallel, an effort to build a NASA-owned combustor is underway. This combustor will be designed and fabricated in-house and has been

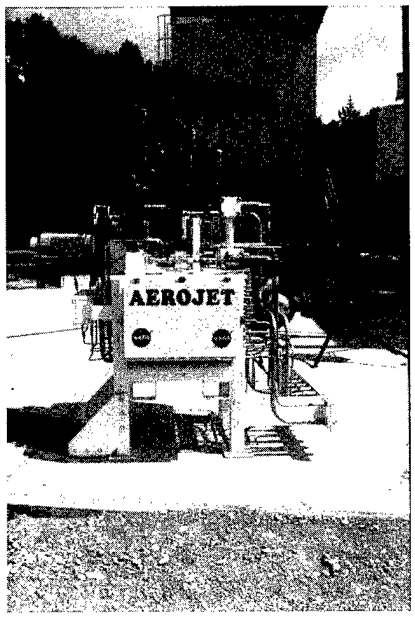

FIGURE 41.—Main and preburner injector technology.

currently designated as the Modular Combustion Test Article. This test article will be designed for higher operating pressures, with the capability of testing single- and multiple-element configurations with liquid-oxygen flow rates up to 4.5 kilograms per second (10 pounds per second). A modular design concept will allow operating pressures of up to 41,300 kiloPascals (6,000 pounds per square inch) to be tested in an unwindowed configuration, with plans to attempt windowed measurements at pressures above 13,800 kiloPascals (3,000 pounds per square inch).The Modular Combustion Test Article will support the engine development for the Reusable Launch Vehicle program. Injector technologies identified for the study include improved fuel-rich preburners with respect to turbine environment and throttleability, oxidizer-rich preburner injector

design, gas-gas injector design, and improved liquid-gas main injectors. The test article has also been identified as a possible test-bed for liquid-oxygen-rich materials testing. The current plan is to phase from the Aerojet test article to the Modular Combustion Test Article in March 1996.

In the past, engine development has involved extensive trial and error testing of much larger hardware with much more limited data, making substantial technology advances prohibitively expensive. Use of small windowed combustors for designing rocket engine injectors represents an application of state-of-the-art technology that will greatly reduce development time and costs of new engine hardware.

Sponsor: Office of Space Access and Technology

Industry Involvement: Aerojet Tech Systems, Pratt & Whitney

University Involvement: Pennsylvania State University, University of Alabama in Huntsville

Tripropellant Injector and Combustion Technology

Huu P. Trinh/EP12
205–544–2260

A tripropellant engine provides an opportunity to burn hydrocarbon fuel with oxygen efficiently during the boost phase and hydrogen with oxygen afterwards. This concept offers possible advantages for application in a reusable launch vehicle for reasons of weight and cost savings, since only one engine needs to be developed.

To advance the state of the art with respect to the development of injection elements, Pennsylvania State University has designed two types for testing. The first one, a tricoaxial swirl injector (fig. 42), uses the swirling liquid RP–1 in the center and is subsequently surrounded by cylindrical co-flowing jets of gaseous hydrogen and gaseous oxygen. The rotating RP–1 leaves the center post and forms a hollow cone at a 35-degree angle. The inner radii of the RP–1, gaseous hydrogen, and gaseous oxygen exit openings are 0.135, 0.165, and 0.345 inch, respectively.

The second type, an effervescent atomizer (fig. 43), is similar in design to a shear coaxial element. The major difference is that both fuels, RP–1 and gaseous hydrogen, share the center post. The gaseous hydrogen flow enters the liquid RP–1 through three holes located upstream of the center post-exit plane and forms the effervescent fluid. The inside diameter of the center post is 0.5 inch, whereas the inner and outer diameters of the gaseous oxygen annulus are 0.18 and 0.5 inch, respectively. During cold-flow testing with gaseous nitrogen and water simulants, liquid drop sizes were obtained from photographs, which

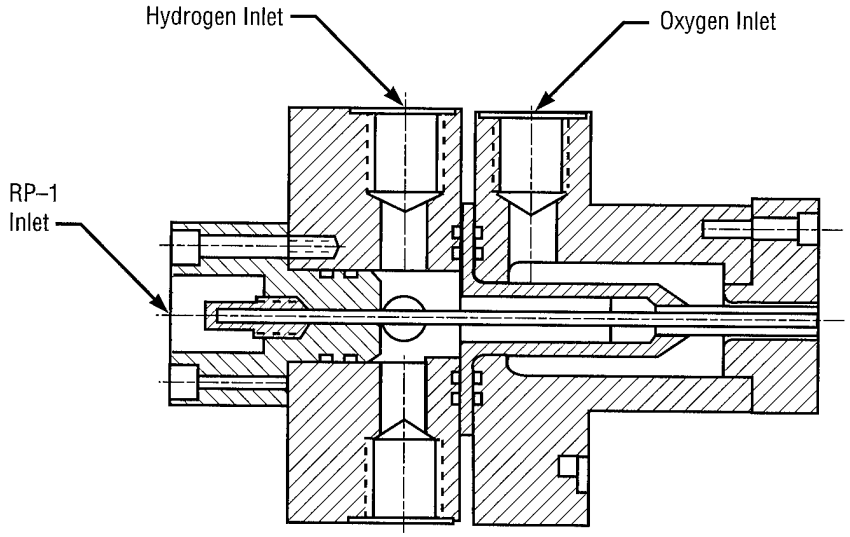

FIGURE 42.—Tricoaxial swirl injector for gaseous oxygen/RP–1/gaseous hydrogen.

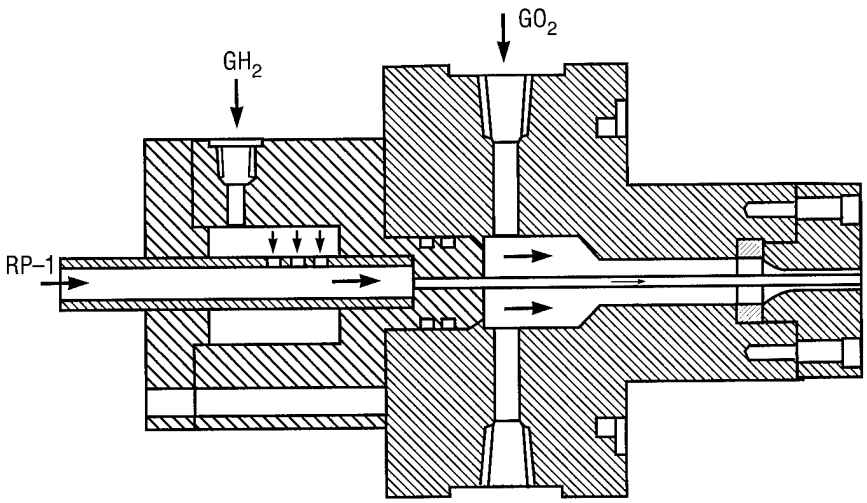

FIGURE 43.—Effervescent injector for gaseous oxygen/RP–1/gaseous hydrogen.

indicate that the liquid atomization improves significantly with increasing the gas-to-liquid volumetric ratio.

An initial series of tests has been conducted with both injection elements, using a 2- by 2-inch unielement combustor. For the tripropellant operation, an overall optimum mixture ratio of oxidizer to fuel was based upon an established mixture ratio of gaseous oxygen/RP–1 of 2.4 (yielding high performance), together with the stochiometric mixture ratio for gaseous oxygen/hydrogen of 8.0 (producing the maximum temperature). Test results using various mass percentages of gaseous hydrogen were then compared with the experiments in which no hydrogen was injected at all. The results revealed that for an increase of hydrogen up to 10 percent, the combustion efficiency, η_{c*}, rose from 82 percent to 98 percent for the tricoaxial swirl-injection element, while an increase from 83 percent to 96 percent was noticed for the effervescent element. The higher combustion efficiency may be caused by a combination of the gaseous oxygen/hydrogen combustion and improved RP–1 atomization due to momentum transfer between the gaseous hydrogen and RP–1 flows.

Penn State is currently performing parametric hot-fire tests to provide details of the combustion flow field and injector performance characteristics.

Sponsor: Office of Space Access and Technology

University Involvement: Robert J. Santoro and Charles Merkle, Propulsion Engineering Research Center, Pennsylvania State University

Effects of Hydrogen Addition on RP–1 Droplet Burning in Oxygen Environment

Huu P. Trinh/EP12
205–544–2260

At present, the knowledge of processes occurring from propellant injection to combustion is limited for the tripropellant operation. Foreign researchers[1] have reported improved combustion efficiencies by adding small amounts of gaseous hydrogen to the gaseous oxygen/RP–1 reaction. Since the physical mechanism is not well understood, MSFC has initiated research in this matter under a NASA Research Announcement with the Propulsion Engineering Research Center of Pennsylvania State University. The results will be used to advance injection technology for tripropellant combustion application.

To investigate the impact of hydrogen addition to the gaseous oxygen/RP–1 combustion, an apparatus (fig. 44) was constructed to conduct experiments at Penn State. The test module is equipped with a droplet generator, flame burner, and a glass chimney for photographic observation. A flash-illumination system and camera were positioned downstream of the burner to record the RP–1 drop-size variation. Experiments were conducted on isolated individual RP–1 droplets burning in a pure oxygen environment, to which co-flowing hydrogen gas was added. From the high-magnification images of the droplets, the droplet velocity and size were determined in addition to other independent measurements. A comparison of the

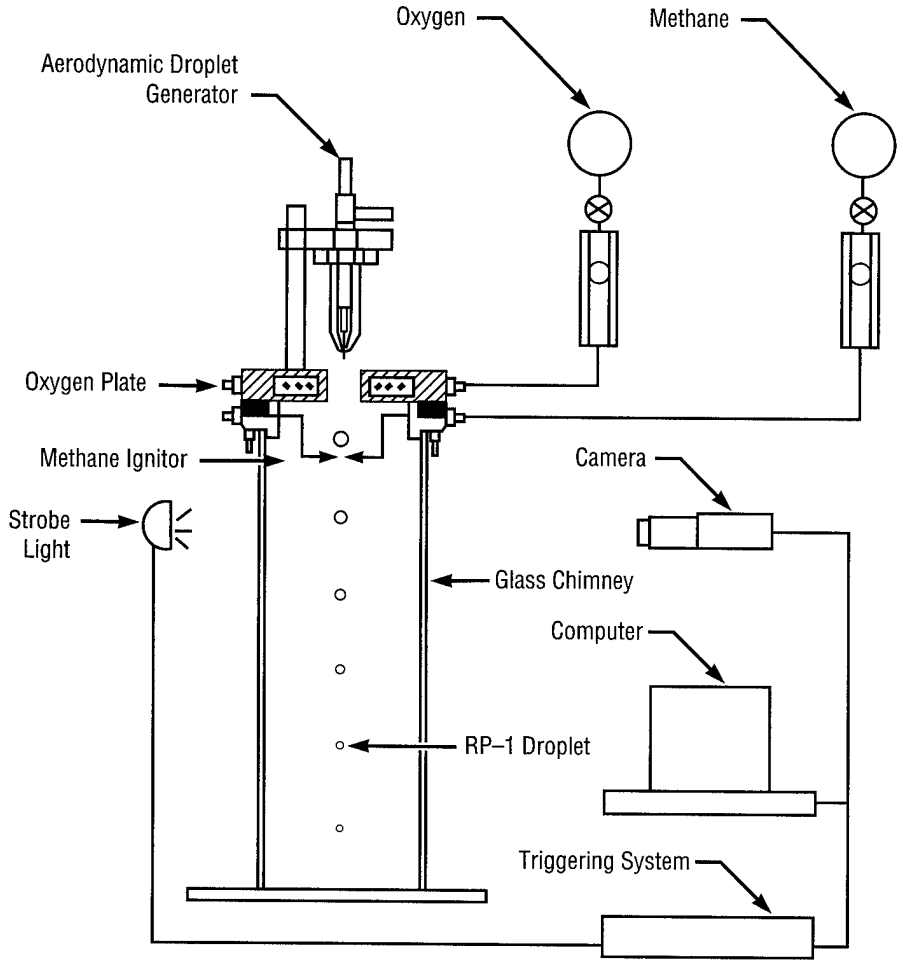

FIGURE 44.—Schematic of the experimental setup.

droplet lifetime burning in an environment with and without hydrogen addition was made (and is shown in fig. 45, together with the respective analytical predictions). The results indicate that the addition of hydrogen has no significant effect on the regression rate of the RP–1 droplet.

Reported improvements of combustion efficiency from other tripropellant combustion studies may be caused by the hydrogen affecting the RP–1 fuel-atomization process.

Penn State independently performs additional detailed measurements to verify the results and provide an experimental data base for future combustion modeling efforts.

[1]Ono, Fumiei, et al. July 1992. Effects of Hydrogen Addition on Combustion Performance of a Lox/Kerosene Rocket. Technical Report of National Aerospace Laboratory, TR–1177.

Sponsor: Office of Space Access and Technology

University Involvement: Robert J. Santoro and Charles Merkle, Propulsion Engineering Research Center, Pennsylvania State University

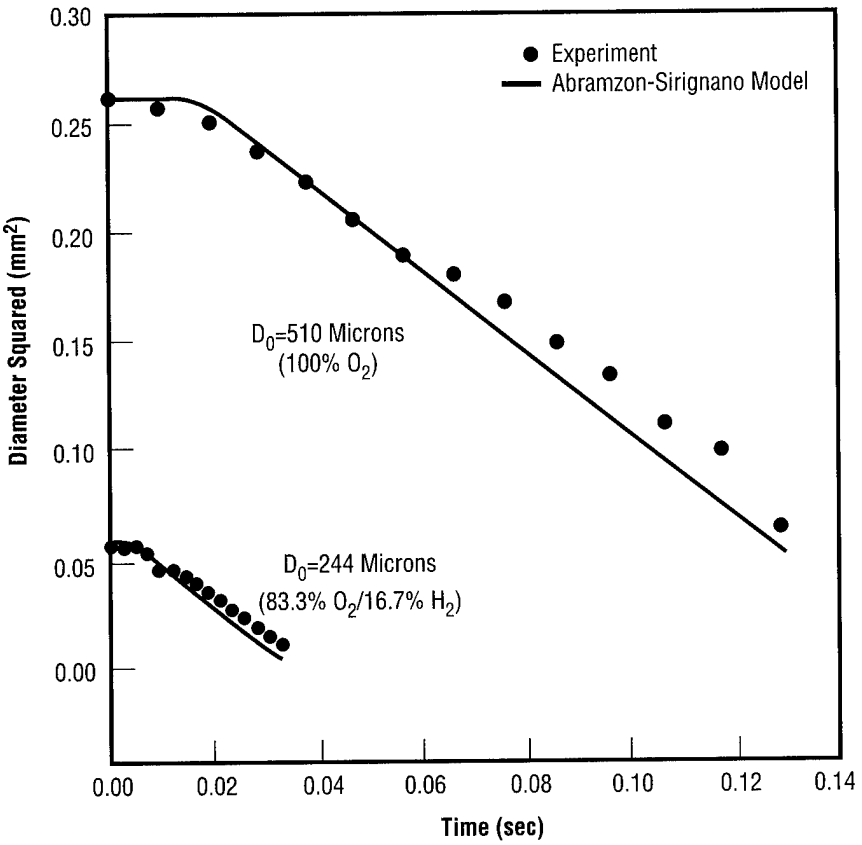

FIGURE 45.—History of RP–1 droplet size in the burning process. (Solid curves generated from Abramzon-Sirignano vaporation model at 100-percent gaseous oxygen.)

Unielement, Oxygen-Rich Preburner

Huu P. Trinh/EP12
205–544–2260

A full-flow, staged combustion cycle using an oxygen-rich preburner has been a candidate for use on the proposed reusable launch vehicle. The oxygen-rich combustion gas used to drive the turbine system would have a high density; consequently, the required turbine power can be obtained by the low-temperature preburner products. This will improve turbopump operability and durability. However, before full-scale engine development can proceed, the issues of ignition characteristics, flame stability, temperature striation, and combustion performance in the preburner at high oxidizer-to-fuel mixture ratio must be resolved (in addition to material compatibility). MSFC and the Propulsion Engineering Research Center of Pennsylvania State University are jointly investigating advanced injection techniques for the oxygen-rich preburner.

In this effort, two types of injection techniques will be examined. The first one, direct injection, has propellants being directly introduced at the injector face of the preburner. The other technique, near-stoichiometric/dilution injection, has the fuel and some oxidizer flow through the injector face at a stoichiometric mixture ratio. The combustion hot gas is then diluted with the rest of the oxidizer downstream. The current effort emphasizes the direct injection technique using a coaxial swirl injector for the liquid oxygen and gaseous hydrogen.

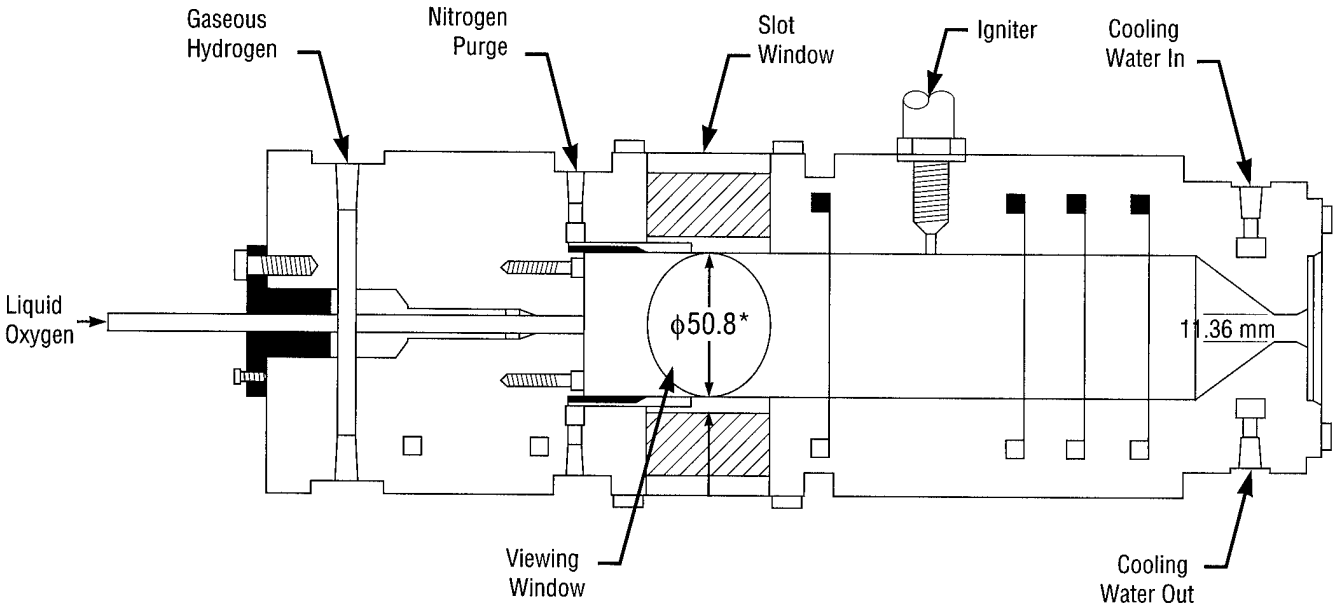

FIGURE 46.—Schematic of unielement combustor.

The experiment was conducted with a 2- by 2-inch square combustor (fig. 46). Liquid oxygen enters into the chamber through the center injection post in a swirling motion, and gaseous hydrogen flows through the outer annulus of the injection element. The hot-fire tests were accomplished for chamber pressures from 140 to 500 pounds per square inch and a mixture ratio range of 3 to 166. (The C* efficiencies for two chamber pressures of 200 and 300 pounds per square inch are shown in fig. 47.) The results show that the efficiency is better than 92 percent for both conditions. For higher chamber pressures, the hydrogen density is proportionally increased and causes a reduced injection velocity for a given flow rate. The associated degradation in liquid-oxygen atomization tends to reduce the combustion efficiency. Typical chamber-pressure traces of the hot-fire tests have been plotted

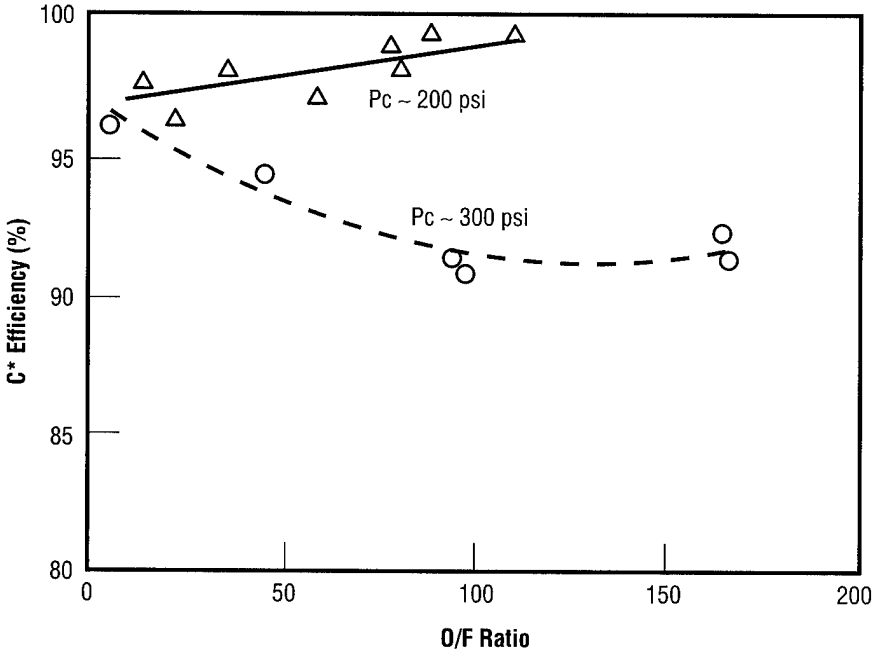

FIGURE 47.—C* efficiency at chamber pressures of 200 and 300 pounds per square inch.

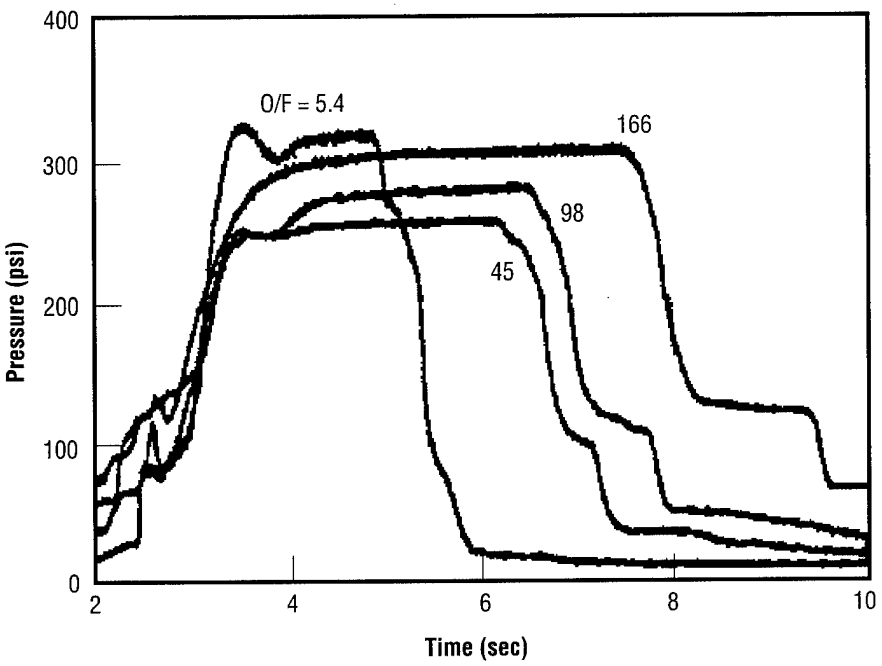

FIGURE 48.—Typical chamber-pressure traces for mixture ratio range from 5.4 to 166.

(fig. 48), and the data indicate stable burning after the ignition period.

At present, Penn State continues testing the swirl coaxial injector to provide detailed information of the combustion behavior and flow-field characteristics. In addition, the injector for the RP–1/liquid-oxygen propellant system and the near-stoichiometric/dilution injector are being designed. MSFC is in the process of testing similar injectors at higher chamber pressures.

Sponsor: Office of Space Access and Technology

University Involvement: Robert J. Santoro and Charles Merkle, Propulsion Engineering Research Center, Pennsylvania State University

Ultrasonic Fuel Regression Measurement in Hybrid Rocket Motors

Dan M. Holt/EP12
205–544–4949

A technique for utilizing ultrasonic transducers to measure hybrid motor fuel regression rates during motor operation was developed and demonstrated on the Large Subscale Solid Rocket Combustion Simulator Program. This technique consisted of installing specially developed ultrasonic transducers into solid rocket combustion simulator motor cases (11 and 24 inches in diameter) configured with a specially formulated hybrid fuel designed to simulate a solid rocket motor exhaust environment.

The transducers, developed by MSFC and contractors Lockheed Martin Astronautics and Thiokol Space Operations, consisted of dual-pitch/catch units installed in a single

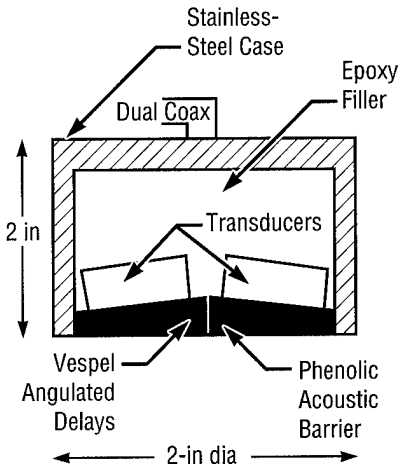

FIGURE 49.—Ultrasonic transducer.

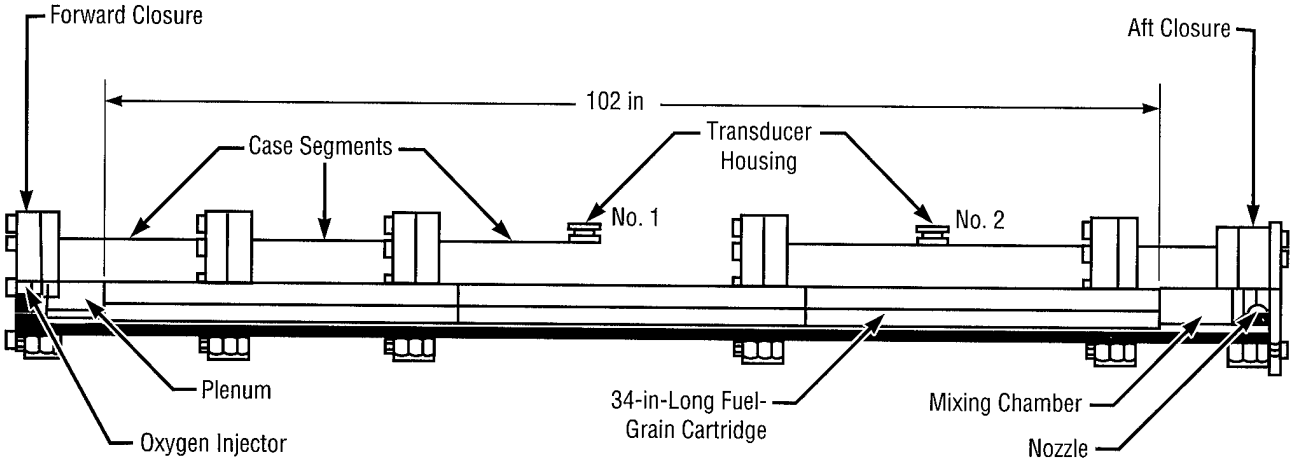

FIGURE 50.—11-inch motor configuration.

stainless-steel housing (fig. 49). The transducers were installed along the length of the motors and successfully measured fuel regression during motor operation by sending ultrasonic signals through the fuel and recording the time it takes for the signal to return to the unit (fig. 50): thus, the terminology "pitch/catch"—one unit pitches the signal, the other catches it. Running controlled samples in the laboratory and on the motors prior to firing allowed the team to establish a known factor for the densities of the fuel and case materials. This factor represents the time for the ultrasonic pulse to travel through a given thickness of fuel and back again. During motor operation, as the fuel regresses (burns back), the thickness changes, thereby measuring the time it takes for the signal to travel back and forth. The transducer sends signals continuously during motor operation, and—with the aid of a personal computer—graphical interpretations are generated to represent grain regression (fig. 51).

Posttest measurements verified the accuracy of the system within 0.002 inch of physical measurements. The incorporation of such an ultrasonic measurement system in future hybrid and solid motor testing will allow substantial cost and time savings over the traditional methods of disassembling motors and performing physical measurements in a number of locations. In addition, ultrasonic fuel regression measurements made in real time during a motor firing allow scientists and engineers to adjust hybrid oxidizer flow rates in real time to obtain steady oxidizer flux rates, if needed, for enhanced solid rocket motor simulation.

The techniques developed and proven on the Solid Propulsion Integrity Program will be used to measure fuel regression rates on motors ranging from 11 to 70 inches in diameter during the Hybrid Propulsion Demonstration Program, beginning in late 1995. The Hybrid Propulsion Demonstration Program is a consortium of industry and government participants utilizing a combination of private and public funding to further develop hybrid propulsion technology. This program will culminate in the test-firing of space booster-sized motors (producing 250,000 pounds of thrust) at MSFC. The real-time measurement of fuel regression during static tests by way of ultrasonic measurements is an integral portion of this important new propulsion technology development.

Boardman, T.A.; Porter, L.G.; Brasfield, F.W.; and Abel, T.M. July 1995. An Ultrasonic Fuel Regression Rate Measurement Technique for Mixture Ratio Control of a Hybrid Motor. Paper 95–3081, 31st American Institute of Aeronautics and Astronautics/ American Society of Mechanical Engineers/Society of Automotive Engineers/American Society of Electrical Engineers Joint Propulsion Conference and Exhibit.

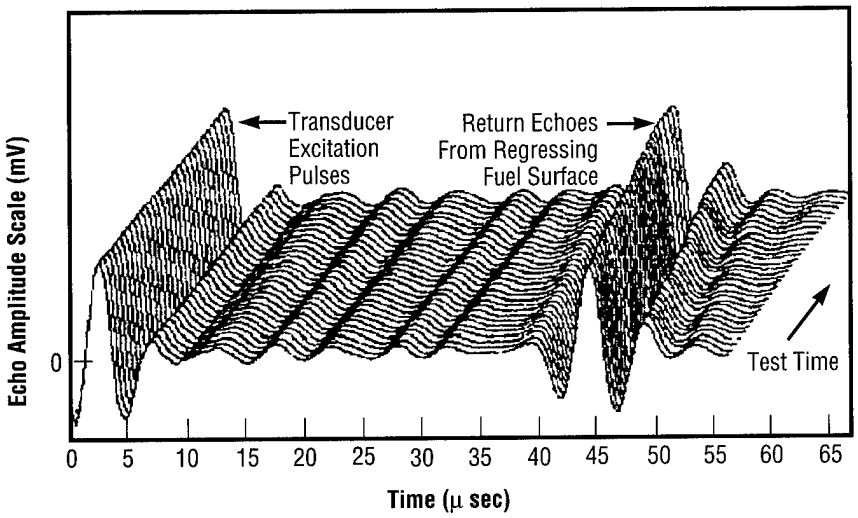

FIGURE 51.—Graphic representation of grain regression measurement.

Sponsor: Office of Space Access and Technology

Industry Involvement: Lockheed Martin Astronautics, Thiokol Space Operations, and Ultran Laboratories

Results of an 11-Inch Liquid-Oxygen Hybrid Rocket Motor Combustion Instability Study

Charles Martin/EP12
205–544–7098

Several test programs have been undertaken at MSFC to study the factors (independent variables) contributing to hybrid motor chamber pressure oscillations. Results from these programs reveal that the hybrid motor is a complex system which can best be understood through logical systematic testing. The test series of eight motors described in this overview uses a design of experiments approach that allows for identification of factors and their interactions. For this study, an interaction exists if—and only if—the effect of one factor depends on the level of another factor. Factors under investigation included liquid-oxygen (lox) flow rate/nozzle throat diameter (flowdt), injector pattern (injpat), and the pressure drop across the injector (deltap). The liquid-oxygen flow rate and throat diameter were perfectly correlated (aliased) in an attempt to maintain a constant chamber pressure. Each factor was set at two levels, resulting in a full factorial matrix with eight tests. All other factors in the test series were to remain constant. The test matrix is illustrated in table 3.

Figure 52 is a schematic of the test article. The levels for all three factors could be accomplished by changes made in the injector, nozzle, and feed system. No intentional changes (other than the planned factor levels) were

TABLE 3.—*Test matrix.*

		Deltap*= 50 psi	Deltap*= 200 psi
injpat = axial	flowdt**= 2 lb/sec and 1.05 in	Test #4 (2/A/50)	Test #2 (2/A/200)
injpat = axial	flowdt**= 5 lb/sec and 1.71 in	Test #8 (5/A/50)	Test #1 (5/A/200)
injpat = soild cone	flowdt**= 2 lb/sec and 1.05 in	Test #5 (2/A/50)	Test #3 (2/A/200)
injpat = soild cone	flowdt**= 5 lb/sec and 1.71 in	Test #7 (5/A/50)	Test #6 (2/A/200)

* Injectors are of the impingement type and were designed to produce the same droplet size in all tests.

** A cavitating venturi was used to regulate flow rate and isolate the feed system from the motor chamber oscillations.

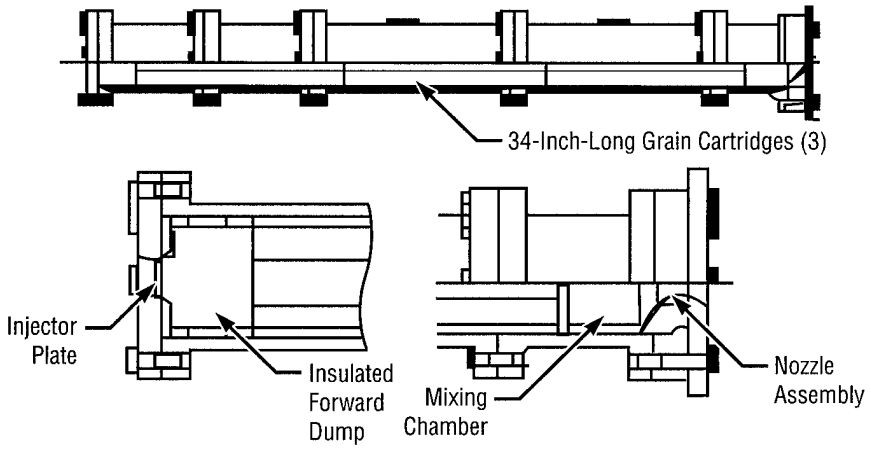

FIGURE 52.—Test article configuration (used with permission from Thiokol Corporation).

made, either to the test article or to the feed system, during the tests.

Following the test series, a statistical analysis was performed on several response (dependent) variables. For each of the response variables, an analysis of variance was performed to determine which factors and factor interactions had significant influence on the behaviors of the response variables. The analysis used a 0.05 level to test for significance. Table 4 defines the response variables.

Flowdt was the primary effect on fuel, fwdbd, aftbd, O/F, tempint, igntim, throat erosion, and frequencies. The flowdt*injpat and the flowdt*deltap interactions have a second-order effect on fwdbd. Several other factors and interactions had third-order effects on some of the response variables. No effects were identified for oscillation amplitude or C*. The proper variables or variable ranges may not have been adequately tested, and some of the results may have been obscured by the small sample size and/or the inability to select the desired independent variable settings.

Several variables had intriguing correlations with each other. These correlations were not within the context of a formal design and, therefore, should not be taken as indications of associations; however, the correlations may be useful in making decisions about the choice of independent variables for future experimental designs. Response variables C* and amplitude had a correlation coefficient of 0.70. The correlation coefficients between amplitude and the chronological order of testing and amplitude and deltap were –0.78 and 0.49, respectively. The correlation coefficient between C* and deltap was 0.63.

Among the four high-flow-rate motors, the motor showing exceptionally high amplitude oscillations also had very low fuel regression at the forward end. While it would have been advantageous to have more data in the axial direction, funding allowed only six axial stations to be measured.

TABLE 4.—*Definitions of response variables.*

Response Variable	Definition
Fuel	Total amount of fuel consumed during each test.
Fwdbd	Fuel regression distance in the forward 3 inches of the forward grain.
Aftbd	Fuel regression distance in the aft 3 inches of the aft grain.
O/F	Total oxygen flow divided by the total fuel consumed.
C*	The product of the pressure integral, average throat area, and the gravity constant divided by the total mass flow. (Not calculated for P2030007 since it dropped out shortly after 10.1 seconds.)
Tempint	Integral term of the aft chamber temperature* from time = 0.0 to time = 10.1 seconds.
Igntim	Time from 0.0 to first peak on the forward chamber pressure.
Throat Erosion	Average throat erosion.
Frequencies	Frequency from Fast Fourier Transforms (FFT) at same time amplitude was chosen.
Amplitude and Roughness	Amplitude — Peak-to-peak amplitude of largest forward chamber pressure oscillations between 8 and 14.2 seconds where a well-organized single frequency could be found using FFT. Roughness — The total vectical length of the forward chamber pressure to 10.1 seconds. (P2030007 dropped out shortly after this time). Amplitude and roughness are attempts at quantifying the magnitude of pressure oscillations. The correlation coefficient between these two is 0.975. This level of agreement suggests that both are good indications of pressure oscillation magnitude.

* The head-end thermocouple does not survive the testing environment.

A logical extension of this work would involve a series of designed experiments to be conducted to investigate droplet size, droplet velocity, droplet direction, characteristic length (L*), chamber pressure, splashblock design (step height), and/or heat addition to the front end of the motor. Once frequencies and amplitudes are understood, burn rates should be investigated.

Pressure Oscillations in Hybrid Rocket Motors

Dan M. Holt/EP12
205–544–4949

Beginning in 1992, a joint government-industry program has been conducted at MSFC to develop hybrid rocket motors. Hybrid rocket motors combine an inert solid fuel grain with a gaseous or liquid oxidizer in an effort to realize the benefits of both liquid and solid rocket motors. This joint effort, funded by both private and public moneys, is known as the Joint Independent Research and Development Hybrid Program.

One of the most significant findings to date has been the recurrence of motor-pressure oscillations under various operating conditions. These oscillations are not unstable in the sense of increasing amplitude, but—in worst-case conditions—they have spiked to double the motor operating pressure before returning to a more uniform pattern. Joint development members MSFC, Thiokol Space Operations, the Rocketdyne Division of Rockwell International, and Lockheed Martin Astronautics are performing extensive research to determine the causes of the observed oscillations and methods for controlling them.

A significant body of research has been devoted to the problem of flame stabilization in ramjets. Two factors that affect flame stabilization are the temperature of incoming gas and the flow field at the entrance to the fuel grain. Because of the similarity of hybrids and ramjets, it is reasonable to assume the same factors will affect

flame stability in hybrid rocket motors. The similarities between hybrids and ramjets and results from an earlier industry independent research and development program provided the basic hypothesis for this program: namely, flame stabilization at the entrance to the fuel grain is required for smooth hybrid motor combustion. This program is investigating the effects of liquid-oxygen flow rates, head-end flow fields, and liquid-oxygen vaporization on hybrid pressure oscillations. Each of these factors is thought to directly affect establishment of a stable flame at the entrance of a fuel-grain port.

To date, all program effort has used a liquid-oxygen-fed motor (24 inches in diameter). Figure 53 is a schematic for the motor. The major case components are forward closure, vaporization chamber, grain sections, mixing chamber, and aft closure. The motor is designed to allow for the lengths and configurations of each of its components to be varied.

All tests use identical, monolithic, seven-port fuel grains (108 inches in length). A typical test duration is 10 seconds. Parameters that have been varied in the program include liquid-oxygen flow rate (10, 20, and 40 pounds mass per second), injector flow pattern (axial and solid cone), fuel configuration in the vaporization chamber (domed or domed with fins), and the degree of coupling between the motor and the feed system.

In tests for which the feed system has not been isolated from the motor, organized 5- to 10-hertz oscillations have occurred. When there has been a high degree of isolation between the motor and the feed system, the motor has operated with only minimal combustion roughness. The isolation has been provided for each by an orifice or venturi close to the injector and by a high-pressure drop across the injector. In each case, the result was a disappearance of the oscillations. Examples of oscillatory and nonoscillatory behavior are shown in figures 54 and 55.

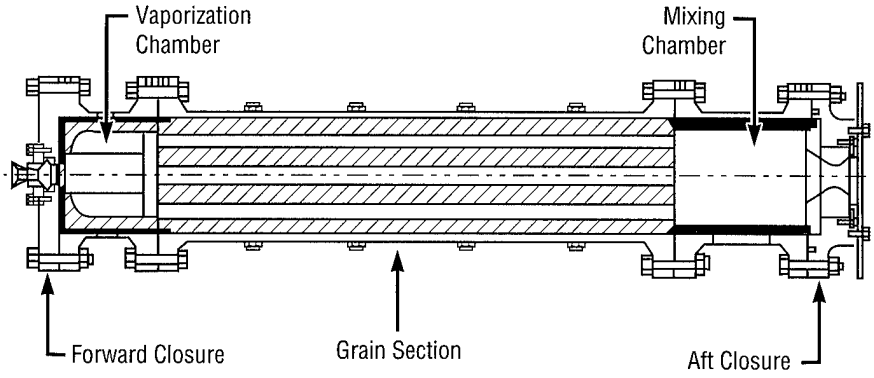

FIGURE 53.—24-inch motor configuration.

To date, the motor has operated without oscillations at all flow rates and with both finned and nonfinned head ends. At fluxes tested thus far (up to 0.73 pound mass per second per square inch), the vaporization chamber fuel configuration has not had a significant impact on the smoothness of the pressure trace. Future testing will push the flux to 1.0 to determine the effect on combustion. These future

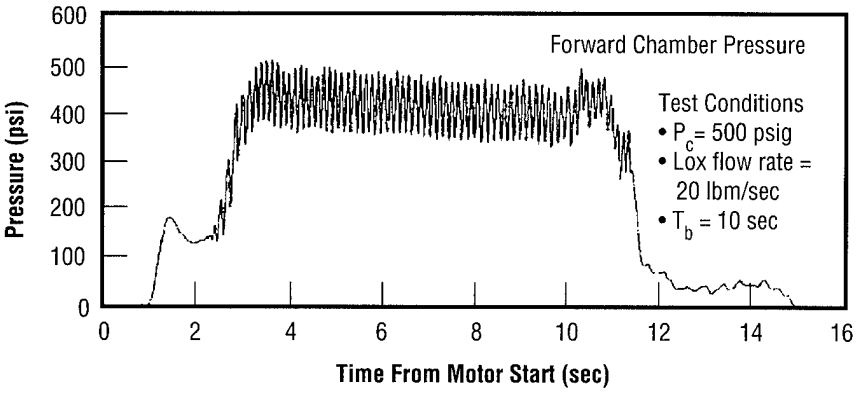

FIGURE 54.—Oscillations resulting from a coupling of motor and feed system.

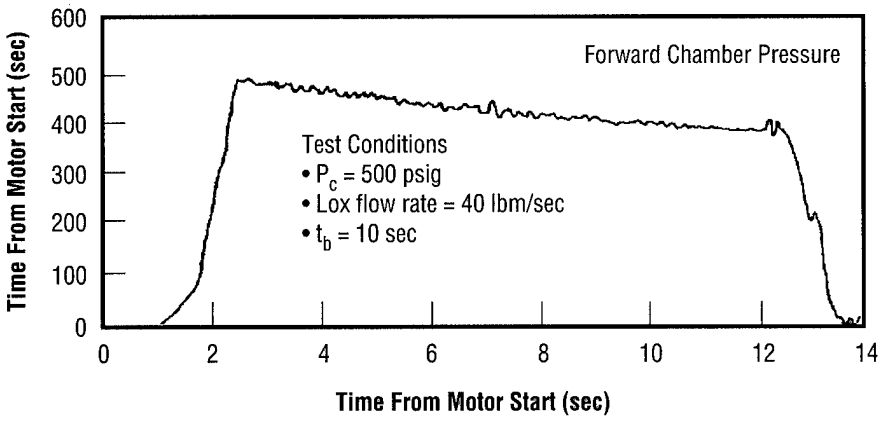

FIGURE 55.—Nonoscillatory combustion that occurs when isolation between motor and feed system is increased.

efforts will be integrated to form a part of the Hybrid Propulsion Demonstration Program.

Boardman, T.A.; Brinton, D.H.; Carpenter, R.L.; and Zoldaz, T.F. July 1995. An Experimental Investigation of Pressure Oscillations and Their Suppression in Subscale Hybrid Rocket Motors. Paper 95–2689, 31st American Institute of Aeronautics and Astrophysics/American Society of Mechanical Engineers/Society of Automotive Engineers/American Society of Electrical Engineers Joint Propulsion Conference and Exhibit.

Carpenter, R.L.; Boardman, T.A.; Claflin, S.E.; and Harwell, R.J. July 1995. Hybrid Propulsion for Launch Vehicle Boosters: a Program Status Update. Paper 95–2688, 31st American Institute of Aeronautics and Astrophysics/American Society of Mechanical Engineers/Society of Automotive Engineers/American Society of Electrical Engineers Joint Propulsion Conference and Exhibit.

Sponsor: NASA/MSFC Propulsion Laboratory Nonreimbursable Space Act Agreement

Industry Involvement: Thiokol Space Operations, Rocketdyne Division of Rockwell International, and Lockheed Martin Astronautics

Solid Rocket Motor Asbestos-Free Insulation

John O. Funkhouser/EP12
205–544–7105

Health-hazard concerns and decreasing availability have necessitated the replacement of the present reusable solid rocket motor asbestos/silicon dioxide-filled, acrylonitrile butadiene rubber internal case insulation material with asbestos-free insulators. The primary objective is to develop and qualify an asbestos-free internal case insulation design that will demonstrate equal or better erosion performance at a reasonable cost.

Material selection procedures with subscale testing have produced two candidate materials which will undergo full-scale testing in late 1995. Aramid-filled, ethylene propylene diene monomer is proposed for both materials. A 7-percent Aramid-filled material is recommended for all of the internal case insulation except for the aft dome, where an 11-percent Aramid-filled insulator may be required. Subscale tests have demonstrated greater erosion resistance with the 11-percent Aramid-filled material in the high-impingement aft dome area.

The design recommendations for the first full-scale motor test were derived primarily from a single 48-inch subscale test motor designed to duplicate the full-scale motor aft dome environment. Analysis had to be based on only three data measurements per station location. This limited data base

precluded any traditional statistical analysis approach. A subjective decision had to be made based on all appropriate comparative methods. Mean values (with corresponding variances) were evaluated, along with maximum loss values. Comparison techniques were prioritized and assigned either a conservative or nonconservative rating. Controversial data from two critical stations provided additional concern and were evaluated with less emphasis. Based on an estimated probability of failure no greater than 1 per 100 motors, a decision was made to approve the full-scale test insulation design with less-than-desired reliability in the aft dome area.

Data evaluation methodology established for the two proposed insulation materials will greatly enhance analysis of data from the first full-scale test motor. A similar evaluation based on very limited data will determine the internal case insulation design for subsequent static and flight motors. The results of this endeavor will be a more efficient reusable solid rocket motor in terms of cost and reliability. Innovations derived for the statistical analysis of solid rocket motor internal case insulation erosion performance with limited data should benefit the entire solid rocket motor industry.

Sponsor: Space Shuttle Projects Office

Industry Involvement: Thiokol Corporation Space Operations

Hybrid Rocket Cold-Flow Modeling

Wendy Cruit/EP12
205–544–1130

Due to recent renewed interest in hybrid rocket motors, MSFC has participated in several hot-fire hybrid test programs. A major concern in several of these tests has been low-frequency pressure oscillations within the motor combustion chamber. The Propulsion Laboratory's Motor Systems Division, in conjunction with Auburn University's Dr. Rhonald Jenkins, submitted a Center Director's Discretionary Fund proposal to investigate such oscillations (approved September 1995). Through ongoing research at MSFC's Structures and Dynamics Laboratory, Fluid Dynamics Division, some of the mechanisms causing the oscillations are now being studied. A laboratory-scale, two-dimensional, water-flow model of a hybrid rocket motor has been built and installed in a closed-loop, water-flow facility to aid in the research.

The hybrid model is patterned after a shear-flow water tunnel developed in 1990 to investigate fluid-flow exiting porous materials.[1] The side walls are constructed of clear acrylic for flow visualization and optical velocity measurements; the top and bottom walls are constructed of a porous metal plate that simulates a solid propellant burning surface, the fuel of a hybrid motor. Oxidizer flow is also simulated with water and enters through an injector of axial or radial orientation (fig. 56). Reference figure 57 for a hybrid cold-flow model installed in a test fixture.

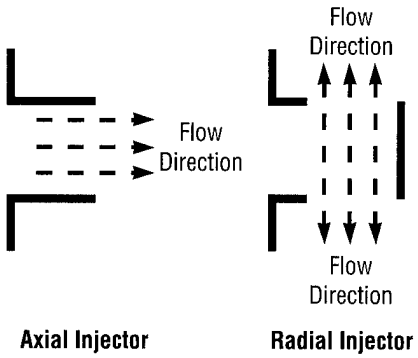

FIGURE 56.—Diagram showing flow direction of axial and radial injectors.

Flow interaction between the hybrid injector and motor sections is qualitatively understood by injecting helium bubbles and recording their movement with a 1,000-frames-per-second video recorder. Currently, the flow patterns are being assessed for the different configurations in the head end and immediately downstream of the head end. The vortex shedding frequencies are also being studied to determine if there is an association between the shedding frequency and the low-frequency pressure oscillations.

Quantitative flow-field mapping is accomplished with a laser Doppler velocimeter. Velocity vectors are constructed from the two components and show the recirculation zones created by the radial injector and the stagnation regions resulting from "flame-holding" steps in the diameter between the injector and motor (fig. 58).

This hybrid modeling effort is contributing to the hybrid community by generating a parametric data base

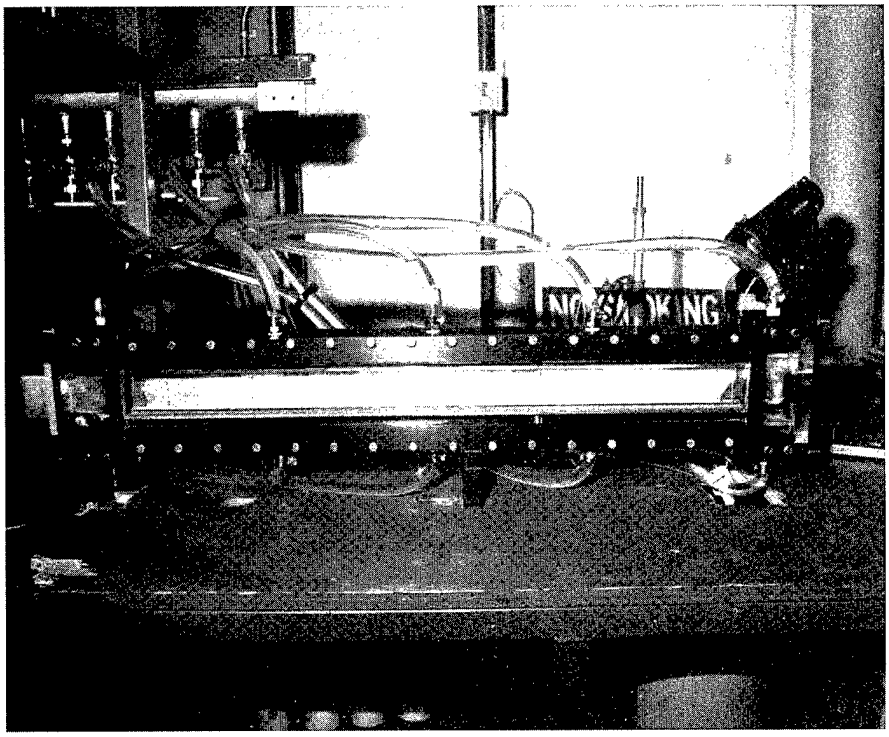

FIGURE 57.—Hybrid cold-flow model installed in test fixture.

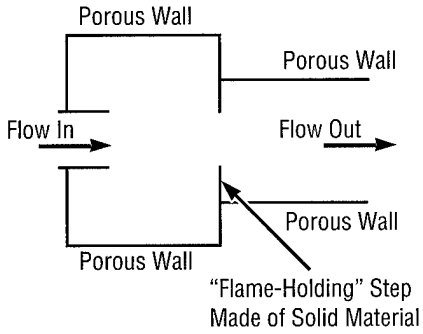

FIGURE 58.—Diagram of model showing "flame-holding" steps.

of the fluid dynamics in such motors and providing test-bed capability to answer current hybrid rocket motor questions and those that will arise in the future.

[1]Smith, A. 1993. Porous Wall Flow Experimental Facilities. *Research and Technology 1993*, 178–179.

Sponsor: Center Director's Discretionary Fund

■■■■■

Development and Demonstration of a 250-Kilopound-Force Hybrid Rocket Test-Bed

Dan M. Holt/EP12
205–544–4949

Recent increased interest in hybrid propulsion technology has prompted the formulation of an industry-led consortium to design, fabricate, and test a 250-kilopound-force thrust hybrid rocket booster system at MSFC's East Test Area. Hybrid rocket motors combine an inert solid-fuel grain with a gaseous or liquid oxidizer in an effort to realize the benefits of both liquid and solid rocket motors.

The new program, the Hybrid Propulsion Demonstration Program, combines efforts from the Hybrid Technology Option Project, the Hybrid Propulsion Technology for Launch Vehicle Boosters program, and the redirected Solid Propulsion Integrity Program. Participants include MSFC, Lockheed Martin Astronautics, Thiokol Space Operations, United Technologies Chemical Systems Division, the Rocketdyne Division of Rockwell International, Allied Signal, Lockheed Martin Manned Space Systems, and Environmental Aeroscience.

Hybrid propulsion activities have been ongoing at MSFC for several years through testing of the 11- and 24-inch motor systems at test stand 500. These motors will continue to be utilized to evaluate critical technology issues, including combustion stability, fuel utilization and web retention, nozzle and insulation materials response, and

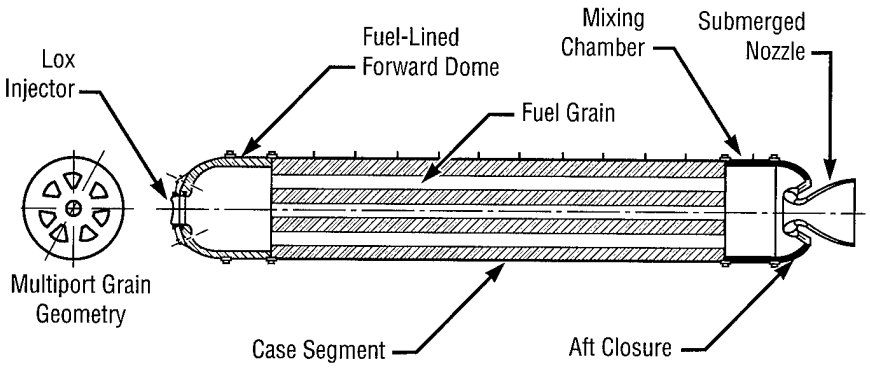

FIGURE 59.—250-kilopound-force hybrid motor design concept.

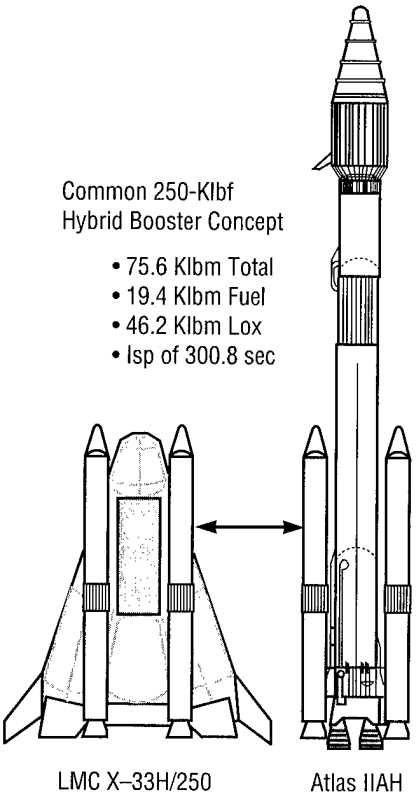

FIGURE 60.—Common hybrid booster concept.

scale-up effects. Test results along with system studies will influence the large motor design. MSFC facilities, including feed, ignition, pressurization, and purge systems, will be expanded to support the testing of the 250-kilopound-force thrust motor system. MSFC science and engineering personnel will also provide for test and evaluation of the nozzle and insulation materials.

Hybrid propulsion is being considered for advanced launch vehicle applications due to advantages gained in safety, cost, environmentally benign combustion products, attractive performance, and mission flexibility relative to current rocket boosters. Recent advancements in the area of hybrid propulsion research have indicated potential application to both the expendable launch vehicle fleet and future launch vehicles. Figure 59 illustrates an early conceptual design for the 250-kilopound-force hybrid motor. The major case components include a domed forward closure, vaporization chamber, grain segment, mixing chamber, and aft closure. A submerged nozzle with exit cone is planned, with initial test capability targeted for December 1996.

The goal of the program is to demonstrate critical hybrid propulsion technologies at the 250-kilopound-force thrust scale to minimize future full-scale development risk. Preliminary concepts of the booster show promise for application to both the X–33 Advanced Technology Demonstrator and the Atlas launch vehicle. Following completion of the X–33's technology demonstration phase, hybrid boosters are being considered to provide for commercialization and mission envelope expansion. Substitution of hybrid rocket boosters on the Atlas launch vehicle increase geosynchronous transfer orbit payload capability from approximately 8.1 to more than 10 kilopound mass in projected evolutionary schemes. Figure 60 illustrates a hybrid booster concept sized to support Lockheed Martin's X–33 Advanced Technology Demonstrator and the Atlas IIAH. Detailed cost studies and booster/launch vehicle trade studies will be performed to optimize these concepts.

Abel, T.M.; Carpenter, R.L.; Claflin, S.A.; Crawford, J.T.; and Holt, D.M. July 1995. Solid Rocket Motor Simulation and Hybrid Propulsion Testing at the Marshall Space Flight Center. Paper 95–2944, 31st American Institute of Aeronautics and Astronautics/American Society of Mechanical Engineers/Society of Automotive Engineers/American Society of Electrical Engineers Joint Propulsion Conference and Exhibit.

Sponsor: Office of Space Access and Technology

Industry Involvement: Lockheed Martin Astronautics, Thiokol Space Operations, United Technologies Chemical Systems Division, Rocketdyne Division of Rockwell International, Allied Signal, Lockheed Martin Manned Space Systems, and Environmental Aeroscience

Other Involvement: Advanced Research Projects Agency, U.S. Air Force Phillips Laboratory

Solid Rocket Combustion Simulation Using the Hybrid Combustion Process

Dan M. Holt/EP12
205–544–4949

Historically, test evaluation of new designs, materials, and processes for solid rocket motor nozzles and insulators at MSFC has been carried out using heavyweight, facility solid rocket motor test-beds. However, if the solid-propellant combustion environment and associated nozzle/insulation material response is simulated using a hybrid motor test-bed, significant cost savings and expanded test flexibility could be achieved. Ongoing testing in the East Test Area, under the Large Subscale Solid Rocket Combustion Simulator program, has led to the development of a family of solid rocket combustion simulators. Testing completed to date includes subscale solid rocket combustion simulators (11 and 24 inches in diameter) that have validated the use of the hybrid combustion process for solid rocket motor simulation.

Utilizing the combustion simulator design approach—which combines an inert solid-fuel grain with a liquid-oxygen injection system in an effort to simulate a solid rocket motor, while maintaining the safety and control attributes of a liquid system—provides a unique national asset not currently available with conventional rocket motor test-beds. The combustion simulator test-beds allow for rocket motor component overtesting, margin testing, and controlled test to failure. The Large Subscale Solid Rocket Combustion Simulator program, initiated by NASA in September 1993, is being performed by Lockheed Martin Astronautics, with Thiokol Space Operations and the Rocketdyne Division of Rockwell International functioning as major subcontractors.

The 11-inch motor was used to develop regression rate correlations for the DX fuel formulation, selected

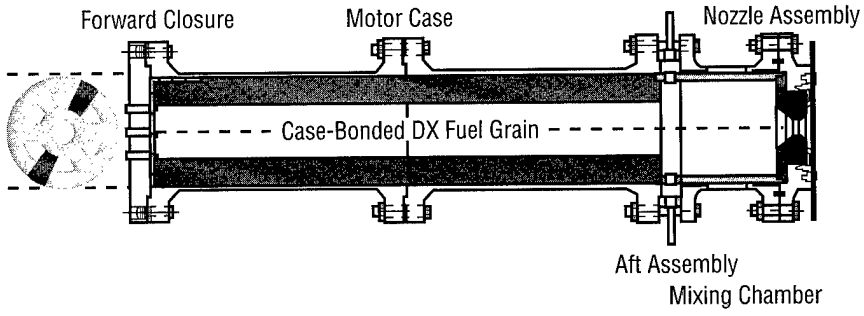

FIGURE 61.—24-inch solid rocket combustion simulator.

to simulate the solid rocket combustion environment. Twenty-four-inch motor testing completed to date has evaluated ballistic scale-up effects, multiport motor effects, fuel overcast capability, and the initiation of a control system to enable motor operation at a constant chamber pressure and mixture ratio.

Figure 61 illustrates the various components that make up the 24-inch combustion simulator system. Testing of the 24-inch-diameter combustion simulator system was completed in July 1995 at MSFC. A total of seven tests were conducted using the circular port configuration over a wide range of motor pressures and oxidizer flow rates. Stable combustion was observed on all tests, with nozzle throat erosion ranging from 3 to 8 mils per second. This performance compares favorably with the performance of a similar-sized solid rocket motor.

In conjunction with these tests, an innovative approach for the measurement of web thickness was demonstrated. Ultrasonic transducers were installed in steel housings welded to the motor case. The development of a pulse-echo thickness measurement technique provided for real-time measurement of web thickness during motor firing. The data obtained by the ultrasonic measurement technique agree closely with pre- and posttest web thickness measurements. This system will provide a real-time estimation of fuel flow rate for use in computing mixture ratio and subsequent mixture-ratio control.

Additional testing utilized a seven-port wagon-wheel grain configuration and provided an increased understanding of the ballistic characteristics of DX fuel. Integration of a closed-loop control system—providing for real-time adjustment of an electrohydraulic valve and the corresponding adjustment in liquid-oxygen flow rate and resulting chamber pressure—was also initiated during this test series.

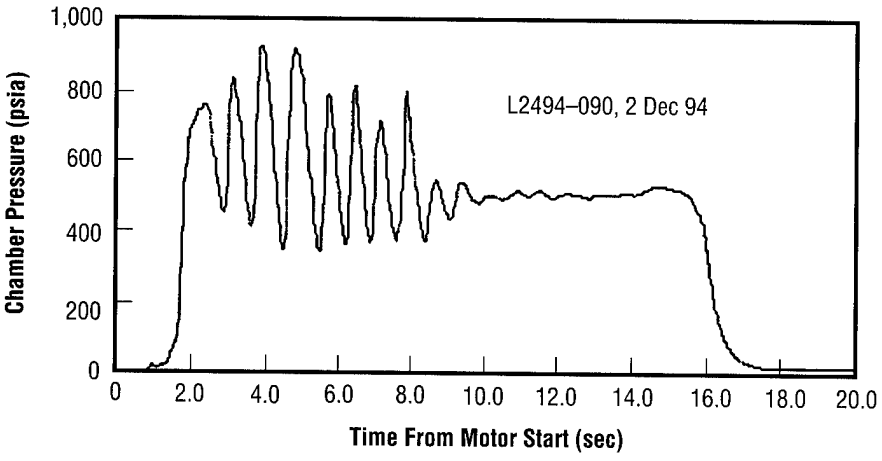

FIGURE 62.—Control system integration test.

Figure 62 illustrates the chamber pressure profile from test L2494–090. The control system gain setting—initially set excessively high in order to respond quickly to chamber pressure deviations—resulted in an unstable control solution. However, a midtest reduction in gain provided for a stable control solution. Test L2494–090 demonstrated a significant advancement in hybrid motor control and chamber pressure (thrust) tailoring.

Testing to date on the Large Subscale Solid Rocket Combustion Simulator program has established the viability of the combustion simulator concept through testing with the 11- and 24-inch solid rocket simulators. A valuable data base has been compiled to allow for future evaluation of advanced solid rocket motor materials and processes. The overall system will provide invaluable advancement of solid propulsion.

Abel, T.M.; Boardman, T.A.; and Crawford, J.T. November 15–17, 1994. Rocket Nozzle Materials Testing Using a Solid Rocket Combustion Simulator. Joint Army, Navy, NASA, and Air Force Rocket Nozzle Technology Subcommittee Meeting, Seattle, Washington.

Sponsor: Office of Space Access and Technology

Industry Involvement: Lockheed Martin Astronautics, Thiokol Space Operations, Rocketdyne Division of Rockwell International

Solar Thermal Propulsion Thrusters and Cryogenic Fluid Management

Leon J. Hastings/EP25
205–544–5434

A number of technologies must mature before full-scale development of the solar thermal propulsion concept can be undertaken. These include the absorber/thruster and the subcritical liquid-hydrogen storage/feed system. Basically, the solar propulsion concept involves focusing sunlight on a high-temperature absorber that heats hydrogen to 2,500 Kelvin and expels it from a nozzle for thrust in the 4.4- to 44.0-Newton range at high specific impulse (800 to 900 seconds). The MSFC effort consists of three basic elements: (1) development of absorber/thruster fabrication and assembly techniques, (2) development of an MSFC solar test facility, and (3) testing of a cryogenic fluid management subsystem. Activities and accomplishments for each of the three elements are summarized below. Reference figures 63 and 64.

Absorber/thruster: High-temperature absorber/thruster operation presents significant technology challenges involving heat transfer and materials selection and design. As presently envisioned, the absorber/thruster will be constructed primarily of a tungsten/rhenium-alloy inner and outer shell surrounded by a carbon foam or graphite insulation. The gaseous hydrogen will flow through the passage between two shells, absorb the energy focused into the inside cavity,

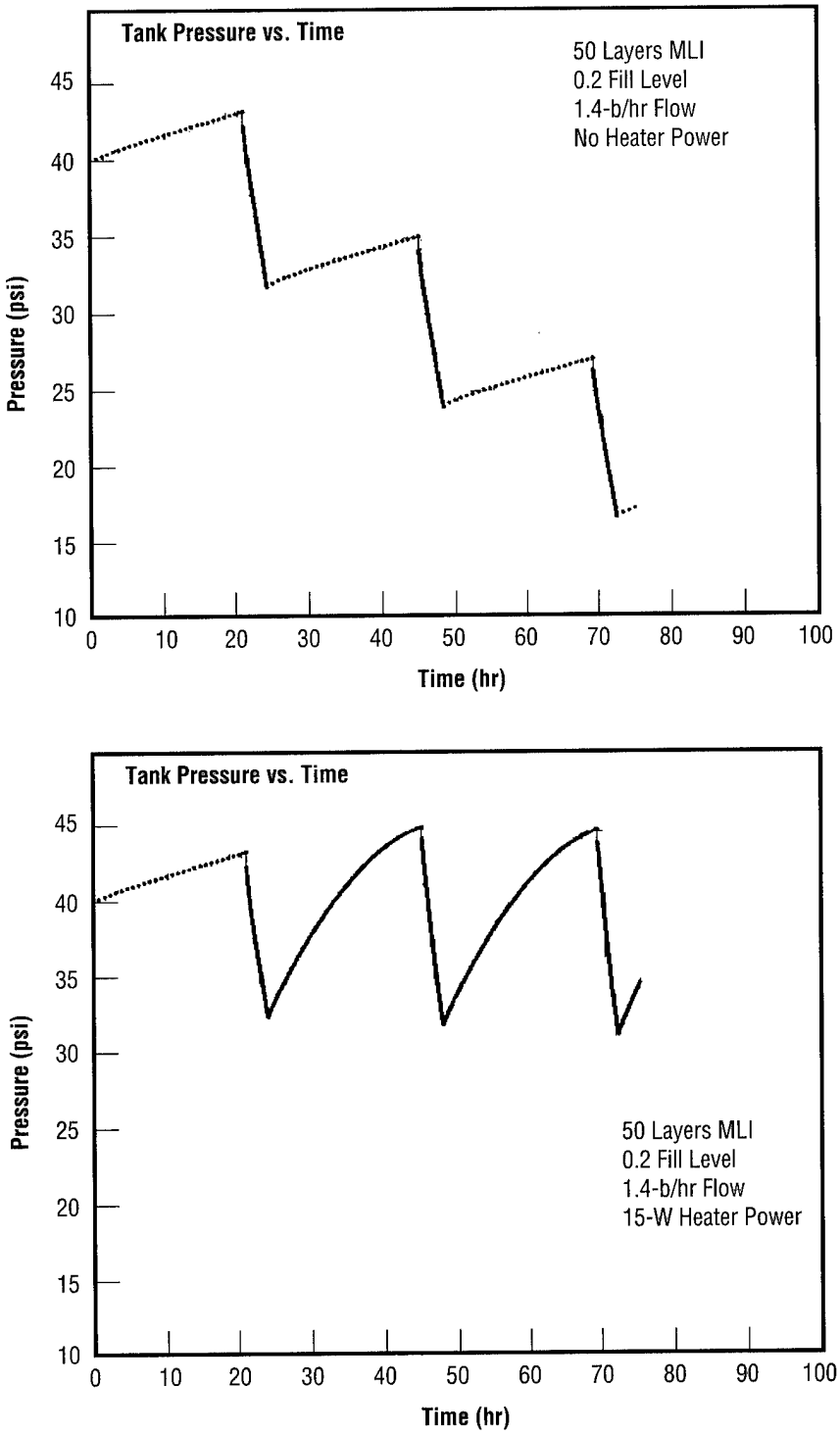

FIGURE 63.—Predicted pressures with vent system feeding the thruster.

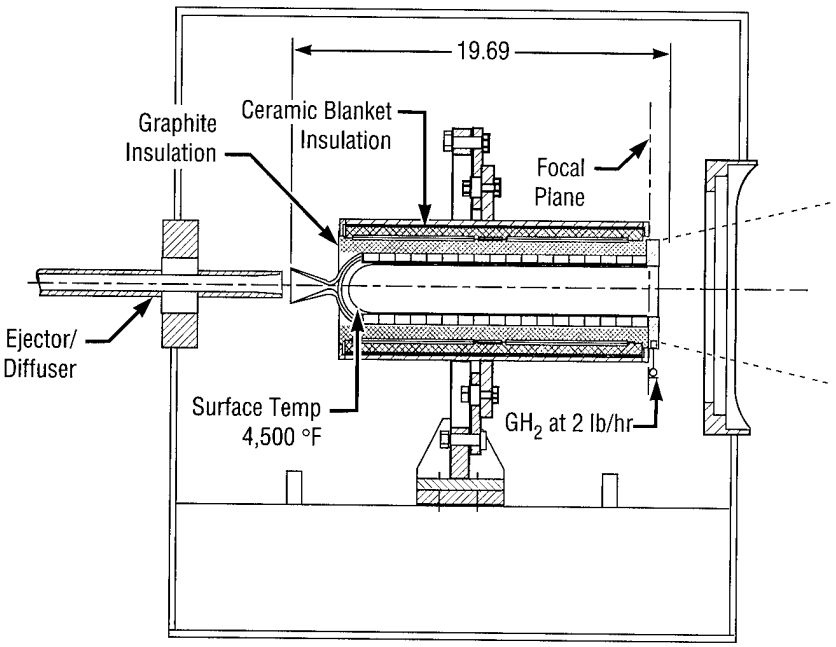

FIGURE 64.—Prototype absorber/thruster mounted in vacuum test chamber.

and then flow to the nozzle. Fabrication techniques are being explored through the development of a subscale absorber/thruster with a 2.2-Newton thrust. The MSFC vacuum plasma spray facilities have produced several tungsten inner and outer shell samples for an initial test article. Efforts are now in progress to establish a heat-exchanger shape that will assure efficient heat exchange between the inside shell and gaseous hydrogen without excessive pressure losses and fabrication expense or complexity. Flow-passage fabrication experimentation completed to date includes:

- Diamond cut machining: slow and costly; rough cuts—basic shell structure damage likely
- Electrical discharge machining with electrodes: improved cuts relative to diamond cut, but thermal stresses embrittle and weaken the tungsten; expensive
- Electrical discharge machining with brass wire: best machining process to date; expensive.

Solar Test Facility: Construction of the test facility in the East Test Area is planned, and preliminary layouts have been completed. The test facility concept consists of a 47-square-meter heliostat mirror, a 5.5-meter-diameter concentrator, a quartz-windowed vacuum test chamber, gaseous-hydrogen plumbing, and an experiment control system. Accomplishments include fabrication of a prototype concentrator segment (in preparation for fabricating all 144 hexagonal segments), 90-percent completion of concentrator support structure design, fabrication of a polished 33-centimeter-diameter quartz window, positioning a vacuum pump/test chamber (for thruster testing), and definition of heliostat design/performance requirements.

Cryogenic Fluid Management Subsystem: MSFC is participating with a consortium in the design of the 2-cubic-meter liquid-hydrogen storage/feed system and performance of the demonstration testing. Elements included are: zero-gravity venting, capillary screen liquid-acquisition device, pressurization/expulsion, and multilayer insulation. Basically, the propellant management subsystem concept consists of utilizing the liquid-acquisition device and thermodynamic vent system to flow 100-percent vapor to the thruster during burn cycles; i.e., the insulation is configured to match the liquid-hydrogen boil-off with the thruster flow rate and mission burn cycle (typically 100 to 200 burns). Accomplishments include preliminary pressure control analyses and definition of test article interfaces in the 6.1-meter-diameter vacuum chamber at test position 300. As an example, pressure-control analyses indicate that tank pressure can be maintained between 310 and 207 kiloNewtons per square meter (45 and 30 pounds per square inch absolute) (requiring engine delivery pressure of approximately 172 kiloNewtons per square meter (25 pounds per square inch absolute) with the assistance of 15 watts of heater power during the coast periods at a fill level of 20 percent.

Sponsors: Aerospace Industry Technology Program, Office of Space Access and Technology, Center Director's Discretionary Fund

A Lightweight, Composite, Liquid-Hydrogen Feedline

Philip Tygielski/EP43
205–544–7169

One of the many technological needs in making a single-stage-to-orbit vehicle a reality is being able to reduce component weight. Making components lightweight can lead to an increase in mass fraction and vehicle performance. One area with potential for substantial weight savings is the use of graphite/epoxy composite feedlines for the vehicle propulsion system. Typical feedlines for vehicles are made from aluminum or stainless-steel materials. An estimated weight savings of nearly 50 percent over conventional metallics could be achieved by using composite feedlines. This potential weight savings makes the use of composite materials a very attractive feature for future single-stage-to-orbit vehicles.

Under a cooperative agreement contract (NRA 8–11) between MSFC and McDonnell Douglas Aerospace, a team was formed to develop and demonstrate the use of a composite feedline for flowing liquid hydrogen. The authority to proceed was given in July 1994, with the objective of delivering a fully flight-qualified feedline in August of 1995. The feedline would then be installed onto the DC–XA vehicle for flight. In order to reduce the development costs of this new technology and also meet the delivery schedule, the work was divided between MSFC and McDonnell Douglas, making the best use of the talent and resources each organization had to offer. McDonnell Douglas was tasked to perform the design and analysis of the composite feedline, while MSFC was tasked to manufacture, assemble, and perform all feedline testing.

The composite feedline designed is used to supply liquid hydrogen at 50 pounds per square inch gauge from the liquid-hydrogen tank sump to the liquid-to-gas conversion system onboard the DC–XA vehicle. The liquid-to-gas conversion system is used to supply propellants to the reaction-control thrusters for vehicle attitude control. This particular feedline incorporates five advanced technology features. The first is the use of graphite/epoxy material, and the second is the manufacture and use of elbows made from composite. (Many feedlines today involve very complex geometries and are rarely straight lengths.) Third is the manufacture and use of flanges made from composite. Fourth is the ability to join a composite tube to a composite tube. (Since some feedlines may not be feasible to make in one piece because of complex geometry or other constraints, it will become necessary to be able to join composite lines together.) Finally, the fifth feature demonstrated is the ability to join a composite tube to a metallic tube. (In propulsion feed systems, there will inevitably be areas where a feedline will contain a metallic component, typically a bellows or flex joint. It then becomes necessary to be able to join that metallic component to the composite part of the feedline.)

The successful demonstration of all five of these technology features is key in the ability to use composites for vehicle feed systems.

The flight composite feedline is 2 inches in diameter (fig. 65). The line consists of a composite flange joined to a 90-degree composite elbow using a composite splice joint. The 90-degree elbow is then joined to a 45-degree elbow using another composite splice joint. The other end of the 45-degree elbow is joined to a reducer made from titanium material. The graphite/epoxy material selected for the elbows and flange was IM7/8552, an eight-harness prepreg weave. The material used for the composite splice joints was unidirectional IM7/8552 prepreg. All three joints (two composite-to-composite joints and one composite-to-titanium joint) were bonded using Hysol EA9394 adhesive. The material selection was based upon materials testing performed by McDonnell Douglas during its development program for the National Aerospace Plane.

Tooling for each composite item was designed and fabricated. Each composite item was then fabricated in MSFC's Productivity Enhancement Complex. Each component was fabricated by hand-layup onto the tooling. Once the part was hand-layed onto its tooling, it was then oven cured. After the oven cure, the composite part was removed from the tooling, and final machining was made on the part to meet its final dimensions. After each composite component passed its final inspection, the components were adhesively

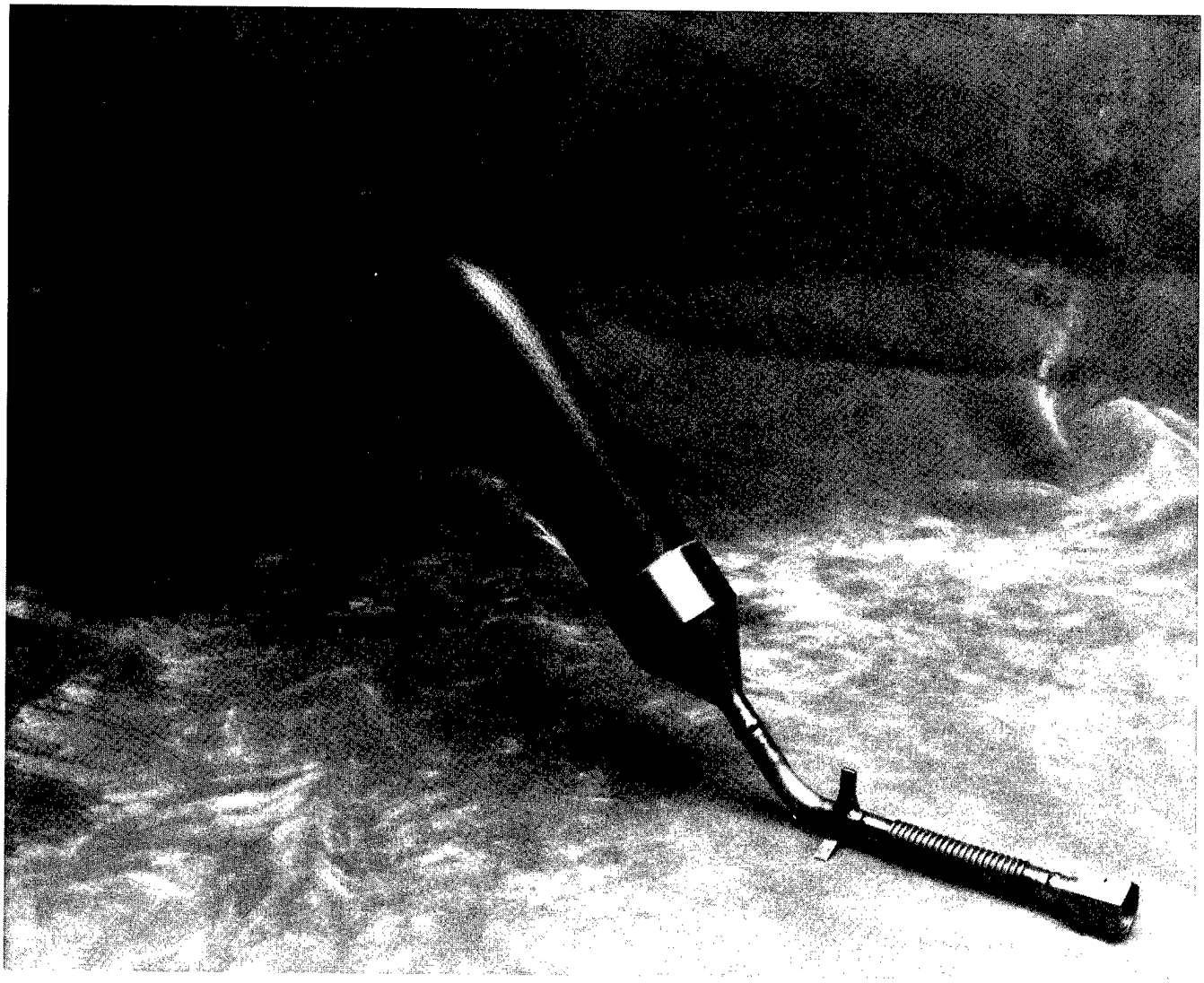

FIGURE 65.—Lightweight, composite, liquid-hydrogen feedline.

bonded together using the splice joints. The best method found for applying adhesive into the splice joints was by injecting the adhesive through four 90-degree clocked holes (0.10 inch in diameter) drilled into each end of the splice. This ensured uniform coverage of the adhesive and proved to be a much simpler process.

After fabrication of the composite items, a rigorous test program was begun to qualify the design for flight. Three development test articles were assembled. Development test article No. 1 incorporated a composite flange, a composite 90-degree elbow, two composite-to-composite splice joints, and a composite-to-titanium joint. This article was subjected to helium-leakage tests, a proof-pressure test at 75 pounds per square inch gauge, a 58-thermal-cycle test between −423 °F and +145 °F, a hydrogen-leakage test, and, finally, a burst-pressure test at 125 pounds per square inch gauge. The test article passed all tests. The helium leakage measured was no greater than 10 E−08 cubic centimeters per second magnitude. The hydrogen leakage from the entire test article was no greater than 0.5 standard cubic inch per minute, which is the lowest threshold of the measurement system used. Development test articles Nos. 2 and 3 were fabricated in order to perform structural strength tests of the adhesive joints at liquid-hydrogen temperature. The composite-to-composite joint failed at 9,215 pounds of axial load. The composite-to-titanium joint failed at 8,709 pounds of axial load.

After successful completion of the development test articles, a prototype feedline was fabricated. This test article was built to the exact configuration of the flight feedline. The prototype feedline was subjected to a vibration life test to qualify the flight feedline for eight DC–XA flights. The feedline was vibration tested to approximately 28 Grms for a duration of 78 minutes in each axis. The vibration test was performed with liquid hydrogen at 50 pounds per square inch gauge inside the feedline to simulate the operating temperature and pressure. The posttest inspections revealed the feedline successfully passed this vibration test. No damage to the feedline was observed, and it passed the posttest helium-leakage test.

The actual flight feedline has been built and has successfully passed its acceptance testing. The feedline was subjected to helium-leakage tests, a proof-pressure test at 75 pounds per square inch gauge, a 10-thermal-cycle acceptance test between −423 °F and +135 °F, and a vibration test.

To date, this work has shown the feasibility of applying composite materials in a feedline design for liquid hydrogen. The feedline has passed all of its critical tests. The feedline is now being integrated into the DC–XA vehicle for its first flight in early 1996.

Sponsor: Office of Space Access and Technology

Industry Involvement: McDonnell Douglas Aerospace, Huntington Beach, California

Structures and Dynamics

Suppression of Transient Acceleration by Levitation Evaluation

Gerald S. Nurre/ED01
205–544–1424

Suppression of Transient Acceleration by Levitation Evaluation is a U.S. Microgravity Laboratory 2 flight experiment scheduled for launch in September 1995. Its objective is to isolate, to microgravity levels, a science experiment (supported on a floating platform) from its surrounding acceleration environment. The payload platform is suspended by three dual-axis, wide-gap electromagnetic actuators configured to provide control in six degrees of freedom. Disturbances to the isolation platform are measured by accelerometers whose responses are processed by a high-bandwidth controller to command the actuators to provide the appropriate forces to counteract the disturbance inputs. In addition to the acceleration controller, a position-feedback loop is employed to maintain centering of the platform at a very low bandwidth. The position loop is necessary to compensate for extremely low frequency disturbances that the electromagnetic actuators' noncontact working area cannot accommodate.

This effort began in the fall of 1993 through Center Director's Discretionary Funds to study various microgravity isolation concepts. In January 1995, work began in earnest on the flight experiment to replace an experiment canceled from the Microgravity Laboratory manifest. Through a Space Act Agreement, a partnership was initiated with McDonnell Douglas Corporation, with their tasks being to design and fabricate three printed circuit boards, an analog acceleration controller board, a digital position loop board, and an actuator amplifier board. The company has also supplied the electromagnetic actuators, while MSFC has designed and fabricated the power supply board, the locker to house the experiment, and the electrical interfaces. In addition, MSFC has also designed and implemented the position-loop controller, developed a detailed six-degrees-of-freedom simulation model, and performed all the system-level hardware tests. This work was performed over a 5-month period.

This concept complements the rack-level isolation system that is currently planned for microgravity payloads on the International Space Station in that it provides for subrack isolation capabilities, which may prove useful in more easily accommodating future microgravity experiments.

The Suppression of Transient Acceleration by Levitation Evaluation experiment demonstrates that microgravity science can be performed using wide-gap electromagnetic actuators. At the same time, the effort highlights the capabilities of the MSFC/McDonnell Douglas team to design, fabricate, integrate, and test the hardware necessary to support a flight experiment.

Sponsor: Center Director's Discretionary Fund, Office of Life and Microgravity Sciences and Applications

Industry Involvement: McDonnell Douglas Corporation

Reusable Launch Vehicle Vertical Lander Guidance and Control Research

Dan J. Coughlin/ED13
205–544–2159

Don R. Krupp/ED13
205-544–1812

Michael W. Gallaher/ED13
205–544–1447

NASA is considering a vertical lander as a candidate concept for a single-stage-to-orbit reusable launch vehicle. This research considers three strategies for guiding and controlling the inversion of a reentering reusable launch vehicle (from a nose-first attitude to a vertical landing) and involves simulating each strategy (from a common reentry state to touchdown) using a common guidance algorithm and different controllers. Results demonstrate the characteristics that typify and distinguish each concept and help to identify peculiar problems, level of guidance and control sophistication required, feasibility concerns, and areas in which stringent subsystem requirements will be imposed by guidance and control.

The reusable launch vehicle vertical lander is envisioned to be a completely autonomous vehicle capable of performing a variety of missions, including the delivery of payload and/or personnel to the planned *International Space Station*. Investigators, serving as members of MSFC's Reusable Launch Vehicle Flight Mechanics Team, concentrated on guidance and control subsystem design and analysis for the reentry, inversion, and landing phases of the mission. A primary objective has been to investigate flight regimes and guidance and control issues not addressed by the DC–X program.

Successful design of a vertical lander spacecraft requires early attention to the vertical landing phase itself—that part of the mission which defines the lander's uniqueness. Despite the immaturity of the vertical lander configuration, preliminary simulation and analysis can yield crucial understanding of the unique challenges associated with the concept. This research has provided valuable insight into many design issues, including peculiar problem areas, the required sophistication of the guidance and control subsystem, feasibility concerns, and the subsystems likely to receive stringent requirements imposed by the guidance and control subsystem.

The vertical lander reentry and landing mission phase will consist of several distinct subphases: deorbit burns, atmospheric reentry, atmospheric flight (hypersonic to subsonic), maneuver-to-vertical landing orientation, terminal descent, and landing. Many of these phases reflect familiar, well-understood problems in space vehicles, for which engineers have established reliable approaches to solving. Other phases present unique challenges that aerospace system developers have never addressed in a functional launch vehicle—in particular, the maneuver-to-vertical orientation, terminal descent, and landing. These phases, tightly constrained by propellant and time considerations, will require closely integrated guidance and control algorithm development and implementation.

Three inversion options were investigated in this research project:

- The aerodynamic inversion concept initiates the maneuver at a "high" altitude and subsonic Mach number (as compared to the other two inversion concepts) by utilizing the vehicle's unstable aerodynamic characteristics: upon retraction of aerodynamic control surfaces, aerodynamic moments cause the vehicle to pitch up. Control torque, furnished by a reaction control system, stabilizes the vehicle in a tail-first attitude and maintains a 180-degree angle of attack until landing guidance is initiated. Upon guidance initiation, the engines ignite and the control system uses guidance commands to achieve a vertical touchdown. Figure 66 illustrates the aerodynamic inversion option.

- The propulsive inversion concept requires an inversion initiated at a lower altitude and Mach number. The vehicle allows the aerodynamic moments to cause a positive pitch (as in the previous concept, by retracting aerodynamic control surfaces and temporarily relinquishing attitude control). The vehicle ignites and gimbals the main engines to stabilize the vehicle in a tail-first attitude, while maintaining a negative flight path angle. Guidance attitude and throttle commands are then followed to touchdown.

- The powered pull-up maneuver concept begins at an even lower

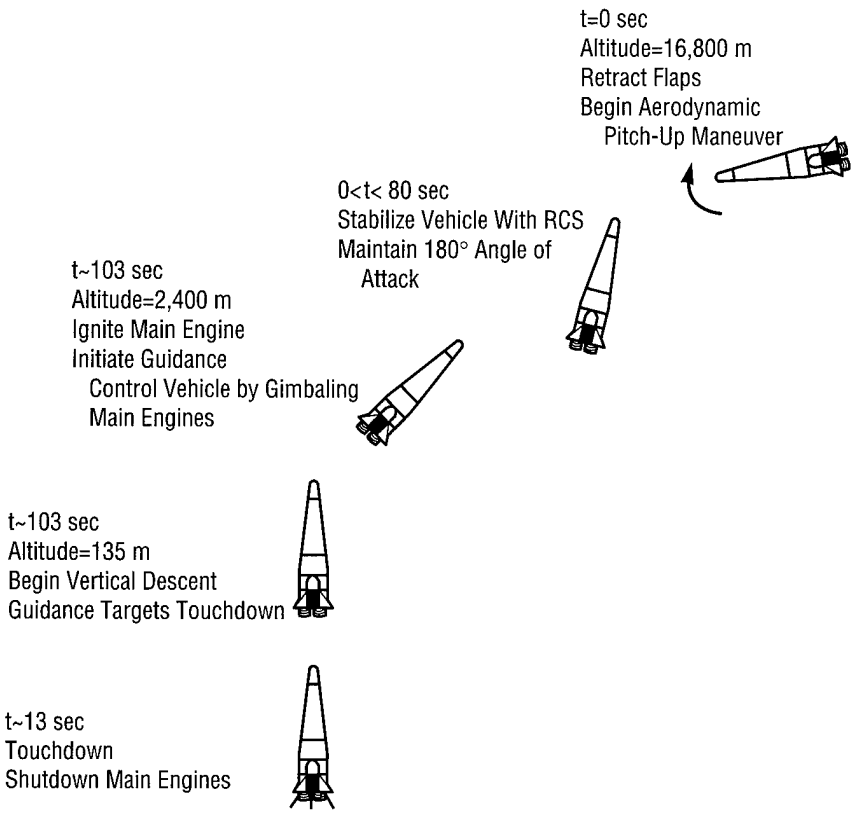

FIGURE 66.—Aerodynamic inversion maneuver.

altitude and Mach number. The main engines are then utilized to control the vehicle in a "pull-up" maneuver that raises the flight path to a positive angle (above the horizontal). This aspect of the maneuver produces a momentary "hover" point. Guidance attitude and throttle commands achieve a vertical touchdown.

Results of the guidance and control analysis indicate that no landing option investigated can be declared infeasible or precludes future analysis. In each landing scheme, a successful touchdown was achieved within the propellant budget. While each of the three simulated concepts touched down successfully, questions still remain about the controllability of this vertical lander configuration. With the current configuration (aerodynamic shape and mass properties), the aerodynamic control surfaces are inadequate to control the vehicle's angle of attack during the reentry flight phases (especially subsonic flight). The vehicle's shape and/or the aerodynamic control surfaces will require redesign or resizing to correct this deficiency.

The final objective of the research is to identify and discuss future analyses that would be required to establish feasibility of the vertical lander concept. Included in this list of analyses are a 6 degree-of-freedom dispersion study, engine-out analysis, and propellant management study.

Results of this research have been published as NASA Technical Memorandum 108500.

Sponsor: Office of Space Access and Technology

TREETOPS Structural Dynamics and Controls Simulation System Upgrade

George Myers/ED12
205–544–1477

The objective for this 18-month effort is to provide current and complete upgrade for the TREETOPS suite of analysis tools. This upgrade will provide the required format for maintaining the current tools as well as accommodations for future enhancements. TREETOPS is a time-history simulation of the motion of a complex multibody flexible structure in a tree topology with active control elements. "TREETOPS" refers to the simulation program, TREETOPS, plus two interactive preprocessors, TREESET and TREEFLX; an interactive postprocessor, TREEPLOT; and an adjunct program, TREESEL.

The simulation provides an advanced capability for analyzing the dynamics and control-related issues of complex flexible structures. The code has been used to analyze and design controllers for a number of large space systems including the Hubble Space Telescope. TREETOPS is capable of simulating the dynamics and control of flexible systems as complex as the space station mission, the rendezvous and docking of spacecraft, and robot tasks and manipulations.

TREETOPS, a multibody dynamics and controls analysis tool, has undergone various upgrades to improve its applicability as well as modeling fidelity. These upgrades have included such basic formulation enhancements as unrestricted boundary conditions for flexible bodies, accommodation of effects due to geometric nonlinearities, additions of sensor and actuator math models, and revisions to increase computational performance. TREETOPS development efforts have been performed largely in a research and development environment, where the emphasis has been on adding analysis features to obtain numerical results. In a strictly simulation development environment, emphasis would be placed on documentation and design details.

As part of the upgrades and enhancements, nonlinear geometric effects in TREETOPS would be addressed, and testing would be done on beam-buckling and plate-buckling problems to address foreshortening effects. The enhancement offers the opportunity for tremendous improvement to the analytical results. Reference figure 67.

Sponsor: NASA Headquarters, Office of Equal Employment Opportunity, Historically Black Colleges and Universities Program

Industry Involvement: Boeing Aerospace, McDonnell Douglas, Martin Marietta, Rockwell International Space Division, General Motors Company

University Involvement: Stanford University, Massachusetts Institute of Technology, Georgia Institute of Technology, University of Iowa, University of Toronto, University of Alabama, Auburn University, University of Alabama in Huntsville, Howard University, University of Maryland, University of Colorado

Other Involvement: Johnson Space Center, Goddard Space Flight Center, Langley Research Center, Stark Draper Laboratory, Sandia National Laboratory, Oak Ridge National Laboratory

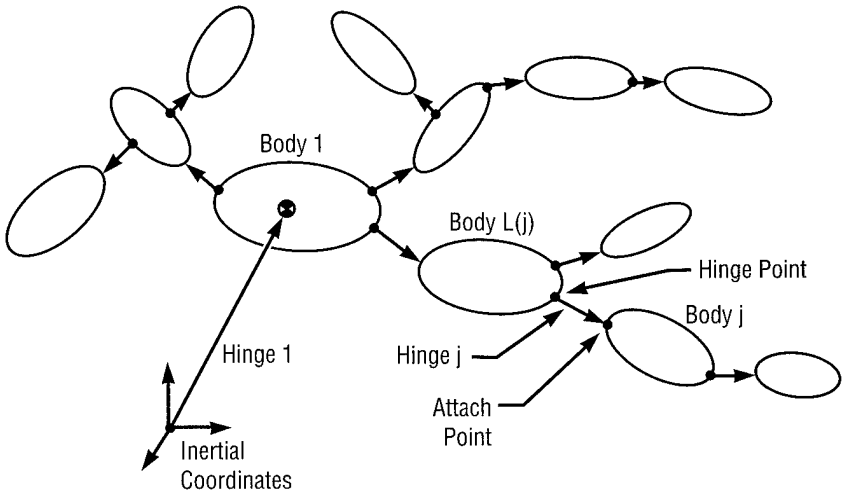

FIGURE 67.—An illustration of the TREE topology.

Segmented Mirror Adaptive Optics

John M. Rakoczy/ED12
205–544–1431

In its pursuit of excellence in advanced optics, MSFC has been developing a test-bed for adaptive optics technology. Adaptive optics is a key technology in establishing the next generation of large space telescopes, as well as improving performance of existing ground-based telescopes.

A particular challenge in dealing with a large-aperture space telescope is the task of getting a large mirror (from 8 to 20 meters in diameter) up in space. Rather than a single monolithic mirror, smaller mirror segments could be fabricated, launched into space, and assembled on orbit. Initial alignment, phasing, and calibration of a segmented-mirror configuration would require an active control system. Once the segments are aligned, the control system would maintain the desired wavefront despite such disturbances to the telescope as thermal transients and structural vibrations. Here lies the motivation for MSFC to develop an adaptive optics test-bed incorporating the controls-optics-structures-thermal initiative.

The Phased-Array Mirror, Extendible Large Aperture is a f/1.5 Cassegrainian telescope. The primary mirror consists of 36 hexagonal segments, 7 centimeters flat-to-flat, and figured to a sphere with a 1.5-meter radius of curvature. A Shack-Hartmann wavefront sensor is used to measure wavefront tip and tilt. Inductive edge sensors measure relative piston motion. Three

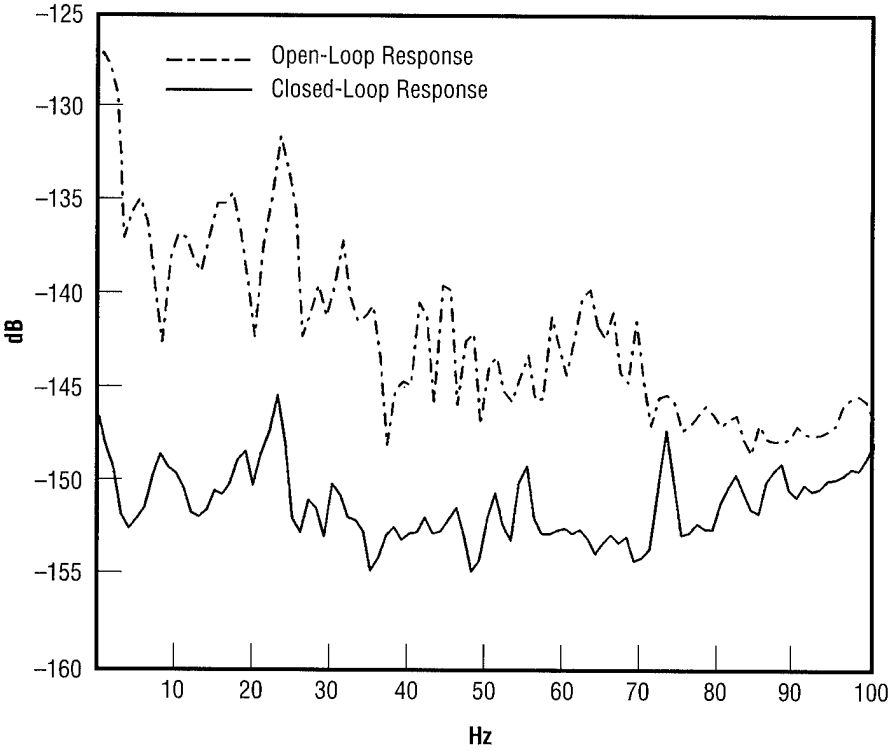

FIGURE 68.—Aberrator plate disturbance power spectral density.

electromagnetic actuators are configured for each segment to effect tip, tilt, and piston motions. Four digital signal processors receive sensor signals, perform control computations, and send actuator commands at a 5,000-Hz sample rate. System components were developed and assembled by Kaman Corporation in Tucson, Arizona. The system was transferred to MSFC in May 1993 when MSFC was tasked with performing integration and testing with funding from the MSFC Center Director's Discretionary Fund.

Program requirements were to control the wavefront of a monochromatic source (helium-neon) to one-tenth of a wavelength at a bandwidth of 100 Hz, which was particularly challenging considering that there were 240 structural vibration modes within the bandwidth of the control system. Furthermore, thermal transients altered the behavior of the wavefront sensors and edge sensors. The effort involved a serious controls-optics-structures-thermal interaction problem.

A control strategy was developed utilizing insights gained from MSFC's Control-Structures Initiative and Large Space Structures Ground Test Facility. (A similar strategy was used in the redesigned Hubble Space Telescope control system in order to accommodate solar array vibration disturbances.) Atmospheric-type disturbances were introduced by mounting a glass aberrator plate on a

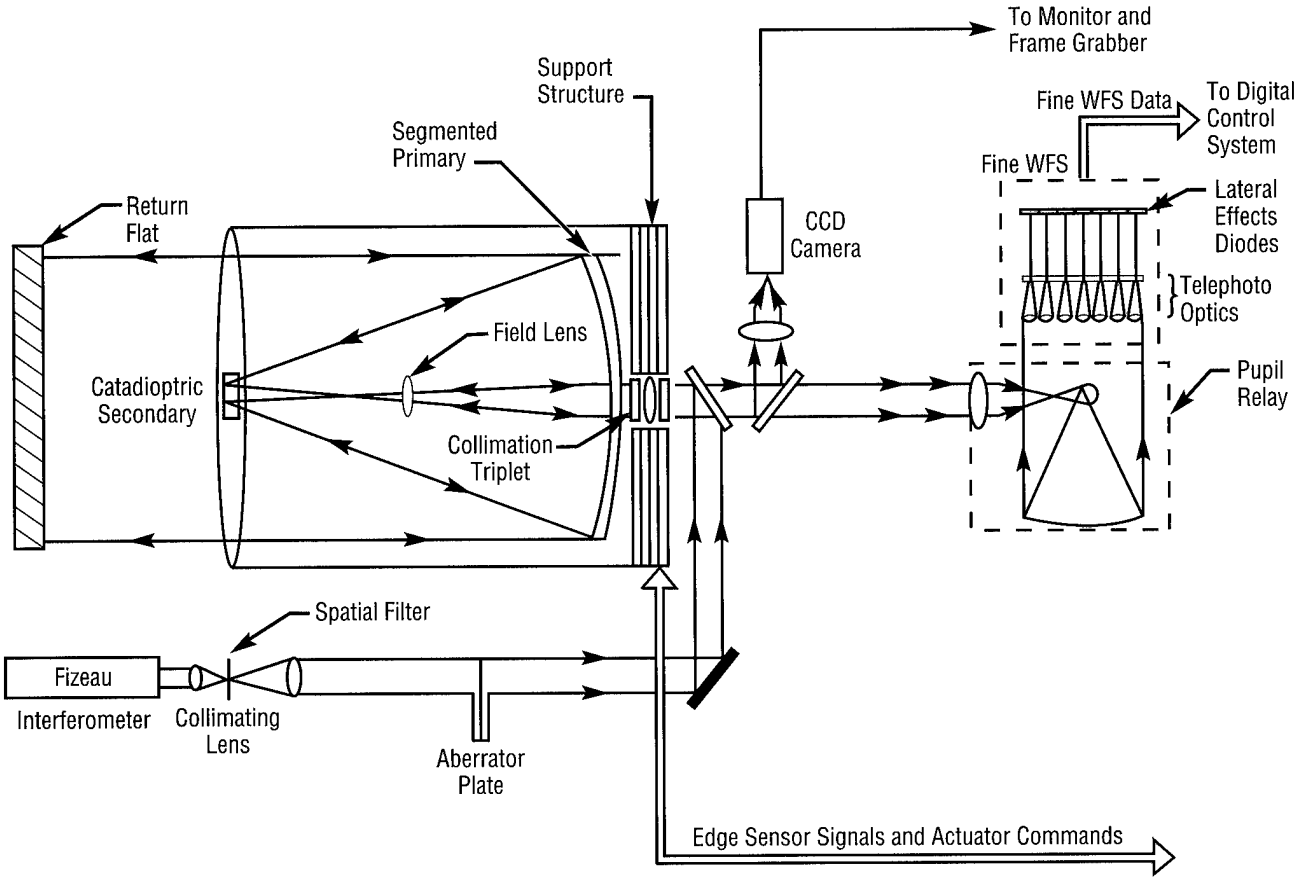

FIGURE 69.—Experimental layout of the system.

motor and rotating it in the optical path of the Phased-Array Mirror, Extendible Large Aperture telescope. Wavefront distortions from the aberrator plate were much more severe than those expected from the atmosphere. Figure 68 shows a power spectral density plot of the aberrated wavefront with and without the control system active. With the completion of this task, MSFC successfully demonstrated the operation of a segmented, primary-mirror adaptive-optics system for tip, tilt, and piston correction up to bandwidths of 100 Hz.

Work is continuing at MSFC to upgrade the system for compatibility with a white light source; specifically, the wavefront sensor will be upgraded for better sensitivity to white light. An automated wavefront sensor calibration and nulling scheme is also under investigation. Absolute distance interferometry is being explored as a way of phasing and calibrating the array in an automatic, turn-key operation. Finally, some of the mirror segments need to be refigured in order to yield better optical performance down to the diffraction limit. When the upgrades are complete, the Phased-Array Mirror, Extendible Large Aperture telescope will be fully operational for visible or infrared astronomy and of possible use as a tertiary component in a major ground observatory.

The success of the integration and testing task depended greatly on a multidisciplinary effort, drawing upon skills from controls, structures, optics, thermal analysis, modal testing, electronics, software, and systems engineering. Team members were awarded an MSFC Research and Technology Group Achievement Award for their efforts in June 1995. The effort will pay high dividends as

inputs to future design activities for the next-generation large space telescope. Reference figure 69.

Gleckler, A.; Ames, G.; Markason, D.; Radau, S.; and Waites, H. March 13–18, 1994. Phased-Array Mirror, Extendible Large Aperture: Progress Report on a 0.5-Meter-Diameter Telescope with a 36-Segment Adaptive Primary Mirror, #2201–95. Society of Photo-optical Engineers: Astronautical Telescopes and Instruments for the 21st Century, Kona, Hawaii.

Ames, G.; Howard, R.; Lindner, J.; Montgomery, E.; Patterson, A.; Rakoczy, J.; Zeiders, G.; and Waites, H. February 4–10, 1995. Phased-Array Mirror, Extendible Large Aperture: Phase I Testing and Verification on a 0.5-Meter-Diameter Telescope With a 36-Segment Adaptive Primary Mirror. Society of Photo-optical Engineers: Photonics West 1995, San Jose, California.

Sponsor: Center Director's Discretionary Fund

Industry Involvement: AmDyn Corporation, Blue Line Engineering, Kaman Aerospace Corporation

Automated Rendezvous and Capture Technology Description

Richard W. Dabney/ED13
205–544–1473

In the past, all U.S. rendezvous and docking operations have been piloted or ground-controlled, but autonomous rendezvous and capture has become a required technology due to the need for resupply of the space station by unmanned rockets. Significantly reduced operations cost and increased repeatability, reliability, and safety are but a few of the benefits automated rendezvous and capture offers.

Although the Russian docking system is available, it is not fully autonomous during all mission phases, requiring ground radar tracking and command for rendezvous and producing high contact velocities, which are not acceptable to space station needs without expensive, energy-absorbing mechanisms or structural enhancements. The current NASA MSFC Automated Rendezvous and Capture project will bring the technology to satisfactory levels by late 1997 if funding continues as budgeted; test facility upgrades are complete, and system integration is well underway. The technology requires no real-time human commanding of the resupply vehicle, allows automated mission design prior to flight, and fully automates vehicle operations, incorporating onboard mission/trajectory updates from real-time navigation data.

A typical automated rendezvous and capture mission flight profile includes chase-vehicle docking from behind (fig. 70); approaches from ahead of and below the target are also supported. A complete system block diagram is shown in figure 71. Necessary hardware consists of a short-range video guidance sensor, global positioning system antennas/receivers for long-range navigation, and a three-point docking mechanism (fig. 72). Software elements include absolute and relative global positioning system navigation filters, as well as guidance, navigation, and control for automated mission planning, automated orbital phasing maneuvers, automated proximity operations and docking, and automated collision avoidance maneuvers.

Maturity of the automated rendezvous and capture system will be substantially increased upon completion of the ongoing ground demonstration project, including verification and documentation of specific hardware and software. Extensive integrated ground testing will be performed to validate reliability and performance of the complete system, followed by flight (if funding permits) of an automated rendezvous and docking experiment as a payload on the shuttle or an expendable vehicle to identify any unexpected problems.

Three-point docking mechanism: As depicted in figure 72, the active three-point docking mechanism consists of three electrically redundant latching mechanisms, a control unit, and supporting structure: the passive part

is composed of three capture trunnions. The latching mechanisms and trunnions will be equally spaced, and docking status (undocked, captured, or locked) will be provided by the mechanism to the resupply vehicle. At least two trunnion bars must be within their capture envelopes before any latch can begin to capture its trunnion, closing to the locked position only after all three latches have reached alignment.

Dabney, R.W., and Howard, R.T. April 28, 1992. Closed-Loop Autonomous Docking System. U.S. Patent 5,109,345.

Howard, R.T.; Dabney, R.W.; and Bryan, T.C. June 4, 1991. Standard Remote Manipulator System Target Augmentation for Automated Docking. U.S. Patent 5,020,876.

Sponsor: Automated Rendezvous and Capture Ground Demonstration Program Office

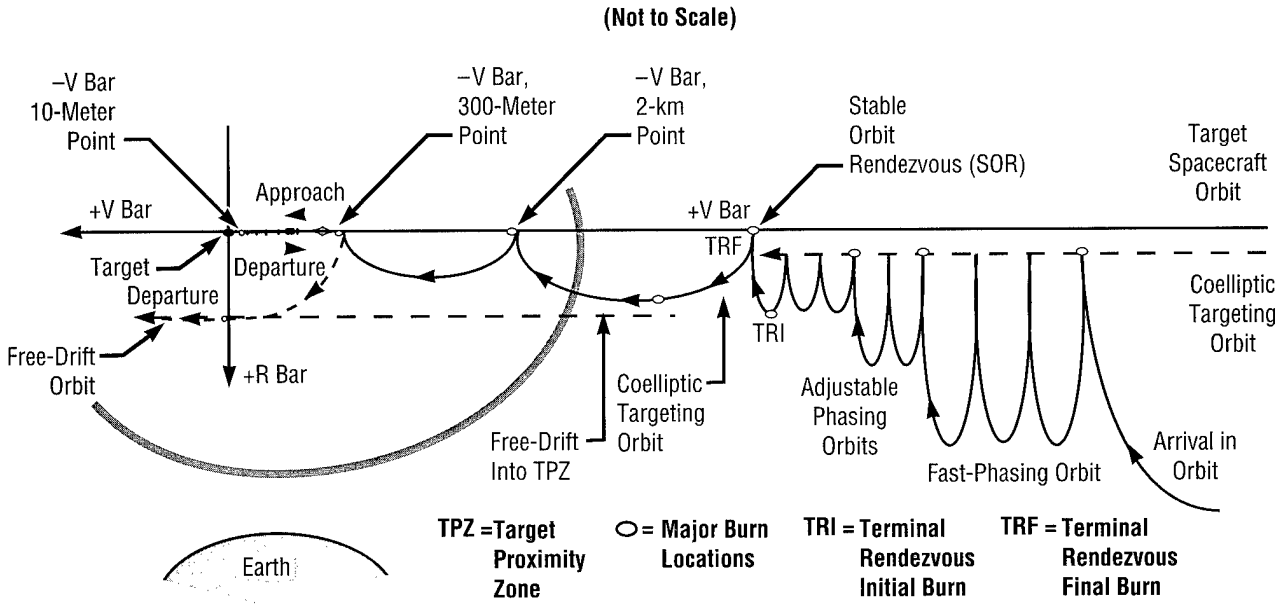

FIGURE 70.—Typical automated rendezvous and capture mission flight profile.

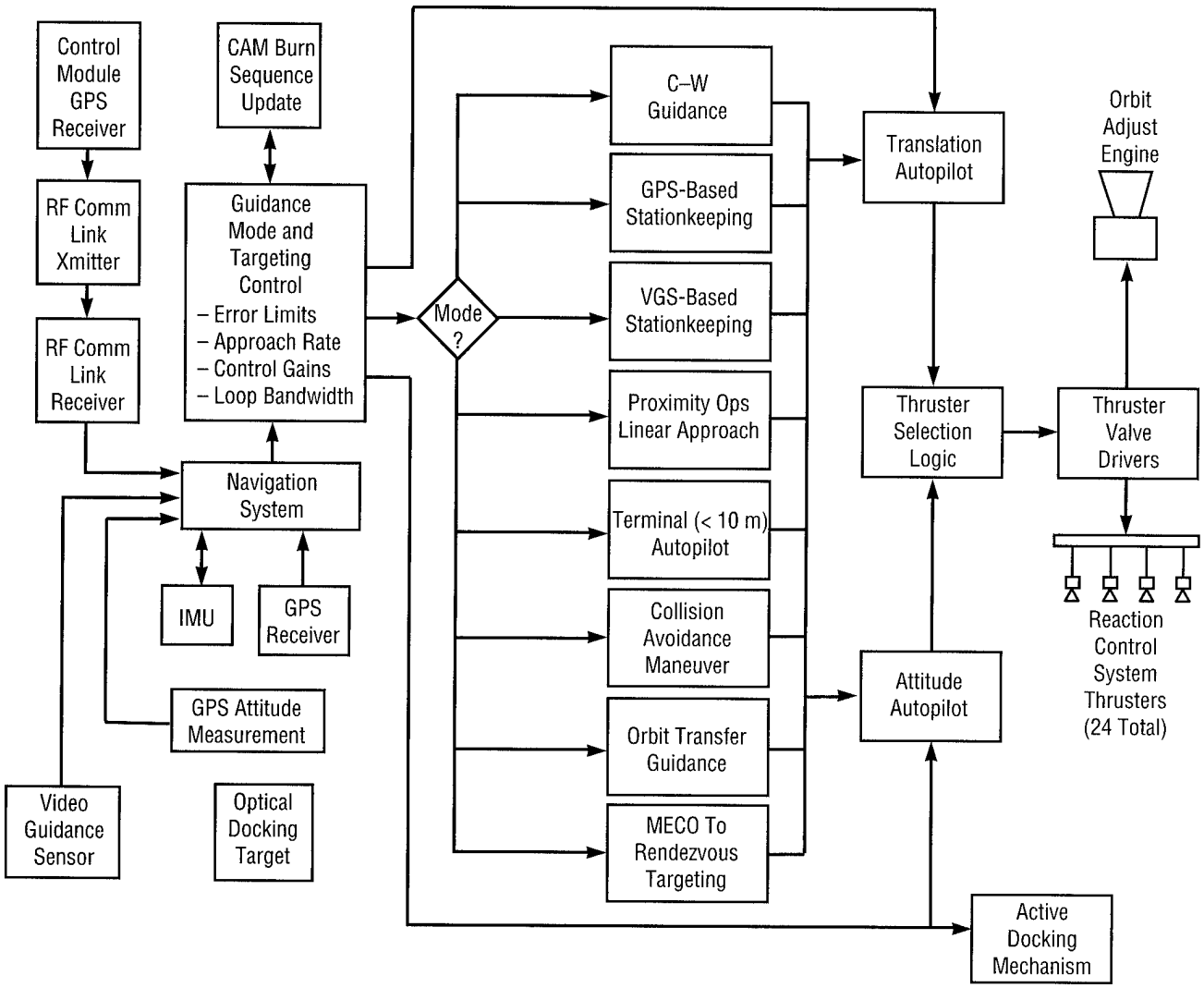

FIGURE 71.—Automated rendezvous and capture system block diagram.

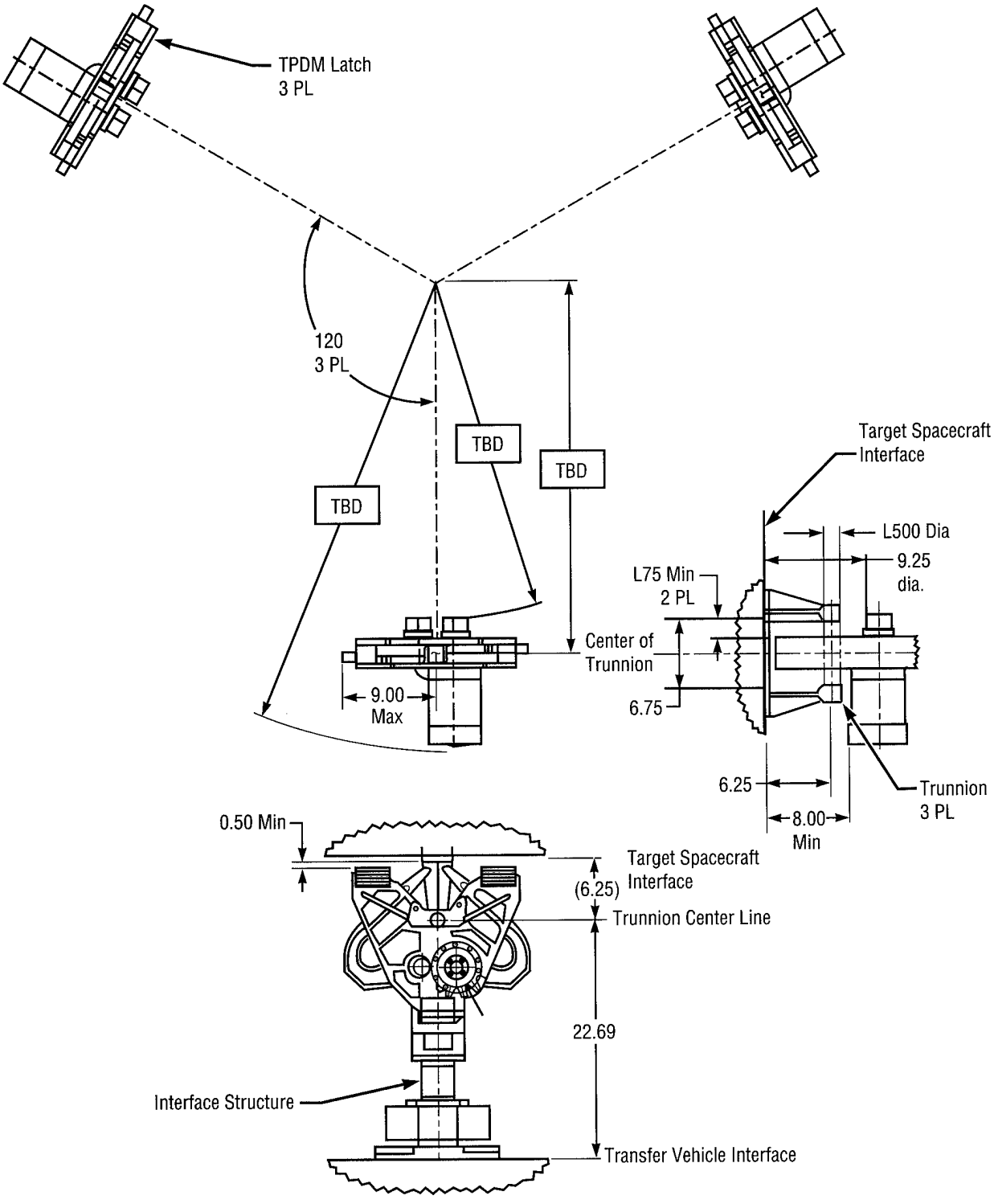

FIGURE 72.—Three-point docking mechanism.

Experimental Determination of Preswirl Effects on Damping Seal Performance

Eric M. Earhart/ED14
205–544–2417

The interactions and phase relations between a rotor's elastic and inertial forces can lead to subsynchronous whirl, a type of self-excited vibration at frequencies near the lowest critical frequency of the rotor. This potentially destructive phenomenon imposes limits on turbomachinery performance. As an example, subsynchronous whirl caused serious development problems on the space shuttle main engine's high-pressure fuel turbopump. Early in the development program, the speed of the turbopump was limited to 22,000 r/min because of destructive subsynchronous whirl. Stiffening the ball-bearing carriers and introducing smooth interstage seals enabled the turbopump to reach its design speed of 36,000 r/min. However, the whirl persisted, although the amplitude was considered acceptable. To combat the problem, MSFC engineer George L. von Pragenau invented the damping seal. Upon replacement of the smooth interstage seals with damping seals, subsynchronous whirl was eliminated from the high-pressure fuel turbopump.

MSFC-developed computer codes have shown that damping seals inhibit subsynchronous whirl by providing more damping than whirl forces. In most applications, fluid comes out of the impeller with very high tangential velocities and enters the damping seal; MSFC's codes indicate this fluid preswirl degrades the damping seal's stabilizing capacity. Unfortunately, no high-Reynolds-number damping seal test data with known preswirl are available to verify this important analytical result.

The subject program objective is to assess (experimentally) the effect of preswirl on damping seal performance. An existing test rig will be used to compare the performance of a smooth seal and a damping seal with two different fluid preswirls. The performance of each seal will be measured with a smooth test rig shaft and fluid preswirl of one-tenth the shaft speed. Tests will be performed in water at 5,000, 10,000, and 20,000 r/min, and 1,000, 1,500, and 2,000 lb/in^2 delta pressure. The test series will then be repeated with a new shaft with paddles to increase the fluid preswirl to the shaft speed. Present analyses predict this will greatly degrade the stabilizing capacity of each seal. Resulting data will be compared to computer code predictions, and anchored computer codes will then be used to design new turbomachinery.

Subsynchronous vibration is a potentially destructive phenomenon that imposes limits on turbomachinery performance. Damping seals have been shown to inhibit subsynchronous whirl by providing more damping than whirl forces. This project will provide the requisite data to relate the stabilizing capacity of the damping seal to the amount of preswirl in the fluid entering the seal.

Sponsor: Center Director's Discretionary Fund

Industry Involvement: Wyle Laboratory

System for Anomaly and Failure Detection

Thomas H. Fox/ED14
205–544–1462

Since ground testing of the space shuttle main engine began in 1975, there have been 28 major incidents. These failures—most of which were during the early phases of development when significant design changes were still taking place—occurred despite an extensive internal system of self-checking and measurement redlines. This number almost seems insignificant when compared to the more than 1,500 tests without major incidents. However, these failures have costs (engine damage, stand damage, etc.) associated with them that belie their small numbers.

Development of the System for Anomaly and Failure Detection was initiated in 1985 and completed in 1994. It has been tested (297 tests to date) using data from actual tests ranging from those that did not have shutdowns or severe damage to those with catastrophic failures (17 tests). Data from existing engine computer models were used to test against failure modes for which no hot-fire data existed.

In all tests in which significant failures occurred, the algorithm has shown improvement over redline methodology by issuing earlier shutdown commands, with the exception of the few catastrophic failures that occurred within a few milliseconds and with no prior warning. The system has also demonstrated that no inadvertent shutdown commands would have been issued. A conservative analysis of the savings that could have been accrued had the system been active during the 17 tests resulting in catastrophic failures indicates a potential savings of approximately $48,000,000.

The algorithm has monitored 32 hot-fire tests on the Technology Test-Bed stand and was an active participant in the last test, which means that the detection system had shutdown authority if an incipient engine failure had been detected. These tests have included a standard all-Rocketdyne engine, a wide-throat engine with Rocketdyne pumps, and several with a wide-throat engine and a mix of Rocketdyne and Pratt & Whitney high-pressure pumps.

The System for Anomaly and Failure Detection system installed on the Technology Test-Bed stand is expected to be moved to Stennis Space Center late in 1995, where it will be used as a stand protection system.

Fox, T.; Cikanek, H.; and Evatt, T. May 18, 1994. Development of the System for Anomaly and Failure Detection. Advanced Earth-to-Orbit Propulsion Technology Conference, NASA/MSFC, Alabama.

Sponsor: Space Transportation System Chief Engineers

Flight-Control Augmentation for Aft Center-of-Gravity Launch Vehicles

Chris Barret/ED15
205–544–7118

The space shuttle was only the first step in achieving routine access to space. Recently, MSFC has been studying a whole spectrum of new launch vehicles for space transportation. Some of these could transport components of the space station to orbit, and some could take us to Mars and beyond to expand our frontiers of knowledge.

In all our future launch vehicle designs, decreasing the structural weight will always be of great concern. This is tantamount to increased payload capability, which, in turn, means reduced cost per pound to orbit. One very significant increase in payload capability has been defined: a sizable weight savings can be realized by a rearrangement of the internal propellant tanks. Studies have been conducted both at MSFC and at Martin Marietta Corporation (maker of the space shuttle external tank) which show that a very substantial weight can be saved by inverting the relative positions of the liquid-hydrogen and liquid-oxygen propellant tanks.

As the vehicle sits on the launch pad in the conventional configuration, the heavier liquid-oxygen tank is located on top of the lighter hydrogen one, requiring a heavy structural member between the two tanks to prevent the lighter tank from being crushed. The configuration also requires large, long,

and even drag-producing liquid-oxygen feedlines running the length of the vehicle on the exterior fuselage. If the relative position of the propellant tanks is inverted, both the heavy structural separation member and the long feedlines could be deleted.

While the structures community at MSFC was elated with this finding, the liquid-oxygen tank aft configuration gave the vehicle an aft center-of-gravity location that surfaced controllability concerns. In the conventional configuration, the launch vehicle is controlled in the ascent trajectory by the gimballing of its rocket engines. Studies have been conducted at MSFC to show that the resulting aft center-of-gravity-configured vehicle would not be adequately controllable with the engine gimballing alone.

Today, more aft center-of-gravity launch vehicles are appearing. In addition to an aft center of gravity being caused by an internal rearrangement of propellant tanks, aft center-of-gravity vehicles are also appearing due to heavier rocket engines and larger numbers of aft engines. Therefore, in the new spectrum of launch vehicles being considered, the controllability of the aft center-of-gravity-configured vehicle must be assessed. When the available control authority has been determined to be inadequate or marginal, some means of flight-control augmentation is required.

This research effort has proposed, designed, and wind tunnel-tested a novel solution to provide the required flight-control augmentation for an aft center-of-gravity-configured vehicle, when needed most in the ascent trajectory during maximum dynamic pressure. The vehicle used in the research is one that has recently been studied at MSFC. The liquid-hydrogen and liquid-oxygen propellant tanks in the external tank have been interchanged, giving the vehicle an aft center of gravity. Research indicates that engine gimballing alone does not offer adequate control; the required flight-control augmentation is provided by aerodynamic flight-control augmentors. This solution not only solves the original problem of augmenting the control of the aft center-of-gravity vehicle, but also can be used in the marginal control configuration to enhance controllability as load alleviators to reduce engine-gimballing requirements, to provide engine actuator failure protection, and to enhance crew safety and vehicle reliability by providing more control in engine-out events.

These devices can reduce the wind restrictions. Conventionally, the launch vehicle loads during ascent are alleviated by turning the vehicle into the wind, thereby reducing the vehicle's angle of attack. Thus, load relief is accomplished at the expense of trajectory deviation. Load-relief control is most necessary when the vehicle experiences maximum dynamic pressure and the aerodynamic loads are greatest, which happens to be when the flight-control augmentors would provide the most significant assistance. The added control capability through the use of these surfaces allows greater tolerance of wind magnitudes and a minimization of bending moments on the vehicle, both during ascent and during launch. For prelaunch, the unfueled vehicle on the pad is assumed to withstand peak loads of 75 knots and, fueled at liftoff, peak winds of 50 knots. The environmental disturbances are multiplied by 1.5 to account for Von Karman vortex shedding effects. Wind profiles show greatest steady wind speeds occurring between 20,000 and 60,000 feet, with a gust overshoot of up to 50 percent. The more the engines are required to gimbal, the more engineering design and cost are involved to have the propellant ducts move with the gimbal action while maintaining a full flow of fuel. The extension, compression, and torsion of the propellant ducts become limiting factors of engine gimballing. Thus, the designed flight-control surfaces of this research provide the required control augmentation, as well as a plethora of additional significant benefits.

Through this effort, current and past uses of launch vehicle aerodynamic surfaces have been reviewed. NASA has a rich national heritage of launch vehicles that have used aerodynamic surfaces, both to provide flight stability and to provide flight control. The Saturn V took humankind to the Moon wearing 300 square feet of aerodynamic surfaces to provide flight stability. Since landing on the Moon, the wealth of smart materials and advanced composites that have been developed allow for the design of very lightweight, strong, and innovative launch vehicle flight-control augmentors. Today, a myriad of launch vehicles have been actively launched from over 15 geographic sites. Aerodynamic surfaces currently being used by other nations on launch vehicles have been reviewed.

The flight-control requirements analyses of this research have been

conducted to determine the amount of flight-control augmentation required. Based on these determined control requirements, the above reviews, the generated vehicle mass properties, and ascent trajectory data, candidate flight-control augmentors have been designed and fabricated, along with experimental launch vehicle test articles. A static wind tunnel test program and a dynamic wind tunnel test program have been conducted at MSFC for these candidate flight-control augmentors and the host experimental aft center-of-gravity launch vehicle. The wind tunnel test programs have produced data for the static stability and dynamic stability derivatives. The wind tunnel test data have been reduced and utilized to conduct the vehicle static stability analyses and dynamic stability analyses. Results have been compared to DATCOM-generated analytic data.

The best candidate designs demonstrate the augmented control authority achievable with the use of the flight-control augmentors. Figure 73 shows the flow chart of this conducted research effort, while figure 74 illustrates the fabricated aft flight-control augmentors tested on the experimental launch vehicle in MSFC's wind tunnel. Figure 75 depicts the fabricated forward flight-control augmentors tested on the launch vehicle. Figure 76 offers the experimental wind tunnel test article with aft devices attached, and figure 77 shows the experimental vehicle test article with forward and aft devices attached.

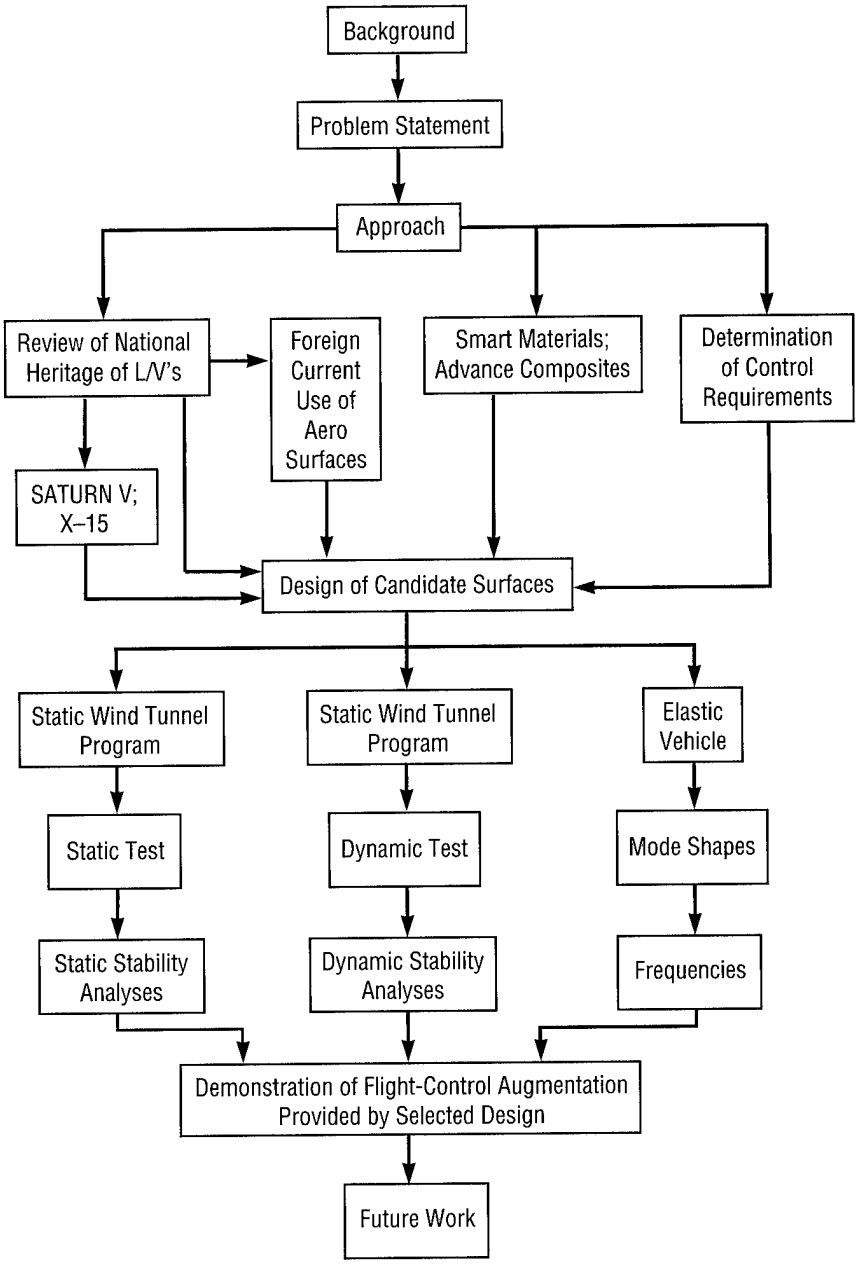

Figure 73.—Flow chart of conducted research.

Sponsor: Center Director's Discretionary Fund

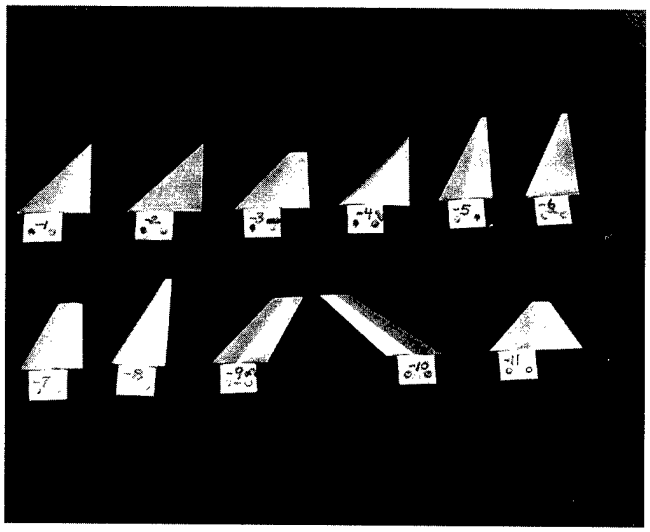

Figure 74.—Fabricated aft launch vehicle flight-control augmentation devices.

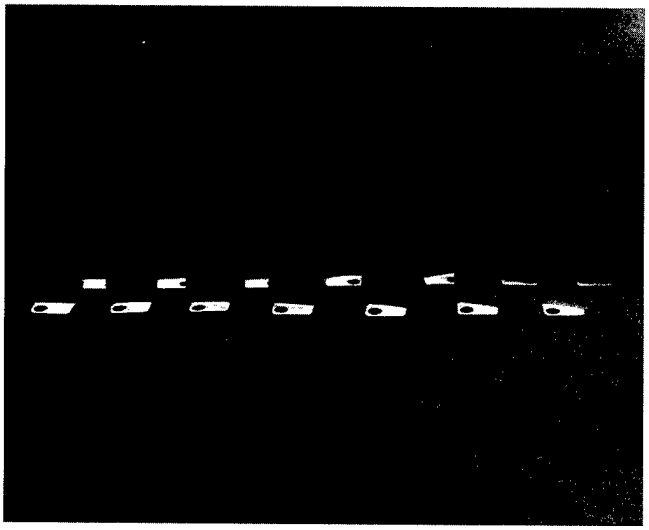

Figure 75.—Fabricated forward launch vehicle flight-control augmentation devices.

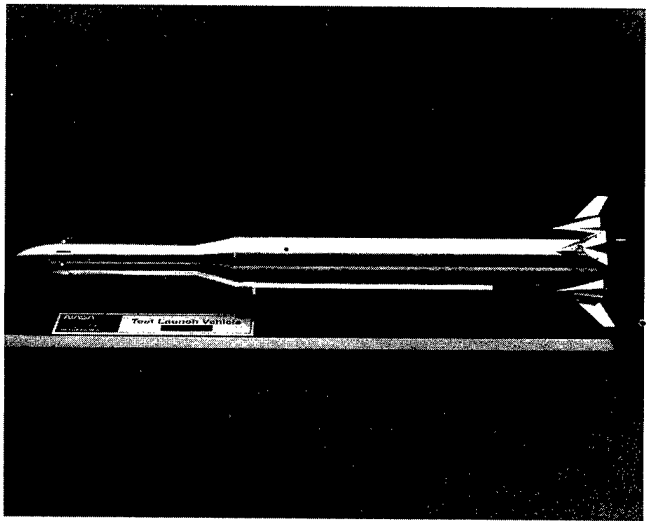

Figure 76.—Fabricated launch vehicle wind tunnel test article with flight-control augmentation devices attached aft.

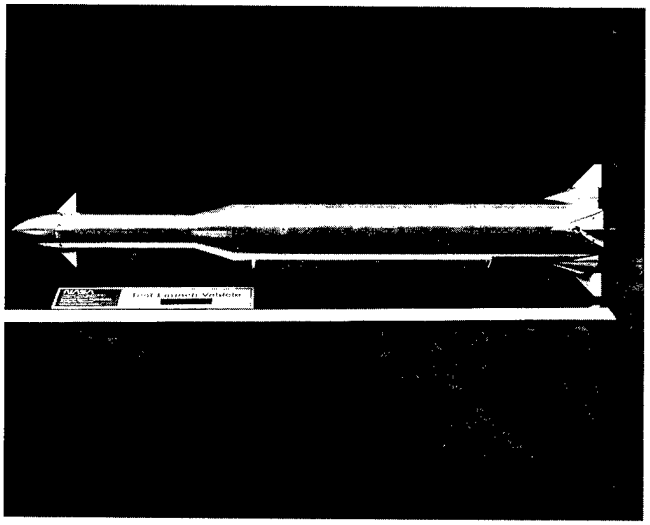

Figure 77.—Fabricated launch vehicle wind tunnel test article with flight-control augmentation devices attached aft and forward.

Composite Integrally Bladed Turbine

Katherine K. Mims/ED22
205–544–1506

A ceramic composite integrally bladed turbine disk (blisk) combines two important technology benefits: (1) reduced weight resulting from both a reduced parts count and from use of a lower-density material and (2) improved damping, a derivative of the inherent damping offered by continuous fiber-reinforced ceramic composites. An added benefit is the possibility of reduced operating costs due to enhanced durability (relative to metals) in the intended gaseous oxygen-rich environment. However, the structural response of these single-piece structures to high-vibration environments must be considered. An unshrouded metallic blisk provides little or no damping; without damping there is a degradation of high-cycle fatigue life, and the blisk may become the turbopump's life-limiting component. Use of composites is anticipated to impart needed internal damping to the configuration to address the vibratory stresses encountered because of the unsteady flow loads (random vibration) through the bladed turbine regions. A team of engineers from MSFC and Lewis Research Center was formed to execute a technology development plan to characterize the extent to which composites can damp these vibrations. In addition, unique, gaseous oxygen-rich environments data will be generated that will broaden the application of composites.

This task will produce enabling technology for single-piece, unshrouded composite turbines for gaseous oxygen-rich operation, and supports long-term/high-payoff concepts where composites may be considered as a means to achieve goals of lower engine weight and life-cycle cost. The effort is aimed at providing advance data for two critical design issues: structural dynamics integrity and gaseous oxygen-rich turbine environmental compatibility. Once these areas are baselined in the Simplex turbopump, demonstration of the design in reusable launch vehicle-type operating conditions will be warranted. This particular task is directed to benchmark ceramic-matrix composite design methodologies required to address the most critical fundamental design issues.

The program is divided into two phases. Phase I involves researching and identifying existing relevant data bases in order to establish the current state of knowledge; establishing a material selection criteria test matrix; selecting and obtaining samples of the fiber/matrix composite candidate(s); performing subscale damping, thermal shock, and liquid-oxygen compatibility bench tests; characterizing candidate composite materials for the Simplex pump environment; and generating a Simplex pump turbine region design configuration based on composite material blisk design. Phase II consists of the actual hardware fabrication and testing. These efforts include generating a preliminary test plan, conducting a preliminary design review for a full-scale blisk, fabricating and delivering a full-size composite blisk sample(s) for baseline technology validation tests, and performing hot-fire turbopump testing and pre- and post-inspection of a blisk.

During the early portion of Phase I, key design issues were addressed: selection of the composite material for the blisk, generation of a materials test matrix, and identification of critical design parameters and attachment issues. An extensive government/industry survey was conducted over a period of several weeks in order to identify the current state of knowledge on design and development issues for a ceramic-matrix composite blisk. Participation included members from the Department of Defense and the Department of Energy; associated engineers from the Lewis Research Center, White Sands Test Facility, and MSFC, and industry fabrication and end-item use companies with experience in similar applications. Teleconferences provided data and visibility into industry capabilities and experiences with composites. Subsequent design actions were then initiated in two major areas: attachment between composite disk and metal shaft and the modification of the inertia-welded Simplex disk to shaft design to accommodate the composite disk and shaft configuration.

For the remainder of fiscal year 1995, work was performed on three parallel fronts: structural assessment, design efforts, and materials characterization. Two carbon fiber architectures, quasi-isotropic (0/±60) fabric layup and polar (0/90) fabric layup (to simulate a polar weave), were selected for material characterization panels. These

panels will be densified using the isothermal chemical vapor infiltration process.

Key issues which have arisen in finalizing the matrices have been the requirements and approach for both high-cycle and low-cycle fatigue testing, oxygen compatibility test requirements and test article geometries, and friction factor/surface effects testing. These issues have been resolved through several detailed discussions involving government and industry participants. Subscale testing will be performed to support materials characterization and attachment design efforts toward the end goal of placing the composite blisk configuration into the Simplex turbopump in fiscal year 1997.

Composites, with potential for damping due to the makeup and interaction of their substructures, provide unique and alternative nonintrusive damping concepts and can be applied in industry where severe vibration environments are experienced (space and nonspace): rotating industrial machinery, automotive or turbomachine systems, and advanced and current liquid rocket engines. MSFC is continuing, as part of its proactive initiative, to examine mechanisms for improved damping for the upcoming designs that promote use of lightweight, single-piece composites. The composite blisk is one of many such potential applications which, when benchmarked through operational environments, could be extended into other industry uses.

Sponsor: Office of Space Access and Technology

Industry Involvement: DuPont/ Lanxide; Southern Research Institute

Other Government Involvement: Department of Defense (Wright Patterson Air Force Base), Department of Energy (Oak Ridge National Laboratory), Lewis Research Center, Johnson Space Center (White Sands Test Facility)

Damping Measurement of Advanced Composite Materials for Turbomachinery Applications

Donald L. Harris/ED22
205–544–6265

A widely held assumption is that fiber-reinforced composite materials possess more inherent material damping than metals or monolithic composites. With this in mind, the objective of this study is to quantify the material damping of fiber-reinforced composite materials that can be used in turbomachinery applications. Fiber-reinforced ceramic-matrix composite materials possess high-strength, low-weight, and high-temperature capabilities—qualities that turbine end-component materials must have. The additional quality of higher damping will allow components to be less complex and able to withstand higher dynamic loading.

This particular damping study was approved in October of 1993 and is scheduled for completion in January of 1996. The idea to study the damping capacity of composite materials came from the realization that, while there is an interest in developing ceramic integrally bladed disk (blisk) components, damping data were not readily available.

The objective of the task is to measure the inherent material damping capacity of composite materials which have promise for use in rocket engine

blisk applications. Such damping information is required for dynamic analysis that can predict the dynamic stress of a component under loading.

Samples of various advanced composite materials were selected for testing. Damping tests were performed on beam samples (20.32 centimeters long by 2.54 centimeters wide by 0.3175 centimeter thick) for several modes of vibration in a free-free boundary condition. These materials represented various types of composite materials: fiber-reinforced ceramic-matrix composites, carbon/carbon composites, monolithic silicon nitride, and Inconel 718. Inconel 718, a nickel-based superalloy currently used in rocket engine turbopump applications, served as the baseline material. Test data revealed that the fiber-reinforced composites provided more material damping than the baseline material—in some cases as much as one-third more damping (see fig. 78).

Two fiber-reinforced ceramic-matrix composite disks (22.86 centimeters in diameter) have been purchased from Oak Ridge National Laboratory for damping tests. These disks are representative of rocket engine turbines, bladed disks, and blisks in size and basic geometry. Two different

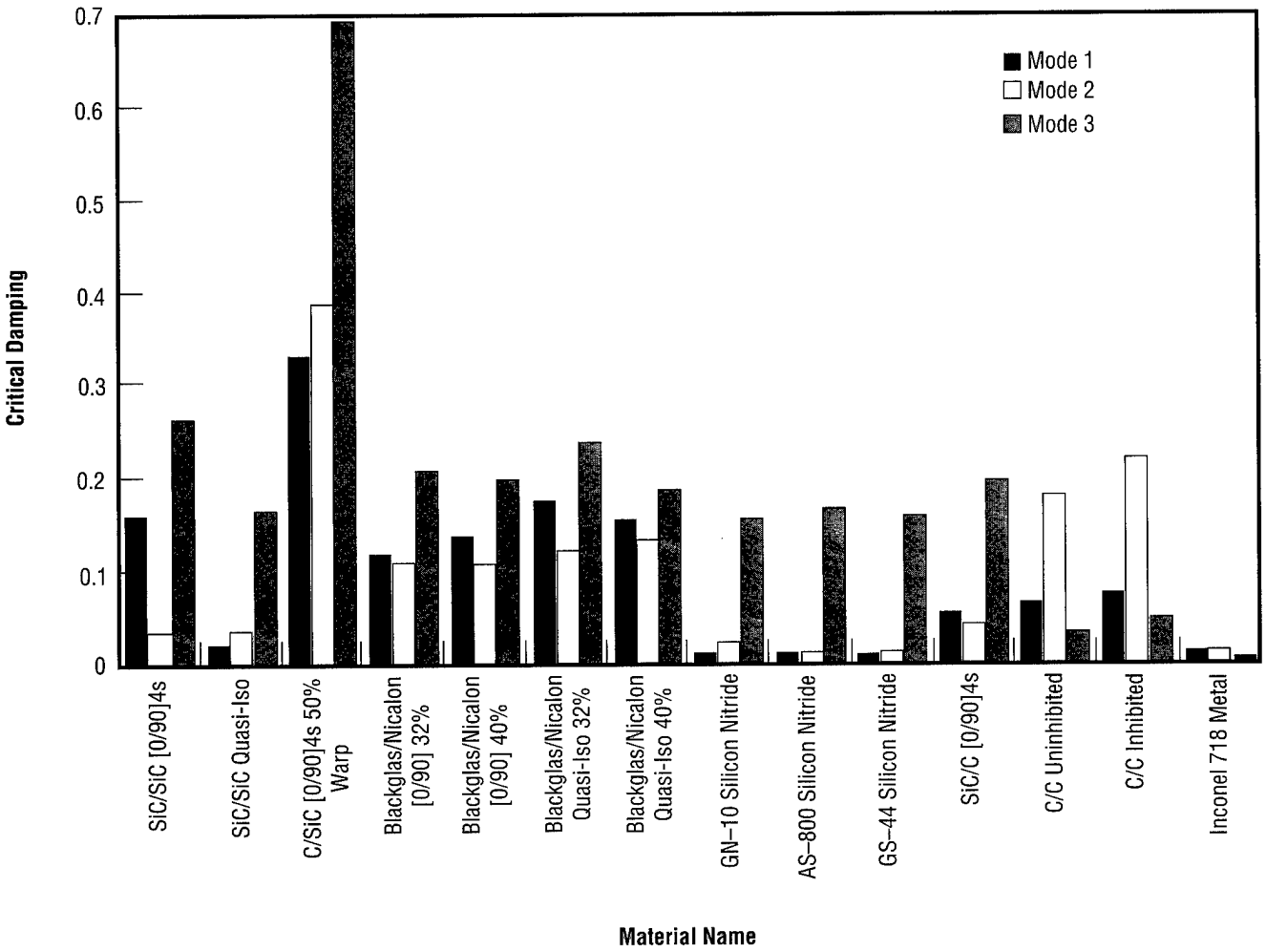

FIGURE 78.—Fiscal year 1995 damping study test results.

fiber architectures are represented: polar and quasi-isotropic cloth layup. The strength of the component is dependent on the fiber type and architecture; polar architecture can provide good strength for turbine applications but is difficult to produce, while the cloth layup is easy to produce but not quite as strong.

The majority of the tests have been performed at MSFC, while additional temperature and vacuum tests have been performed at the Lewis Research Center. Damping tests in vacuum provide the best results because the damping caused by air resistance has been eliminated. Test data are stored in a data base developed using the commercially available materials data base software M/Vision.

Test data can aid in the selection of materials for turbomachinery applications. Turbopump components produced from composite materials will allow the engine to be lighter, thus providing an improved thrust-to-weight ratio. Composites in the turbine area could allow the engine to run at higher temperatures, thereby increasing performance and equating to larger payloads (or the delivery of smaller payloads to higher orbits).

With the commercialization of space, this data can be utilized by private companies in the development of space vehicles that will be lighter, be able to perform better, and do so at lower development and operations costs.

Composite materials can offer lighter weight and less costly components for rocket engine applications. Test data have shown that fiber-reinforced composites provide higher material damping than the selected baseline advanced metal alloy. Additionally, with their higher damping, composites may increase the life of components subjected to high-vibration environments.

Sponsor: Center Director's Discretionary Fund

Synchronous Phase-Averaging Method for Machinery Diagnostics

Tony R. Fiorucci/ED23
205–544–1551

Turbomachinery health monitoring and fault diagnosis have always been significant technical challenges in the space and transportation industries. A reliable health-monitoring system can prevent catastrophic failures and costly engine downtime due to false alarms. To enhance engine safety and reliability, efficient and reliable diagnostic signal analysis techniques must be developed that can reduce catastrophic system failure risks and expedite the evaluation of both flight and ground test data, thereby reducing launch turnaround time.

A new algorithm, synchronous phase averaging, is being developed to provide superior signal enhancement performance for diagnostic evaluation over that of the conventional synchronous time-averaging method. A quasiperiodic synchronous (Sync) component is transformed into a pure-tone discrete component using the phase-synchronized enhancement method. Time domain averaging can then be directly applied to the resultant signal to achieve signal enhancement. The technique also eliminates the required tachometer monitoring instrumentation and allows direct application to remote sensing, such as gearbox diagnostics using a single acoustic or accelerometer measurement.

Successful application examples have been utilized to demonstrate the performance of the proposed

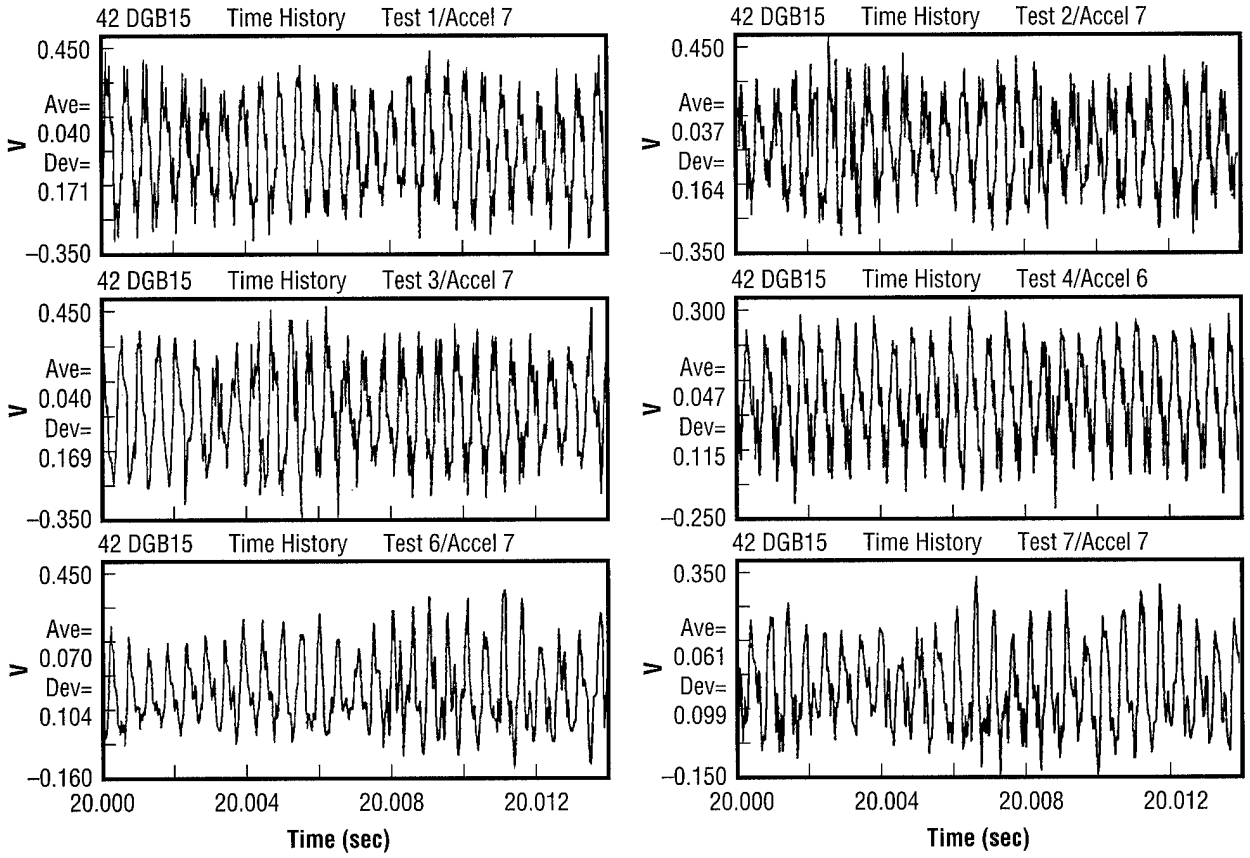

FIGURE 79.—Raw signal of gearbox test data with 500 average (fundamental frequency = Sync).

synchronous phase-averaging techniques for gearbox diagnostics. The test data were captured from externally mounted accelerometers of a gearbox, with both input pinion and output gears having 27 teeth. The shaft rotational frequency (known as synchronous and denoted as N) is run at approximately 71.7 hertz during the tests; therefore, the predicted gear-mesh frequency is approximately 1,935 hertz (the 27th harmonic of Sync). Figure 79 shows the raw time history of an accelerometer measurement for six sets of gearbox data used to demonstrate the phase averaging during one revolution of shaft rotation. The waveforms of these raw signals have all been corrupted by background noise. To perform synchronous phase averaging, these raw accelerometer data were first synchronized to the gear-mesh frequency using the phase-synchronized enhancement method. Time domain averaging was then directly applied to the data using a fundamental frequency of 71.7 hertz (Sync). Figure 80 shows the resulting enhanced signals, each over a full cycle of shaft rotation for the six tests. The number of ensemble averages performed in the analysis is 500. Within this full cycle of shaft revolution, an enhanced signal with 27 cycles of oscillation is observed, which corresponds to the tooth-mesh waveform. In examining the smoothness of this waveform, a noticeable discontinuity or irregularity is readily observed in tests 6 and 7 at the 26th oscillation cycle. The discontinuity repeatedly shows up in the phase-averaged enhanced signal at other time periods within the test, indicating a gear-tooth fault within the hardware used in tests 6 and 7.

The synchronous phase-averaging analysis does not require tachometer or key-phaser input, such as the synchronous time-averaging method would require. The synchronization can be directly performed within a vibration measurement signal at any gear-mesh frequency of a chosen rotor. Since the amplitude of the gear-mesh

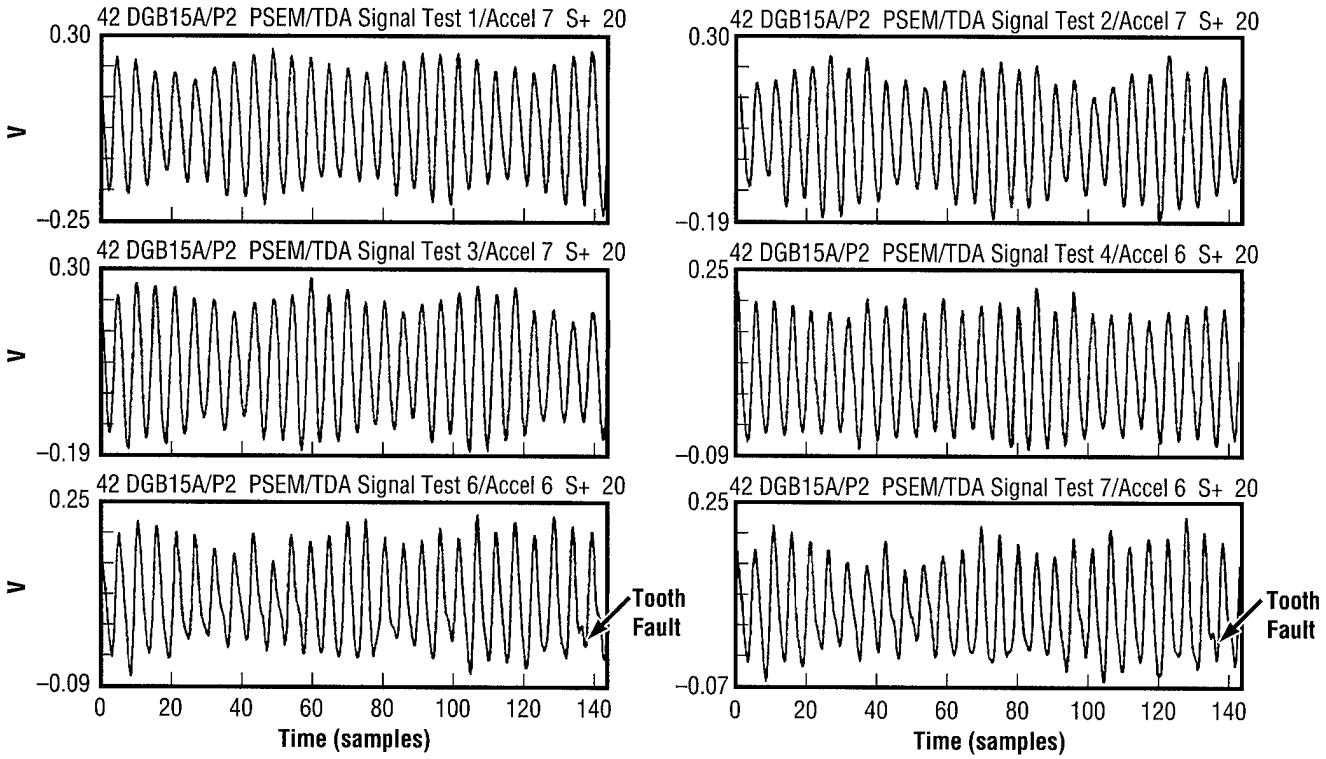

FIGURE 80.—Synchronous phase-averaged signal of gearbox test data with 500 averages (fundamental frequency = Sync).

component measured by a vibration sensor is typically strong, synchronization to various rotational frequencies within a single measurement can be achieved by tuning the phase-synchronized enhancement method reference frequency to the desired gear-mesh frequency. Therefore, the complexity of the instrumentation and data acquisition requirements is reduced.

The synchronous phase-averaging technique has considerable commercial application potential outside NASA's propulsion area. As demonstrated with the gearbox test data, this method could greatly enhance the performance for diagnostic evaluation, which is a common and critical mechanical component for many industrial machinery systems, including those used in the power plant, transportation, and manufacturing sectors.

Fiorucci, T., and McBride, J. 1994. Phase-Synchronized Enhancement Method for Machinery Diagnostics. *Research and Technology 1994.*

Jong, J.; Jones, J.; McBride, J.; and Coffin, T. December 1991. Correlation Identification Between Spectral Components in Turbomachinery Measurements by Generalized Hyper-Coherence. Third International Machinery Monitoring and Diagnostic Conference.

Jong, J.; Jones, J.; McBride, J.; Fiorucci, T.; and Zoladz, T. 1994. Phase-Synchronized Enhancement Method for Space Shuttle Main Engine Diagnostics. NASA Conference on Advanced Earth-to-Orbit Propulsion Technology.

Sponsor: Space Shuttle Main Engine Office

Single-Cycle Versus Multicycle Proof Testing

Henry M. Lee/ED25
205–544–4619

The overall objective of this effort is to assess the relative advantages and disadvantages of single-cycle versus multicycle proof testing and to understand and develop the optimum proof test logic.

Previous work done under this task has included an historical review of multicycle testing experiences and typical defects. The surface crack growth in Inconel 718 was experimentally characterized; a simple analytical model that used the reference stress estimates of J (elastic-plastic stress intensity) was developed; and resistance curves for surface cracks were developed to support the model that used a bounding approach for multicycle growth. Several critical experiments were performed, including studying the relationship between fatigue crack growth and ductile tearing, fractographic studies, acoustic emission monitoring, proper characterization of elastic-plastic fatigue crack growth, and conditions for identifying multicycle failure under load control. From the results of the above work, a second analytical model based on the tear-fatigue theory was developed.

Which is better: single-cycle or multicycle proof tests? The answer is not simple. The question must be asked in the right way. Looking at the question from a strictly deterministic view, for a single component that survives a proof test, multicycle proof testing will cause more crack growth than a single cycle. If the component survives, it will always be worse with multicycle proof testing. Looking at the question from a probabilistic basis, one must consider a population of components before versus after testing. Multicycle testing will cause more crack growth than single cycle, but it will remove more defective components from the population.

Service reliability is influenced by many factors, including material properties, service and proof loading, and component and crack geometry. Specific calculations of in-service reliability requires detailed fracture mechanics analysis coupled with probabilistic analysis. Specification of a single, simple, multicycle proof test protocol in every application is not feasible.

Other issues must also be considered when comparing single-cycle versus multicycle tests. Researchers must approach such other concerns as cracks at stress concentrators, hold-time effects, multicycle proof test failure due to damage coalescence, flaw shape changes, and weldment issues.

An engineering guidelines handbook for proof test design is being developed with emphasis on theory and validation of tear-fatigue algorithm for multicycle growth, as well as evaluation of single-cycle versus multicycle proof testing based on fleet reliability.

Sponsor: Office of Space Access and Technology

■■■■■

Development of State-of-the-Art Proof-Test Methodology

Charles L. Denniston/ED25
205–544–7248

MSFC is currently funding the Southwest Research Institute to provide the Center with an updated, state-of-the-art, proof-testing guidelines document for metallic pressure vessels. The current guidelines document, NASA–SP–8040, was released in 1970, is out of date, and is based on a linear analysis approach that is no longer in wide use.

Southwest Research is utilizing two new pieces of technology to develop the new document. The first piece provides a way of solving elastic-plastic fracture mechanics problems by estimating a flaw's J-integral value via the Electric Power Research Institute J-integral estimation scheme. The second technology being incorporated into the evolving guidelines document is the Failure Assessment Diagram, which is to be used to evaluate flaw growth behavior, including the initiation of ductile tearing and instability in the vicinity of the flow. Both of the approaches represent relatively new ways to solve the type of fracture mechanics problems faced when an engineer designs proof tests.

The J-integral estimation scheme provides a means for estimating the J-integral value for a flaw responding to a particular loading in a certain geometry. While methods for calculating actual J-integral values for flaws do exist, these solutions are only for a limited range of problem types

and are not generally easy to determine. The Electric Power Research Institute scheme approaches the problem of estimating *J*-integrals by assuming the total *J*-integral for a particular problem can be expressed as the sum of exclusively elastic and purely plastic solutions.

$$J_{\text{Total}} = J_e + J_p$$

The J_e term represents the elastic portion of the total *J*-integral and is defined as:

$$J_e = \frac{K^2(a_e)}{E'} \text{ with :}$$

$$E' = \begin{cases} E; & \text{for plane stress} \\ \dfrac{E}{(1-\mu^2)}; & \text{for plane strain} \end{cases}$$

where:

$K(a_e)$ = Linear stress intensity factor (pounds per square inch $\sqrt{\text{inch}}$)

a_e = An equivalent crack size (inches)

E = Material's modulus of elasticity (pounds per square inch)

m = Material's Poisson's ratio $\left(\text{inch}/\text{inch}\right)$.

The nonlinear (plastic) contribution to the total *J*-integral is:

$$J_p = \alpha(\sigma_0)(\varepsilon_0)(c)(h_1\{a,n\})\left(\frac{P}{P_0}\right)^{n+1}$$

where:

a = Ramberg-Osgood equation constant

s_0 = Material's yield strength (pounds per square inch)

e_0 = Corresponding strain to s_0

c = Uncracked ligament length (inches)

h_1 = Electric Power Research Institute elastic-plastic fracture mechanics expression (function of material and geometry)

a = Actual crack size [or depth] (inches)

n = Ramberg-Osgood equation exponent

P = Applied load [either tensile (pound mass force) or moment (inches per pound mass force)]

P_0 = Characterizing yield load (pound mass force or inches per pound mass force).

The estimation of the *J*-integral for a particular problem now only involves the acquisition of what is generally readily available information.

Obtaining a value for a flaws *J*-integral is a vital part of any proof-test philosophy, but it is not sufficient. As an example, one only has to consider a leak-before-burst calculation for a potential flaw in the side of a thin-walled pressure vessel consisting of a ductile metal. This type of leak-before-burst problem can easily become a nonlinear problem with significant yielding around the flaw when pressures are high. The yielding complicates the calculation of a *J*-integral and reduces the material's resistance to failure. Any proof-test philosophy that will work with thin-walled pressure vessels of ductile

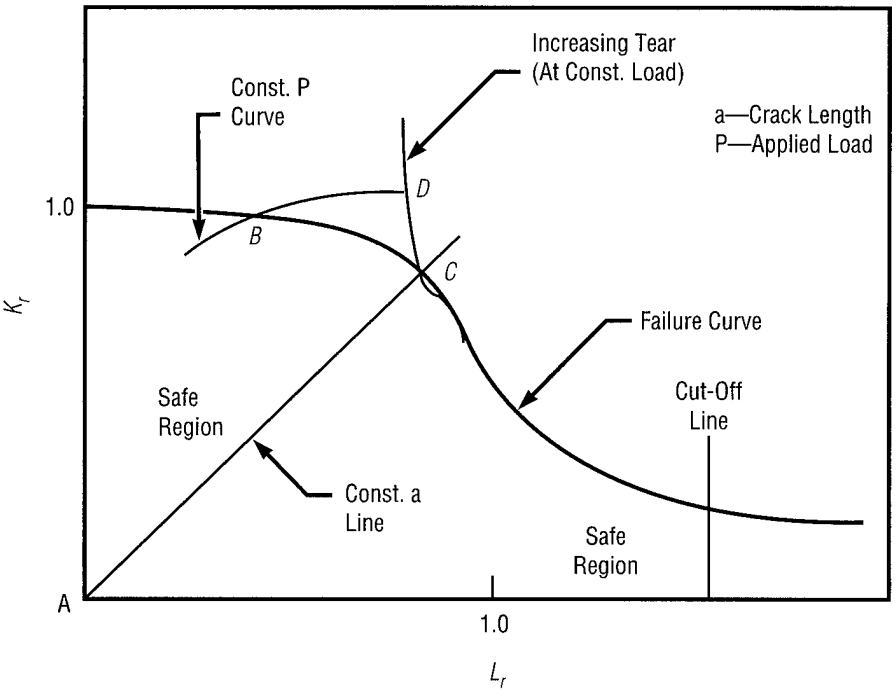

Figure 81.—Failure Assessment Diagram with tearing.

metals must be capable of handling this loss of toughness brought about with increased local loading.

Southwest Research plans to account for this loss of toughness in the guidelines they are developing by using Failure Assessment Diagrams. Figure 81 provides an example in which the "failure curve" illustrates the reduction in material toughness with increased loading. The K_r and L_r terms are defined below.

$$K_r = f\left\{\frac{\sqrt{J_{\text{Apply}}}}{\sqrt{J_{\text{Apply}}}}\right\};$$

$$L_r = g\left\{\frac{P_{\text{Applied}}}{P_{\text{Reference}}}\right\}$$

Failure Assessment Diagrams can be used to do more than just determine material allowables. They can also be used to solve flaw-tearing problems in ductile metals. Figure 81 illustrates a situation where a certain flaw is growing due to a constant load, P. When the flaw growth reaches point B, initiation of tearing is predicted. At the flaw's tip, the stress and *J*-integral can be predicted by using the corresponding K_r and L_r values at point B. Tearing is predicted to be arrested at point C, where the stress and *J*-integral at tearing arrest can be determined from examining the K_r and L_r values corresponding to that point. However, if the "increasing tear" curve were tangent to the "failure curve," then the instability of the flaw would be imminent, and the tearing of the flaw might not stop. In such a case, a failure, e.g., a pipe burst, would be predicted.

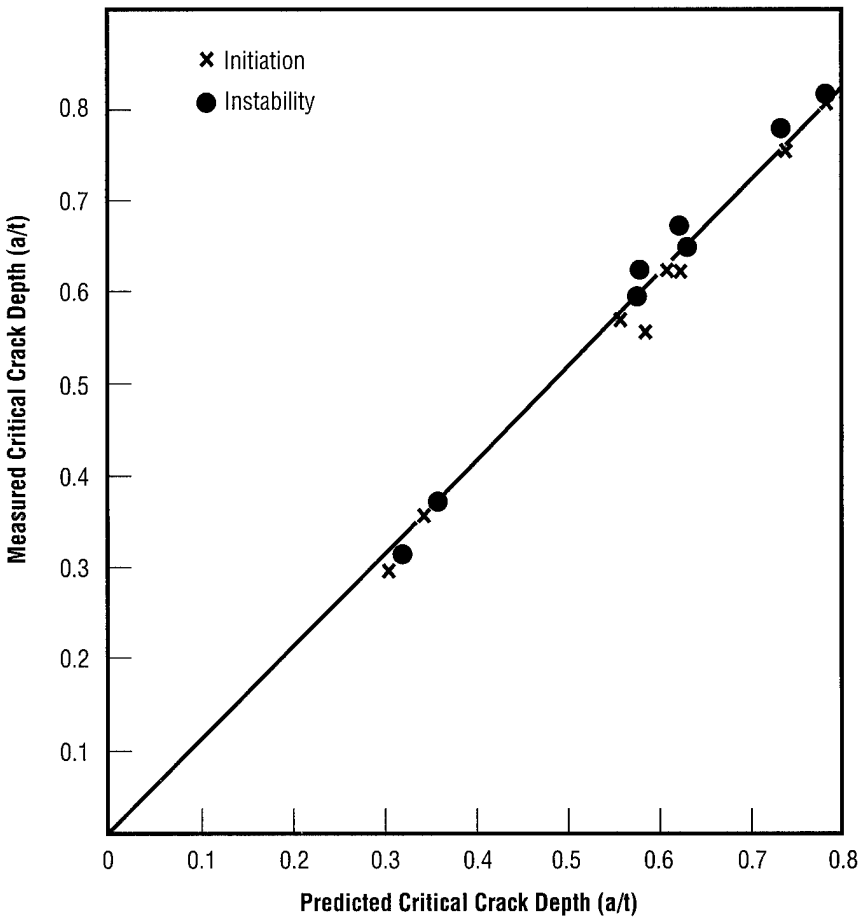

Figure 82.—Comparison of measured and predicted crack depths at the initiation of stable tearing and instability for Inconel 718 test specimens.

Southwest Research is currently running tests to verify the Failure Assessment Diagram approach to predicting tearing behavior. In figure 82, a plot comparing the measured critical crack depth to the predicted critical crack depth is shown for surface flaws in Inconel 718 test specimens. A similar plot could be shown for measured versus predicted critical loads. Southwest has been able to predict the initiation and instability behavior of tearing flaws generally within ±10 percent.

The final phase of testing to verify the philosophy to be incorporated into the proof-testing guidelines is underway. In the final phase of Failure Assessment Diagram testing, space shuttle main engine ducts are having surface flaws placed in them and their ends sealed. Each of these three ducts will then be pressurized until failure. The growth of each flaw placed in the duct wall will be examined and compared to what the approach to be incorporated into the proof-testing guidelines predicts. Once these three

tests are completed, the actual writing of guidelines should commence. The proof-testing guidelines document is scheduled to be delivered to MSFC by the end of the 1996 fiscal year.

Sponsor: Office of Space Access and Technology

Industry Involvement: Southwest Research Institute

Hybrid Method for Measurement of Rotational Structural Dynamic Properties

Michael L. Tinker/ED23
205–544–4973

Rotational structural dynamic responses are typically not measured in modal survey testing due to the lack of adequate procedures or instrumentation. In the residual flexibility free-suspension method, the inclusion of rotational terms could (1) improve the process of updating finite element models using test data and (2) enhance the applicability of the residual technique for various industries. Due to the difficulty of measuring rotational residual flexibilities, the current study considers the possibility of attaching rectangular masses to the interface regions, or trunnions, of a space shuttle payload simulator (fig. 83) to amplify rotational motion of the trunnions and enhance their measurement.

The purpose of this research is to investigate use of a hybrid free-suspension modal testing method for measurement of rotational frequency response functions and residual flexibility. The work is part of an ongoing effort to perform shuttle payload modal vibration testing more accurately and less expensively than in the past.

The subject hybrid technique combines the mass-additive and residual flexibility techniques that have been studied for potential application to shuttle payloads during the past several years at MSFC. The mass-additive approach involves the measurement and use of free-free modes of the structure with mass-loaded boundaries or interface degrees of freedom, and the residual flexibility method requires the free-free modes and residual flexibility of the interfaces. In both cases, shuttle orbiter-constrained modes are derived using a summation of free-boundary modes.

Although ongoing in-house research has shown that the mass-additive approach is less desirable than the residual flexibility method for verifying shuttle payload models, it has features that are very attractive when considered in terms of a hybrid modal test method. In particular, rotational measurements for the payload interfaces (trunnions) become possible when a rectangular mass is used to increase the angular motions and provide a means of using translational accelerometers. Measurement of rotational structural dynamic properties historically has been very difficult, and it appears that a practical rotational accelerometer has yet to be developed. For this reason, only translational data is generally taken during modal tests. Although payload interface rotations are not constrained by the orbiter, the availability of rotational frequency response function data could be useful in model correlation. Further, rotational measurements are of great interest to the structural dynamics community in general. One drawback to the residual flexibility approach has been the difficulty in obtaining rotational data for general boundary conditions.

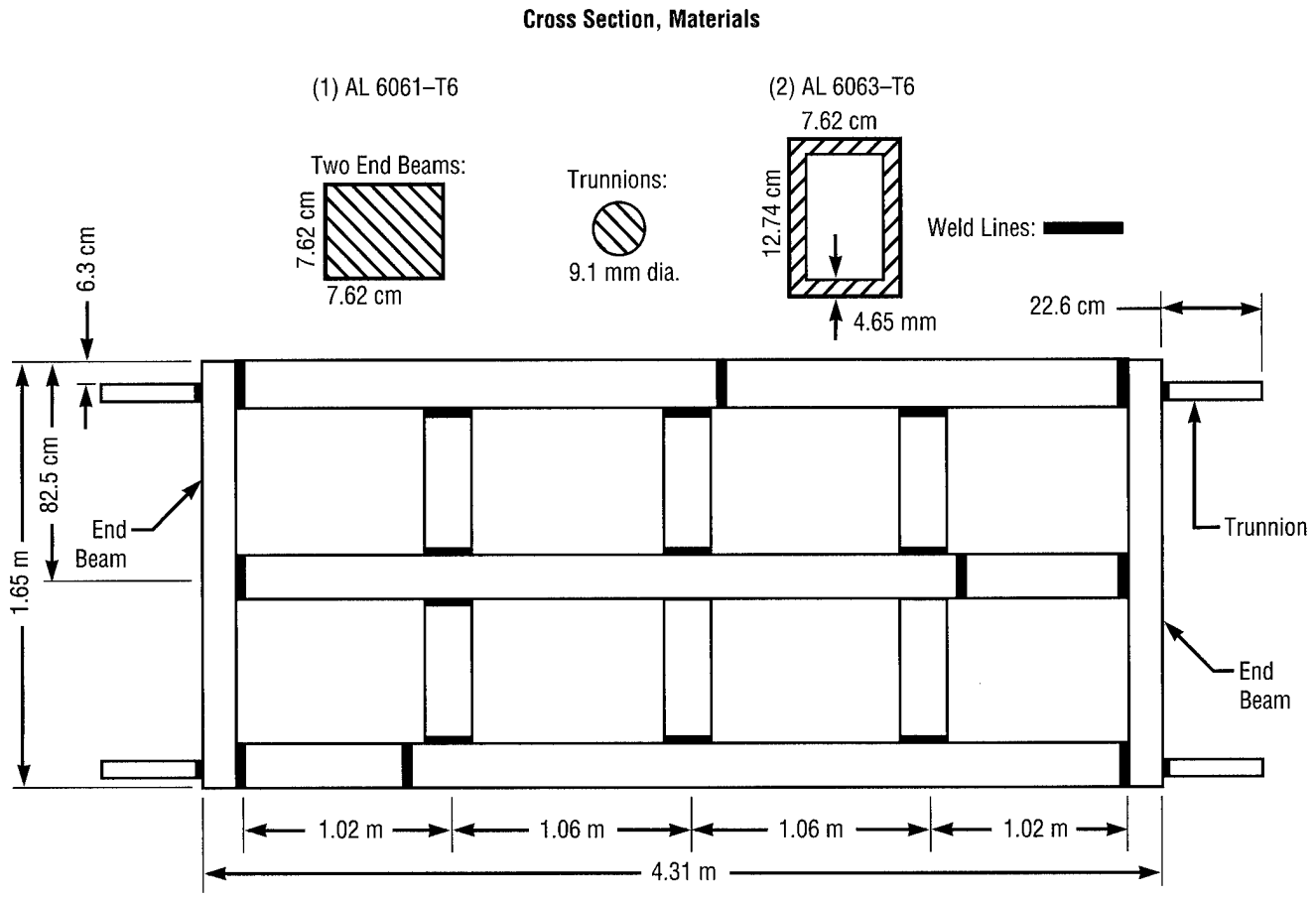

Figure 83.—Space shuttle payload simulator.

The research includes the following tasks: (1) derivation of hybrid equations; (2) use of a simple test article dynamically similar to shuttle payloads (fig. 83), at least in the orbiter interface regions; (3) calculation of free-free mode shapes, frequencies, and interface residual flexibilities for the article with mass-loaded interfaces; (4) measurement of free-free modes, frequencies, and residuals for the simple test article with a mass-loaded trunnion interface; (5) estimation of rotational frequency response and residual functions in the absence of interface mass-loading; and (6) discussion of using rotational frequency response function data for model correlation. Step 5 provides the desired result: the rotational frequency response (acceleration/force ratio) and residual flexibility estimated for the trunnion without mass-loading. This requires some analytical work once the mass-loaded rotations have been measured.

Hybrid equations have been derived for the residual approach to allow the use of mass-loading at desired points on the structure. The effects of the masses have been analytically removed to derive the constrained mode shapes of the structure without mass-loading. In the past year, rotational frequency response measurements were made using a simple payload simulator structure having trunnion interfaces (fig. 83). A small mass was attached to one of the four trunnions (fig. 84), and was instrumented with accelerometers to allow estimation of the trunnion attach-point rotations.

Work remaining to be done is as follows: (1) calculate rotational trunnion responses for the payload

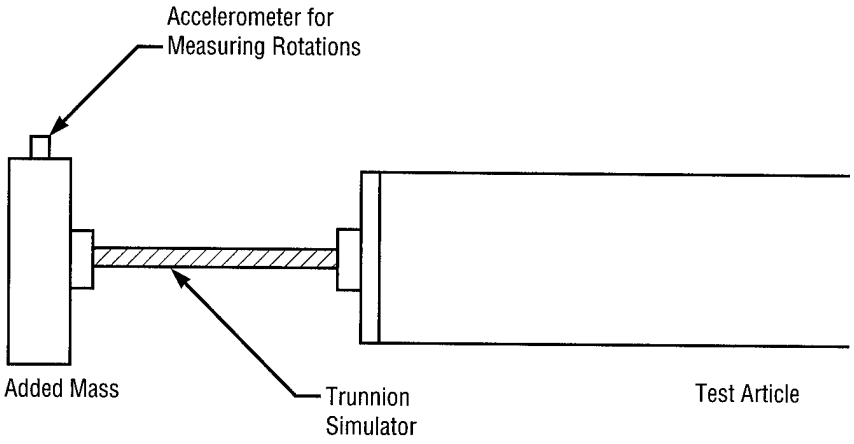

Figure 84.—Illustration of test setup for measuring rotational response.

simulator structure with mass-loading and compare with the measurements made this past year, (2) write computer code to estimate the rotational responses without mass-loaded trunnions, and (3) complete checkout of the code that was modified in fiscal year 1994 to include mass addition in the computation of residual flexibility. A fourth task is being considered to measure rotations with a mobile mass unit that can be attached at any desired point on the structure.

Admire, J.R.; Tinker, M.L.; and Ivey, E.W. January 1994. Residual Flexibility Test Method for Verification of Constrained Structural Models. *American Institute of Aeronautics and Astronautics Journal*, 32:1:170–175.

Admire, J.R.; Tinker, M.L.; and Ivey, E.W. November 1993. Mass-Additive Modal Test Method for Verification of Constrained Structural Models. *American Institute of Aeronautics and Astronautics Journal*, 31:11:2, 148–53.

Sponsor: Center Director's Discretionary Fund

Life Prediction of Ceramic-and Metal-Matrix Composites

James B. Min/ED25
205–544–1564

In order to save weight and increase performance, new rocket systems will continue to make use of ceramic- and metal-matrix composites. Currently, MSFC is developing a design analysis tool to determine the useful life of rocket engine components made with ceramic-matrix and metal-matrix composites.

The technical objectives of the project have included the development of a new analysis technique that combines micromechanics, fracture mechanics, and statistical principles to model and predict the mechanical response and failure mechanisms of such composites. The proposed technique uses the coefficient of friction at the fiber-matrix interface as the interface parameter which, unlike the interfacial shear-stress parameter in the earlier models, can account for the effects of fiber diameter, fiber volume fraction, loading, transverse stress, and thermal effects. Thus, a single parameter can now be used to correlate data for different temperatures, as well as fiber volume fractions and loadings, which was not possible with earlier models.

For continuously reinforced composites, the failure mechanisms involve fiber-matrix debonding, fiber-bridged matrix cracking, and fiber failure in the wake of the matrix crack (fig. 85). The micromechanics, shear-lag, and continuum fracture mechanics models will be integrated with a

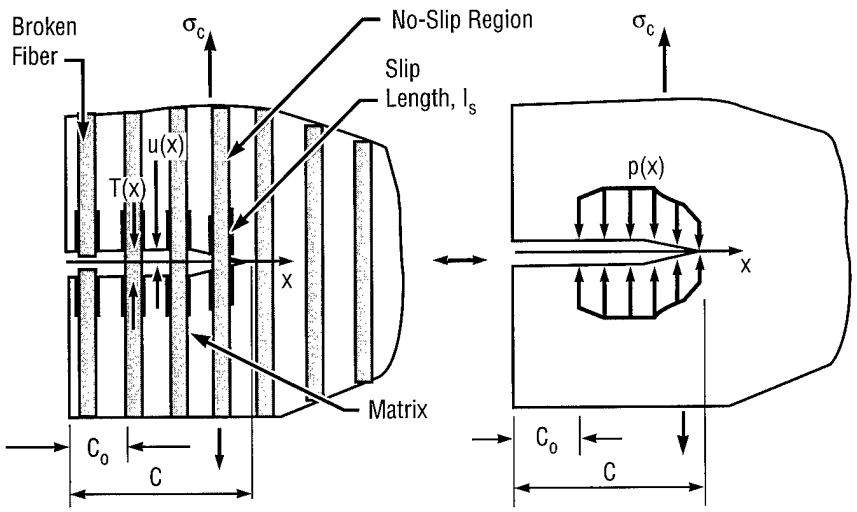

FIGURE 85.—Schematic representation of failure modes in ceramic- and metal-matrix composites with corresponding continuum idealization.

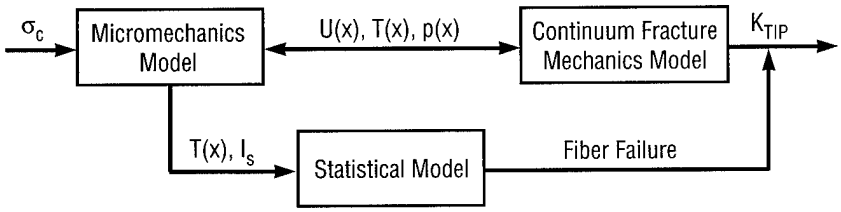

FIGURE 86.—Flow chart describing analytical techniques.

statistical model to develop a general-purpose ceramic- and metal-matrix composite life-prediction analysis code (fig. 86).

The successful completion of this effort will result in the development of a new, analytical tool called "CMLife." The tool will be used for fatigue life prediction of laminated and textile ceramic-matrix and metal-matrix composites, thereby fulfilling a critical need in the design of high-temperature components at NASA and in industry. A menu-driven, point-and-click user interface will enhance its appeal to engineers and designers, and it will be seamlessly integrated with a commercial finite element code for life prediction of ceramic- and metal-matrix composites.

Sponsor: Office of Advanced Concepts and Technology, Small Business Innovation Research

Industry Involvement: Analytical Services and Materials, Inc.

Elastic-Plastic and Fully Plastic Fatigue Crack Growth

Wayne Gregg/ED27
205–544–5501

The objective of the elastic-plastic and fully plastic fatigue crack growth research effort is to develop methods and computer programs for analytically predicting lifetimes of flawed metallic structures that experience appreciable plastic crack-tip stresses. In order to reach this objective, existing elastic-plastic stress intensity (J-integral) solutions from the Electric Power Research Institute have been collected and combined with new analytical solutions developed from finite element solutions with the reference stress method. The list of available J-integral solutions is the most extensive ever collected. An overview of the solutions is as follows:

J-integral solutions for primary loads based on Electric Power Research Institute solutions and the reference stress method:

- Two-dimensional axial flaws in pressurized cylinders
- Two-dimensional circumferential flaws in cylinders, axial end force
- Two-dimensional crack from a hole in biaxial stress field
- Two-dimensional single-edge cracked plate (plane stress and plane strain)
- Two-dimensional center-cracked plate (plane stress and plane strain)
- Through wall circumferential crack, axial end force
- Through wall circumferential crack, bending moment.

J-integral solutions for primary loads based on newly developed finite element solutions and the reference stress method:

- Three-dimensional surface flaw in a finite width plate subjected to a tensile end force (two degrees of freedom—near surface and deepest point)
- Three-dimensional corner flaw in a finite width plate subjected to a tensile end force (two degrees of freedom—near surface points).

Existing linear-elastic stress intensity solutions from the NASA/FLAGRO software have been combined with limit-load solutions and cyclic stress-strain curves to provide estimates for the J solutions with the reference stress method. A listing of these FLAGRO geometries includes:

- TC01: through center crack subjected to tension
- TC02: through edge crack subjected to tension or bending
- TC03: through crack from an offset hole in a plate
- TC04: through crack from hole in lug
- TC05: through crack from hole in a plate with a row of holes subjected to tension or bending
- TC06: through crack in a sphere
- TC07: axial through crack in a cylinder
- TC08: circumferential through crack in a cylinder subjected to tension or bending
- TC10: circumferential through crack from a hole in a cylinder
- EC01: embedded elliptical crack subjected to tension
- CC01: corner crack in a rectangular plate subjected to tension or through wall bending
- CC02: corner crack from a hole in a plate subjected to a bending moment
- CC03: corner crack from a hole in a lug
- SC01: surface crack in a rectangular plate subjected to tension or bending
- SC03: surface crack in a spherical pressure vessel
- SC04: longitudinal surface crack in a hollow cylinder
- SC05: thumbnail crack in a hollow cylinder subjected to tension or bending
- SC07: thumbnail crack in a solid cylinder subjected to tension or bending
- SC08: thumbnail crack in a thread root in a cylinder subjected to tension or bending
- SC09: circumferential crack at a thread root in a cylinder subjected to tension or bending.

In addition to J-integral solutions, crack-growth algorithms have been developed for some of the flaw geometries. The associated algorithm topics include:

- Monotonic loading
- Cyclic loading
- Primary and secondary loading (mechanical and thermal)
- Combined primary loading (tension and bending)
- Crack failure
- Crack closure
- Ductile tearing
- Materials data base.

Current plans are to incorporate these solutions into the NASA/FLAGRO software in order to allow free access to interested industries and other government agencies. A preliminary list of prioritized solutions to be coded into FLAGRO will include TC01, EC01, CC01, and SC01. These solutions will have a portion of the capabilities from each crack growth algorithm currently available.

Sponsor: Office of Space Access and Technology

Industry Involvement: Southwest Research Institute, Rocketdyne Division of Rockwell International

Life-Prediction Methodology for Ceramic-Matrix Composites

Rene Ortega/ED27
205–544–5448

The lack of utilization of high-temperature monolithic ceramics in rocket engine components is primarily due to their low fracture toughness. Reinforcement of the ceramic matrix with ceramic fibers (ceramic-matrix composites) can significantly increase the damage tolerance of these materials by various crack-tip shielding mechanisms, such as fiber-bridging in the crack wake, crack deflection, and crack-tip blunting. These mechanisms have been shown to increase fracture toughness from 4 to 5 Ksi $\sqrt{in}$ for monolithic ceramics to 20–35 Ksi $\sqrt{in}$ for ceramic-matrix composites, even though the elongation at failure has remained in the 0.4- to 0.8-percent range. However, the durability of these materials under cyclic loading is unknown, as is their resistance to attack under severe environmental conditions present in the rocket engines.

Very large flaw populations inherent in the manufacturing processes for some of the more promising ceramic-matrix composite candidates present some unique problems in the development of a life-prediction methodology for these materials. The stress intensity solutions for the large crack arrays are lacking, and crack-interaction effects are difficult to model even without other crack-tip shielding mechanisms mentioned earlier. Because of these problems, the few attempts at life prediction have abandoned the damage-tolerance approach and have concentrated on attempting to predict damage accumulation through the reduction of stiffness. While these efforts have been promising, they are only in the initial stages and tend to be highly empirical.

MSFC, along with the expertise of Lewis Research Center personnel, has begun a program with the overall goal of developing, codifying, and validating a life-prediction methodology for ceramic-matrix composite engine components. The critical-damage mechanisms will be identified through a large number of interrupted high-temperature cyclic and monotonic tests. Test coupons will be evaluated through both nondestructive and vibratory dampening testing to ascertain the degree of damage. Also, sequential through-the-thickness polishing and microscopical evaluation will be performed to determine the ongoing damage mechanisms, as well as measure the crack density and crack-size distribution. The effect of time at different temperatures (i.e., environmental stability) will be considered by pre-exposing selected specimens to high temperatures for appropriate times prior to testing. The evolving cyclic or time-dependent flaw population and distribution will be quantified, correlated to the nondestructive evaluation, and used in analytical modeling. Further cyclic and monotonic data and other material properties of the selected ceramic-matrix composite will be obtained by testing—and supplemented by literature search where possible.

In order to maximize the success of the life-modeling developmental effort, both the damage accumulation methodology and a probabilistic-based fracture mechanics method will be investigated at the outset to determine the most promising approach. Both will be based on the identified physical damage processes and will utilize the quantified measurements of material damage as a function of load and temperature history. The use of probabilistic fracture mechanics is driven by the need to describe a complex flaw population and has a greater chance of success than the deterministic damage tolerance approach. Other methodologies may be investigated if appropriate. After evaluation, the most promising methodology will be down-selected for life-code development. The life-prediction code will be validated through subcomponent cyclic and monotonic testing of such complex geometries as bolt holes or notches at appropriate test conditions.

Sponsor: Office of Space Access and Technology

Coherent-Phase Cavitation-Monitoring System for Turbomachinery

Tom E. Nesman/ED32
205–544–1546

Cavitation is the process of boiling fluid that occurs when local fluid dynamic pressures in the areas of accelerated flow drop below the vapor pressure of the fluid. When cavitation occurs within the turbopumps of liquid rocket engine propulsion systems, it can severely degrade overall system performance, cause excessive structural vibration, and damage turbopump blades. The Coherent-Phase Cavitation-Monitoring System will utilize an innovative coherent-phase wide-band demodulation technique to accurately detect the cavitation inception point occurrence, its severity, and the type of cavitation, with an on-line, continuous monitoring system. The method's effectiveness is attributed to its unique ability to accurately extract cavitation-generated signatures without being subject to commonly encountered high-frequency discrete interference.

Traditionally, the performance of turbomachinery and other fluid dynamic systems has been very difficult to determine. Therefore, a reliable method for determining cavitation losses in turbomachinery systems is crucial in assessing overall system performance. The principle for cavitation detection is based on a unique phenomenon associated with cavitation physics, i.e., when cavitation occurs in a rotating system, the periodic rotational components (such as revolutions per minute and their harmonics) will amplitude modulate the wide-band, high-frequency noise generated from the collapse of cavitation bubbles. Such a wide-band modulation phenomenon (a narrow-band discrete signal multiplied by wide-band random noise) will generate hidden periodicity in a monitored dynamic response signal, thus providing a unique signature in the high-frequency region conducive to cavitation detection. However, because of lacking nonlinear-phase information, conventional linear spectral analysis is unable to identify such hidden periodicity within a cavitation-generated wide-band modulation signal.

Prior techniques for cavitation detection have utilized full-wave rectification spectral analysis to perform wide-band demodulation on monitored dynamic measurement signals. The full-wave rectification wide-band demodulation method detects a cavitation signature by demodulating the dynamic signal over an isolated band of high-frequency noise floor using the principle of envelope detection. The onset and existence of cavitation are determined by the recovery of the hidden periodicity within the cavitation-generated wide-band modulation signature. The magnitude of the modulation is used to determine the cavitation severity as a function of system operational parameters (rotational speed, impeller geometry, developed heat, etc.).

In actual applications, the conventional cavitation detection technique suffers from a severe limitation. Since the hidden periodicity is recovered from the

envelope signal of a wide-band high-frequency noise floor, any discrete components present in this high-frequency region of the raw signal will erroneously generate discrete peaks in the resulting demodulated signal, appearing to be recovered hidden periodicity. This limitation is critical in assessing the performance of rocket engines under severe operational environments in which other vibration sources contribute many high-frequency components that can corrupt the demodulation signal.

The new coherent-phase wide-band demodulation technique provides an effective method to avoid such discrete interference. The method is based on the fact that for an ordinary (linear) wide-band noise signal, the spectral components at different frequencies are statistically independent of each other. However, for a wide-band modulation noise signal with hidden periodicity (nonlinear), a unique coherent-phase relationship exists among all interacting components.

The new technique can thus identify hidden periodicity by searching for such a coherent-phase relationship. An inherent characteristic (also a highly desirable one) of the method is that it would not be affected by any linearly superimposed discrete component since only the phase information is utilized for cavitation signature detection. As a result, the coherent-phase information provides an effective way to overcome the critical limitation of discrete interference suffered by the conventional method. The new technique utilizes a phase-only filtering technique along with an envelope detector to search for the unique cavitation-generated coherent-phase relationship.

Application examples to the alternate turbopump development high-pressure fuel turbopump test data have been utilized to demonstrate the performance of the new techniques. Figures 87(a) and 87(b) show the raw power spectral densities of two different pressure measurements during test TTB–038. 6N sideband anomalies are present in the first measurements, but are not observable at all in the raw spectral densities of the second measurement.

In order to determine whether these anomalies were related to cavitation-induced vibration, wide-band demodulation has been performed to identify whether a cavitation-generated hidden periodicity was presented in the wide-band noise floor of the two measurements (figs. 87(c) and 87(d)). No hidden periodic components were recovered in the first measurement (fig. 87(c)); however, the wide-band demodulation spectral density of the second measurement recovered strong hidden periodicity at 6N±a from the wide-band noise floor. The periodic modulating components of the wide-band modulation signal were composed of not only the 6N component, but also its sideband components (the 6N±a anomalies). Such nonsynchronous-related modulating components associated with the cavitation phenomenon were also observed in other pump tests and in inducer MSFC water-flow tests, indicating that the 6N±a sideband anomalies should be a cavitation-related phenomenon.

In summary, cavitation within the turbopumps of liquid rocket engine propulsion systems can: (1) severely degrade overall system performance, (2) cause excessive structural vibration, and (3) create erosion damage to turbopump blades. Therefore, an effective on-line cavitation detection and monitoring system must provide critical performance information during the engineering development of efficient fluid dynamic elements. Moreover, the system must provide this same capability in monitoring operation fluid dynamic systems in the field. Ultimate benefits include efficient turbine designs, lower maintenance costs of on-line systems, and reduced risks of catastrophic failure of on-line fluid dynamic systems.

An effective cavitation detection and monitoring method has strong commercial applications for various turbomachinery systems. In particular, the hydropower industry (almost all hydroturbines experience cavitation and undergo excessive erosion and performance degradation), the nuclear power industry (boiler feedwater pumps), and the U.S. shipbuilding industry (commercial and military surface ship propellers) could all benefit from on-line cavitation monitoring systems.

Nesman, T.; Bordelon, W.; Jong, J. 1995. Dynamic Water-Flow Tests Using Four-Bladed Axial-Flow Inducers. Workshop for Computational Fluid Dynamics Applications in Rocket Propulsion and Launch Vehicle Technology.

Jong, J.; Jones, J.; Jones, P.; Nesman, T.; Zoladz, T.; and Coffin, T. April 1994. Nonlinear Correlation Analysis for Rocket Engine Turbomachinery Vibration Diagnostics. Forty-Eighth Meeting

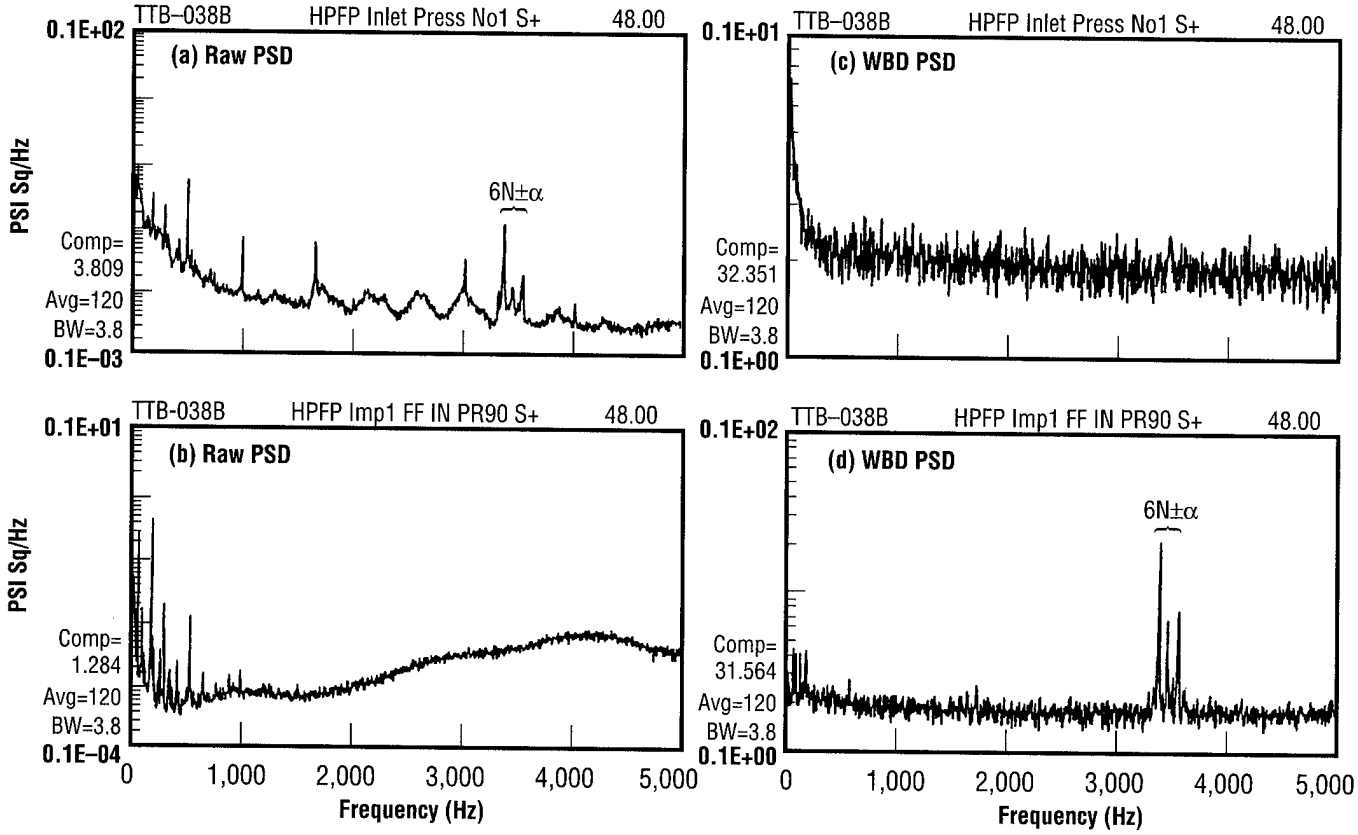

FIGURE 87.—Power spectral densities of alternate turbopump development high-pressure fuel turbopumps: (a) raw power spectral density—inlet pressure number 1; (b) raw spectral density—first-stage impeller pressure; (c) wide-band demodulation spectral density—inlet pressure number 1; (d) wide-band demodulation—first-stage impeller pressure.

of the Mechanical Failure Prevention Group.

Sponsor: Small Business Innovation Research

Investigation of Inducer Steady and Unsteady Blade Loads

Stephen W. Gaddis/ED34
205–544–1612

During the development of the alternate turbopump development liquid-oxygen turbopump, scientists questioned the unsteady hydrodynamic blade load used to determine the inducer blade high-cycle fatigue life. Consequently, a full-scale water-flow inducer test article (fig. 88) was used to investigate inducer steady and unsteady blade loads. Conducted in MSFC's Inducer Test Loop, tests were performed at reduced shaft speeds and ambient water temperature, and were successfully completed in March 1995. The four-bladed, unshrouded, 14.6-degree inducer was tested at scaled water-flow conditions simulating the design-flow coefficient and a range of suction-specific speeds from 5,000 to 16,000 (head falloff). Steady and unsteady measurements—inducer pressure rise, unsteady shroud pressure, and steady and unsteady blade strains—were recorded in both stationary and rotating reference frames. Four strain gauges were mounted per blade. Each was spaced equally chordwise along the blade, approximately 33 percent radially from the inducer hub. Testing was conducted at design conditions to measure steady and cavitation-generated unsteady blade loads to verify the inducer blade high-cycle fatigue life.

Steady strains for blades 1 and 3 (fig. 88) indicated: (1) higher steady strain at the blade leading edge and trailing edge; and (2) at higher suction-specific speeds, the blade chordwise strains tended to be more evenly distributed. At different suction-specific speeds, three inducer cavitation modes were observed: blade-tip vortex, blade alternating, and asymmetric. These cavitation modes changed the inducer unsteady blade loads depending upon the particular mode experienced. At the 38-percent chord position, the blade unsteady strains for all four blades (fig. 89) indicated the change in unsteady strain as the cavitation modes varied with increasing suction-specific speed.

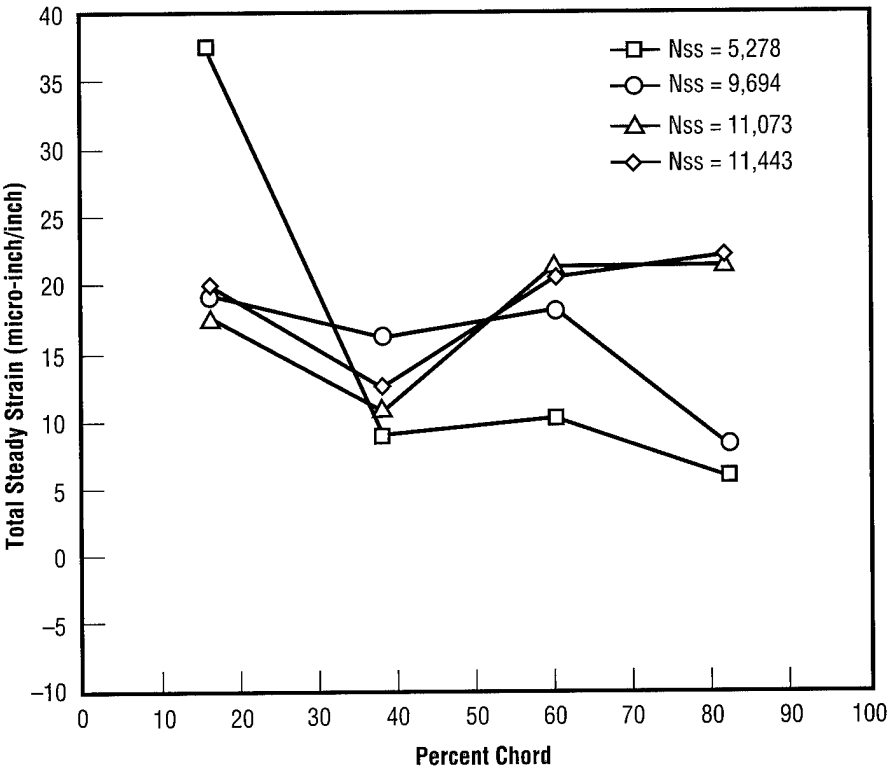

FIGURE 88.—Steady-state hydrodynamic microstrain for blade 1 only versus blade chord for different suction-specific speeds (Test #ITL0006, 14.6-degree inducer, 30-mil-tip clearance, 100-percent Q/N, running 36/0, 37/0, 38/1, 39/0).

Testing concluded that a maximum strain ratio of unsteady to steady blade hydrodynamic strains to be 14 percent, which confirmed adequate inducer life for the alternate turbopump development high-pressure liquid-oxygen pump program. Testing also upheld the conservative design practice of using a strain ratio of 20 to 30 percent to account for unsteady hydrodynamic loads.

Sponsor: Office of Advanced Concepts and Technology, Alternate Turbopump Development Project Office

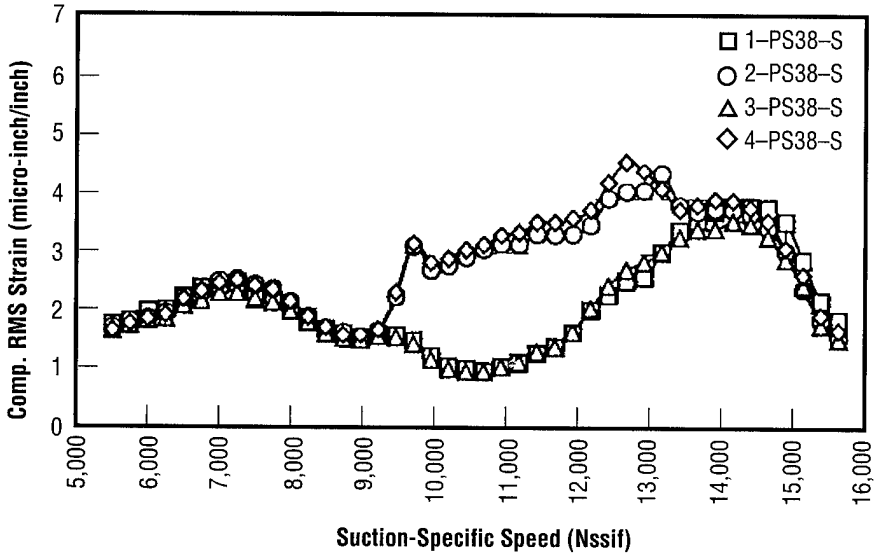

FIGURE 89.—MSFC inducer blade strain test (ITL0006) (run 40/1, 14.6 degrees, 0.030-inch tip cir., 4,200 revolutions per minute, composite RMS unsteady blade strain).

Investigation of Flow Through a Power-Steering Flow-Control Valve

Stephen E. Skelley/ED34
205–544–1574

The complex flow-path intersections within today's power-steering pumps must be designed to minimize fluid aeration and cavitation since the noise and vibration that result not only affect the automobile's power-steering system performance, but also directly impact passenger comfort. At the same time, by design, the flow-control valve must regulate flow through the power-steering system across a wide range of engine speeds and steering maneuvers. Fluid-borne noise and cavitation at fluid pressures near 6,900 kiloPascals (1,000 pounds per square inch absolute) result from the extreme operating conditions that these power-steering flow-control valves experience. A simplified cross section of the flow-control valve in its open position (fig. 90) illustrates that the vented flow joins the flow from the steering system and "supercharges" it before entering the power-steering pump. The cavitating jet and the mixing of the two flows produce noise and reduce the quality of flow entering the pump. Delphi Saginaw Steering Systems builds thousands of flow-control valves a day, yet continues to evaluate each new design by building and testing each one individually. In response, MSFC has entered into a Space Act Agreement to transfer its experience gained in evaluating rocket engine components with experimental and computational techniques.

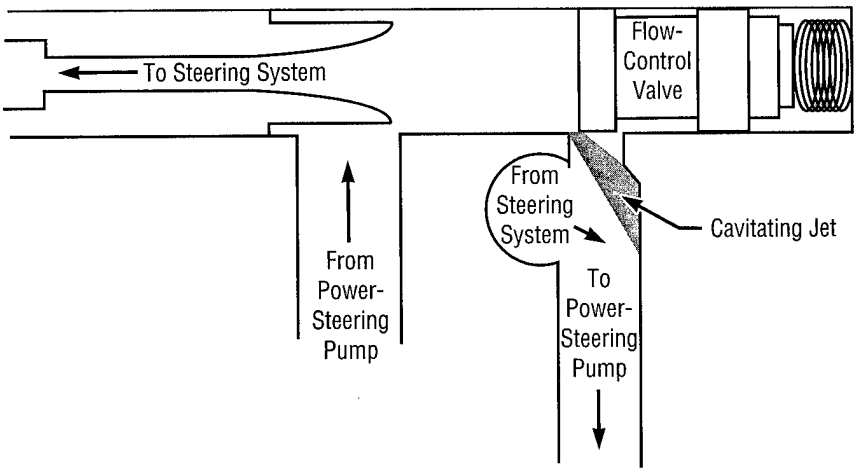

FIGURE 90.—Cross section of open flow-control valve.

MSFC will design a superscale acrylic model of a flow-control valve and test the model under simulated pump-operating conditions with water as the test fluid. With valve flow-path diameters on the order of 12.7 millimeters (0.5 inch), the scaled-up model reduces the operating pressures to a more manageable 104 kiloPascals (15 pounds per square inch absolute) and provides adequate room for measurement access and visual inspection of the flow. Detailed pressure, velocity, and turbulence intensity measurements and qualitative flow visualization in the superscale model will document the flow environment across the entire valve-operating envelope. A parallel effort will develop a computational fluid dynamic model of the flow-path geometry. This model will be calibrated with the experimental data. The resulting computational model will then be used to evaluate the performance of alternate flow-control valve designs, providing valuable predictions of cavitation incipience, flow separation, and system pressure losses. Finally, an optimized flow-path design derived from the baseline experimental test results and the computational fluid dynamics design optimization will be developed.

Industry Involvement: Delphi Saginaw Steering Systems

■■■■■

Experimental Microthruster Evaluation at Simulated Orbital Conditions

Andrew W. Smith/ED36
205–544–4932

Why try to measure a force equivalent to the weight of a paper clip? In the absence of gravity, such minuscule forces can accomplish impressive tasks, like correcting the position of a satellite in Earth orbit. "Microthrusters" is the term given to the class of nozzles that generate these microforces, and are generally classified by a throat Reynolds Number of below 10,000. To quantify the performance characteristics, MSFC maintains test equipment to evaluate microthrusters at simulated orbital conditions.

Experiments are conducted in a 5-cubic-meter vacuum chamber with diffusion pumps capable of evacuating air at 196 cubic meters per second to a chamber pressure of 1E–7 millimeters of mercury absolute. This pressure simulates the density of the atmosphere at approximately 200 miles altitude. A force stand in the chamber measure microthruster forces over a range of 5 to 3,000 dynes. Supporting instrumentation measures gas flow rate, model pressures, and chamber pressure.

The most recent addition to the MSFC data base is the microthruster for the Gravity Probe B Space Science satellite (fig. 91). The Gravity Probe B

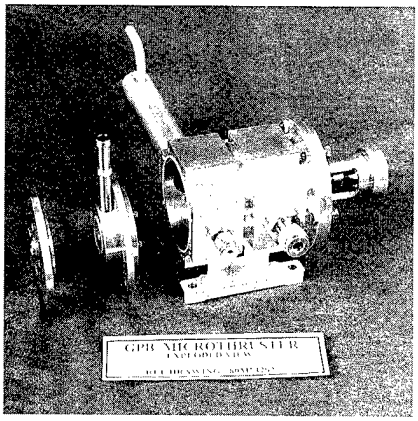

FIGURE 91.—Gravity Probe B microthruster model: exploded view.

is designed to watch the position of a gyro as it orbits the Earth, looking for slight changes as predicted by relativity theory. The satellite's microthrusters are being designed and built by Lockheed–Palo Alto, California. The original purpose of the MSFC testing was to provide an independent confirmation of the microthruster's performance, but grew into a test-bed service for Lockheed when they need to change the design. The test matrix consisted of five plenum pressures versus 18 flow rates. Thrust and discharge coefficients were found to be highly dependent on the throat Reynolds number. The performance was further benchmarked by comparison with a classic sharp-edged orifice nozzle (fig. 92).

MSFC's orbital simulation facilities will continue to be used to participate in analytical studies (Droege),[1] conduct fundamental research (Russell),[2] and provide private industry a test-bed service (Carter).[3]

[1]Droege, A. 1994. Direct Simulation Monte Carlo Analysis of Microthruster Rarefied Flow Characteristics. *Research and Technology 1994*, 208–209.

[2]Russell, C. 1992. Welding in Space Experiments, EH25.

[3]Carter, J. 1995. Experimental Study of the Performance of Gravity Probe B Microthruster. NAS8–39743 Task 034 Final Report.

Sponsor: Science Payload Project Office

Industry Involvement: Lockheed–Palo Alto, California

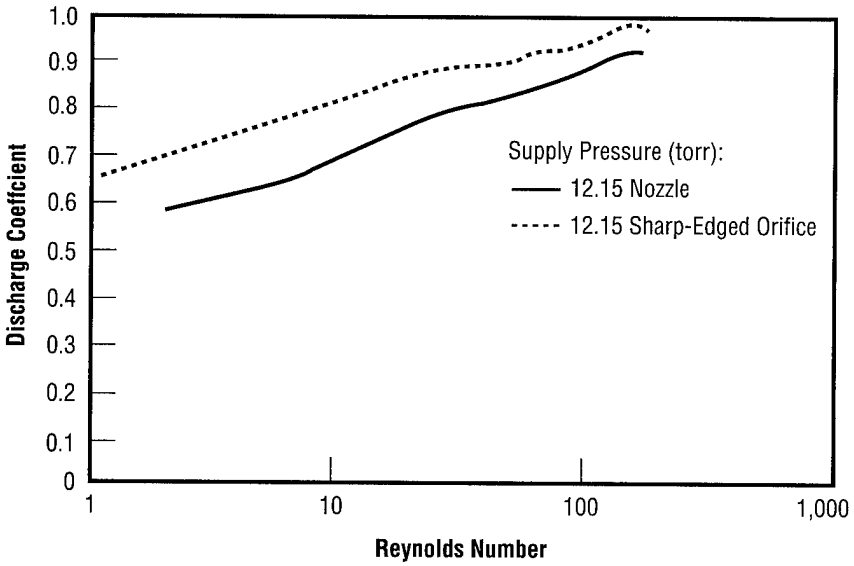

FIGURE 92.—Laval nozzle versus sharp-edged orifice: discharge coefficient = F(Reynolds No.).

Determination of Composite Material Sensitivity to Permeability Depending Upon Lay-Up Configuration

Robert W. Carrigan/ED52
205–544–1227

The purpose of this study is to investigate how permeability is affected by fiber orientation (i.e., lamination sequence) at cryogenic temperatures for a given stress level. The test bottles will be designed to handle liquid hydrogen and fabricated using the automated filament-winding machine in the Productivity Enhancement Complex. The major objective of this research is to quantify the level of hydrogen permeability based upon a specific fiber orientation for a test bottle without a liner.

The effort to reduce launch vehicle weight significantly while still meeting mission objectives has led to the increasing use of high-modulus, high-strength composite materials for major structural elements. Under the National Aerospace Plane program, a rectangular composite liquid-hydrogen tank was designed and built to demonstrate that composite materials can be used to manufacture cryogenic tankage. However, one of the major problems that confronts the use of composite materials for linerless cryogenic tanks is permeability, which is further complicated when pressure and thermal cycling loads are taken into account.

A program has been initiated at MSFC to design, fabricate, and test a series of subscale test bottles to determine the effect that the lay-up configuration may or may not have regarding its permeability. The fabrication and testing of the bottles will be performed in four phases. The first phase will consist of 12 bottles—separated into four subsets of three bottles. Each group of three will be fabricated using the same material and fiber orientation. It is important to note that the materials used when comparing each group of three to each other may or may not be the same. Phases II, III, and IV will also consist of 12 bottles each. The bottles for phases II, III, and IV will not be fabricated until the bottles from phase I (or the previous phase) have been tested and the data analyzed.

This research will provide NASA with a valuable technology for the Reusable Launch Vehicle initiative. Once proven, the technology will provide a data point for acceptable permeability, directly benefiting the industrial partners working toward a reusable launch vehicle.

Sponsor: Center Director's Discretionary Fund

Industry Involvement: Thiokol Corporation

Composite Intertank

Donald B. Ford/ED52
205–544–2454

Pete I. Rodriguez/ED52
205–544–7006

The development of reusable graphite/epoxy composite primary structures is critical to both expendable and reusable launch vehicle configurations. A composite structure, lighter than a comparable metallic structure, means a lower vehicle cost. Optimization can reduce both the mass of composite structures and the manufacturing cost of large components.

Primary structures include the fuel tank, oxidizer tank, and intertank. MSFC is developing the intertank—the cylindrical structure connecting the fuel and oxidizer tanks—to be compatible with an industry partner's composite fuel tank. The intertank's design addresses the parameters of a reusable structure and is relevant to any of NASA's reusable launch vehicles. A reusable structure must handle all loads in the expected design envelope without any failure during its operational lifetime. Simultaneously, the reusable concept requires minimum mass structures; therefore, the design of the intertank optimizes to a zero-margin structure.

The intertank is an 8-foot-diameter structure[1] developed by MSFC to support testing of a liquid-hydrogen composite propellant tank.[2] A thorough understanding of design criteria, analysis, failure prediction, manufacturing, and test setup all contribute to achieving the best

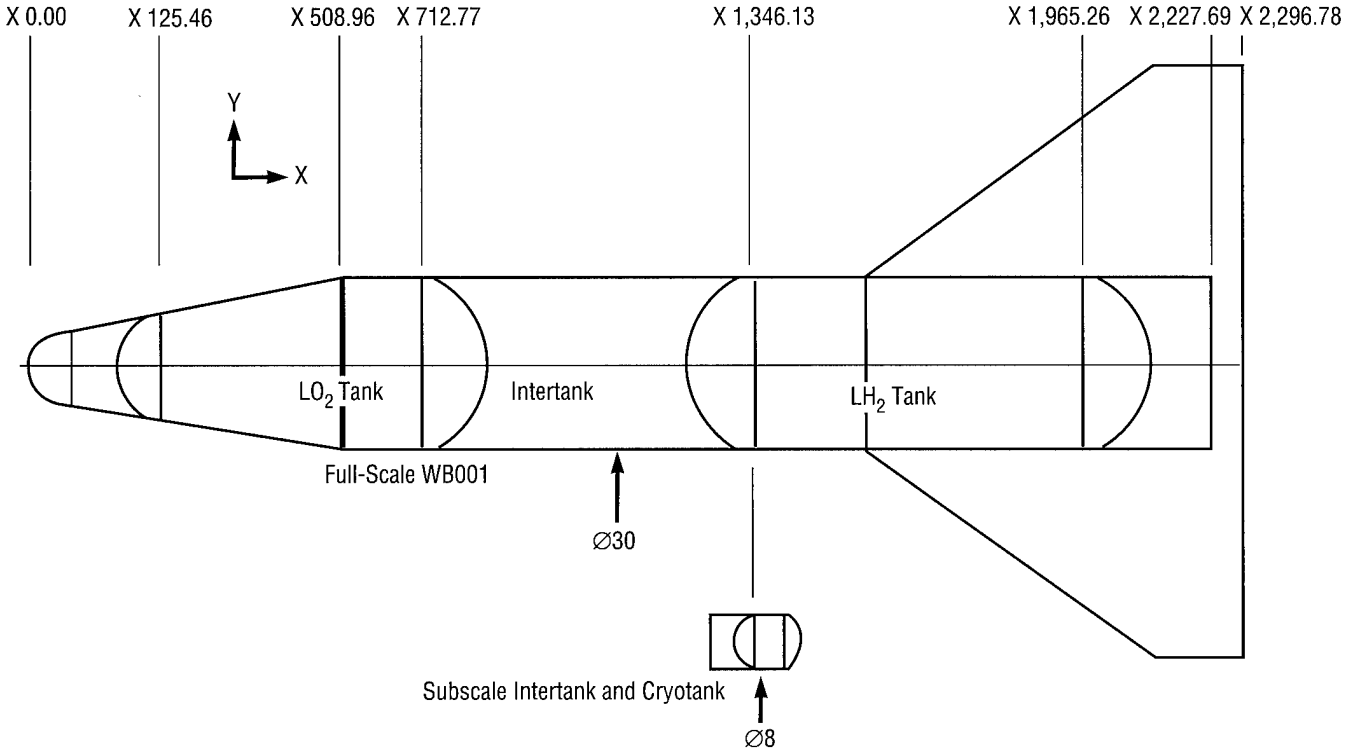

FIGURE 93.—Winged-body configuration reusable launch vehicle.

design. Even though the tests involved represent a large aerospace structure, the derived information applies to composite structures in general. The design criteria for the test specimen are derived from the requirements placed on a full-scale reusable launch vehicle intertank. A winged-body configuration (fig. 93) trade study[3] provided the loading conditions. The loads used for a subscale technology demonstration test were to envelop any launch vehicle configuration. Government- and industry-standard design practices determined the appropriate safety, peaking, and distribution factors applied to the load. Material properties were obtained from the manufacturer's data[4] and past projects.[5]

The design covers the aspects of honeycomb sandwich shell construction. Particular focus has been on the interface at each end of the shell. Any advantage in an optimally designed shell can be lost if heavy over-designed end fittings attach the intertank to the propellant tanks. The design has incorporated a genetic algorithm optimization to simultaneously trade both cylindrical shell and end-joint parameters. Shell variables include ply orientation, balance, symmetry, and core thickness, while end-joint variables include joint build-up geometry, edge distance, and bolted interface criteria (bolt mass, diameter, strength). The design alters the variable constituents to meet cylindrical buckling, dimpling, wrinkling, and strength requirements of the shell and to meet local-bearing, net-tension, wedge-splitting, shear-out, and bolt-stress requirements in the end joint.

The technology developed with the composite intertank produces lighter launch vehicles, which enables smaller vehicles with lower operational costs to perform the same functions as older boosters. The technology is also necessary to make advanced launch vehicle concepts feasible. The results of development apply not only to aerospace structures, but can benefit the everyday design of transportation—from airplanes to automobiles.

[1]Composite Primary Structures. NASA Regulation Announcement 8–11.

[2]Composite Cryotank. NASA Regulation Announcement 8–12. Rockwell International.

[3]Winged-Body WB001 Trade Study, MSFC/PD22 WB001 (Liquid-Oxygen Tank Forward) Data Loads. June 5, 1994. CorrectCoord.Excel.

[4]Graphite/Epoxy IM7/8552 System Data. Hercules Aerospace Company.

[5]Lightweight Composite Intertank Structure. March 1993. General Dynamics Space Systems Division, NAS8–37138 MSFC ALS–NLS ADP 3102.

Sponsor: NASA Regulation Announcement 8–11, NASA Regulation Announcement 8–12

Industry Involvement: Rockwell International

Orbital Debris Penetration Effects in Spacecraft Interiors

Joel E. Williamsen/ED52
205–544–7007

Orbital debris penetration of manned spacecraft is accompanied by a number of atmospheric effects that can pose a serious hazard to spacecraft and crew survival. These atmospheric effects can include overpressure, light flash, and temperature rise as hot particles from the penetration process impinge the atmosphere of a manned spacecraft. The objectives of this research have been: (1) to conduct a series of hypervelocity impact tests at the University of Alabama in Huntsville's Aerophysics Research Center to measure these effects, and (2) to formulate a mathematical model for these results for predicting the onset of dangerous levels of overpressure, light, and temperature for a given spacecraft shield design and interior layout.

In these tests, a light gas gun was used to fire orbital debris particle simulants from 0.375 to 0.625 inch in diameter through target simulants into a large test chamber simulating the interior cabin of a spacecraft at 1 atmosphere. The test chamber was instrumented with pressure transducers, light sensors, and temperature gauges to measure the level of blast hazard associated with differing target and penetrator conditions at various distances from the target site (fig. 94). The mitigating effects of interior equipment ranks and spall blankets were also measured by placing these elements inside the test chamber against the simulated "pressure wall" of the spacecraft.

Note that overpressure measurements from these tests (table 5) taper off considerably with the distance from the penetrating event (sensors 2 and 3 show lower overpressures than sensor 1) and the presence of internal equipment racks (tests 9, 10, and 13). The peak overpressure measurements occurred at roughly the same time that the internal debris cloud from the penetrated pressure wall passed the overpressure sensors. Temperature test results showed a curious trend toward higher temperatures farther from the point of penetration, although these temperatures occurred much later in time (several hundred milliseconds after impact) than when the debris cloud passed by the sensors (only several milliseconds after impact). These data have led to the theorization that the heated air nearest the point of impact slowly moves through the module, combining with additionally shocked and heated air (downstream) to reach increasingly high overall air temperatures (280+ °C in some cases). Light levels were measured at above 40,000 watts/steradian (27.2 million candles) when directly viewing the target—levels sufficient to cause temporary blindness. However, the level of light as viewed from 90 degrees (i.e., from the side) was less than 20 watts per steradian—well within safe levels.

Given these data, an analytical model predicting the level of overpressure and temperature experienced within the spacecraft cabin as a function of impinging particle characteristics (mass, velocity), shield design, and distance from the penetrating event was generated. This model is being

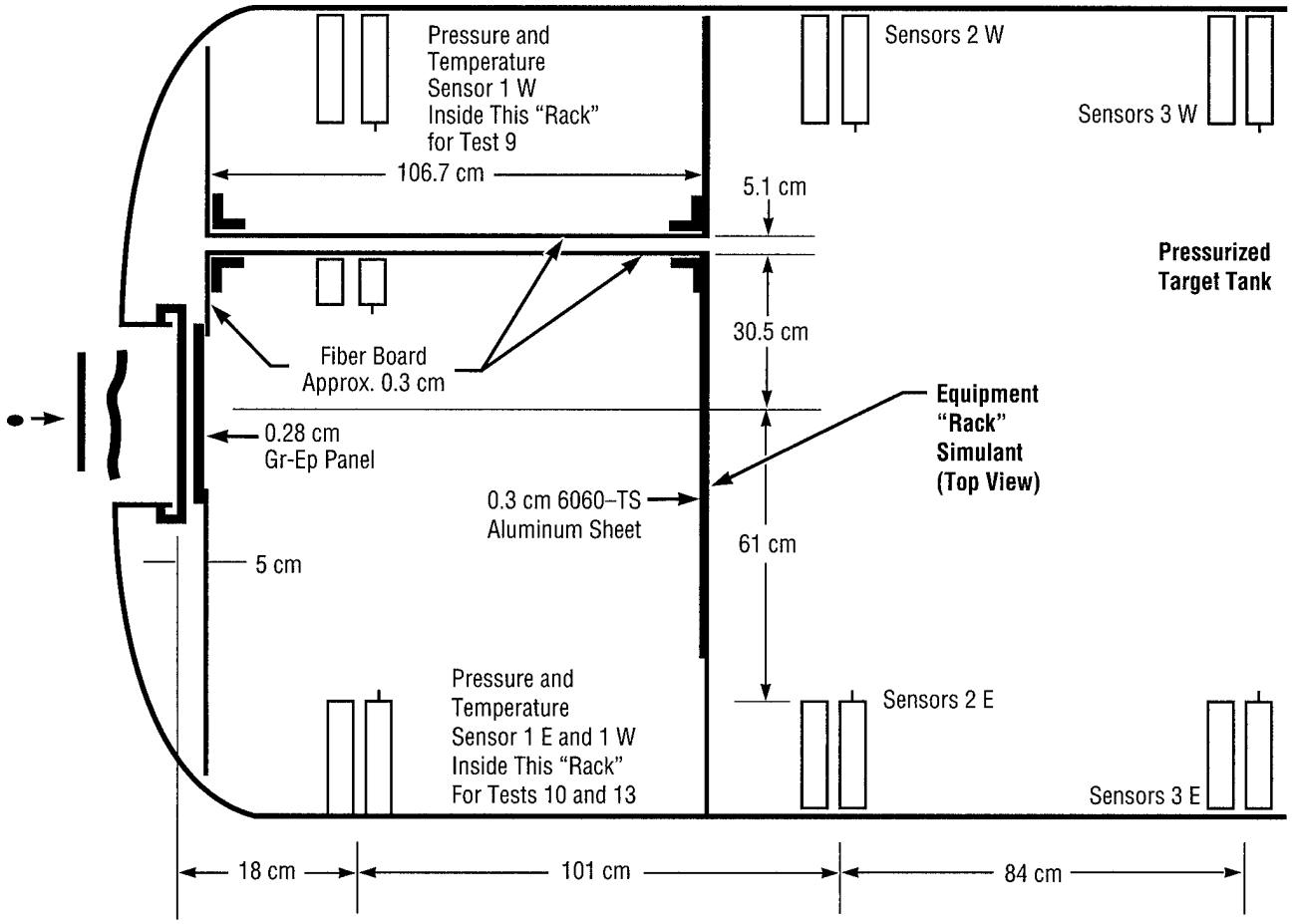

FIGURE 94.—Target chamber arrangement with internal equipment rack simulant.

used in conjunction with previously existing military models to quantify and reduce the likelihood of crew injury given these hazardous levels of overpressure, light, and temperature effects in the *International Space Station*. By quantifying the likelihood of loss, specific procedures for measurably increasing crew safety from the unlikely event of orbital debris penetration are being developed.

This series of internal effects research was successful in meeting its primary and secondary objectives: (1) to establish, through experimentation, the level of spacecraft cabin overpressure, light, and temperature that accompanies penetration of typical orbital debris shielding as a function of penetration parameters, shield type, interior equipment, and distance from the source of penetration; and (2) to formulate a mathematical model of these results for predicting the onset of dangerous levels of overpressure, light, and temperature for a given spacecraft shield design and interior layout. A comprehensive NASA/ University of Alabama in Huntsville report on these findings will be released at the close of the contract in December 1995.

Williamsen, J.E., and Serrano, J. April 10–12, 1995. Atmospheric Effects in Spacecraft Interiors Following Orbital Debris Penetration. Paper 2483–03, Society of Photo-optical Instrumentation Engineers, AeroSense 1995 Symposium, Orlando, Florida.

TABLE 5.—*Overpressure test results.*

Target		1	1	1	2	3	1+ Blanket	1+ Rack	2+ Rack	2+ Rack
Test Number		1	3	6	5	8	11	10		13
Projectile Diameter		1.27 cm 0.500 in	1.59 cm 0.625 in	1.59 cm 0.625 in	1.59 cm 0.625 in	0.95 cm 0.375 in	1.27 cm 0.500 in	1.59 cm 0.625 in	1.59 cm 0.625 in	1.59 cm 0.625 in
Velocity (k/s)		6.70	6.42	6.50	6.58	6.64	6.46	6.63	6.21	6.52
Sensor 1E	Peak Overpressure	117 kPa 17 psi	141 kPa 20.5 psi	110 kPa 16.0 psi	234 kPa 34.0 psi	262 kPa 38.0 psi	38 kPa 5.5 psi	55 kPa 8.0 psi	—	145 kPa 21.0 psi
	Duration of Peak	0.35 msec	0.50 msec	0.45 msec	0.45 msec	0.35 msec	0.20 msec	0.10 msec	—	0.10 msec
Sensor 1W	Peak Overpressure	121 kPa 17.5 psi	148 kPa 21.5 psi	214 kPa 31.0 psi	276 kPa 40.0 psi	193 kPa 28.0 psi	—	97 kPa 14.0 psi	3 kPa* 0.4 psi	207 kPa 30.0 psi
	Duration of Peak	0.35 msec	0.50 msec	0.40 msec	0.40 msec	0.40 msec	—	0.10 msec	0.10* msec	0.10 msec
Sensor 2E	Peak Overpressure	31 kPa 4.5 psi	117 kPa 17.0 psi	103 kPa 15.0 psi	69 kPa 10.0 psi	48 kPa 7.0 psi	—	9 kPa 1.3 psi	5 kPa 0.7 psi	10 kPa 1.4 psi
Sensor 2W	Peak Overpressure	41 kPa 6.0 psi	145 kPa 21.0 psi	97 kPa 14.0 psi	103 kPa 15.0 psi	45 kPa 6.5 psi	24 kPa 18.0 psi	9 kpa 1.3 kPa	3 kPa 0.5 psi	6 kPa 0.9 psi
Sensor 3E	Peak Overpressure	21 kPa 3.0 psi	55 kPa 8.0 psi	83 kPa 12.0 psi	21 kPa 3.0 psi	7 kPa 1.0 psi	34 kPa 5.0 psi	9 kPa 1.3 psi	10 kPa 1.5 psi	8 kPa 1.2 psi
Sensor 3W	Peak Overpressure	17 kPa 2.5 psi	55 kPa 8.0 psi	48 kPa 7.0 psi	28 kPa 4.0 psi	7 kPa 1.0 psi	21 kPa 3.0 psi	9 kPa 1.3 psi	3 kPa 0.5 psi	4 kPa 0.6 psi

*Pressure sensor located in adjacent equipment rack.

Tests with Internal Equipment Present

Sponsor: Office of Space Flight,
Space Station Program Office

University Involvement: University
of Alabama in Huntsville

Nonautoclave Curing of Composite Flight Structures

Jeffrey L. Finckenor/ED52
205–544–7041

The high specific strength and stiffness of fiber composites make them excellent choices for use in the aerospace industry. Typically, composite parts are cured under high temperature and pressure in an autoclave, but, because the parts are so large, they often require very expensive autoclaves. Significant cost savings could come from using oven cures instead of autoclave cures. If the variations due to different layup techniques and part thicknesses are quantified, then both part weight and cost could be optimized.

This research project has two phases, with four objectives each. All samples are being made in the Productivity Enhancement Complex in Building 4707. Testing will take place in Building 4619.

Phase I: (1) quantify effects of cure, layup, and thickness; (2) ensure predictability of oven- and autoclave-cured composite honeycomb structures; (3) evaluate bonded composite structural joints; and (4) evaluate embedded fiber-optic health monitoring.

Objective 1: Cure, layup, and thickness. Autoclaves are used to provide pressure to compact plies of the laminate together so strong bonds are formed. Using an oven, or doing a hand layup, provides less compaction. This experiment determines if there is a significant loss in material properties due to methods that provide less compaction.

The effects and interaction of the factors will be studied with a 2^3 factorial experiment with two replicates. Compression and shear tests will provide material properties. The design factors and their levels are: (1) cure: oven and autoclave, (2) layup: hand- and tape-laying machine, and (3) thickness: 8- and 52-ply. The tests will be done on three material systems: AS4/3501–6, IM7/8551–7, and IM7/F655 (Bismaleimide). An additional material, IM7/F584, may also be studied.

An additional set of tests with more replicates will be conducted on AS4/3501–6 to compare only the oven and autoclave properties. Results will include all nine in-plane material properties and strengths.

Objective 2: Oven and autoclave honeycomb predictability. Using the same three materials as for Objective 1, three point-bend tests and column-buckling tests will be performed and compared with predicted failures.

Objective 3: Bonded joints. Bonded joints are a simple and economical way of joining composite structures, but adhesive bonds are very difficult to analyze reliably. These tests will provide data for future designs requiring bonded joints.

Aluminum and composite double-lap splices will be used to bond together composite plates and composite honeycomb samples. Aluminum channels will also be bonded and co-cured on the inside of a composite honeycomb, then bolted together to simulate a thrusting-type payload shroud separation joint.

Objective 4: Embedded sensors. Vehicle health monitoring is becoming more important to the aerospace industry. One method uses embedded fiber-optic strain sensors in composite structures. This experiment will provide data for using sensors on a flight-like structure.

The panel-splice tests will incorporate a fiber-optic sensor in the composite splices. The strain-sensors are Fabry-Perot differential strain-measuring devices. For comparison, a uniaxial strain gauge and a coating of photostress material will be employed on the same parts.

Phase II: (1) study predictability of post first-ply failure behavior; (2) evaluate single-lap bonded and bolted joints; (3) develop a time-load-strain relationship; and (4) apply information from phase I to a large-scale cylinder.

Objective 1: Post first-ply failure. Many current failure theories used on composites are very weak in theory, but are still commonly used for lack of a better analysis. To study failure, bend tests will be conducted on 12- and 40-ply IM7/8552 layups and optimized by classical lamination theory and the Tsai-Hill failure criterion for the maximum number of ply failures before ultimate failure. The actual and predicted load-deflection curves will be compared.

Objective 2: Single-lap joints. Single-lap joints are structurally much less efficient than double-lap joints, but

design constraints may occasionally force a single-lap joint. Composites have more potential problems with this than metals because of the low material properties through the thickness. Tension samples of IM7/8552 will be tested using single-bolted, double-bolted, and bonded single-lap joints.

Objective 3: Time-load-strain. The matrix of many fiber composites is a viscoelastic material—meaning the strain is a function of load and time. While this effect is largely mitigated by the fibers in the 0-degree direction, the 90-degree direction can be strongly affected.

Tape-layed AS4/3501–6, 0-, 90-, and ±45-degree (shear) samples will be loaded at 30, 60, and 90 percent of their ultimate load, and the strain will be recorded over time. This information will allow the development of a time-load relationship for material stiffnesses.

Objective 4: Large cylinder. To apply the information learned from the other tests, a cylinder (3 feet in diameter and 6 feet long) will be fiber-placed using IM7/8552. It will be cut in half, bonded together, and then tested to failure. This cylinder will weigh 50 pounds and be able to support 900,000 pounds.

Conclusion. These tests will provide a significant experience data base for the development of future launch vehicles at MSFC.

The study of oven-cured parts will quantify the effect on material properties due to less-expensive manufacturing methods, which could reduce the cost of manufacturing many composite parts.

Sponsor: Center Director's Discretionary Fund

Orbital Debris Penetration Resistance of Reusable Launch Vehicles

Jennifer H. Robinson/ED52
205–544–7013

A preliminary set of orbital debris impact simulation tests has recently been completed in support of the NASA Reusable Launch Vehicle program. The results of these tests were used to estimate the probability of no penetration of a typical launch vehicle. Several different thermal protection system and structure design specimens were tested, with the objective of determining the most promising combination to resist penetration by meteoroids and orbital debris in low-Earth orbit.

During the 1995 fiscal year, MSFC performed hypervelocity impact tests on 63 thermal protection system/structure designs in the Debris Impact Simulation Facility operated by the Space Environmental Effects Branch within the Materials and Processes Laboratory. Test results, analyzed by the Structural Development Branch of the Structures and Dynamics Laboratory, were used to determine the penetration probability of a typical reusable launch vehicle for its expected lifetime over a baselined set of missions. Results indicated "penetration" or "no penetration" for various aluminum spherical particle diameters, all at approximately 6-kilometers-per-second impact velocity. By extrapolating the data to represent the higher velocities expected on-orbit and particles of

more dense material, a "critical" penetrating particle was estimated for the average expected impact velocity. Next, using the NASA meteoroid and orbital debris environment models for low-Earth orbit, an estimation of "critical" particle impact probability was estimated. In addition, an equation to predict the penetration resistance of thermal protection/ structural systems has been developed. Further tests and analyses are expected to be performed in the 1996 fiscal year.

Accomplishments gained contribute significantly to NASA and industry capabilities for future evaluation of thermal protection systems and structures for use on low-Earth orbit spacecraft. Before this task was completed, no known equations existed that could predict the penetration resistance of such complicated systems. The commercial potential for this effort is immediate and significant. Private industry is already using the data in the preliminary designs of reusable launch vehicles for commercial use in the next 10 years, including current work to optimize system weight. Other potential uses include space station crew return vehicles, space shuttle design improvements, and other reusable vehicles that must return to Earth through the harsh reentry environment.

Sponsor: Office of Space Access and Technology

Industry Involvement: Rockwell International, Space Systems Division

Composite Redesign of Obstetrical Forceps

Stan S. Smeltzer, III/ED52
205–544–9051

The goal of this technology development project is to design, test, and manufacture a set of obstetrical forceps using state-of-the-art instrumentation technology and fiber-reinforced polymer materials. A fiber-optic strain sensor will be embedded into a specific position of the polymer during fabrication to enable the physician to read the amount of compression and tensile load being applied to an infant's head during delivery. A tailored thickness portion of the forceps will utilize the elasticity of the polymer material and provide a fail-safe method to prevent the physician from placing an unsafe amount of force on an infant's head under normal delivery conditions. The major objective of this work is to develop a set of instrumented forceps to be used to perform clinical trial studies.

On March 5, 1993, NASA/MSFC received a problem statement from Dr. Jason Collins of the Collins Clinic identifying a need for improving the function of obstetrical forceps. The request was for assistance in redesigning the current stainless-steel Simpson-type forceps, so as to reduce the risk of injury to infants and mothers during a forceps-type delivery, while at the same time keeping as much of the traditional appearance and functionality of the forceps as possible.

The forces induced onto the fetal head during a forceps delivery are primarily the traction or pull force (tensile) and the compressive force needed to overcome the friction or resistance of the maternal tissues. According to previous studies by Fleming, Pearse, Wylie, and Ullery, the major factors that influence the performance of forceps are: (1) the structure of the instrument; (2) the fetal head that the forceps must grasp; (3) the resistance of the maternal tissues; and (4) the force applied by the attendant. Studies of the amount of pull force and compressive force applied to infants during delivery have been limited. Strain gauges for measuring total force and calibrated instruments like the axis-tractionometer for measuring traction have been used with limited success to gain useful data with respect to measuring those forces imposed on the infant by the use of the forceps for delivery. Although no limits have been established, measurements from these field tests do give valuable data for this redesign effort.

The redesign of the obstetrical forceps will begin with coupon testing of candidate thermoplastic materials embedded with fiber-optic gauging at MSFC. After the characteristics of the material and sensor sensitivity have been determined, a final design of the forceps will be completed. The Collins Clinic will provide the manufacturing expertise to produce a prototype set of forceps for MSFC characterization. Once the technology has been proven in the laboratory, clinical studies at the Pregnancy Institute will take place. A patent application has been

completed and filed with the Chief Council's Office detailing this technology development.

This project is an excellent application of NASA reinvestment into the community. Once proven, the technology will provide a safer delivery process for both mother and baby.

Ullery, J.C.; Teteris, N.J.; Botschner, A.W.; and McDaniels, B. 1963. Traction and Compression Forces Exerted by Obstetric Forceps and Their Effect on Fetal Heart Rate. Columbia, Ohio.

Morey, W.W., Jr.; Dunphy; and Meltz, G. 1991. Multiplexing Fiber Bragg Grating Sensors. United Technologies Research Center, East Hartford, Connecticut.

Lawson, S.W., and Smeltzer, S.S. December 1993. Composite Redesign of Obstetrical Forceps. Fourth National Technology Transfer Conference and Exposition, Anaheim, California.

Sponsor: Technology Utilization Office (Space Act Agreement)

Industry Involvement: Collins Clinic, Fiber and Sensor Technology

Composite Dome and Polar-Boss Leakage Validation

Stan S. Smeltzer III/ED52
205–544–9051

The goal of this research project is to demonstrate the design, analysis, manufacture, and test of a composite spherical dome cap and polar-boss assembly on the Cryostat Test Facility. The dome cap will be designed for 75-pounds-per-square-inch internal pressure with liquid hydrogen and a circular cutout to accept candidate polar-boss assemblies. The composite dome cap will be fabricated using a combination of fiber placement and hand layup in MSFC's Productivity Enhancement Complex. The major objective of the research is to demonstrate an acceptable level of hydrogen leakage for a composite dome and metallic polar-boss assembly subjected to thermal and pressure cyclic loading.

The effort to significantly reduce launch vehicle weight while still meeting mission objectives has led to increasing use of high-modulus, high-strength composite materials for major structural elements. Under the National Aerospace Plane program, a rectangular composite liquid-hydrogen tank was designed and built to demonstrate that composite materials can be used to manufacture cryogenic tankage. However, most launch vehicle cryogenic tanks are cylindrical and contain dome/polar-boss assemblies which enclose the tank ends, as opposed to the flat, square bulkheads used on the rectangular National Aerospace Plane tank. In order to obtain credible membrane permeability data, a polar-boss joint with minimal leakage would be necessary. During the 1995 fiscal year, six subscale composite tanks were tested with liquid nitrogen to determine the integrity of the polar-boss/dome joint. The first five test tanks leaked during or after the first cryogenic pressure cycle. Although the test of the sixth configuration provided no detectable leakage with bubble solution after the first cycle, further pressure/thermal cycling compromised the integrity of the polar-boss/dome joint, rendering the joint unacceptable. Therefore, the current investigation will determine an acceptable polar-boss/composite dome joint configuration.

Once the composite spherical dome cap has been fabricated, the cap will be installed along with a containment shell on the Cryostat Test Facility. Phase I testing will consist of liquid-nitrogen/gaseous-helium testing to characterize the leakage associated with the dome cap installed in the facility. Once phase I testing is complete and the data have been analyzed, a circular cutout will be machined in the top of the composite dome cap to accept candidate polar-boss configurations. Phase II testing will follow the same testing plan as phase I in order to characterize the polar-boss leakage, and will include the testing of three to four polar-boss configurations until an acceptable configuration is determined. Once an acceptable polar-boss configuration has been determined, liquid-hydrogen testing of the polar-boss/dome-cap joint for leakage will be completed. All of the testing is based on availability of the Cryostat Test Facility in the West Test Area at MSFC.

This research will provide NASA with a valuable technology for the Reusable Launch Vehicle initiative. At the time this article was written, no commercial or government agency had proven an acceptable metallic polar-boss and composite tank interface. Once proven, this technology will directly benefit the industrial partners working toward a reusable launch vehicle by providing a data point for acceptable joint leakage.

Sponsor: Center Director's Discretionary Fund

Industry Involvement: Thiokol Corporation

Poisoning Characteristics of a Palladium-Based Trace Contaminant Control System Catalyst

Jay L. Perry/ED62
205–544–2730

Mary S. Traweek/ED62
205–544–7397

Removal of trace chemical contaminants (resulting from materials offgassing and human metabolic processes) from a spacecraft cabin atmosphere is necessary to provide crew members with an acceptable environment in which to live and work in space. Current spacecraft systems for controlling contaminants employ either adsorption, catalytic oxidation, or a combination of these technologies. In particular, the contamination control system designed for the *International Space Station* uses both adsorption by activated charcoal and high-temperature catalytic oxidation using a commercially available palladium catalyst. Charcoal is used to remove volatile organic compounds, while the catalytic process targets hydrocarbons that are poorly removed by the charcoal. As the activated charcoal adsorption capacity is consumed, trace contaminants such as chlorocarbons, chlorofluorocarbons, and sulfides which can adversely affect the catalytic oxidation of hydrocarbons can enter the catalytic reactor. A thorough understanding of the effects of these compounds on catalytic oxidation of hydrocarbons is necessary to adequately maintain the contamination control systems used onboard spacecraft.

The major objective of the project is to study the effects of catalytic poisons on the ability of a palladium-based catalyst to oxidize hydrocarbons effectively. Also, the reversibility in these effects is being investigated to help determine onboard maintenance requirements for the system. Of particular interest to the investigation are the effects of dichloromethane, hydrogen sulfide, 1,1,2-trichloro-1,2,2-trifluoroethane, and bromotrifluoromethane on the catalytic oxidation activity for methane. Such chemicals are frequently observed in spacecraft cabin atmospheres and include compounds considered as keys in the design of spacecraft contamination control systems. Methane was chosen as the reference hydrocarbon because it is difficult to oxidize. Also, the palladium catalyst performance for methane oxidation has demonstrated a high degree of sensitivity to the selected poisoning compounds. Understanding the effects of varying poison concentration is central to the investigation.

The catalyst, a one-eighth-inch cylindrical alumina pellet supporting a 0.5-percent palladium catalyst, is placed in an automated test rig and heated to 400 °C. At that temperature, methane oxidation is nearly 100 percent. The fresh catalyst is operated in the absence of poisons until thermal stability is achieved—a process that takes approximately 3 days. Baseline tests are then performed for each poisoning compound at different concentrations. During the baseline runs, thermal ramps between ambient

and normal operating temperatures are conducted to determine the effects of the poison on the methane reaction rate. The products of the poisoning compound's oxidation are also determined at this time. After the baseline runs are completed, a cyclic poisoning study is conducted in which catalyst poisons are injected into the test rig to produce a poisoning effect; the injection is then stopped to allow the catalytic activity to recover.

Results have shown that the catalyst is irreversibly poisoned by sulfide compounds; concentration of the sulfide compound entering the catalytic reactor only affects the rate at which poisoning occurs. Fortunately, since sulfide production onboard a spacecraft is a very small component of human metabolism, the adsorption processes used before the catalytic reactor can protect it from harm. Chlorocarbon poisoning has been shown to be repeatedly reversible to the same activity level after more than the equivalent of 2 years of cyclic exposure. Although complete recovery of methane oxidation activity is not achieved, the single-pass efficiency recovers to between 85 and 90 percent after each exposure to dichloromethane. This result is important in determining the useful life of both the charcoal and catalyst beds.

Project findings indicate that the sulfide breakthrough of the charcoal bed is the most critical element to be considered for scheduling system maintenance activities. Future work on the effects of chlorofluorocarbons on methane oxidation performance are planned. The effects of fluorine on catalytic activity are unknown, as is their degree of reversibility.

The results of the research are helping to design and operate trace contaminant control systems used onboard spacecraft more effectively and may be useful in designing commercial emissions control systems.

Sponsor: *International Space Station* Program Office

Industry Involvement: Ion Electronics, subcontract to TDA Research, Inc.

■■■■■

Trace Chemical Contaminant Control System Performance Simulation

Jay L. Perry/ED62
205–544–2730

Charles Ray/ED62
205–544–7227

Buildup of atmospheric trace contaminants in such closed habitats as a spacecraft cabin may lead to potentially serious health problems for its occupants. For this reason, control methods are implemented for minimizing contaminant concentrations to acceptable levels that ensure the occupants' long-term health and well-being. Designing such systems is difficult since temperature, humidity, and other environmental factors can affect their performance over time. Time-consuming and expensive testing is normally required to verify system capabilities before they can be used effectively. A means to minimize the need for large-scale testing has been developed.

Trace contaminant control can be achieved through various means. Typical technologies used onboard spacecraft include physical adsorption on granular-activated charcoal or other adsorbents, chemical adsorption using impregnated granular-activated charcoals and granular lithium hydroxide, ambient temperature catalytic oxidation, and high-temperature catalytic oxidation. Other significant means include absorption in water via condensing humidity and habitat leakage. Many of these techniques are used commercially in

building construction and aircraft design. Usually, in order to design and evaluate the effectiveness of a chosen contamination control system, pilot-scale testing must be conducted. In order to reduce the need for large-scale, expensive tests to assess the many design parameters that must be addressed to achieve the most efficient design, a computer program has been developed that allows basic contamination control techniques to be simulated. Results from the program can be used in assessing different technology combinations, hardware sizing, and life-cycle economics. Commercial applications include building construction, industrial emissions control analyses, and aircraft ventilation system design. Computer program documentation has been developed, including a user's guide and a description of the current program version. With input and output manipulation via commercial spreadsheet programs, the simulation tool can be run on a personal computer. Program validation and uncertainty analyses have been conducted which demonstrate it delivers results within the observed uncertainty of contamination control system tests.

Perry, J.L. April 1994. A Users' Guide to the Trace Contaminant Control Simulation Computer Program. NASA TM–108456.

Perry, J.L. May 1994. Trace Contaminant Control Simulation Computer Program. Version 8.1. NASA TM–108457.

Perry, J.L. June 23, 1995. Validation of the Trace Contaminant Control Simulation Computer Program and Its Use for Supporting Flight Hardware Qualification. NASA MSFC Memo ED62(39–95).

Sponsor: *International Space Station* Program Office

Small, Efficient Metal-Substrate Catalytic Converter for Trace Contaminant Control

Jay L. Perry/ED62
205–544–2730

Spacecraft air-cleaning systems need to minimize weight, volume, power consumption, and requirements for replacement components. NASA Small Business Innovation Research phase II contractor, Precision Combustion, Inc., has developed a very lightweight, compact, high-conversion efficiency "Microlith™" catalyst system (U.S. Patent 5,051,241) for the trace contaminant control system. Earthbound versions of the Microlith™ system being developed for the *International Space Station* are currently in automobile emissions control testing with the top three U.S. domestic auto manufacturers and with a manufacturer of advanced industrial process fume control equipment. Hamilton Standard is exploring putting the technology on aircraft for cabin air cleaning.

The system replaces conventional "monolithic" catalyst substrates with a series of very short, lightweight, highly effective metal substrates, and achieves both rapid lightoff and a ten-fold reduction in size and weight compared to conventional monolithic converters. In the space station application, weight savings are even greater, as the current system relies heavily upon disposable filters. Precision estimates the weight savings represent a dollar savings of up to $4 million per year in station operating costs.

The key feature of Microlith™ technology is its improved geometry/reaction rate. The improved catalytic metal monolith design significantly enhances surface-gas contact through the use of Microlith™ structures with high open areas, small channel diameters, and short channel lengths. Short channel length prevents the significant boundary-layer buildup typical of conventional honeycomb converters. The greatly enhanced mass transfer efficiency becomes especially important for low concentrations of target species. Direct electric heating of the catalytic segment provides positive control over the catalyst temperature and also allows periodic regeneration of the catalyst.

The proof-of-concept phase I prototype test achieved greater than 99-percent destruction of trace organic components per pass through the system, using a small amount of electrical heating at low inlet air temperatures. The phase I Microlith™ test reactor operated at a space velocity of around 40,000 per hour, with greater than 99-percent destruction efficiency of xylene, methanol, 2-propanol, and acetone, as well as methane and ammonia. These conversions demonstrate the ability of the Microlith™ converter to serve as an effective contaminant control system through direct electrical heating of the catalyst. Actual system power requirements for these conversions are being assessed in the continuing phase II work. Efficient packaging of the Microlith™ reactor and determination of optimized operating conditions in a full-scale working prototype are now in progress.

The same technology that offers such fast lightoff and efficiency in the space station is being applied to terrestrial air-pollution problems. Automotive exhaust is the source of nearly half of all U.S. manmade air pollution. With new California and national standards seeking to cut automotive emissions by 75 percent, Precision reports considerable interest from automotive manufacturers and suppliers of exhaust systems, and now has joint development or test programs underway with a number of these companies. Testing to date by automotive manufacturers of prototype designs without any electrical heating have demonstrated that this low-cost, fast-lightoff approach (estimated at less than $50 per vehicle) allows emissions substantially lower than even California's tightest ultra-low emission vehicle standards. For industrial emissions, the small size and rapid lightoff of the technology allow design of point-of-source catalytic oxidation units, offering better individual process control and reduced costs for plant infrastructure. Precision is now in a joint development program with a catalytic fume-burner manufacturer to enter this market.

In a third market, the unit's very low weight and volume offer potential for use in aircraft, for example, in cleaning up aircraft cabin air. Precision and Hamilton Standard are exploring the potential for this application. Precision reports that six U.S. patents have been issued on the technology, and a number more are pending.

Sponsor: Small Business Innovation Research

Industry Involvement: Precision Combustion, Inc.

Catalysts for the Oxidation of Trace Contaminants

Jay L. Perry/ED62
205–544–2730

As human exploration of space requires missions of longer duration, spacecraft trace contaminant control systems with improved logistics and power requirements must be developed. Central to this need is the development of a new oxidation catalyst that exhibits improved activity and poisoning resistance combined with the ability to effectively control a large spectrum of trace chemical contaminants observed in spacecraft cabin atmospheres. Of special importance is the controlling of hydrocarbons in the presence of known catalyst poisons such as chlorocarbons, chlorofluorocarbons, and sulfides.

The primary objectives of the project are to develop a suitable co-precipitated metal/metal-oxide catalyst, investigate the effects of various dopants on its capabilities to oxidize trace hydrocarbons at high temperatures and carbon monoxide at room temperature, characterize its activity and poisoning characteristics, develop repeatable processing and fabrication techniques, and deliver a catalyst on a support suitable for use in the design and development testing of future spacecraft contamination control systems.

Initial work on co-precipitated gold/cobalt-oxide catalysts during phase I of the project produced catalysts which had methane oxidation activity comparable to the best commercially available platinum- and palladium-based catalysts. This catalyst also exhibited very high activity for carbon monoxide oxidation at temperatures as low as –70 °C. However, the phase II work demonstrated that the high-temperature catalyst was strongly poisoned by sulfur compounds and was only moderately stable at high temperatures. Phase II work also resulted in the development of an oxide catalyst that exhibits higher room temperature carbon monoxide oxidation activity than any commercially available catalyst. The use of this catalyst can dramatically lower the power requirements for catalytic oxidation because carbon monoxide's high generation rates from offgassing and crew metabolism and high toxicity make it the contaminant which sets the flow rate through the catalytic oxidation system. If the carbon monoxide can be oxidized at room temperature, the flow rate and power requirements of the catalytic oxidizer can be greatly reduced.

Opportunities are now being pursued to commercialize the newly developed catalyst. Applications include removal of carbon monoxide from closed environments, automotive cold-start emissions control and negative emissions vehicles, portable carbon monoxide sensors, and closed-cycle carbon dioxide lasers.

Sponsor: Office of Commercial Programs, Small Business Innovation Research

Industry Involvement: TDA Research, Inc.

■■■■■

Trace Chemical Contaminant Generation Rates for System Design of Closed Habitats

Jay L. Perry/ED62
205–544–2730

A spacecraft, or any closed habitat, presents a unique design challenge with respect to providing a comfortable environment in which people can live and work. All aspects of the environmental design, including inhabitable volume, temperature, relative humidity, and composition, must be considered to ensure the comfort and health of the occupants. The crew members and the materials selected for outfitting the spacecraft play an integral part in designing a closed habitat because material offgassing and human metabolism are the primary sources for continuous trace chemical contaminant generation inside it. Since these contamination sources cannot be completely eliminated, active control processes must be designed and deployed to assure an acceptably clean cabin atmosphere. Knowledge of the expected rates at which contaminants are generated is very important to the design of these processes. Data from past spacecraft missions and human contaminant production studies have been researched and analyzed to provide this knowledge. The resulting compilation of contaminants and generation rates serves as a firm basis for past, present, and future contamination control system designs for space and aeronautics applications.

Material offgassing data obtained from six Spacelab module missions were collected and analyzed statistically to develop an equipment offgassing rate listing for more than 200 chemical compounds. Also, the literature on past closed chamber tests conducted in the United States and Russia was researched to obtain a broad reference base for trace contaminants produced by human metabolic processes. The listing is central to the design and development of future spacecraft contamination control systems and may also be used in applications for the commercial aircraft industry.

Perry, J.L. August 1995. Trace Chemical Contaminant Generation Rates for Spacecraft Contamination Control System Design. NASA TM–108497.

Sponsor: *International Space Station* Program Office

Urine Pretreatment Methods for Microgravity

Cindy F. Hutchens/ED62
205–544–2313

Pretreatment of urine is required in space station waste-water recovery systems to control urea and its resulting odors and microbial growth. Also, recent testing and experience on the shuttle orbiter waste-water plumbing indicated that pretreatment is required for long-term use of urine separator hardware to reduce or eliminate fouling of the hardware and plumbing with urine precipitates. This is important for *International Space Station* application because the amount of maintenance time for cleaning and repairing hardware must be minimized. The method of choice for urine pretreatment for the U.S. water reclamation system is Oxone®, a monopersulfate compound, and sulfuric acid (H_2SO_4). Development and initial testing of an effective method to inject these into a urine stream in microgravity is the focus of this effort. The first phase of this work concentrated on Oxone® and was performed from September 1994 to May 1995. The sulfuric acid injection design is continuing through 1995.

The method of introducing Oxone® into the urine stream on-orbit is quite a technical challenge. Oxone® in a powder form is not easily metered into a fluid stream in microgravity, and the efficacy in solution significantly degrades over time so that it is not practical to launch the chemical in a liquid form that would be easy to inject into the system.[1]

A trade study to determine an appropriate method of injecting Oxone® indicated that a solid tablet of Oxone® added at the inlet of the urinal would adequately pretreat the urine and protect the urinal. The tablet was a mixture of Oxone® powder and polyethylene glycol, and was encased in the same material currently used for the urinal inlet filter. The tablets were first tested in a dissolution test; then the prototype filter and tablets were used in a 30-day test to validate the ability for treating real urine.

The dissolution test determined a baseline dissolution rate, allowed visual observation of fluid flowpatterns, and measured and recorded the pressure drop across the solid Oxone® in several configurations using water at body temperature.[2] Figure 95 shows the data measured in the baseline dissolution test. As the tablets dissolve (the rate of dissolution decreased as the tablets got smaller), the surface area of the tablet became smaller, and less pretreatment was added to the stream. The test used six tablets, weighing 31.8 grams total. The tablets tended to dissolve from the outside first, did not break apart, and dissolved in one piece (staying inside the filter encasement so that no undissolved Oxone® went downstream to the separator).

After dissolution testing, a 30-day test to evaluate the prototype method for injecting proper levels of Oxone® safely and conveniently into the separator was completed. Tablet dissolution was measured on a batch basis: a batch of urine consisted of the amount of urine needed to dissolve nearly all of the Oxone® in the filter. The remaining Oxone® was measured

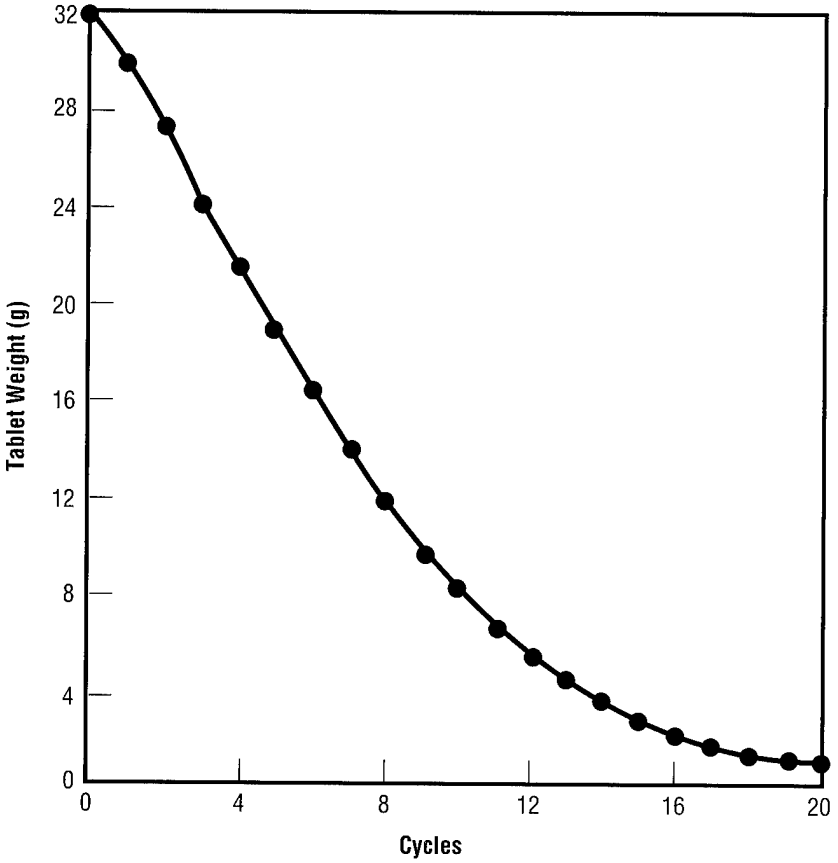

FIGURE 95.—Oxone® tablet dissolution rate.

to get a ratio of the pretreatment and urine which had gone through the filter. Data on the pretreated urine were collected to measure the efficacy of the pretreatment used in this method. (The pretreatment was modified slightly during the test in order to optimize the amount of Oxone® used.)

The 30-day prototype test data are shown in figure 96. After several batches, the percent of polyethylene glycol by weight was modified to increase the binding efficacy, and the method of compressing the tablets was improved so that the tablets were more consistent. This caused the pretreatment/urine ratio to be closer to the goal of 5 grams of Oxone® per liter of urine (fig. 96). The pH of the pretreated urine was generally between 4 and 5, which is exactly what would be expected when pretreating with Oxone® alone. The oxidation potential in the stored pretreated urine was very low (an average of 0.016 percent), indicating that the pretreatment was adequately pretreating the urine but had not been exhausted. The amount of Oxone® left at the end of the batch averaged 0.22 grams. Subjective judgment of the odor/bacteria filter during the test indicated that the odor/bacteria filter was loading at a lower rate than with no pretreatment. (The low odor level will lead to logistics savings.) After forty test days and processing a total of 750 pounds of urine, the separator and adjoining plumbing were disassembled for a thorough inspection and found to be completely free of precipitates. The separator pitot tube was clear of any residue, and all of the hoses were clean.

The trade study completed in this effort pointed to a simple method of urine pretreatment that will optimize weight, power, and volume. The success of this testing has been a major step in finding a final urine pretreatment design for the *International Space Station* and for ensuring prevention of urine collection hardware degradation due to fouling and urine solids buildup. This translates as less maintenance and lower logistics. Work is underway to find a suitable injection method for sulfuric acid.

[1]Oxone®-Monopersulfate Compound Technical Sheet, DuPont.

[2]Rethke, D.W. February 1995. Test Plan for Urine Pretreat Injection System. Hamilton Standard, Space and Sea Systems, Windsor Locks, Connecticut.

Sponsor: *International Space Station* Program Office

Industry Involvement: Hamilton Standard, Windsor Locks, Connecticut; ION Electronics, Huntsville, Alabama

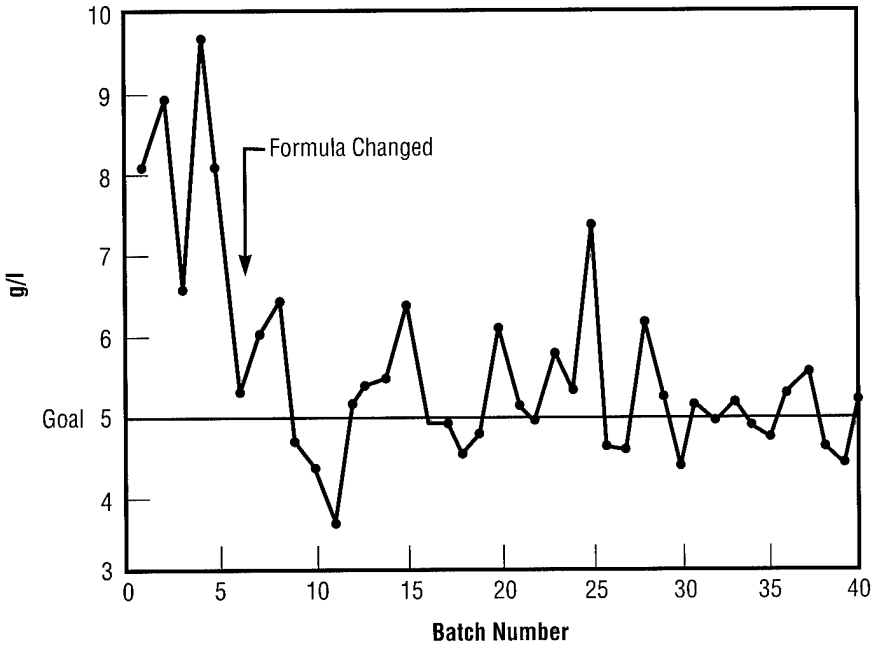

FIGURE 96.—Pretreatment-to-urine ratio per batch.

Developing a Microbial Monitor With Polymerase Chain-Reaction Technology

Monserrate C. Roman/ED62
205–544–4071

Future manned spacecraft development for long-duration missions will require water reclamation to avoid frequent resupply of water. Monitoring the water-recovery system for potential system process failures and microbial contamination is critical. This project addresses activities needed to further develop available polymerase chain-reaction technology for microbial water monitoring that could be adapted to the *International Space Station* water system. The monitor will be capable of quantifying the total viable microbial population and detecting and identifying viable pathogenic microorganisms in the processed water on a real-time basis.

Ensuring the microbiological quality of potable and processing waters requires the detection of indicator microorganisms. Because the use of conventional methods for the microbial detection and identification are slow and labor-intensive, these methods are not suitable for applications where information is needed within hours. Therefore, development of a water-quality monitor that uses the polymerase chain-reaction technology will enhance the design of the *International Space Station* water-recovery system.

Monitoring the microbial populations and identifying changes in relative populations would indicate that a steady-state balance is not being maintained and will serve as an early warning that the water-recovery system is not functioning properly. The development of a technology for real-time microbial water monitoring will allow consumption of recycled water shortly after processing, reducing the need for prolonged water storage prior to use and thereby reducing the number and size of storage tanks needed.

The University of Alabama in Birmingham, through a subcontract with ION Electronics, addressed the feasibility of polymerase chain reaction technology to develop a microbial water-quality monitor for use on the *International Space Station*. Polymerase chain-reaction is a genetic-based method in which a deoxyribonucleic acid segment of the target microorganism is detected by enzymatic amplification of a single segment to a million fold. The chain-reaction procedure consists of three steps (cycles): (1) the double-stranded helix is heat-denatured, (2) two primers (short single-stranded oligonucleotides—the nucleotide sequence located at the two ends of the target to be amplified) are annealed at low temperature, and (3) the primers are enzymatically extended by deoxyribonucleic acid polymerase (TaqMan) at an intermediate temperature. An exponential increase of the target acid occurs by repetition of each cycle. The chain-reaction amplification is accomplished by using an instrument called a thermocycler, which repeatedly changes the temperature of the sample. University researchers evaluated scientific literature and designed a set of oligonucleotides that could be used to detect potential pathogens in recycled water.

Monitoring the water-recovery system aboard the space station for potential system process failures and microbial contamination is essential for crew health. By developing existing chain-reaction technology, a water-quality monitor could be adapted for space station use and beyond. The monitor could provide rapid detection of target microorganisms with high sensitivity and meet NASA's needs for low power and simple operation.

In addition to potential space applications, a microbial monitor would have Earth applications as well. Potential uses include hospitals, the food industry, water-processing plants, and chemical/pharmaceutical laboratories. Once fully developed, the microbial monitors could become instrumental tools in laboratories concerned with microbial contaminants.

Polymerase chain-reaction technology is relatively new; however, there is an increased application as a method of diagnosis and microbial identification in environmental, clinical, and industrial samples. Collaborations with other interested government agencies could further develop the technology for different applications and prevent duplication of research efforts.

Bej, A., and Gauthier, J.J. 1992. Final Report—Identification of Microorganisms by Polymerase Chain Reaction During Stage 7 of the Water-Recovery Test. ED62 (76–92).

Cassell, G.H.; Glass, J.I.; and Elliot, E.J. 1995. Final Report—Polymerase Chain-Reaction-Based Microbial Monitor for Analysis of Recycled Water Aboard the *International Space Station Alpha*: Issues and Prospects. ED62 (61–95).

Sponsor: *International Space Station* Program Office

University/Industry Involvement: University of Alabama in Birmingham under subcontract with ION Electronics

Development of a Packed-Bed Adsorption Model With Predictive Capabilities

James C. Knox/ED62
205–544–4887

Continuous carbon-dioxide removal from the cabin air is a critical life-support system function on manned space missions. On the *International Space Station*, the carbon-dioxide removal assembly design must maintain a cabin carbon-dioxide concentration of less than 0.7 percent in atmospheric pressure. Several additional constraints are placed upon the design: it must function quietly and extremely reliably in microgravity; exist and operate within tight mass, volume, and power envelopes; and must produce high-purity carbon dioxide suitable for subsequent processing that will extract and return oxygen to the cabin. Furthermore, it must use a minimal amount of consumables to reduce the costs and reliability considerations of logistics.

The carbon-dioxide separation technology chosen for the U.S. portion of the space station—based on selective adsorption equilibria—is called "four-bed molecular sieve," and is being designed and built by the Allied Signal Corporation under subcontract to Boeing.[1] Four adsorbent beds (two desiccating, two carbon-dioxide removing) operate in a thermal/vacuum swing cycle. A diurnal cycle is also imposed on the operation. The unit produces a carbon-dioxide stream of 99-percent purity. The removing beds (which contain a 5A zeolite) use a honeycomb heater core to provide the energy for desorption.

A half-cycle schematic (fig. 97) illustrates the four-bed molecular sieve carbon-dioxide removal assembly for the U.S. Laboratory and Habitation modules on the *International Space*

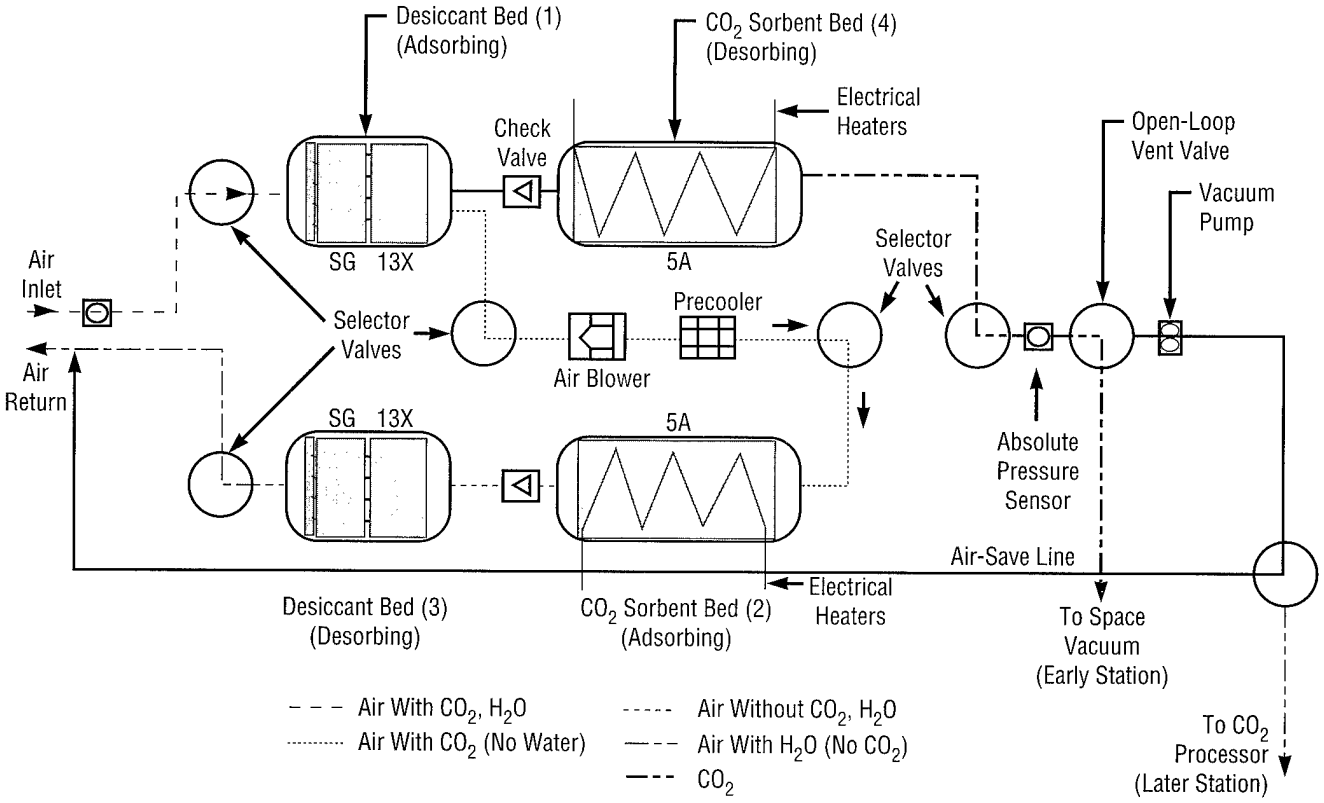

FIGURE 97.—Half-cycle schematic of the four-bed molecular sieve carbon-dioxide removal assembly.

Station. Inlet air is first drawn through the desiccant bed, after which it is directed through a precooler and the carbon-dioxide adsorbent bed. The warm air then desorbs water from the other desiccant bed and returns, humidified, to the cabin. Meanwhile, carbon dioxide is desorbed from the regenerating adsorbent bed and is released to space or stored for reduction and oxygen generation. Nitrogen and oxygen that desorb ahead of the carbon dioxide are returned to the cabin via the air-save line.

In order to predict the consequences of processor design changes, tune the processor's operating conditions and cycling schedule, and ascertain the effects of its operation on the cabin environment, the four-bed processor is being modeled and simulated using a finite-difference method. The honeycombs present in the carbon-dioxide removing beds introduce a significant amount of channeling, and necessitate the use of a two-dimensional (axial and radial) model. Verification testing has been conducted on laboratory-scale packed beds to determine empirically lumped mass-transfer coefficients and to verify and refine the computer models. Researchers have also undertaken a study of the multicomponent equilibria important to the processor's operation and, in particular, the co-adsorption of water, nitrogen, and carbon dioxide on the materials used for the separation. Inclusion of these and other significant phenomena present in the carbon-dioxide removal process are critical to the development of a computer model with the capability to predict processor operation when large changes are made in its configuration.

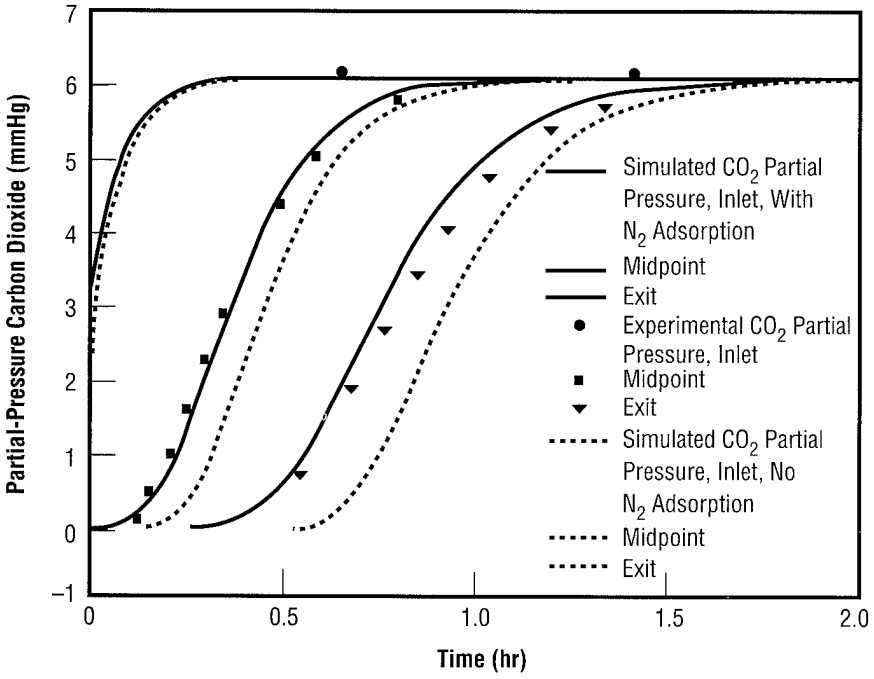

FIGURE 98.—Experimental and simulated carbon-dioxide breakthrough with and without nitrogen co-adsorption.

Researchers have successfully developed models of the packed sorbent beds in a stand-alone configuration.[2] The simulations and experimental results demonstrate the importance of incorporating the thermal effects of adsorption and the interactions between adsorbates, particularly nitrogen and carbon dioxide, in this processor. (Figure 98 illustrates the consequence of neglecting nitrogen on the simulation of packed-bed carbon-dioxide breakthrough.) Ongoing efforts are focused on the integration of the stand-alone models into an integrated model of the four-bed molecular sieve removal assembly.

The model being developed in this effort is expected to enhance understanding of the carbon-dioxide removal assembly and facilitate the optimization of the system to address the design issues associated with meeting the severe requirements of such a separation system for space. It will provide a tool for investigation of alternative methods already in use in the U.S. shuttle and Russian Mir programs, and alternative designs under consideration aimed at maintaining a lower cabin carbon-dioxide concentration and involving kinetic adsorptive separations, resistance heating of sorbents, hydrophobic adsorbents, and other techniques. Commercial applications include the investigation and optimization of sorbent systems, used

widely in the petroleum and gas-separation industries.

[1]Atmospheric Revitalization Subsystem Description. 1993. Boeing Corporation (NAS8–50000), D683–15003–1.

[2]Mohamadinejad, H., and Knox, J.C. 1994. Development and Verification Testing of a Hardware-Independent Molecular Sieve Model. Second International Conference on Life Support and Biosphere Sciences, Huntsville, Alabama.

Sponsor: *International Space Station* Program Office

Pulse-Tube Refrigeration for Spacecraft and Commercial Applications

Douglas G. Westra/ED63
205–544–3120

A pulse-tube refrigerator breadboard unit has been built and tested by Dean Applied Technology Company under a phase II Small Business Innovation Research contract (NAS8–39917). Pulse-tube refrigeration, offering a viable alternative to chlorofluorocarbon/hydrochlorofluorocarbon systems, uses helium as the working fluid and is, therefore, nontoxic to humans and totally harmless to the environment. Microgravity-compatible because they require no boiling or condensing zero-gravity heat transfer, pulse-tube refrigerators can be operated over a wide range of temperatures and are directly applicable to numerous space and commercial refrigeration requirements. These include food refrigerator/freezers, laboratory freezers, freeze dryers, and computer cooling, as well as detector and electronics cooling. The pulse-tube refrigerator that was built operates in a temperature range required for food freezers, where pulse-tube refrigerators have never been applied before. This technology is applicable to the space shuttle, the *International Space Station* and Mir, and future NASA missions.

The Pulse-Tube Refrigeration Cycle is a relative newcomer compared to other refrigeration cycles. In 1963, Professor Gifford of Syracuse University and his graduate student, R. Longsworth, noticed that blanked-off plumbing lines connected to gas compressors became hot at the closed end.[1]

In 1982, Dr. Pete Kittle of NASA's Ames Research Center joined with Dr. Ray Radebaugh of the National Institute of Standards and Technology and began developing pulse tubes. In 1983, they made a breakthrough when, without adding any moving components, they were able to improve the efficiency of the pulse-tube refrigerator by increasing the phase shift between the pressure and the mass flow. This improvement—done by connecting an orifice and a reservoir to the hot end of the pulse tube—became the standard pulse-tube refrigerator configuration known as the orifice pulse tube. Single-stage orifice pulse-tube refrigerators (fig. 99) have reached 30 Kelvin, while a three-stage orifice pulse tube has reached 3.6 Kelvin.

One of the major motivations for development of this technology is as an alternative to the current space station food refrigerator/freezer technology. The current technology is thermo-electric, which is very reliable and has virtually no vibration. However, thermo-electric refrigerators are also very inefficient. In fact, as the temperature lift increases, the power consumption for thermo-electric refrigerators increases exponentially. Pulse-tube refrigeration offers high reliability, low vibration, and much higher efficiencies. Electrical power consumption on the space station is extremely critical; therefore, development of alternative technologies such as pulse-tube refrigeration technology is necessary.

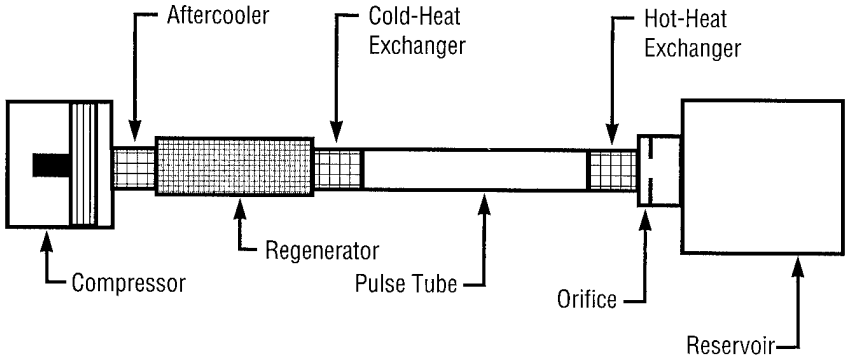

FIGURE 99.—Single-stage orifice pulse-tube refrigerator.

The pulse-tube refrigerator demonstration unit built by Dean Applied Technology Company, Inc. has been designed and built to operate at a temperature range and load level needed for typical food freezers and laboratory freezers. As far as is known, this is the first time that such a refrigerator has been applied to this temperature range. Details of the design are given in reference 2.

After design and fabrication, this pulse-tube refrigeration development model was subjected to numerous tests. A temperature of – 45 °C (–50 °F) has been reached, which is well below the temperature required for food freezers. The next step will be to improve efficiency, reduce cost, and gain experience in integration with freezer cabinets and power sources.

Although the development unit was built primarily for zero-gravity application, it has numerous possibilities as a commercial technology, including use in home food refrigerator/freezers, laboratory freezers, medical/cryobiology applications, cooling of electronics, and superconductivity research.

[1]Kittel, P. 1994. A Short History of Pulse-Tube Refrigerators. Eighth International Cryocooler Conference.

[2]Dean, W.G., and Westra, D.G. October 24–26, 1995. Pulse-Tube Refrigeration for Spacecraft and Commercial Applications. Presented at NASA Technology 2005 Conference, Chicago, Illinois.

Sponsor: Small Business Innovation Program

■■■■■

Low-Temperature Stirling-Cycle Refrigerator for Spacecraft Refrigeration Systems

Douglas G. Westra/ED63
205–544–3120

A Stirling-cycle refrigerator breadboard unit has been built and tested by Stirling Technology Company under a phase II Small Business Innovation Research contract (NAS8–40172). Stirling-cycle refrigeration, offering a viable alternative to the currently used chlorofluorocarbon/hydrochlorofluorocarbon systems, uses helium as the working fluid and is, therefore, nontoxic to humans and totally harmless to the environment. Stirling-cycle refrigerators can be operated over a wide range of temperatures, have few moving parts, and provide high reliability and low vibration. This technology is applicable to numerous space and commercial refrigeration requirements, including food refrigerator/freezers, laboratory freezers, and freeze dryers, as well as detector and electronics cooling. The refrigerator described herein operates in a temperature range required for food freezers. Consult Walker[1] for a detailed description of the theory and operation behind the Stirling cycle.

The Stirling-cycle refrigerator developed under this project was designed to meet the requirements of the space station food refrigerator/freezer. The vapor-compression cycle, although very efficient on the ground, has many features that make it less

suitable for zero-gravity operation, including a requirement for liquid/vapor separation in the condenser and a lubricant reservoir. In addition, most manned space applications require high reliability, low vibration, and nontoxic working fluids. Vapor-compression systems, which contain freon refrigerants and have many brazed or soldered connections, must be double- or triple-contained to meet safety standards, thereby decreasing system efficiency. Also, Spacecraft Maximum Allowable Concentration standards often limit the amount of refrigerant that can be used in the system, which sometimes causes further reductions in efficiency and has, in the past, caused intermittent operation (due to frost buildup).

The current baseline technology for the space station food refrigerator/freezer, thermo-electric, offers many required specifications, including high reliability, low vibration (no moving parts), and no toxicity (no working fluid required). However, it has very low efficiencies (coefficient of performance less than 0.2) and limited capacity. The Stirling-cycle refrigerator provides baseline capabilities with moderate efficiency (coefficient of performance greater than 1.1), and the use of a nontoxic working fluid (helium). In addition, its ability to easily achieve lower temperatures makes it adaptable to other space station applications, including a –70 °C freezer and freeze drier, a –183 °C freezer, and a –196 °C snap freezer.

The unit built by the Stirling Technology Company (fig. 100) has been designed and built to operate at a temperature range and load level needed for typical food freezers and laboratory freezers. This refrigerator makes use of a linear motor, which leads to extremely simple and mechanically compact systems by negating the necessity for converting rotary motion to reciprocating motion. Efficiency and reliability improvements in the linear motor are among the innovations used in this project. Another innovation, the use of flexural bearings, enables the moving components to operate efficiently and without wear, even though a lubricant is not employed. When properly implemented, the forces provided by the flexure totally eliminate the possibility of contact between the moving and stationary parts. Probably the most innovative concept employed is the free-piston Stirling-cycle concept. In this configuration, the moving components within the device are not mechanically coupled to the drive motor via a conventional kinetic linkage; rather, the components (i.e., the displacer) oscillate under the influence of the gas forces occurring within the Stirling cycle.

The internal cycle innovations described above would not have practical benefits without an efficient means of accepting heat from the load to produce cooling while rejecting heat to the heat sink. Consequently, Stirling Technology has also come up with some innovative methods for the heat acceptor (heat load) and the heat rejector (heat sink), including proprietary helium-to-air heat exchangers. For more details of this unit, consult Penswick.[2]

Test results to date have been very promising. The breadboard test unit has supported a heat load of 130 watts at –26 °C (–15 °F) (with a coefficient of performance of 1.1). By simply changing the temperature setpoint, the same unit has achieved a temperature of –70 °C (–94 °F) at a heat load of 60 watts, suggesting that this unit could be used to meet the requirements of the space station laboratory support equipment's –70 °C freezer and freeze drier. Reliability tests on individual components, e.g., the flexures, also show promising results. Subsequent tests are planned to prove the reliability of the entire Stirling-cycle refrigerator system.

[1]Walker, G. *Cryocoolers*, Parts 1 and 2. Plenum Press.

[2]Penswick, B.L. October 24–26, 1995. Long-Life, High-Reliability, Environmentally Sound Electric Generators and Coolers. Presented at the NASA Technology 2005 Conference, Chicago, Illinois.

Sponsor: Small Business Innovation Research

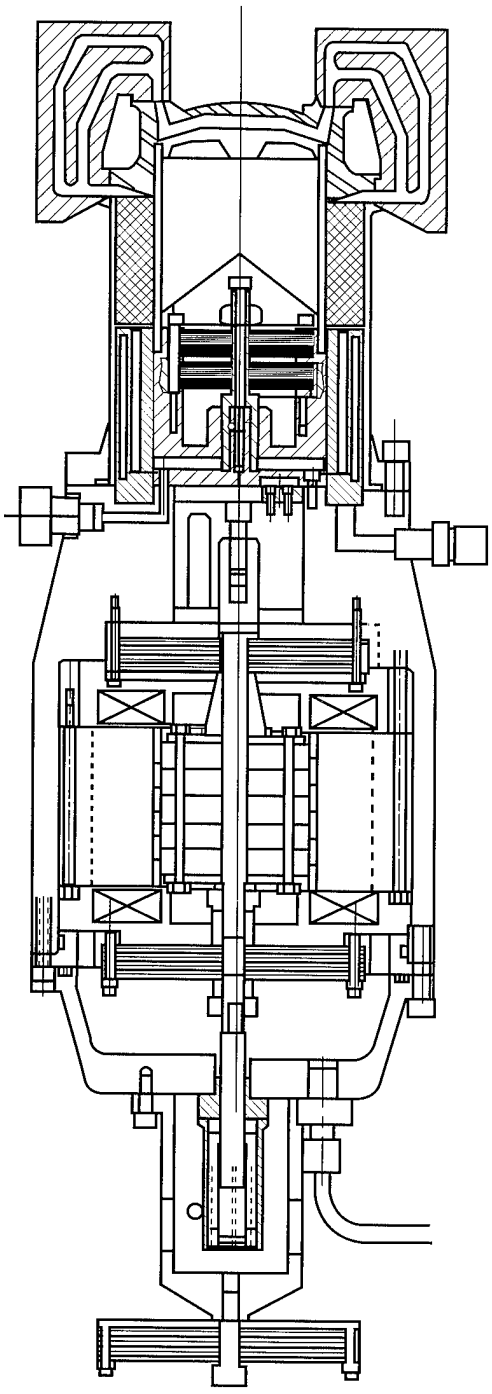

FIGURE 100.—Low-temperature Stirling-cycle refrigerator configuration with advanced cold head (shown vertically).

Materials and Manufacturing Processes

Localized Corrosion in Aluminum Alloys by the Scanning Reference Electrode Technique

Merlin D. Danford/EH23
205–544–2612

Corrosion of aluminum alloys is generally measured on a macroscopic scale using a relatively large surface area of a test specimen and measuring the corrosion currents. However, the corrosion generally is not uniform on a microscopic scale. Work with aluminum-lithium alloys indicates that they are susceptible to pitting corrosion,[1] a localized corrosion phenomenon. Recently, MSFC has employed the Scanning Reference Electrode Technique for measuring such localized corrosion.

The Scanning Reference Electrode Technique instrument (fig. 101) is commercially available, has the capability to measure microgalvanic potentials close to the surface of materials, and allows in-situ examination and quantification (on a microscopic scale) of electrochemical activity as it occurs. The tool is microprocessor-controlled, and electrical potentials are measured by a special probe capable of translation in the X and Y directions. The specimen, in the form of a cylinder, is held in a vertical position and rotated around the Y-axis. The scan is synchronized with a display monitor, and the resultant data are shown in the form of line scans or two-dimensional area maps. The width of the area maps (X direction) can be set at will using the zoom-in feature of the experimental setup. The height of the area maps (Y direction) is set automatically by the control software according to the proper aspect ratio. Movement of the scanning probe during data collection is in the Y direction. Direct measurement of surface potentials, showing anodic and cathodic areas, at discrete positions on the sample surface may be taken and stored for time-related studies. Because the minimum detectable signal is on the order of 1 milliamp per square centimeter, a potential must be applied to the sample to increase the corrosion current to at least this level. This is accomplished by means of a separate potentiostat coupled to the Scanning Reference Electrode Technique system.

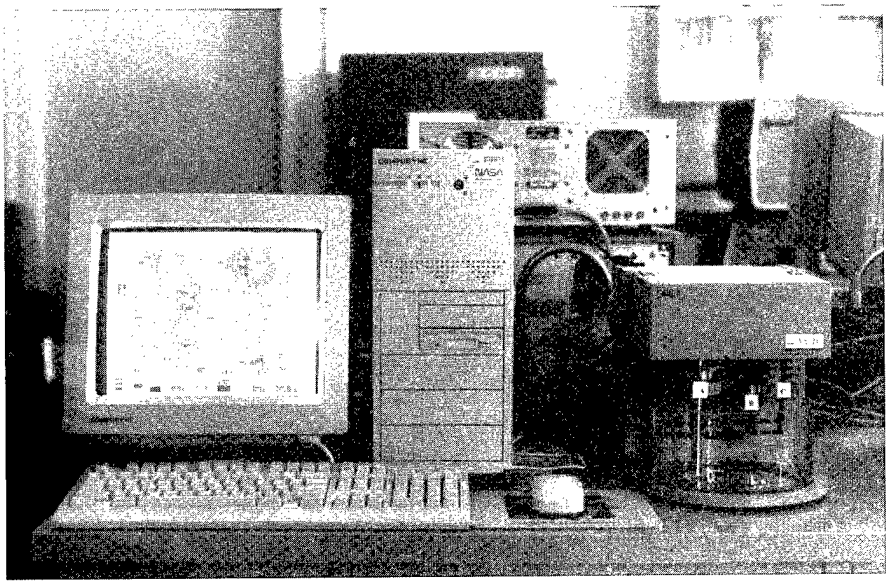

FIGURE 101.—The Scanning Reference Electrode Technique.

Corrosion testing specimens consisted of cylindrical metal rods approximately 1.27 centimeters (0.5 inch) in diameter and 10.2 centimeters (4 inches) in length. In the case of welded samples, a longitudinal V-groove was machined along the entire length of the rod (Y direction). The groove was then filled using 4043 filler by tungsten inert-gas welding and subsequently machined down to a smooth circular surface. Samples were immersed in a corrosive medium consisting of 3.5-percent sodium-chloride solution. A potential was then applied to each sample, as the sample was rotated at 100 revolutions per minute during the scan. The experiments were set up in such a way that all maps had a width of 3.0 centimeters (X direction) and a height of 2.25 centimeters (Y direction). After data collection, each map was displayed on the computer screen and the proper palette for the display of map features was selected. Topography measurements of the various map features (potentials for anodic and cathodic regions) were then made. All cathodic features have

positive signs, while all anodic features are negative.

Area map scans for the wrought 2195 aluminum-lithium alloy (fig. 102) and the welded material (4043 filler) (fig. 103) were recently made. The scales of both maps are expanded by a factor of approximately four over those actually occurring in the samples. The map scan for the wrought material (fig. 102) shows many strongly anodic and cathodic features, indicating a strong tendency toward pitting for this material. In contrast, the map scan for the welded material (fig. 103) is highly striated in the direction of the weld. The area containing the weld is entirely cathodic and extends slightly into the heat-affected zone. Strong anodic regions border the weld on both sides, indicating a high propensity for corrosion in these areas.

From these results, it is clear that the Scanning Reference Electrode Technique provides an excellent means for studying localized corrosion on a microscopic scale, showing a marked change in the corrosion characteristics brought about through the welding of materials. Such information is not available from conventional corrosion measurements, through which only overall corrosion rates can be obtained. Soon, however, it will be possible to correlate the overall corrosion rate measurements with the localized corrosion measurements provided by this new technique, delivering an even greater understanding for the corrosion behavior of various materials.

[1]Walsh, D.W. August 1994. NASA/ American Society for Engineering Education Summer Faculty Fellow.

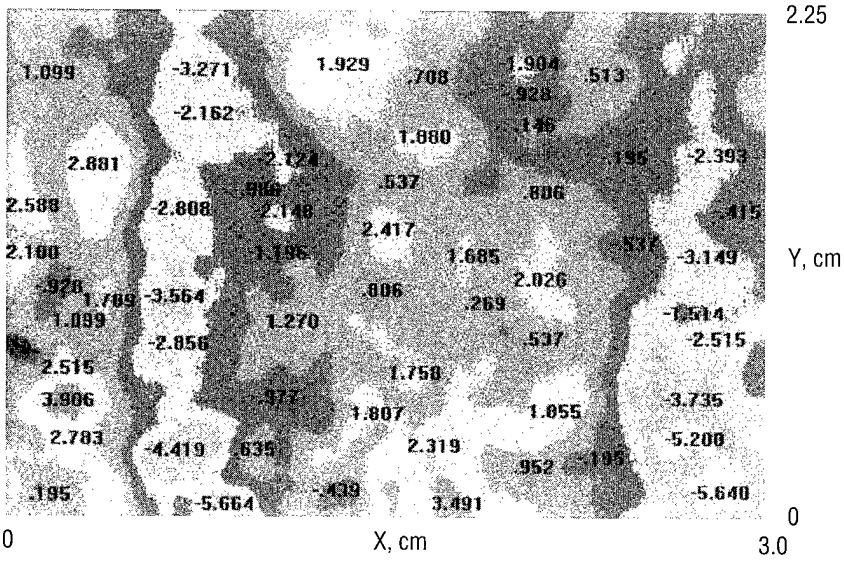

FIGURE 102.—Localized corrosion in wrought 2195 aluminum-lithium alloy.

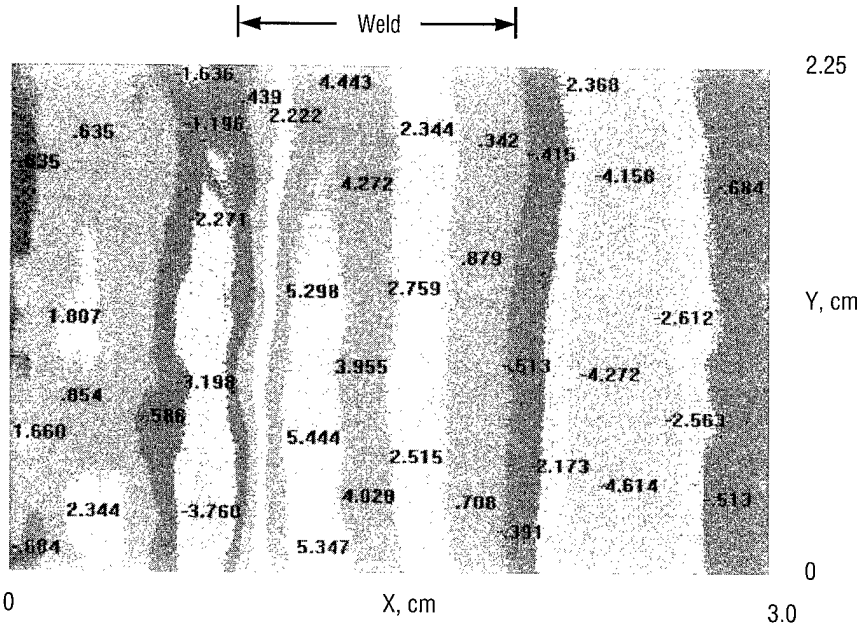

FIGURE 103.—Localized corrosion in welded 2195 aluminum-lithium alloy (4043 filler).

Sponsor: Office of Space Flight

Development of Low Thermal Conductivity, Polyacrylonitrile-Based Fibers

Raymond G. Clinton, Jr./EH34
205–544–2682

During the past 6 years, the Materials and Processes Laboratory—in cooperation with the Solid Propulsion Integrity Program and the U.S. solid rocket motor industry—has conducted a research program to develop and evaluate low thermal conductivity, polyacrylonitrile-based carbon fibers as potential replacements for rayon-based carbon fibers currently used as reinforcement for phenolic-matrix composites in solid rocket motor nozzle applications. Progress of the research program has been documented in past volumes of Research and Technology[1] and elsewhere.[2] As part of this ongoing effort, material performance results have been collected from the Reusable Solid Rocket Motor–4 MNASA static motor firing that occurred in the summer of 1994.

Both polyacrylonitrile-based materials tested, FM5950 and FM5952, were prepregged by B.P. Chemicals using Ironsides 91LD phenolic resin. Table 6 offers fiber, fabric, and composite properties and descriptions of these two materials for both MNASA tests. Placement of the test materials in the throat ring and identification of other nozzle components are provided in figure 104. The throat was designed with a split-ring configuration to enable comparison of the two low thermal conductivity, polyacrylonitrile candidates to each other and to a baseline rayon-based ablative (MX4926).

The FM5952 throat section was constructed from material containing the same fiber lot of Amoco T350–25 as used in the Solid Propulsion Integrity Program–3 MNASA nozzle, but a prepreg lot with a lower resin content was used. The FM5950 throat section represented the same Hercules LF–2 fiber lot and the same prepreg lot as used in the Solid Propulsion Integrity Program–3 MNASA, but the piece was postcured to reduce volatile content and to increase its permeability (by causing an increase in matrix microcracking). As can be seen from the data contained in table 085a, the permeability values of these materials as measured at room temperature were significantly higher than the similar materials tested in the Solid Propulsion Integrity Program–3 MNASA. To fully evaluate the criticality of permeability effects,

TABLE 6.—Low thermal conductivity, polyacrylonitrile materials in the Solid Propulsion Integrity Program–3 and Reusable Solid Rocket Motor–4 MNASA motors.

	FM5950		FM5952	
	SPIP–3	RSRM–4	SPIP–3	RSRM–4
Fiber	LF–2; 6K	LF–2; 6K	T350–25; 6K	T350–25; 6K
Fiber Tensile Strength, Ksi	370	370	351	351
Weave	5HS, 13×13	5HS, 13×13	5HS, 13×13	5HS, 13×13
Shear Treat	Yes	Yes	Yes	Yes
Sizing	GP	GP	UC322	UC322
Specific Gravity	1.62	1.61	1.63	1.61
Resin Content, %	34.0	35.0	33.5	29
Residual Volatiles, %	1.5	1.5 As Cured 0.2 Postcured	1.0	3.9
Postcured	No	Yes*	No	No*
Room Temp. Permeability, Log D'Arcy Constant	–12.2	–11.39	< –20	–13.9
Pocketing	Severe	Severe	Severe	None

* Exposed to overwrap cure after initial cure

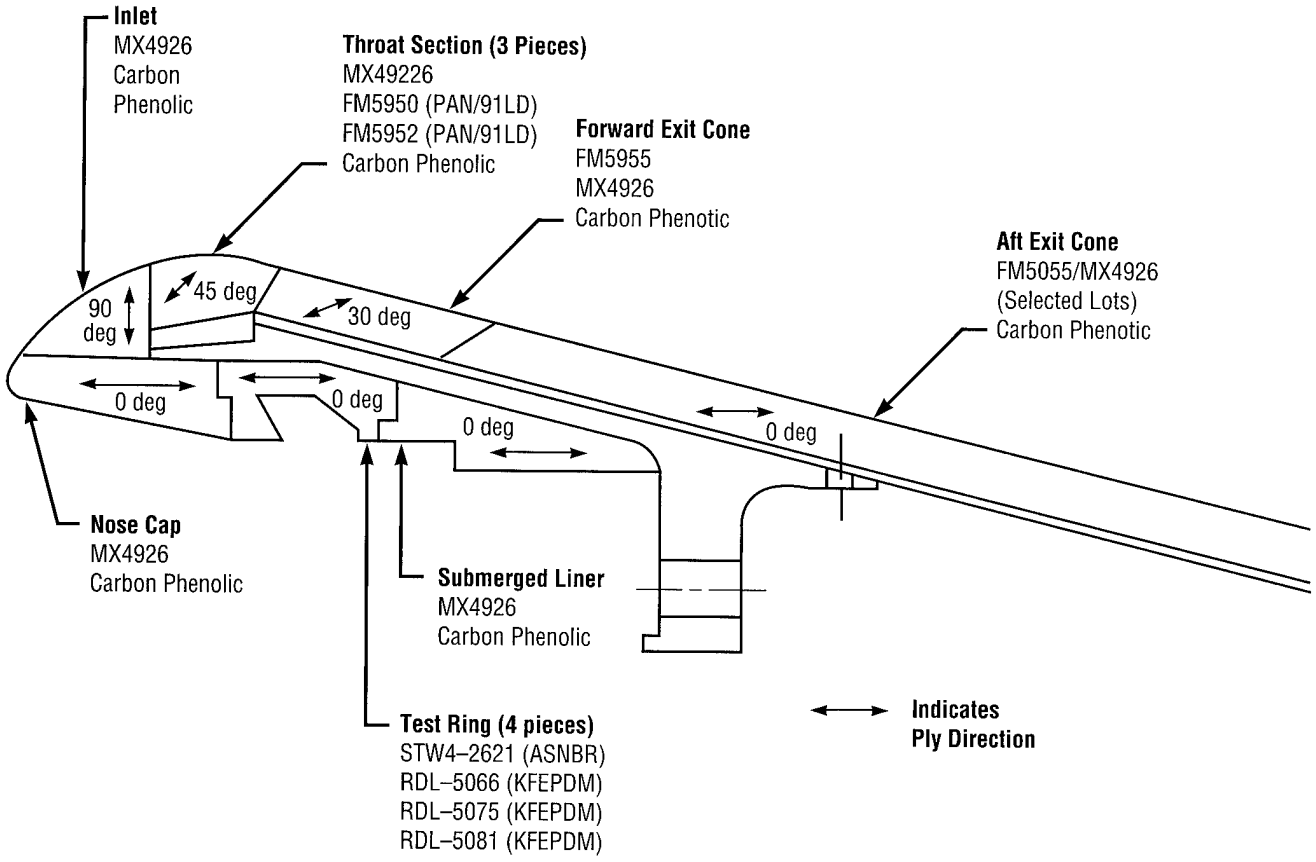

FIGURE 104.—MNASA motor, Reusable Solid Rocket Motor–4, nozzle configuration.

however, more data concerning permeability at the temperatures of the pocketing event are required.

Performance results are summarized as follows. The FM5952 material performed anomaly-free. As the Solid Propulsion Integrity Program–3 MNASA data had suggested—in the absence of pocketing—the low thermal conductivity, polyacrylonitrile-based materials exhibited erosion performance similar to that of the baseline rayon-based ablatives. Using the MSFC check gauge to measure erosion, data were obtained from ten azimuths for the FM5952 and MX4926 sections from the Reusable Solid Rocket Motor–4 MNASA throat. Analysis of these data indicates that the erosion performance of the two materials is statistically indistinguishable at confidence levels exceeding 95 percent. The postcured FM5950 material pocketed as severely as the nonpostcured material in the Solid Propulsion Integrity Program–3 MNASA nozzle, indicating that postcuring does not resolve the polyacrylonitrile pocketing issue. Due to pocketing, erosion measurements for comparison to other throat materials were not made.

A thorough study of potential factors contributing to pocketing was conducted after the Solid Propulsion Integrity Program–3 MNASA tests in an effort to understand the reasons behind, and to appropriately select materials and process conditions to maximize information gained from, the Reusable Solid Rocket Motor–4 MNASA test. In addition to postcuring/permeability, the other variable examined was resin content. (As shown in table 6, the FM5952 resin content was significantly lower than other materials.) The data plotted in figure 105 indicated resin content as

an apparent discriminator between materials that have pocketed and those that have not. Reusable Solid Rocket Motor–4 MNASA material performed in accordance with this trend. Also, laboratory-scale tests of these same materials conducted using the nozzle ablative simulation apparatus at Southern Research Institute produced similar results, i.e., the FM5950 pocketed and the FM5952 did not.

Unfortunately, due to the transition/ termination of the Solid Propulsion Integrity Program, efforts to fully understand and characterize critical performance drivers and to provide the fundamental science and engineering foundation enabling confident nozzle design with alternate polyacrylonitrile fiber-reinforced ablatives will not be furthered. An excellent summary of the accomplishments in material development and the status of the design potential for polyacrylonitrile-based ablative materials is provided by Emery et al.[3] The most advanced work continuing in this area is being conducted at Thiokol/Wasatch Operations and Alliant Techsystems, Inc./Bacchus Works.

[1]Clinton, R.G., 1994. Development of Low Thermal Conductivity, Polyacrylonitrile-Based Fibers for Solid Rocket Motor Nozzle Applications. *Research and Technology 1994.*

[2]Hill, K.H.; Wendel, G.M.; and Tillery, S.W. November 1994. Applicability of Polyacrylonitrile-Based Carbon Phenolic to Solid Rocket Motor Nozzles. Joint Army, Navy, NASA, and Air Force Rocket Nozzle Technology Subcommittee Meeting. Boeing Defense and Space Group, Kent, Washington.

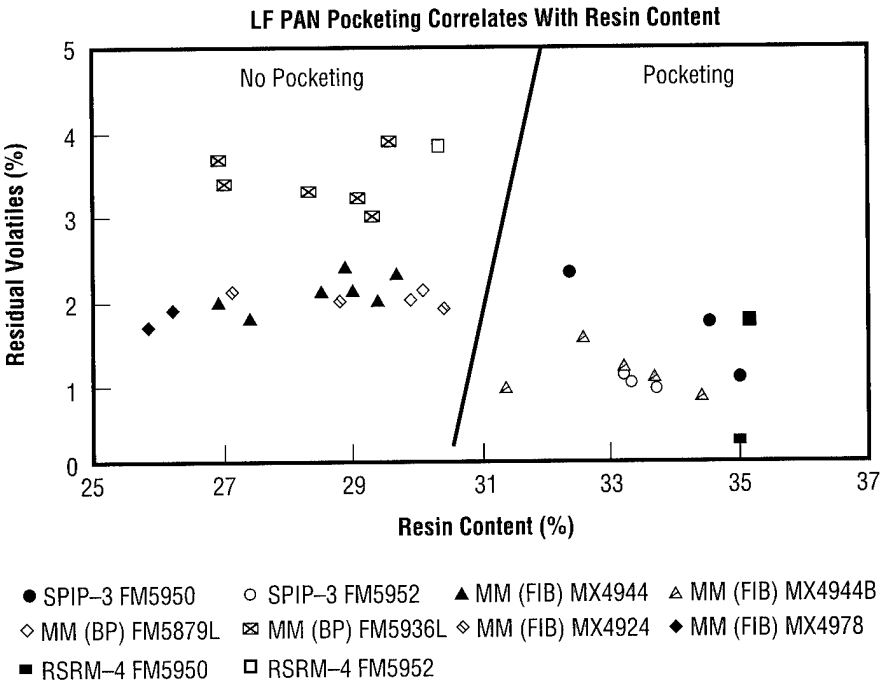

FIGURE 105.—Pocketing versus resin content and residual volatiles.

[3]Emery, E.A.; Heyborne, C.M.; Hill, K.H.; York, J.L.; Canfield, A.R.; Thompson, A.P.; and Wendel, G.M. December 1994. Assessment of the Design Potential of Polyacrylonitrile-Based Materials for Ablative Applications. Solid Propulsion Integrity Program Final Report, Document HI–070F/1.2.9.

Sponsor: Office of Space Systems Development

Industry Involvement: Thiokol/ Wasatch Operations, Alliant Techsystems, Inc./Bacchus Works

Improved Single-Crystal Superalloys Tailored for Hydrogen Service

Deborah D. Schmidt/EH23
205–544–4943

This research and development program is geared toward significantly improving fatigue properties of rocket engine components exposed to a high-pressure hydrogen environment, e.g., the space shuttle main engine turbine blades and nozzles. The ultimate goals are improved fatigue and fracture capability at the maximum debit condition (26 °C, 35 megaPascals of gaseous-hydrogen exposure) and improved, elevated, service-temperature cyclic properties with minimum impact on monatomic properties.

Current Rocketdyne and Pratt & Whitney high-pressure turbopump blade lives are limited by their low-cycle, high-cycle, and thermal-fatigue properties. Both turbopumps contain blades—either directionally solidified or single-crystal—which have microstructures not optimal for service-life extension. Certain microstructural defects, such as porosity and eutectic phase,[1,2] limit fatigue life in both hydrogen-burning space shuttle main engines and air-breathing gas-turbine engines.

Removal of the eutectic phase has been accomplished in two candidate Pratt & Whitney alloys: 1482 and 1484. These were selected because their chemical compositions have wider heat-treating (solutionizing and diffusing) windows. The porosity was removed by optimizing the hot isostatic pressing procedure such that recrystallization would not occur. Improved fatigue crack growth resistance was accomplished through development of a modified ("bimodal" or "duplex") gamma-prime precipitate morphology. This approach was used because cracks tend to follow the path of least resistance.

Traditionally, gamma prime is precipitated by a discreet, ordered cuboidal morphology for optimal creep-rupture properties. Because gamma prime is stronger than the matrix, the cracks tend to propagate along the interface of the gamma-prime phase and the matrix. With this in mind, a bimodal gamma prime was precipitated with morphologies of enlarged and irregular shapes, as well as cuboidal gamma prime. This, in essence, forced the cracks to follow a more tortuous path, slowing their progression.[3]

All initial program goals have been met. Fatigue properties in hydrogen have been improved by a factor of 100 by the removal of the eutectic phase and porosity, and the crack growth rate has been reduced at least by a factor of 4. Enlargement of the data base is continuing by further strain-controlled fatigue tests and creep-rupture tests, with test data analysis also continuing.

If research and development results continue to be favorable, both of the eutectic-free, bimodal, gamma-prime alloys (1482 and 1484) will be candidates for flight certification for space shuttle main engine turbine blades and nozzles. Such microstructural improvements might also be considered for the next generation of propulsion systems.

Commercial research and development is currently underway to utilize the technology for the Department of Defense, the Department of Energy, and other applications. The commercialization focal point is to utilize the superalloys with improved microstructures for applications that require high strength at elevated service temperatures. Enhancements in thin rolled sheets for weight control is only one example.

[1]Schmidt, D.D.; Alter, W.S.; Hamilton, W.D.; and Parr, R.A. August 1989. The Effects of Temperature Gradient and Growth Rate on the Morphology and Fatigue Properties of MAR–M246 (Hf), NASA TM–100374.

[2]Schmidt, et al. Directional Solidification of Superalloys. U.S. Patent Number 4,964,453.

[3]Biondo, C.M.; DeLuca, D.P.; Peters, B.J.; and Schmidt, D.D. 1994. The Influence of Thermal Processing and Microstructure on the Mechanical Properties of Single Crystals in Hydrogen. Advanced Earth-to-Orbit Propulsion Technology, NASA/MSFC Conference Publication 3282, 1:10–19.

Sponsor: Earth-to-Orbit Propulsion Technology

Industry Involvement: Pratt & Whitney

Characterizing Metal Brittleness

Arthur C. Nunes, Jr./EH23
205–544–2699

In many applications, it is enough to specify where brittle behavior occurs so that it can be avoided; in welding, however, it may be necessary to pass through a region of brittle behavior. This can occur when metal grain boundaries remain liquid at temperatures substantially below the bulk melting temperature of the alloy, so that the metal is "hot short" or brittle below the bulk melting temperature. Even then, there might not be cause for concern if the hot metal were not subject to tensile stresses, but it is. Right after a weld pool solidifies, the environment heats up and expands. The expansion can pull apart microfissures (tiny cracks) in the heat-affected zone of the weld. Other crack morphologies, e.g., fusion line cracking, can result from other modes of brittle behavior.

To deal with welding cracking, in one way or another, one must be able to specify the level of abuse the metal can withstand inside its region of brittle behavior. Then it is possible to compare the tolerable abuse with the anticipated abuse to see whether defects will occur in the weld. While necessary, such measurements are not often made by those who characterize metal properties.

At MSFC, researchers have found it useful to represent the tolerable level of abuse of a metal in a regime of brittle behavior by a function relating the isothermal critical cracking strain, ε_c, to temperature, T. If the temperature coordinate is vertical, $\varepsilon_c(T)$ represents a nose-like curve resembling the "pearlite nose" on an isothermal phase-transformation diagram.

Strictly speaking, the isothermal critical cracking strain is also a function of time, $\varepsilon_c(T,t)$. Embrittling liquid boundaries eventually disappear as diffusive homogenization takes place. However, for the short times needed for welding solidification, the time effect may not be important. In fact, researchers have gotten reasonably good agreement between microfissuring predictions and data for a superalloy using an empirical function, $\varepsilon_c(T)$, obtained from observations of cracks and strains on the surface of a hot tensile test specimen.

As in the case of a hardening quench, where it is necessary to avoid the pearlite nose in order to form martensite, it is also necessary (in the vicinity of a weld) to avoid strains within the isothermal critical cracking strain regime as the metal cools from the melting temperature in order to avoid cracks. A means is required in each of the above cases to compare the isothermal values (times or strains) with the nonisothermal cool-down values. In the case of the cool-down strains, $\varepsilon(T,t)$, researchers chose a damage theory in which cracking was assumed to occur whenever:

$$\int \frac{d\varepsilon(T,t)}{\varepsilon_c(T)} = 1.$$

Although the damage theory seemed to work in microfissuring computations, a more clearly motivated cracking criterion is desirable, perhaps to emerge from an analysis of the mechanics of power absorption by various possible fracture modes. The form of the $\varepsilon_c(T)$ function used in the subject analysis was:

$$\varepsilon_c(T) = \varepsilon_{co} 2^{\left(\frac{GS-4}{2}\right)} e^{\frac{(T-T_G)^2}{B}}$$

where ε_{co}, T_G, and B are constants. GS represents the grain size and is incorporated into the expression to reflect the hypothesis that it is actually the displacement across a grain boundary that is critical, so that bigger grains that distribute a larger part of the overall strain to each grain boundary can tolerate less overall strain.

This kind of representation of data on the cracking tendency of an alloy is particularly useful in combination with an analysis yielding local strains. Current work is underway to predict the cracking of a light metal alloy as a function of weld process parameters, and to see whether an electron-beam raster pattern can be found to eliminate microfissuring in a superalloy.

Nunes, A.C., Jr. June 1983. Interim Report on Microfissuring of Inconel 718. NASA Technical Memorandum (TM–82531).

Sponsor: Office of Space Flight

Casting Modeling Technology

Douglas N. Wells/EH23
205–544–3300

Modeling of the casting process has the potential to revolutionize the manner in which complex cast parts are developed. The technology allows the casting designer to predict all aspects of the casting process: molten metal flow, heat transfer, solidification, residual stresses, and the resulting microstructure within the metal casting. With such knowledge, the designer can go to the foundry with a design that preempts casting problems. The results include a shorter development time, less scrap, and higher quality castings. MSFC's Materials and Processes Laboratory is actively developing this technology to improve the quality of cast hardware for aerospace and other applications throughout the casting industry.

NASA is a member of the National Institute of Standards and Technology Consortium on Casting of Aerospace Alloys. This consortium is focused on the cooperative development of the casting modeling technology. Efforts include improving the software code and process sensors, determining fundamental thermophysical data, and validating the resulting improvements. MSFC is currently working with Howmet Corporation and United Technologies/Pratt & Whitney to support the consortium's validation task, while simultaneously improving the quality of space shuttle main engine cast hardware. This program involves modeling the casting of two main engine high-pressure oxidizer turbopump components. The first turbopump component to be modeled, the pump discharge housing, is a fairly well-understood casting, which will provide strong validation of the thermophysical data and code improvements produced by other consortium tasks. A second turbopump component, the turbine inlet housing, will provide validation data for a different material, as well as provide an opportunity to improve a casting process that has proven difficult to refine. The effort has been planned so that the results will be beneficial to all parties involved.

The Materials and Processes Laboratory is pursuing further research and development of the subject technology for application in various MSFC missions. Examples include evaluating the castability of in-house-designed cast parts, predicting the solidification behavior of castings poured in microgravity, and validating thermophysical properties determined for new, advanced alloys such as MSFC-developed NASA–23.

Casting modeling technology will provide invaluable information for future space programs and industries that rely on castings. The time and money saved by eliminating the trial-and-error casting development process will present new opportunities for cost savings and allow those programs dependent on castings to achieve their goals in a timely and cost-effective manner.

Sponsors: Office of Space Access and Technology, Center Director's Discretionary Fund

Industry Involvement: Howmet Corporation, Whitehall, Michigan; United Technologies/Pratt & Whitney, West Palm Beach, Florida.

Development of a High-Strength, Low-Cost Aluminum Piston Alloy

Jonathan A. Lee/EH23
205–544–9290

A technology partnership program to develop a new, high-strength, low-cost alloy for automobile engine pistons is being proposed jointly by NASA and Ford Motor Company of Dearborn, Michigan. This is a continuation of the Government's Partnership for a New Generation of Vehicles program with the U.S. automobile industry, in which NASA is playing an important role. The proposed new aluminum-alloy pistons are expected to withstand more heat than conventional piston materials, produce less air pollution, and may improve gas mileage. NASA's contribution to the effort will be performed by MSFC's Materials and Processes Laboratory.

Through a Space Act Agreement, MSFC/Ford's program objective is to formulate a low-cost, high-strength aluminum-silicon alloy to meet future automobile industry regulations for reducing exhaust emissions. The new piston alloy will have at least a 30-percent improvement in high-cycle fatigue strength when operating at temperatures as high as 300 °C. While some existing advanced, lightweight alloys and composite materials could be used to make pistons for high-temperature operations, these are too costly for broad commercial applications in the auto industry where low cost is a significant production factor. Today's typical piston materials cost is about $1 per pound. This program's target cost will be less than $2 per pound of material to develop a better performance piston for future U.S. auto engines.

The proposed 4-year piston development program calls for MSFC-led development for the first 2 years, with Ford taking over for the remainder. MSFC will perform an extensive literature survey of similar works that have already been accomplished, establish a material data base, develop the new piston alloy, and perform preliminary tests. Ford will lead in the development of new casting techniques, as well as in the design and manufacture of the new pistons. Several methodologies will be explored by MSFC in the attempt to formulate the advanced piston alloy, including various ways of changing the alloy microstructure to obtain the desired mechanical properties. Two of the most promising methods are dispersion strengthening and microalloying: dispersion strengthening entails blending aluminum alloys with finely dispersed carbide or oxide particles, while microalloying requires mixing a very minute amount of a special element in the alloy. The preliminary tensile and fatigue testing will be done at MSFC, with Ford doing the final piston testing and qualification. Under the present terms of the partnership, NASA and other federal government agencies will have the right to use the advanced alloy, as desired.

This program will combine NASA's materials expertise (advanced materials programs) with Ford's piston suppliers (casting technology) and Ford's experience in automotive engine design (piston qualification testing) in a cost-sharing, cooperative-development effort. The partnership between government and industry will enhance U.S. automobile competitiveness overseas. At the same time, the dual-use technology program will also benefit NASA and MSFC directly. For instance, the aluminum-silicon alloy developed from this program will have potential applications in NASA's reusable launch vehicle efforts, where low-cost, castable, high-strength aluminum alloys are required.

Sponsor: Office of Space Access and Technology

Industry Involvement: Ford Motor Company, Dearborn, Michigan

Avionics

Clamp-On Flow-Velocity and Density Transducers for Cryofluids in Thin-Walled Conduits

William T. Powers/EB22
205–544–3452

In principle, it seems possible to measure the mass flow rate, M_f, of cryofluids under single-phase and under some two-phase conditions using external acoustic or ultrasonic transducers that clamp onto the outside of the conduit without penetrating or thinning the conduit. The mass flow rate velocity measurement would consist of a combination of flow (V) sensors and fluid density (ρ) sensors. The flow sensors utilize contrapropagation for fluid that is substantially single-phase, but utilize stroboscopic tracking of scatterers in a reflection mode when bubbles in the fluid scatter the interrogating wave so much that the signal-to-noise ratio obtained with wall-to-wall transmission is inadequate. The fluid density sensors utilize a mass-loading effect on flexural (bending) waves. Reference figure 106.

The near-term objective of this program is to measure flow and mass flow rate in stainless steel and Inconel ducts having diameters near 33 millimeters and near 100 millimeters and wall thickness near 3 millimeters. For this wall thickness, one is able to take advantage of utilizing the small clamp-on ultrasonic transducer developed under contract NAS8–38429 to measure flow either

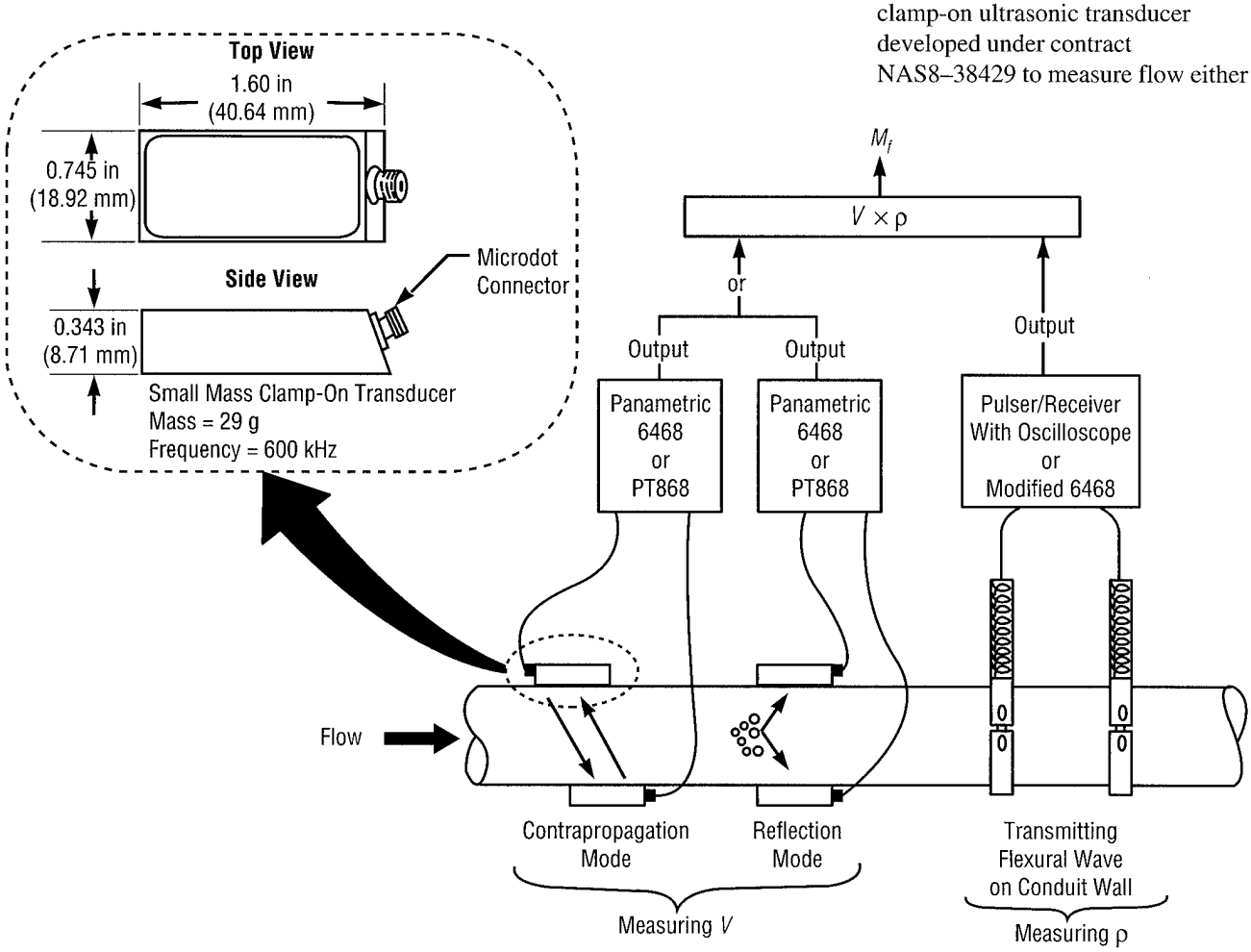

FIGURE 106.—Test configuration to determine mass flow rate.

in the contrapropagation or the reflection mode of the interrogation. In the contrapropagation mode, the clamp-on transducer operates satisfactorily as long as the cryofluid (liquid nitrogen) is single-phase and the flow condition is not "too violent."

Preliminary piggyback testing with liquid oxygen flowing in the high-pressure oxidizer turbopump discharge duct (4.37 inches in diameter by 175 inches in width) and in the fuel preburner supply (1.996 inches in diameter by 127 inches in width) of the space shuttle main engine at the MSFC test stand showed that the transducers operated in conjunction with two commercial ultrasonic flow meters (Panametrics Models 6468 and PT868. Although they have some difficulty measuring flow in the contrapropagation mode, these meters survive the vibration of the duct and the cryogenic temperature of the liquid oxygen).

When the cryofluid is not single-phase, it will have scatterers for the reflection mode of interrogation. A simple test where air bubbles were introduced into water inside a pipe capped at one end demonstrates that this transducer is also able to detect the bubbles as reflectors.

The clamp-on density sensors, in contrast to the flow sensors, do not depend on the continuity of the fluid in the pipe. These sensors are attached orthogonally to the pipe. If operated at a sufficiently low frequency, or stated equivalently, at a sufficiently long flexural wavelength, λ_{flex}, the fluid density sensors launch and detect bending or flexural waves having a phase velocity, c_{flex}, that—for a given pipe—depends on the average density of the fluid in the pipe, or the amount of a given liquid in the pipe. This latter dependence is the basis for liquid presence/liquid level (H) sensing. Analysis of phase velocity in a 1-inch stainless-steel pipe (dia. >> λ_{flex}) and in a flat stainless-steel plate (tank "dia." >> λ_{flex}) has now been carried to the point of explaining the main observations.

More testing is needed to determine the limitations of (1) the operation of the clamp-on transducer in the contrapropagation and reflection mode when cryofluid is single- and two-phase, respectively, and (2) the performance of the clamp-on density sensor in detecting cryofluid density/void fraction. The test will be performed first in a laboratory water-flow loop where conditions are easily controlled. Later the test will be conducted on the liquid-oxygen duct of the space shuttle main engine at the MSFC test stand.

Lynnworth, L.C.; Nguyen, T.H.; Liu, Y.; and Stein, P. September 1994. Clamp-On Flow Velocity and Density Transducers for Liquid Nitrogen and Other Cryogenic Applications, Especially in Thin-Walled Conduits. 1994 Conference on Advanced Earth-to-Orbit Propulsion Technology, vol. 1:97–104.

Sponsor: Office of Aeronautics, Exploration, and Technology

■■■■■

Ground-Based Optical Leak Detection

William T. Powers/EB22
205–544–3452

Leak checks on liquid-propellant rocket engines are labor- and time-intensive and rely upon technician judgment. Ground-based optical leak detection was developed to accelerate and automate the leak detection and location process in response to demands for shorter turnaround times, reduced life-cycle costs, and enhanced mission confidence. It is a remote, near-real-time, computer-based, passive optical infrared imaging method that utilizes differential absorption of the nitrous oxide tracer gas. Providing sensitive leak detection and location, the system eliminates inconsistent technician evaluations and reduces leak inspection cycle time from 3 days to just a few hours. A portable optical leak detection system has been developed and successfully used in laboratory, shop floor, outdoor, and test stand environments.

Space shuttle main engine leak inspections include a subjective, time-consuming, manual soap-solution test of over 140 joints. An extension of this technique to all joints, welds, and brazes on the engine would be prohibitively difficult and expensive. However, approximate leak rates for the leak locations of these 140 joints are known. Helium bag leak checks are very sensitive, but the location of the leak cannot be determined except by performing subsequent soap-solution inspection. The present leak testing

process (soap and bagging) takes roughly 3 days for flight applications, contributing to the turnaround duration of the orbiter.

The Rocketdyne Division of Rockwell International Corporation is developing optical leak detection to reduce leak inspection time and increase mission confidence by rendering leaks within the field of view of an infrared focal plane array video camera instantly visible to the inspector via a television or computer monitor. The engine is pressurized with nitrous oxide, which strongly absorbs infrared radiation. Use on the space shuttle main engine was approved after an extensive compatibility study. The leaking gas is imaged with a filtered infrared camera, and the leaking gas absorbs the incident ambient or lamp infrared radiation, appearing as a dark billowing cloud on the television monitor. Unfortunately, if the leak is small, the dark cloud may be impossible for the human eye to discern.

To automate the process and make small leaks visible to the human eye, camera images are digitally processed. The resulting image of the leaking gas is highlighted in white and superimposed over an initial image, clearly showing the location and extent of the detected leak. Overlaid images are displayed four times per second.

The portable system, designed and assembled by Rocketdyne, consists of a 128- by 128-array InSta™ infrared camera on a wheeled tripod and a wheeled console containing a computer hosting an image processor, monitor, television monitor, video cassette recorder, and the camera electronics. The console can also be lifted by crane or hoist.

Laboratory and shop floor testing with simulated leaks of 0.25 standard cubic inches per minute was successful. Due to cool air-conditioned temperatures, use of a heat lamp or studio-type quartz lamp enhanced the sensitivity of the system. Wind tests, up to 900 feet per minute, were conducted. Results at velocities up to 100 feet per minute were strikingly good. At flow rates above 100 feet per minute, the leak became gradually more obscured due to gas flow away from the leak location and cooling effects. Outdoor sunlight tests were also very successful despite wind gusts that caused cooling effects.

Final testing was performed on the oxidizer side of the space shuttle main engine in the NASA/MSFC Technology Test-Bed test stand. The engine was filled with nitrous oxide through the helium pressurization line. During the first test, with winds gusting between 8 and 15 miles per hour, no leaks were detected. The test stand engineer verified that there were no leaks (no false positives). The test time was only 2 hours, including rechecking, adjustments for the extreme wind conditions, and waiting for gas-bottle exchange. Testing indicated that, with little practice, the entire engine could be done in only slightly more time.

Despite the high gusting winds, a known fuzz leak was detected easily. The leak was shown to be visible well below soap-solution detectability limits. An undisclosed leak was then created and easily detected. The leak was quickly determined to be in a 4-inch cube volume in the space between and behind the high-pressure oxidizer turbopump and the pogo system hardware. Detectability was measured at class 3, class 1, and fuzz-leak levels with excellent results. By moving the camera around the engine, the leak source was triangulated. At the appropriate viewing angle, the leak was detected as coming from a sensor port on the backside of the duct that carries liquid oxygen from the oxidizer turbopump to the fuel preburner in a location hidden by the ducts running between the turbopump and the pogo system. With the majority of joints, direct visual access is possible. To completely locate all leaks, it will be necessary to move the camera around the engine or place multiple cameras in strategic locations around the engine.

A new portable system that uses a staring focal-plane-array infrared detector has been developed. This system can detect leaks with ambient illumination, rather than the laser illumination required for its predecessor. Ground-based optical leak detection has successfully demonstrated a unique capability for detecting and locating small leaks (level 1, fuzz, and smaller) remotely and rapidly (4-Hz frame rate) in the laboratory, shop floor, outdoor environments, and on an engine test stand, showing great promise as an important future tool in rapid, reliable, and remote engine inspection under a variety of conditions. Benefits of using the optical leak detection system include a significant increase in sensitivity and repeatability over soap leak inspection and a significant reduction in the time required to perform leak checks.

Maram, J.; Wyett, L.M.; Delcher, R.C.; and Reinert, J.W. Optical Methods for Remote Rocket Engine Condition Monitoring. Proceedings of the 1988 Conference on Advanced Earth-to-Orbit Propulsion.

Sponsor: Office of Space Access and Technology

Industry Involvement: Rocketdyne Division of Rockwell International Corporation

In-Flight Leak Detection: A Hydrogen/Oxygen Leak-Imaging Sensor

William T. Powers/EB22
205–544–3452

Hydrogen and oxygen propellant leaks are difficult to detect in a spacecraft environment due to the issues of size, weight, and availability of sensors. Tracer gas techniques can identify leaks during the initial checkout phase, but cannot identify leaks caused by cryogenic cool-down of joints and cannot function when the spacecraft is fueled and on the launching pad (or in flight). A need exists for various types of sensors, including imaging sensors, that can, for example, visualize a leak from a joint.

Optical leak sensors offer the advantages of fast detection, remote detection, and lack of contamination problems. Hydrogen is difficult to detect optically because it lacks an absorption spectrum (due to the symmetric, diatomic-molecule structure of this gas). The strongest optical signature from hydrogen and oxygen is the Raman scattering effect. Spontaneous Raman scattering is a very weak effect: in an imaging context, every photon of probe laser light may return 10^{-16} photons of Raman signal light from a 1-atmosphere (pressure) hydrogen leak.

Such detection schemes are actually well within the limits of conventional low-level light-detection techniques. These techniques include pulsed probe lasers and time-gating of single-photo light detectors (in the 5-nanosecond range) and optical filters to reject the probe laser light and stray background light. The wavelength-shifting property of Raman scattering is crucial in this context, as it allows the signal light to be isolated from the probe light.

The caveat in the preceding scenario is the word "conventional." When performing spectroscopic work, one always keeps the optical axis of the detector perpendicular to the probe beam. With an imaging sensor, however, the optical axis of the detector must be precisely aligned to the axis of the outgoing probe beam, which introduces severe problems due to the fluorescence of metal surfaces in the field of view of the detector. Even a narrow-bandwidth, gated detector is easily overwhelmed by background fluorescence.

An innovation in the optical system (fig. 107) of an imaging detector can dramatically lower the background fluorescence problem. The concept involves focusing the probe laser to a point in open space and precisely aligning a pinhole fieldstop such that only light scattered from the focal region may enter the detector. This isolates the background fluorescence from the detector to a large degree. The innovation is called a "confocal" telescope, which allows limited three-dimensional imaging. A key part of the concept is that it allows probe laser intensities to be used that are far below the threshold for gaseous ignition.

The current status of the project is that a breadboard version of a confocal telescope has been constructed and that some data have been taken. The breadboard is 2 by 3 feet in size and contains a continuous-wave doubled-

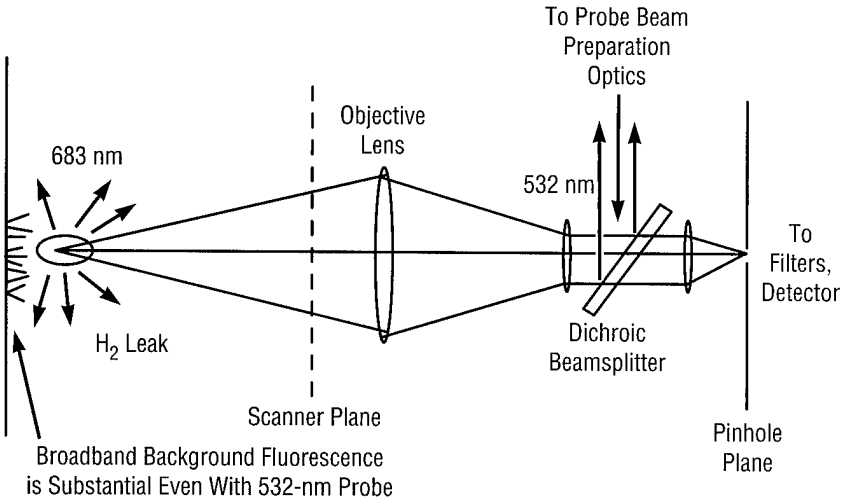

FIGURE 107.—Confocal telescope concept dramatically raises signal-to-fluorescence ratio.

YAG probe source, photomultiplier tube and housing, and an optical scanner for fast scanning. A spacecraft sensor would be much smaller and more lightweight.

In addition to the optical concept, one other critical component of this imaging technology is a fast-control system to manage the imaging process and display the processed data in real time. Conventional real-time operating systems are not fast enough to deal with the submillisecond event scales involved. Instead, hybrid software has been created that allows a fast-control system to be constructed on an MS–DOS environment. The software uses a 32-bit extended disk operating system and an architecture that prevents mode switching during interrupts and their associated overhead. The real-time part of the software will migrate to an embedded instrument-mounted system.

This technology is general in nature and can be commercialized in such areas as hydrogen facility leak detection, forensic analysis, and automated surface inspection. The technology is also a good starting point for more exotic technologies (e.g., stimulated Raman and Coherent Anti-Stakes Raman Spectroscopy techniques).

Duryea, T.W. May 1994. Raman Leak Detection Development. Proceedings of NASA Advanced Earth-to-Orbit Conference, MSFC.

Duryea, T.W. May 1992. Raman-Based Leak Detection. Proceedings of NASA Advanced Earth-to-Orbit Propulsion Technology Conference, MSFC.

Sponsor: Office of Space Access and Technology

Industry Involvement: Rocketdyne Division of Rockwell International Corporation

Installation Integrity Measurement for Various Sensors

Morrison R. Burns, Jr./EB22
205–544–2556

Analysis and Measurement Services Corporation is working with NASA/MSFC under a Small Business Innovation Research agreement, phase II, to develop techniques for measuring the installation integrity of various sensors. The main effort of this contract has been to advance the use of the loop-current step-response technique to measure the installation integrity and dynamic response characteristics of a thermocouple, as installed in composite materials. Sensors being studied include various types of thermocouples, strain gauges, thermistors, platinum resistance thermometers, and other resistance temperature devices.

The loop-current step-response test is based on heating the sensor internally by applying a small electric current to its leads. For thermocouples, the current is applied for a few seconds and removed; thermocouple output is then recorded as it cools to ambient temperature. The output is an exponential transient that can be analyzed to yield the response time of the installed thermocouple, as well as determine bond integrity. This technique can test sensors as they are installed in the field. Because it is not necessary to remove sensors being tested, loop-current step-response testing is very useful when inspecting sensors installed in inaccessible locations. Access to the sensor's leads is all that is required; the actual sensor can be a significant distance from the testing site.

For the Solid Propulsion Integrity Program, hundreds of thermocouples have been tested, both in the laboratory and in the field, to aid in program efforts to test new materials for suitability as nozzle material in solid rocket motor nozzles. Numerous thermocouples have been installed at varying locations and depths in a small solid rocket motor test article to determine the temperature profile of the nozzle. Thermocouple time response and installation integrity have been critical factors in the Solid Propulsion Integrity Program testing.

A typical, normalized loop-current step-response transient test is shown in figure 108. While the feasibility of using the loop-current step-response technique was demonstrated during phase I of this effort, phase II has shown conclusively that this type of testing is a highly useful and very practical tool for testing thermocouples installed in solid materials.

Extensive laboratory testing on strain gauges has illustrated the practicality of using the loop-current step-response technique to determine bond integrity of strain gauges. For comparison, self-heating index tests

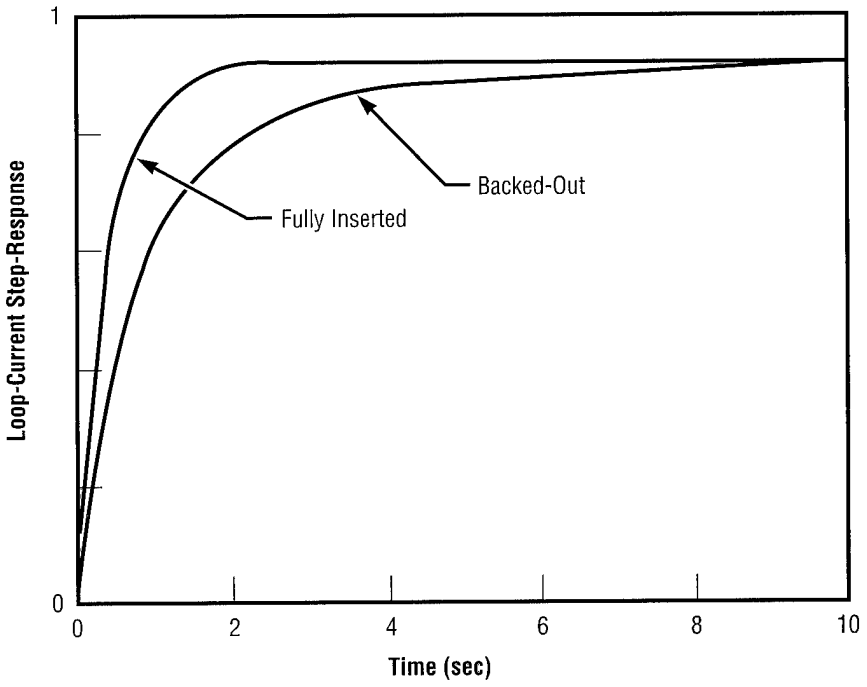

FIGURE 108.—Normalized loop-current step-response transients showing the difference in response time between a fully inserted and a backed-out thermocouple (fully inserted then backed out of the hole by a small amount, leaving a void). Thermocouples were installed in sample nozzle material and tested at room temperature.

were also performed; the results were consistent with the loop-current step-response tests. While Analysis and Measurement Services has performed some strain-gauge field testing at MSFC—and results have been encouraging—the testing has been too small-scale to show anything other than feasibility.

Several commercially available thermistors have been loop-current step-response tested. Initial results gave response times that were nonconservative when compared with conventional plunge test results. This effect was attributed to the variation in power provided to the thermistors during the tests, resulting in a self-catalytic effect. When minor modifications were made to test equipment to eliminate this problem, the retested results were comparable to the standard plunge test results, indicating that the loop-current step-response test method can be used effectively for testing the installation integrity of thermistors.

The bond quality of the six surface-mounted platinum resistance thermometers currently used on each space shuttle main engine has been a concern to NASA. In view of this, Analysis and Measures Services purchased several flight-type platinum resistance thermometers (nonflight-qualified) for laboratory testing. Both loop-current step-response and self-heating index tests were performed. Results indicated good correlation between the two tests, and good bonds were detectable from partial bonds. Some field testing has also been performed on several flight platinum resistance thermometers. Testing to date has shown the feasibility of using the loop-current step-response technique, but more field testing will be necessary to obtain reliable results.

Because the loop-current step-response test pulses the platinum resistance thermometer with a small current, some concern has arisen about its impact on calibration. (A normal test will pulse 15 to 20 milliamperes of current through the thermometer.) In one test, a new platinum resistance thermometer was calibrated, then repeatedly subjected to a 60-milliampere current pulse for 24 hours, and finally recalibrated. Results indicated a calibration shift of less than 0.2 °F, which suggests that a normal loop-current step-response test will not appreciably affect calibration.

The loop-current step-response technique has proven to be a very valuable diagnostic tool for various sensors. Its only drawback is that it cannot give reliable results for a single sensor installation. Reliability of the loop-current step-response test increases with the number of sensor installations being tested. This technique is especially useful for testing large numbers of sensors with similar installations, when accessibility to the sensor is not needed.

Hashemian, H.M.; Mitchell, D.W.; Shell, C.S.; and Farmer, J.P. July 1993. Improved Temperature Measurement in Composite Material for Aerospace Applications. Final Report, Small Business Innovation Research, Phase I. Contract NAS8–39814, Report NASA9306R0.

Sponsor: Small Business Innovation Research

Industry Involvement: Analysis and Measurement Services Corporation

Optical Plume Anomaly Detection Engine Diagnostic Filtering System

William T. Powers/EB22
205–544–3452

From the early days of rocket engine development, engineers have intently observed the exhaust plume during test and in actual flight—their trained eye seeking out a spectral signature of a healthy, properly operating propulsion system. During each observation, this spectral signature is compared with real-time performance and integrated in the "mind's eye" to pick up on anomalies or glitches that would indicate improper operation. Several years ago, MSFC engineers began a serious, more sophisticated look at techniques for detecting anomalies in the operation of the space shuttle main engine through observation of the exhaust plume. These efforts have resulted in considerable progress in the physics of observational devices and have provided encouragement relative to the potential value of such a capability. This success has led to the point of definition of the Optical Plume Anomaly Detection system. State-of-the-art technology in anomaly detection spectroscopy has demonstrated the ability to discern trace amounts (parts per billion) of metals involved in the space shuttle main engine's plume.

However, once these trace amounts are detected, what is the proper process for extracting valid and useful information? The defined process—the Optical Plume Anomaly Detection Engine Diagnostic Filtering System—is an aggressive effort not only to address the initial analysis of the myriad of data, but also to ultimately bring the detection system to future rocket engines as a viable tool for real-time health monitoring. A few of the major tasks within the program include preprocessing algorithms, neural net development of real-time quantification of species, and validation of spectroscopic/atomic models (fig. 109).

The area of model validation is of primary importance. The MSFC team for this effort seeks to validate its systems using plume-seeding data from the space shuttle main engine and the Diagnostic Test Facility. If good performance for analyses of

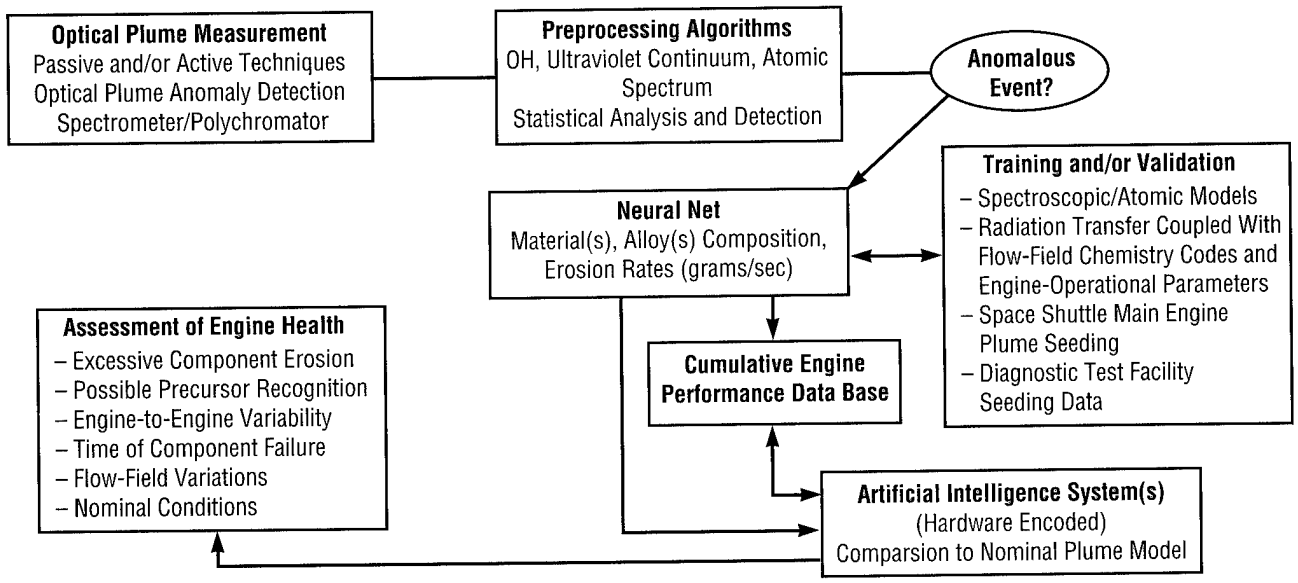

FIGURE 109.—Proposed Optical Plume Anomaly Detection Engine Diagnostic Filtering System process path.

spectral data from both engines can be achieved, then confidence can be placed in the physics, plume codes, and data processing, rather than using seeding data from one source as a calibration for the other. This form of self-consistent validation methodology, supported by team members from the Arnold Engineering Development Center in Tullahoma, Tennessee, will provide versatile spectral analysis systems to meet future demands for application to different rocket propulsion systems and different instrumentation for in-flight or ground-level measurements of spontaneous emission and stimulated emission/absorption of atoms. Recent success with seeding the flow of the shuttle's main engine at MSFC's Technology Test-Bed with a known quantity of substance affords the team with direct validation data for the main engine and also allows confirmation of secondary validation using Diagnostic Test Facility spectral data.

Before exhaust plume spectra can be analyzed for optical activity of atomic species, one must remove the baseline or discriminate between atomic transitions from spectral shapes and emission features normally found in the nominal baseline plume. In the shuttle main engine, one finds extremely high overtone excitation in the (0,0) and associated harmonics as well as a continuum region of emission that extends from the blue, visible far- into the near-ultraviolet spectrum. Preprocessing algorithms developed by Ames Research Center have attempted to address these issues. Initially, the data are registered in angstrom units that, in turn, allow correlation of anomaly detection data across tests and detection of emissions near the "noise level" or in the active OH region of the signal. Statistical tools are in place that characterize the detectability of elements of interest during transient and main-stage periods of a test with a 99-percent confidence level.

Test TTB036 (reference fig. 110 for depiction of various metals of interest) was the first test of the Pratt & Whitney fuel turbopump at the Technology Test-Bed. Propulsion engineers were interested in possible loss of cobalt-based "rub-stop" material. (Cobalt is not an element normally seen during Technology Test-Bed tests, but is clearly present in the anomaly detection spectral plot.) Essentially, with the click of a button, 4,096 data points are compared and statistically evaluated for each 0.5 second of data. Each test-bed test is an average of 170 seconds in duration. Other tools permit animation of data and engine data correlation on-line.

The Ames Research Center has also created an optimization routine to correlate neural net predictions with given spectral data sets. Radial basis function neural nets are under development at the University of Alabama in Tuscaloosa. Initially, multiple networks will be trained with the spectral model and compared to Diagnostic Test Facility data. Once an iterative process between model and neural network developers has produced a first set of "reasonable networks" and a validated spectral model has been achieved using Diagnostic Test Facility and space shuttle main engine data as previously mentioned, most robust networks can be trained quickly.

The neural network approach was chosen to address future needs for real-time applications. The spectral model takes species concentrations and produces a theoretical spectrum. However, the goal is to solve the inverse problem: given a measured spectrum, determine the "correct" specie concentrations. In previous applications of line-by-line codes used to determine specie number densities from path-integrated emission/absorption measurements, this problem is solved by linearized least-squares methods for minimizing the root-mean-square difference between the measured and predicted spectrum. However, while least-squares methods work well for narrow wavelength ranges in a posttest environment where real-time response is not an issue, the requirements of real-time response preclude this method due to generally long processing times. The University of Alabama has developed a solution to the inverse problem using neural networks that "learn" how the spectral line-by-line model works. Basically, the time-consuming computational part is performed pretest, and may take many hours, but the finished product can perform the inverse problem in real time, on the order of milliseconds, with no special hardware.

While other somewhat similar tasks may be underway, research indicates that the present MSFC-guided team of phenomenologists and spectroscopists from the Arnold Engineering Development Center, university professors, graduate students, Ames Research Center, and MSFC's own personnel will provide the best opportunity for the successful application of optical plume anomaly

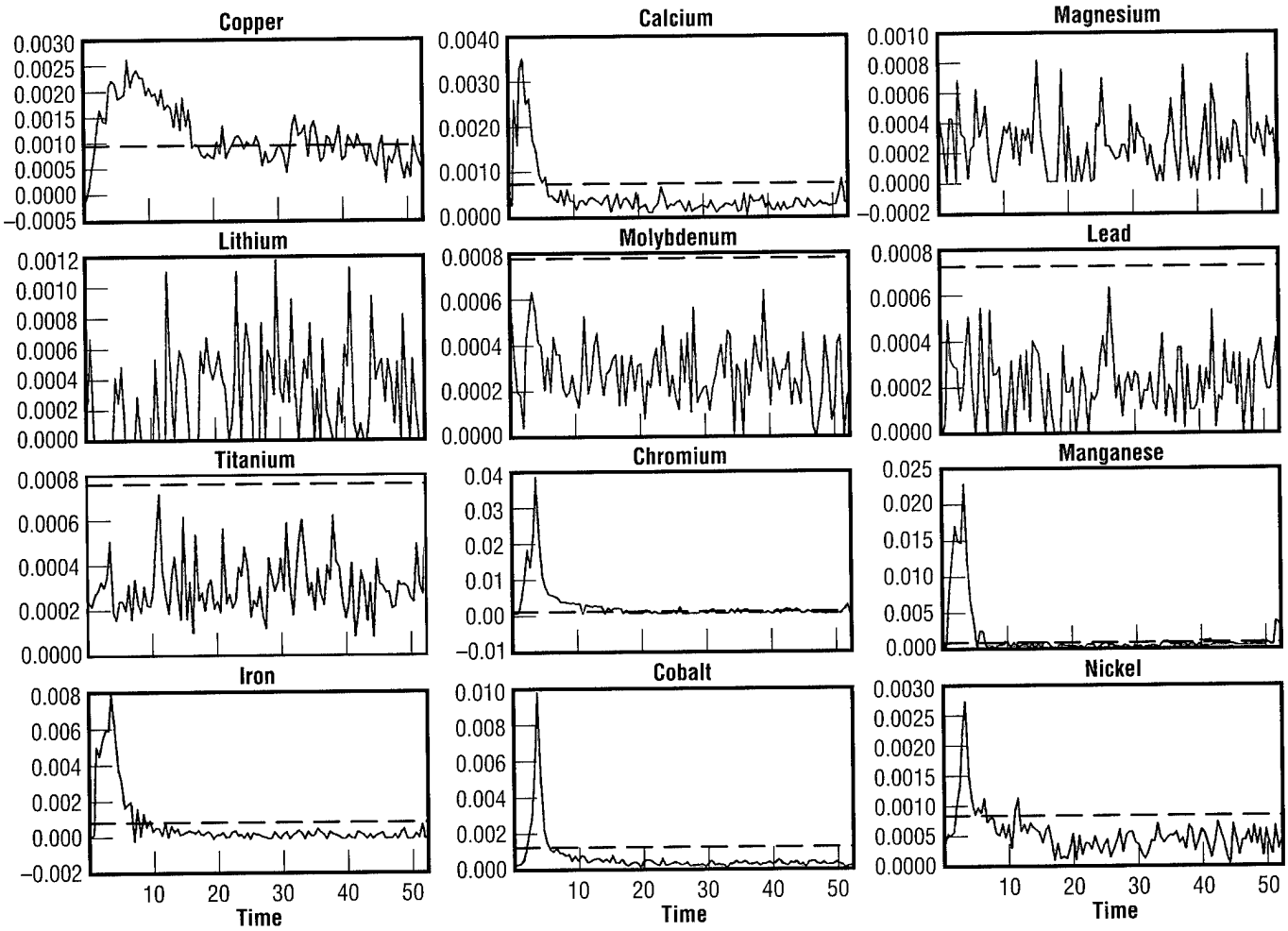

FIGURE 110.—Metals for test TTB036.

detection to future rocket engine operations. To date, the program has provided educational support through various grants to ten graduate and undergraduate students over the past few years.

Buntine, W. May 1994. Optical Plume Anomaly Detection Data Analysis. RIACS, NASA Ames Research Center, Earth-to-Orbit Conference, MSFC.

Wallace, T.L.; Powers, W.T.; and Cooper, A.E. May 1994. An Integrated Methodology for Rocket Engine Plume Spectral Analysis. Earth-to-Orbit Conference, MSFC.

Sponsor: Office of Space Access and Technology

University Involvement: University of Alabama

Other Government Involvement: Ames Research Center, Air Force/ Arnold Engineering Development Center

Flight-Qualifiable, Three-Point Docking Mechanism Control Electronics for Automated Docking

William Jacobs/EB23
205–544–3522

The control electronics (fig. 111) are an instrumental part of the three-point docking mechanism (fig. 112). They provide power and control to the latches and status to a vehicle's onboard computer. This three-point

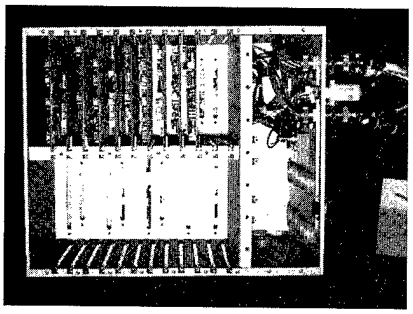

FIGURE 111.—Three-point docking mechanism controller (one string of electronics showing).

docking mechanism is one of the flight-qualifiable systems that make up the automated rendezvous and capture system, and the objective of the controller is to provide for autonomous docking with a target vehicle. The latest three-point docking mechanism design (third generation) includes three-phase, brushless, direct-current motors; two-phase, brushless resolvers; and trunnion presence sensors. Electronically, this is radically different from previous versions of the mechanism. As a result, a new electronic design was developed to control the latches. Another aspect of the new design is the inclusion of redundant motors, resolvers, and sensors. The redundancy is included in the controller design as two single strings of electronics.

The motors are driven by a Metal Oxide Semiconductor Field Effect Transistor inverter using a six-step technique. Hall-effect devices are used for motor commutation. The resolvers are used to provide position for set-point monitoring and derived velocity for closed-loop rate feedback control. Logic has been developed that uses the presence sensors (infrared light-emitting diodes and frequency-matched phototransistors) to determine the presence, as well as direction of movement, of the trunnions in the capture envelope. Requirements placed on the mechanism are to capture a "docking trunnion" within 3 seconds and then close to alignment position in about 20 seconds or longer (about 4.5 millimeters per second of trunnion movement). The controller has pre-

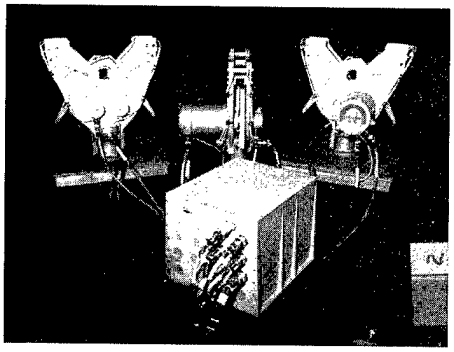

FIGURE 112.—Three-point docking mechanism system with latches, cables, and controller.

established capture and closing rates and selects which rate to command based on the position of the latch's fingers. Using the presence sensors, the control electronics, when armed, waits until two of the three trunnions are in the capture envelopes of the latches before initiating capture. Before the latches close to full dock, all three must be at the "alignment" position. The controller receives "high-level" commands from a remote source, such as an onboard computer, through an RS–422 interface. These commands can be used to do a precheck of the latches, arm the controller for automated capture, or override the automation and force the latches to open either in normal rate or emergency rate if required. The controller also sends out sensor status, latch position status, and engineering data such as motor current, rate command, rate feedback, and resolver position to the onboard computer. These data can be used by the computer to perform redundancy management. As part of the redundancy of the controller, the presence sensors of both sides are always active so that either side of electronics has knowledge of trunnion presence in the case that control must be switched over to the other side. The three-point docking mechanism system has already been baselined for such future flight applications as the space station resupply module and possible future satellite servicer vehicles.

Reference: MSFC–SPEC–2483

Sponsor: Automated Rendezvous and Capture Program Office, Office of Science and Applications Projects

Modular Rocket Engine Control Software

Richard H. Beckham/EB42
205–544–3747

NASA is conducting studies with the goal of enhancing and furthering the technology base to support high-priority programs. To support propulsion system activities, basic research and technology must be accomplished in the engine-control and health-monitoring arena. To accommodate evolving technologies, this system must be modular to allow interface redesign as system requirements change. The Modular Rocket Engine Control Software, which is being developed by Loral Space Information Systems, is a research and technology effort whose primary purpose is to demonstrate software development and maintenance cost reduction by implementing a modular, flexible software architecture.

Approximately 40 people are presently working full time to support the development, verification, and validation of the space shuttle main engine controller software, including laboratory hardware and support software maintenance. A significant percentage of the time and manpower required for this effort centers on the verification and validation of main engine software. Software logic changes resulting from flight requirement changes and/or software logic corrections, plus the need for special test software, have occurred at a relatively high frequency, with each new version requiring verification and validation. Fifteen software versions have been flown on 45 space shuttle missions since return to flight in 1988—an average of a new software version every three flights.

The purpose of the Modular Rocket Engine Control Software contract is to determine and develop a mobile approach to software that allows the incorporation of new system requirements and technology developments in sensors, actuators, input/output, connectors, and health/safety-monitoring techniques with fewer software impacts and, thus, reduced costs. The modular software concept creates a "fire wall" between modules such that when the code is changed, only the affected module needs to be re-verified. Some of the logic errors discovered in the current main engine software might not have occurred with more compartmentalized software.

The Marshall Avionics System Test-Bed is being used to develop program software and for demonstrations of this software at key milestone events. An engine controller system has been installed in the Avionics Test-Bed laboratory, and verification of the software is in progress. A demonstration of a sensor input task was performed in June, with a proof-of-concept demonstration (including an engine health-management task) scheduled for September. Tasks planned for fiscal years 1996 and 1997 include actuator control, vehicle input processing, ground checkout, telemetry processing, and additional health management.

Modular main propulsion system software has been identified as a task item in the Reusable Launch Vehicle Long-Term/High-Payoff Technologies Program. The Modular Rocket Engine Control Software is anticipated to be a stepping stone in the evolving effort. Preliminary results from this contract indicate that it is the proper approach for future software. The reduction in time and manpower required for the verification and validation of software should result in significant cost savings.

Sponsor: Office of Space Access and Technology

Industry Involvement: Loral Space Information Systems

Missions Operations

The Use of Virtual Reality in the Design Analysis of a Space Station Control Room

Joseph P. Hale II/EO23
205–544–2193

MSFC's Crew/Systems Engineering Branch became involved with the spatial layout of Space Station *Freedom* at the 30-percent design review of the building addition that would have housed, among other things, the payload control area. At that time, the primary interests of the architectural engineers included issues such as adequacy of room size (floor space) and their relative dimensions (aspect ratio), as well as ceiling heights and the relative floor heights of the payload control area and its public viewing area. In order to properly support the design review, it was determined that it would be necessary to develop and assess several feasible spatial layouts of operator consoles and support equipment within the proposed payload control area room. Virtual reality was among the analytical tools used to assess the various layouts.

In the Space Station *Freedom* Program, payload operations and integration functions were to be handled out of MSFC, with one of the payload operations and integration functions being real-time payload operations management and control. Although this is a somewhat distributed function, both inside and outside the Payload Operations Integration Center, the payload control area was to serve as the "front room" control room for this function. The Payload Operations Integration Center has four functional discipline teams: the operations integration team, the data management team, the operations control team, and the mission planning team.

Various design analysis tools were used during the design review: scaled drawings, two-dimensional computer-aided design drawings, and immersive virtual reality. The drawings were used to support such analyses as video wall maintenance access, translation path clearances, adjacency, information flow and access comparisons, and video wall viewing analyses.

Immersive virtual reality was used as, among other things, a human factors design analysis tool for the work areas and other architectural spaces. The use of virtual reality in the macroergonomic analyses of work area topological design enables the consideration of the fields of view from a variety of eye reference points and can include operationally driven components, such as translation paths among the various worksites.[1] Examples of "spaces" include control rooms, space stations, and orbiting telescopes.[2] A validation study for "control room class" ergonomic applications—to help characterize possible distortions or filtering of relevant perceptions in a virtual world—was recently completed at MSFC.[3, 4] The primary objective of the experiment was to begin the process of validating and calibrating the use of virtual reality as a human factors analytical tool.

Although the focus of the 30-percent design review was not spatial layout per se, feasible layouts had to be developed in order to assess the adequacy of particular features of the proposed design. The requirements definition and analyses provided both direction for the design effort and criteria for design analyses. Consoles were first defined and then used as building blocks to develop various configuration options. In reality, this is an iterative process, where console layout affects payload control area layout options, which, in turn, affect console layout options. (Locations for printers, fax machines, document stowage, etc., must also be factored into the payload control area layout.) Several configurations of the console floor plan layout, including large video screens and a public viewing area, were developed using scaled drawings and two-dimensional computer-aided design drawings (fig. 113). These were then modeled in virtual reality. Engineers, management, and the Public Affairs Office utilized the system to visualize the various configurations immersively. Based, in part, on the findings of the virtual reality control room validation study referenced above (regarding subjective and objective assessment accuracy/sensitivity of "virtual" control rooms versus "real" control rooms), researchers determined that the level and type of comparative assessments employed in these analyses fall within the comfort zone of supportable, hence legitimate, judgments.

Engineers and management were able to focus on the operationally driven design features, such as the team-based grouping and layout of the consoles. The virtual reality environment provided a unique method of visualizing the control room "space" not otherwise possible.

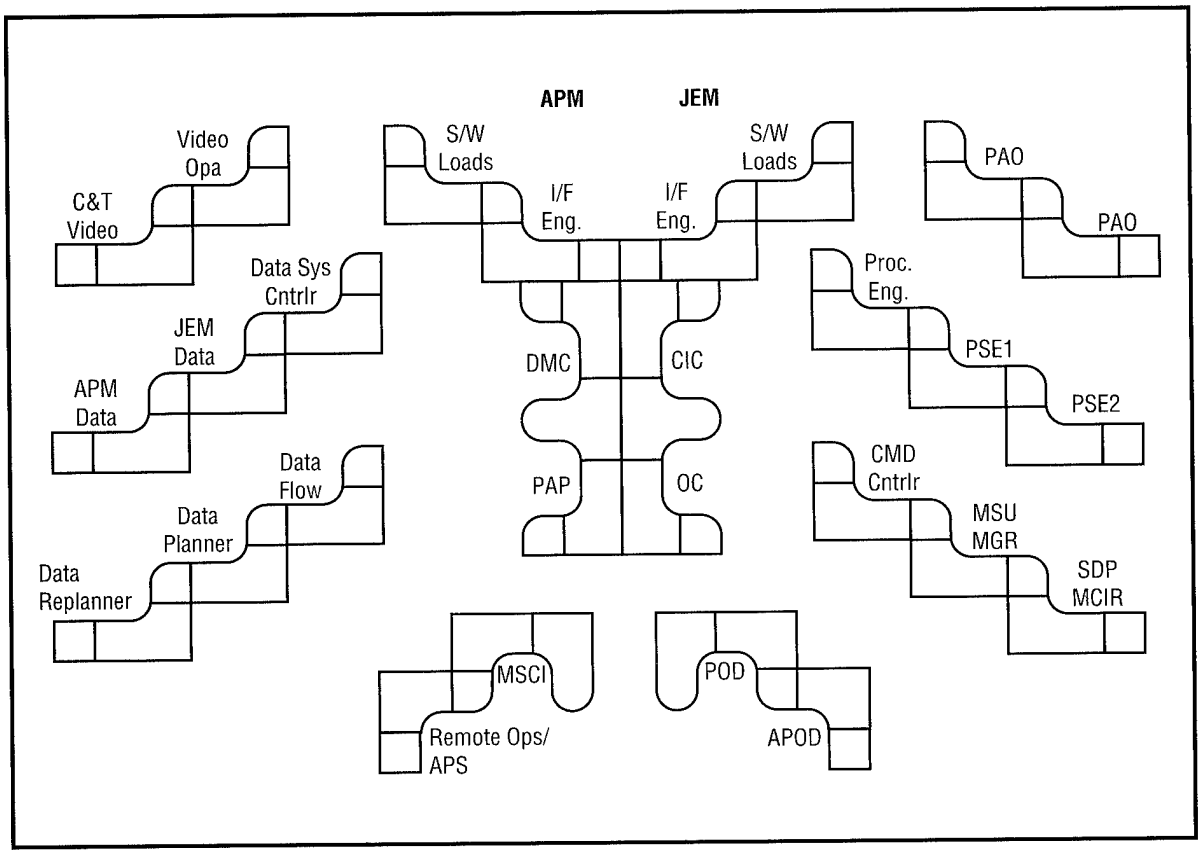

FIGURE 113.—Computer-aided design landscape configuration of the operationally driven payload control area.

Scale and architectural features and relationships that are not—at least immediately—perceptible in plan drawings were much more obvious in the virtual environment, providing better comparative insights and impressions among the various configurations.

Of particular note were the viewing analyses. One issue to be addressed for the 30-percent design review was the relative floor heights of the payload control area and its public viewing area, i.e., how much higher should the floor in the viewing area be above the floor in the payload control area to give the people in the viewing area the best view of control area activities. Part of each of the virtual reality environments was the ability to raise and lower the viewing area floor during a virtual reality session. Simultaneously, the virtual eye height of the user could be adjusted to reflect the full anthropometric design range (e.g., 3.5 feet for 6-year-olds, 6.5 feet for adults). The Public Affairs Office evaluated the view from the public viewing area, considering what a range of visitor sizes might be able to see from the range of viewing area floor heights. The office was also able to perform a preliminary camera viewing analysis, "flying" to various possible camera locations to inspect the composition of the possible camera fields of view. The ability to pan and tilt and change "lenses" (i.e., narrow- to wide-angle fields of view) in real time was especially useful.

These analyses helped answer several specific control room architectural questions posed by the architectural

engineers (e.g., adequacy of room size, control room and public viewing area relationships, camera secondary structure locations, etc.). The most important result, from a human factors perspective, was the general change in thinking on what a control room should look like and what should drive its configuration. The focus on the team and on features that enhance and enable more efficient team operations became more visible and important drivers for control room layout. Classic control room layouts with all consoles in parallel rows, facing forward towards the video wall, were viewed as less desirable and less conducive to efficient team operations than a configuration with grouped consoles based on inter- and intrateam operational considerations.

[1]Hale, J.P. 1993. Virtual Reality as a Human Factors Design Analysis Tool. Proceedings of the Southeastern Simulation Conference, Huntsville, Alabama, 140–144.

[2]Null, C.H., and Jenkins, J.P. (eds.) 1993. *NASA Virtual Environment Research, Applications, and Technology.* National Aeronautics and Space Administration.

[3]Dittmar, M.L., and Hale, J.P. 1994. Virtual Reality as a Human Factors Design Analysis Tool for Architectural Spaces—Control Rooms to Space Stations II: Subjective Measures. Proceedings of the Human Factors Society 36th Annual Meeting, Santa Monica, California: Human Factors Society, 280–283.

[4]Hale, J.P., and Dittmar, M.L. 1994. Virtual Reality as a Human Factors Design Analysis Tool for Architectural Spaces—Control Rooms to Space Stations I: Objective Measures. Proceedings of the Human Factors Society 36th Annual Meeting, Santa Monica, California: Human Factors Society, 275–279.

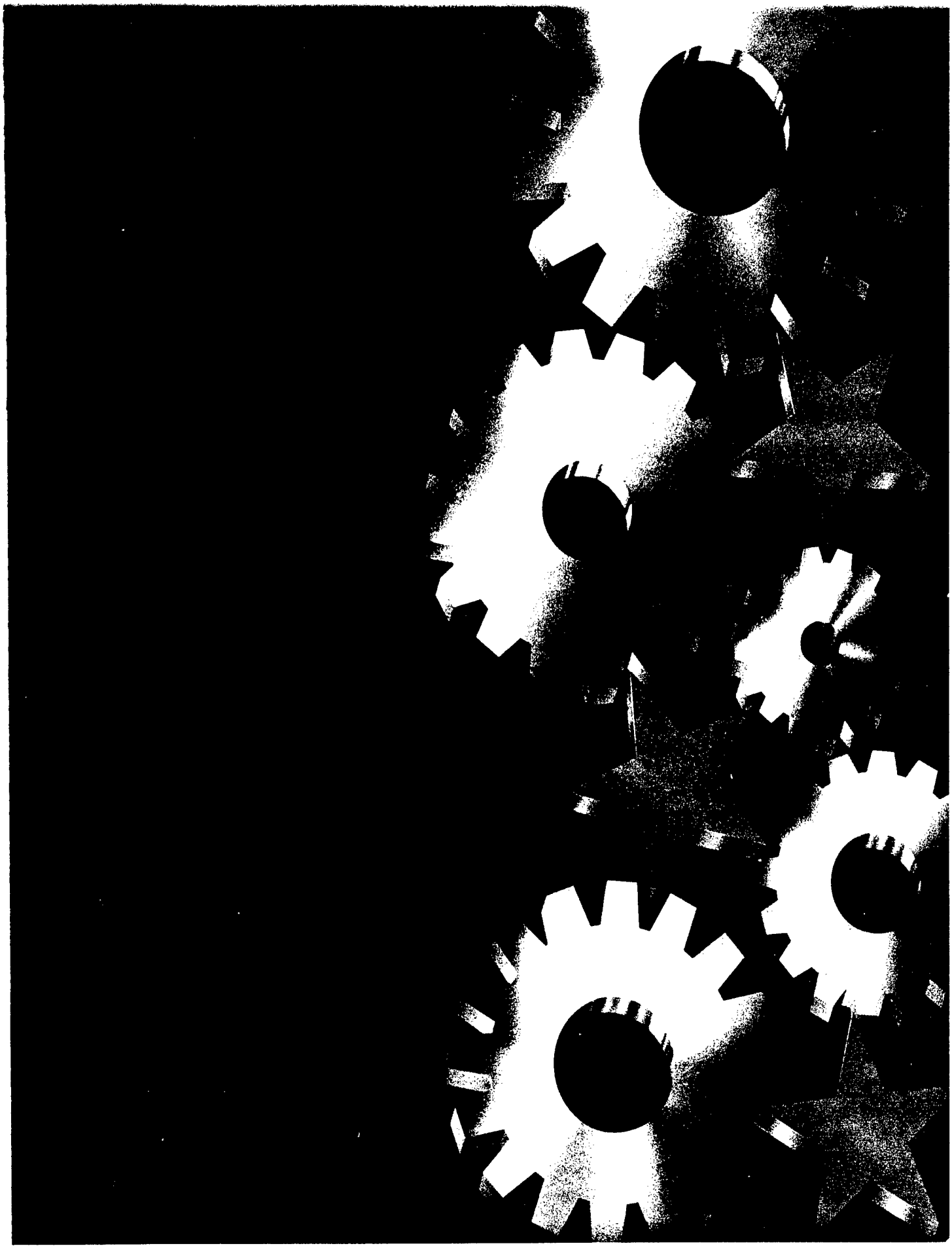

Technology Transfer

In a continuing effort to expand the transfer of technology developed by NASA and its contractors, three field centers—MSFC in Alabama, Kennedy Space Center in Florida, and Stennis Space Center in Mississippi—have joined with the Southern Technology Applications Center in Florida to form a Southeast Regional Technology Transfer Alliance.

While the effort is not limited exclusively to the Southeastern United States (e.g., MSFC has transfer programs of various kinds in nearly two-thirds of the United States), this region is the primary focus of the three centers' efforts. Part of the reason for this is budgetary; while the centers would like to reach out with a total program to all 50 states, limited funds and personnel availability preclude greater efforts. Also, many states fall within the sponsorship of other NASA field centers, all of which operate technology transfer activities. At present, MSFC and/or the Alliance have Memorandums of Understanding with the States of Alabama, Georgia, Tennessee, North Carolina, South Carolina, Kentucky, Arkansas, Florida, Mississippi, and Louisiana.

The Southeast Alliance is providing a synergistic effect, whereby the resources of all three centers are brought to bear on specific problem areas, creating a complementary approach to a solution.

Persons interested in learning more about the NASA technology transfer program can call toll free, 1-800-USA-NASA.

Harry G. Craft, Jr.
Manager
Technology Transfer Office

MSFC Small Business Innovation Research

Helen C. Stinson/LA40
205–544–7239

Timothy A. Self/LA40
205–544–7413

Small Business Innovation Research (SBIR) program objectives established by law include stimulating technological innovation in the private sector, strengthening the roles of small-business concerns in meeting federal research and development needs, increasing the commercial application of federally supported research results, and fostering and encouraging participation by socially and economically disadvantaged persons and women-owned small businesses in technological innovation.

There are three phases in the Small Business Innovation Research program. The purpose of phase I is to determine the technical feasibility of the proposed innovation and the quality of the performance of the small-business concern with a relatively small NASA investment before consideration of further federal support. The performance period is 6 months, with funding up to $70,000. To be eligible for phase I selection, a proposal must be based on an innovation having high technical or scientific merit that is responsive to a NASA need.

The objective of phase II is to continue development of selected innovations shown feasible in phase I that have the highest potential value to NASA and the U.S. economy. Phase II awards may not necessarily complete the research and development required to satisfy commercial and federal needs beyond the Small Business Innovation Research program, but completion of the research and development as well as commercializing the results should be pursued in phase III. Phase II lasts 2 years, with funding up to $600,000.

Phase III is pursuit by Small Business Innovation Research contractors of commercial application of their project results using private-sector funds. This is in support of the government's policy to stimulate technological innovation and provide for return on investment from government-funded research/research and development that is in aid of the national economy. Phase III may also be follow-on, non-Small Business Innovation Research-funded contracts with the government for Small Business Innovation Research-derived products or processes for use by the federal government.

Small Business Technology Transfer is a pilot program with similar objectives to Small Business Innovation Research. This program is a cooperative research and development effort conducted by a small business concern and a research institution. The phase I performance period is 1 year, with funding up to $100,000. Phase II lasts up to 2 years, with funding up to $500,000.

Contact the MSFC Small Business Innovation Research/Small Business Technology Transfer program manager for more information about a particular program. A representation of completed contracts with the phase II results and commercialization of the end products/processes is provided as follows:

Company Name: Accurate Automation Corporation
Contract Number: NAS–8–38967
Project Title: Advanced Telerobotic Control Using Neural Networks

The phase II end product of this endeavor was a new hybrid neural/adaptive robot system with a controller that is unique in that it can be readily adapted from one robot to another without modifying the control software.

By updating the training of the underlying neural network each time the robot arm is moved, the controller automatically learns to improve its performance each time it is used. The system was designed around a unique neural-network coprocessor developed by Accurate Automation Corporation in support of this and other related Small Business Innovation Research programs. The neural-network coprocessor has since been commercialized and is presently being marketed. It has licensees in both PC and Versa Module Eurocard form factors.

Follow-on applications of the technology include aircraft actuator control and the control of a four-motor electric car. Silicon Graphics has provided Accurate Automation Corporation with a considerable amount of equipment as a result of this contract. Unisys, who developed the dual Digital Signal Processor board for the Neural Network Processor, has also invested heavily in the board. This has resulted in sales to Phillips Laboratory, Texas Instruments, Lockheed Martin, Pratt & Whitney, and others for the Versa Module Eurocard board.

The target application arena for this technology includes use in environments dangerous for humans, including underwater ship cleaning and inspection and assembly applications.

Company Name: Engineering Sciences, Inc.
Contract Number: NAS–8–40175
Project Title: A Fast Algorithm for Transient All-Speed Flows and Finite-Rate Chemistry

The phase II end product of this effort was a highly efficient algorithm that can be incorporated into any computational fluid dynamics code for a more efficient and reliable analysis of multiphase flow fluid dynamics and thermodynamics inside liquid-propellant rocket engine combustion devices.

With the technology developed during the first two phases of this effort, Engineering Systems, Inc., has modeled spray-coating processes in an effort to understand the physics of the thermal protection layer coating of the shuttle program's solid rocket boosters. United Space Boosters, Inc., is funding this activity. During 1994 and 1995, Pratt & Whitney employed Engineering Systems' technology to enhance the computational efficiency of the NASTAR code, and last year Engineering Systems utilized the technology to model steam-sterilization processes for Baxter Healthcare Corporation.

NASA has now provided further funding for the development of a code that will address combustion issues relevant to the performance of tripropellant engine preburners/injectors. The technology initiated under the auspices of the Small Business Innovation Research program are now aimed at the development of next-generation launch vehicle propulsion.

Company Name: Plasma Processes, Inc.
Contract Number: NAS–8–40585
Project Title: Innovative Plasma Nozzle Techniques for Eliminating Overspray

This project's phase II end product was a bell-contoured plasma nozzle configuration that reduces overspray, optimizing material-deposition efficiency and quality of vacuum- and air-plasma spray coatings and structures.

Plasma Processes, Inc., designed bell-contoured vacuum plasma spray nozzles that have reduced overspray by 50 percent when spraying copper and copper alloys. The company has also reduced tungsten overspray, producing denser, less-porous coatings than previously achievable. As a result, nozzles have been used to successfully spray-form tungsten crystal-growth furnace cartridge tubes which will be used to process materials in microgravity.

Bell-contoured vacuum plasma spray nozzles have been designed for the Department of Energy to spray gradient materials on plasma-facing components of a nuclear-fusion reactor. In addition, a leading thermal spray equipment and consumables manufacturer has committed to test the nozzles at its own cost to evaluate the nozzles' potential for use in its equipment, and the world's largest producer of plasma spray equipment has issued a letter of intent to purchase a specified number of the nozzles. Plasma Processes, Inc., is currently employing bell-contoured nozzles in a phase II contract to fabricate crystal-growth furnace cartridge tubes for NASA. They will also be used to spray toxic materials (e.g., beryllium) for Department of Energy projects and to fabricate "smart materials" that function as proximity sensors.

Company Name: SECA, Inc.
Contract Number: NAS–8–40583
Project Title: Propulsion Chemistry for Computational Fluid Dynamics Applications

During the phase II portion of this effort, predictive methodology was developed to determine the effect of using real-fluid thermodynamics and physical properties in computational fluid dynamics codes when analyzing propulsion system performance and operational characteristics.

Utilizing Small Business Innovation Research funding, SECA has developed real-fluid thermodynamic and caloric equations of state, transport properties, surface tension, and mixture rules to describe multicomponent fluids at an extreme range of states for propellant and exhaust components. These properties are described in subroutines for use with computational fluid dynamic codes for improving RP–1 injector-element and hybrid-propellant combustion efficiencies considering soot formation, fuel pyrolosis, and burn rate.

These new thermodynamic codes are being used by SECA for Lockheed Martin to analyze and design hybrid rocket motors for the Integrated Hybrid Propulsion Development

Program. SECA's effort in this work will continue through 1997.
The new property subroutines are also being used to predict spray combustion behavior of RP–1 when used alone and with a tripropellant system for the reusable launch vehicle designs of the X–33 and X–34. These tripropellant computational fluid design codes are being developed under a NASA/MSFC phase III Small Business Innovation Research study.

Sponsor: Office of Space Access and Technology; Small Business Innovation Research Program

Dual-Use Hydrostatic Bearing Technology

Christopher J. Bramon/LA40
205–544–2800

A multiagency, multicontractor team is developing a reliable, long-life, cost-effective rotor support system for advanced chillers and liquid rocket-engine turbomachinery. The incorporation of hydrostatic bearings into advanced air-conditioning systems is key to creating a high-efficiency product line that will save $58 million of electricity annually. Long-life turbopumps will significantly reduce military and commercial payload costs and help the United States become cost-competitive and reclaim a majority share of the international launch vehicle market.

Current bearing systems limit the life, reliability, and performance of air-conditioning compressors and rocket engine turbopumps. Hydrostatic bearings replace conventional rolling-element bearings with high-pressure fluid in a noncontacting, low-friction, highly reliable bearing that emphasizes design simplicity, low cost, and long life. Life limitations due to continuous wear of contacting components are eliminated with this system. Critical issues in the design of hydrostatic bearings are the effects of short-duration transient wear during start and stop cycles and the performance of the bearing when using compressible fluids. This program will validate a design system to address these issues and transition the technology to new production programs.

Specific objectives include:

- Validating a hydrostatic bearing design code for compressible fluids
- Conducting transient wear tests of rub-tolerant materials in R134a and liquid hydrogen
- Measuring static and dynamic performance of hydrostatic bearings operating in a compressible liquid (varying supply pressure, pocket-area ratio, pocket depth, orifice geometry, orifice orientation, fluid-bulk compressibility, speed, and operating eccentricity)
- Testing heating, ventilation, and air-conditioning bearings in chiller/compressor components and in new chiller prototype system.

The Dual-Use Hydrostatic Bearing Technology Program started in March 1995 as a 2-year base program with two 1-year options. The base program is dedicated to conducting extensive component performance and wear testing. Options provide for technology transition of an advanced industrial chiller prototype incorporating hydrostatic bearings. This technology could have a pervasive impact on both the space-propulsion and the heating, ventilation, and air-conditioning industries.

A typical industrial chiller unit consists of a centrifugal compressor driven through a set of gears by a hermetically sealed electric motor. The compressor pressurizes the refrigerant,

which passes through both an evaporator and a condenser. Oil is used to ensure proper lubrication of the gears and bearings. Although essential for the successful operation of existing systems, oil reduces heat-transfer efficiency in the condenser and evaporator. The elimination of oil requires a new and innovative approach to the entire system. Carrier Corporation has selected an approach that employs a direct-drive (motor-to-compressor), high-speed system incorporating process-lubricated hydrostatic bearings to remove the need for oil-lubricated gears and bearings.

The resulting direct-drive system will be more efficient due to the elimination of gear mechanical losses, improved aerothermomechanical design, and improved heat-transfer performance in the evaporator and condenser. Compared to the current product line, this new family of direct-drive centrifugal equipment incorporating hydrostatic bearings will be 18 percent more efficient. For a typical 400-ton unit user in Atlanta, Georgia, a power savings of $16,000 annually is expected. Based on the increased market projected for 1997, the average annual power savings for the new Carrier units will be $58 million.

Rapid, reliable, and low-cost access to space is absolutely critical for supporting and maintaining the Nation's space assets with no degradation in mission capability. Current U.S. expendable and reusable space launch vehicles, which typically have launch-preparation times ranging from 85 to 365 calendar days, simply do not meet the launch-on-demand criteria required for responsive and timely replenishment of space assets. Without exception, the propulsion systems of these launch vehicles are characterized by short lifetimes, high maintenance, and extensive ground support. As a result, launches are infrequent, costly, and militarily unresponsive.

To achieve the goals of military responsiveness and affordable commercial launch services, advanced propulsion systems must combine low operational and maintenance costs with increased safety and reliability. A cost analysis of a long-life reusable turbopump, comparing rolling-element bearings versus hydrostatic bearings, indicated a savings of $1.8 million per hour of turbopump operation over hydrostatic bearings. The U.S. commercial launch industry is competing in the work market with private launch vehicles derived from ballistic missiles developed in the 1950's and 1960's. Although the U.S. once dominated the market for commercial launch services (fig. 114), continued reliance on these aging expendable launch vehicles and propulsion systems has significantly reduced cost competitiveness. The U.S. has lost the leadership in commercial launch services to France and is facing further challenges by highly subsidized Japanese, Chinese, and Russian aerospace companies. Launch costs reductions in excess of 50 percent may be required. The National Space Council's 10-Year Space-Launch Technology Plan sets forth a cost goal of $1,000 per pound, which is 22 percent of the current U.S. cost.

Hydrostatic bearings used as the primary rotor support system for cryogenic turbomachinery offer significant design, performance, and durability improvements compared to conventional rolling-element bearing systems. Unlike rolling-element bearings, hydrostatic bearings have no DN (bore diameter × rotor speed) limitations and are not prone to stress-corrosion cracking, rolling-contact

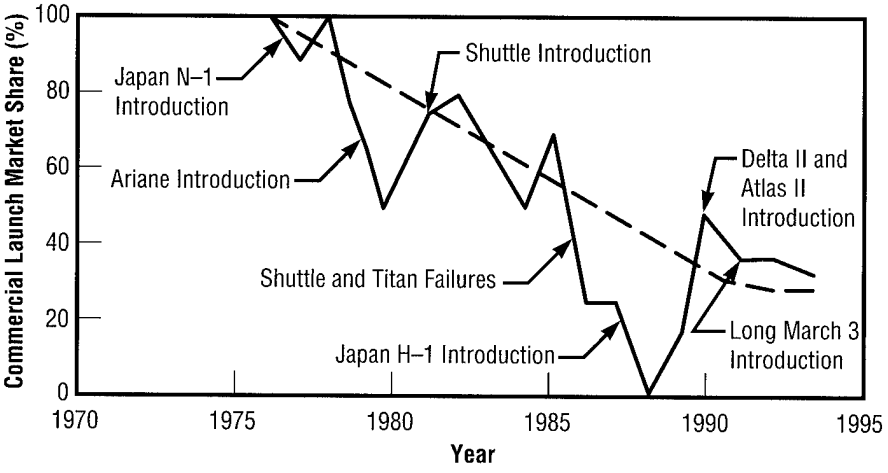

FIGURE 114.—U.S. share of commercial launch market (from National Space Council's 10-Year Space-Launch Technology Plan).

fatigue, or bulk-ring fractures due to material or manufacturing defects. Free of these constraints, the shaft speed can be increased for higher operating efficiency. Increased operating speed also helps to reduce the size and weight of the turbomachinery. Additional desirable characteristics include mechanical simplicity, accuracy of rotor position, high or low stiffness, lack of rotating-to-static part contact during steady-state operation, and excellent damping characteristics for improved rotordynamic performance. These key features enable significant reductions in part count and complexity, the use of high-performance unshrouded impellers, and smaller operating clearances that result in increased performance and longer life at a lower cost.

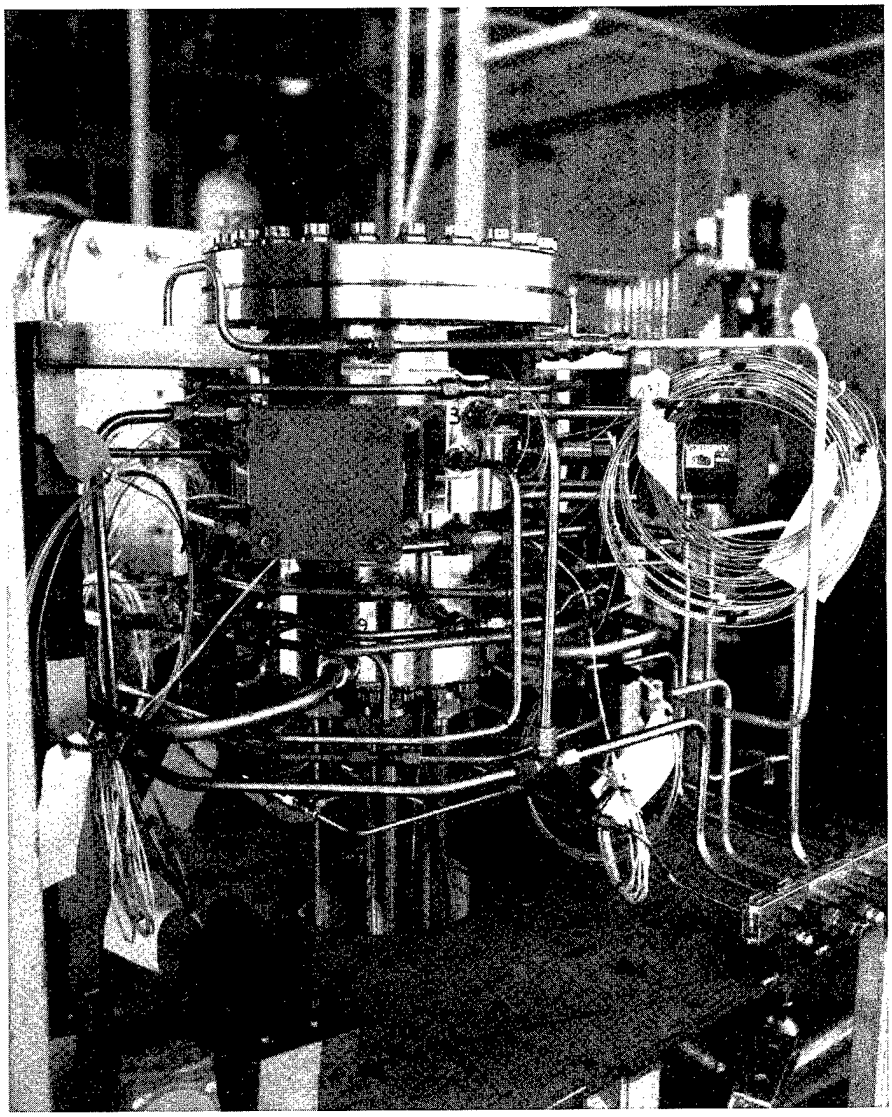

FIGURE 115.—Hydrostatic bearing test rig.

Two major factors that determine the successful operation of a hydrostatic bearing are performance and durability. Performance includes such factors as flow rate, load capacity, drag torque, stability, and the dynamic coefficients—stiffness, damping, and inertia. Pratt & Whitney's test program will evaluate bearing performance, while the Phillips Laboratory will address rub tolerance of various shaft/stator material combinations. The hydrostatic bearing test rig being used in this program is shown in figure 115. In addition to developing the advanced chiller system, Carrier has fabricated and delivered a high-pressure, self-contained, closed-loop R134a system to support the extensive test program. This system allows testing with an ambient-temperature fluid that approaches the compressibility of cryogenic liquid hydrogen at a significantly lower cost. By the end of 1995, the Phillips Laboratory will have concluded the liquid-hydrogen material test program and Pratt & Whitney will have started the R134a performance testing.

Both the aerospace and the heating, ventilation, and air-conditioning industries require advanced rotor-support systems to improve reliability, efficiency, and life, while lowering procurement and operating costs. These advanced rotating machinery systems are necessary to position the United States to compete successfully in the growing international marketplace. Joint technology investment programs, using the

expertise and resources of both government and private industry, are a cost-effective means to meet military and economic security goals.

Sponsor: Technology Reinvestment Project through the MSFC Technology Investment Office

Industry Involvement: Pratt & Whitney, Government Engines and Space Propulsion, West Palm Beach, Florida; Carrier Corporation, Syracuse, New York

Other Government Involvement: U.S. Air Force Phillips Laboratory, Edwards Air Force Base, California

Space Vehicle to Save Launch Costs

Vernotto C. McMillan/LA40
205–544–2615

High launch costs, resulting from the weight and fuel required to deliver a satellite to the proper orbit, are a prohibiting factor in the commercial satellite industry. If additional thrust could be created once in space, less fuel would be required, thereby also reducing weight factors.

Under the Aerospace Industry Technology Program, an industry, academia, and government consortium was formed on April 24, 1995, to develop a new space vehicle to save on launch costs. The consortium, led by McDonnell Douglas Aerospace in Huntington Beach, California, includes United Applied Technologies in Huntsville, Alabama; Thiokol Corporation in Brigham City, Utah; the University of Alabama in Huntsville, Huntsville, Alabama; the U.S. Air Force Phillips Laboratory at Edwards Air Force Base, California; Lewis Research Center in Cleveland, Ohio; and MSFC.

The consortium's goal is to develop a Solar Thermal Upper Stage (fig. 116)—a space vehicle with a unique propulsion system. The planned propulsion system uses large concentrating mirrors to focus sunlight on an energy-absorbing engine. The engine heats hydrogen propellant to high temperatures and releases it through a nozzle to create thrust. Once developed, the system can efficiently transport satellites from low-Earth orbit to geosynchronous equatorial orbit in 15 to 30 days. For communication and Earth-sensing satellites, the geosynchronous orbit is preferred because satellites orbit together with the Earth's rotation and appear to be stationary points over the Earth's surface. The propulsion efficiency of the Solar Thermal Upper Stage allows it to transfer satellites about twice as large as chemical-propulsion (hydrogen/oxygen) transfer vehicles. This, in turn, enables satellite owners to use a smaller, less costly, expendable launch vehicle for the same payload, resulting in a significant cost savings of up to $150 million per launch.

Single-stage-to-orbit vehicles, as currently envisioned, have no capability to place satellites in geosynchronous transfer orbit or in geosynchronous equatorial orbit; the Solar Thermal Upper Stage can provide this capability. Its development will enable the U.S. commercial expendable launch vehicle business to be more cost-competitive with the French, Russian, or Chinese launchers.

The roles of the consortium member are as follows: McDonnell Douglas provides consortium/program management, system design and integration, and liquid-hydrogen storage/feed-system development; United Applied Technologies manages concentrator development; Thiokol Corporation provides concentrator support development; MSFC leads absorber/engine development and testing of the hydrogen storage/feed system; Lewis Research Center develops the flight-type hydrogen tank; the U.S. Air Force's Phillips Laboratory undertakes the testing of the concentrator, absorber/engine; and

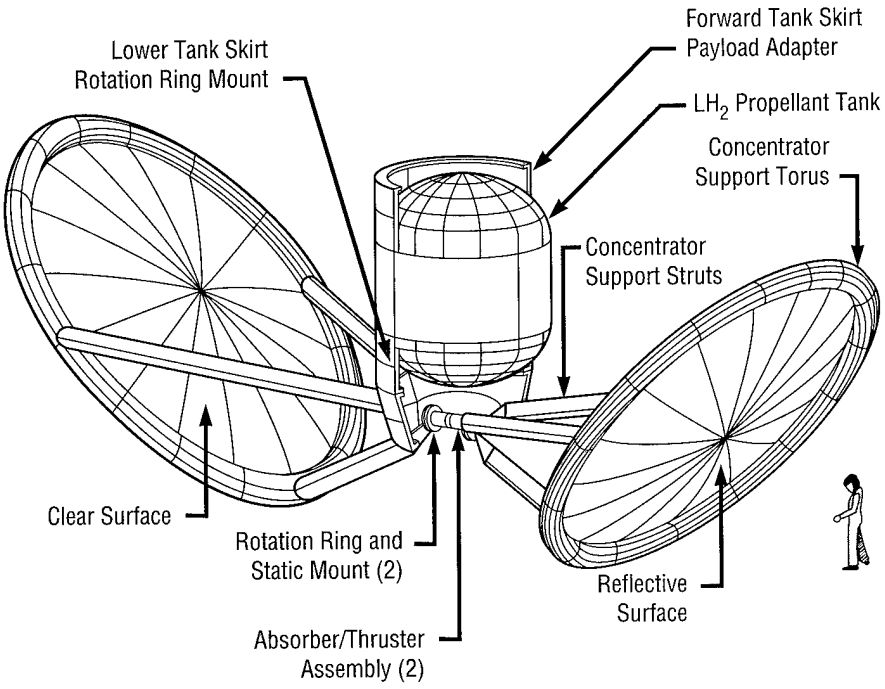

FIGURE 116.—The Solar Thermal Upper Stage uses large, inflatable, parabolic concentrators to focus sunlight on a high-temperature absorber. The absorber is cooled by heating hydrogen gas circulating through it. The hot (2,600-Kelvin) hydrogen is expanded through a nozzle to provide thrust (1 to 10 pounds) at high specific impulse (800 to 1,000 seconds). The fuel is stored as subcritical liquid hydrogen. The Solar Thermal Upper Stage is autonomously guided as it requires about 130 burns (orbits) on its 30-day transfer mission from low-Earth orbit to geosynchronous equatorial orbit.

the University of Alabama in Huntsville conducts data analysis and diagnostics.

The program is valued around $2.65 million, which is a 50-percent cost-share by industry over 30 months beginning in April 1995. Although many of the technologies have been demonstrated at the component level by one of the partnership members, no system demonstration of these various elements together has been demonstrated (on ground or in space), as the capabilities are spread across a number of entities.

Sponsors: NASA Jet Propulsion Laboratory; Office of Technology Transfer

Industry Involvement: McDonnell Douglas Aerospace, Huntington Beach, California; United Applied Technologies, Huntsville, Alabama; Thiokol Corporation, Brigham City, Utah

University Involvement: University of Alabama in Huntsville, Huntsville, Alabama

Other Government Involvement: Phillips Laboratory, Edwards Air Force Base, California; Lewis Research Center, Cleveland, Ohio

Structural Ceramics for Advanced Turbomachinery Applications

Christopher J. Bramon/LA40
205–544–2800

Gary G. Genge/EP32
205–544–4941

The team of Allied Signal Aerospace Equipment Systems, Allied Signal Ceramic Components, Allied Signal Research and Technology, Lockheed Martin Manned Space Systems, and MSFC has entered into a cooperative agreement under the NASA Aerospace Industry Technology Program to develop and demonstrate dual-use ceramic turbine wheel technology applicable to turbopumps, turbochargers, and turbogenerators for hybrid electric vehicles.

The primary goal of this project is to develop a reduced-cost ceramic component manufacturing process ready for commercialization. An additional thrust is the development and demonstration of ceramic turbine wheels in a turbopump application, which will benefit launch vehicles due to improved performance and reduced weight. See table 7 for other benefits.

Commercialization of ceramic turbine wheel technology for advanced turbomachinery applications requires significant reduction in production costs. The team will develop and demonstrate low-cost, high-yield ceramic manufacturing processes. The objective will be met by accomplishing three technology advances: (1) developing gelcasting as a low-cost, high-yield ceramic forming process; (2) developing brazing as a high-load capacity, low-cost ceramic-to-metal attachment; and (3) demonstrating ceramic turbine wheels in a cryogenic turbopump. Technical objectives are shown in table 8.

TABLE 7.—*Commercial and NASA benefits.*

Issue	Aspect	Benefit
Scientific and Technical Merit	• Turbopump With Ceramic Turbine Wheel • Production-Ready Gelcasting Technique • Viable Braze Attachment	• Reduced Weight, Increased Temperature • Commercially Viable Ceramic Components • Increased Torque Capacity
Commerical and NASA Applications	• Improved-Performance, Low-Weight Turbopumps • Turbochargers for Automotive and Off-Road • Turbogenerators for Hybrid Electric Vehicles	• Increased Payload Launchers • Domestic Production of Turbochargers • Improved-Performance Hybrid Electric Vehicles
Benefits	• Reduced Launch Costs	• Increased Launch System Affordability

The manufacturing process development will build on experience with gelcasting; the new ceramic-to-metal attachment will build on current brazing experience. The technology will be demonstrated by producing turbine wheels and testing them in an Aerospace Equipment Systems-developed cryogenic turbopump. Tests will be conducted using the turbopump and a NASA gas generator adapted for oxygen-rich operation, while also using steam-generating equipment being developed by Lockheed for hybrid rocket applications. Two turbine wheel configurations will be tested: an axial impulse turbine, applicable to turbopumps and turboalternators, and a radial turbine, applicable to turbochargers and turbogenerators for hybrid electric vehicles.

Aerospace Equipment Systems is designing the turbine wheels and components needed to adapt the turbine wheels to the existing turbopump, as MSFC designs the hardware required to adapt an existing thrust chamber for use as an oxygen-rich gas generator. These two team members will conduct tests of the turbopump jointly. Ceramic Components is developing the gelcasting technique, conducting material characterization tests, and will produce the turbine wheels. While Allied Signal Research and Technology will develop the ceramic-to-metal brazing technique and transfer this technology to Ceramic Components and Aerospace Equipment Systems, Lockheed Martin will provide hybrid rocket motor-based steam-generation equipment used to test the turbopump. without interlayer materials to

TABLE 8.—*Technical objectives.*

Objective	Approach	Benefit
Develop a Low-Cost, High-Yield Ceramic Forming Process	• Fabricate Axial and Radial Turbine Wheels	• Opens New Automotive Markets for Ceramic Components
Develop a High-Torque-Capacity Ceramic/Metal Attachment	• Braze Wheels to Metal Shafts	• Enables Application of Ceramic Turbines to Turbopumps
Build and Test Two Configurations of Ceramic Turbine Wheels	• Adapt Ceramic Wheels to Existing Turbopump • Test Turbopump With Steam Drive • Test Turbopump With Hot-Gas Drive	• Demonstates Potential for Improved-Performance, Reduced-Weight Turbopumps

The turbopump will undergo mechanical integrity verification tests, first with the steam generator in ambient conditions, and then tests under cryogenic conditions. Oxygen-rich, 1,000 °F gas will be used to drive the turbine while pumping liquid oxygen. The hot-gas/liquid-oxygen testing will demonstrate the ceramic turbine wheel/shaft attachment system capability with high thermal gradients, and will verify the capability of the ceramic turbine wheel material. Table 9 lists testing approaches and objectives.

Since the program kickoff on April 4, 1995, Aerospace Equipment Systems has completed conceptual design layouts of both axial and radial turbopump configurations and has begun detailed design and analysis. The radial turbine aerodynamic design is being performed in conjunction with an automotive turbogenerator program currently underway. Preliminary drawings of the turbine wheels have been released to allow Ceramic Components to fabricate tooling to be used for process development.

Ceramic Components has begun process optimization; work to date has focused on design of experiments for optimization of the binder burnout and densification phases of the gelcasting process. The company is reviewing past history of mold designs for gelcasting research programs for optimization under the Aerospace Industry Technology Program. Design and procurement of development molds have begun, and the company has planned a program to cast existing turbine wheel designs to evaluate dimensional control and repeatability.

Allied Signal Research and Technology has conducted a number of tests of brazed shaft attachments using a variety of sizes, materials, and geometric configurations. Full torque strength has been achieved in a full sizer joint using a simple geometry consisting of a Si_3N_4 (silicon nitride) stub shaft brazed into a Kovar cup. Braze materials and techniques have been refined, improving repeatability. Near-term work will consist of brazing to preferred turbopump shaft materials using butt joints, with and

TABLE 9.—*Test approaches and objectives.*

Test	Approach	Purpose and Results
Turbopump Reference Fluid Tests	• Full-Pressure Air Tests • Full Flow-Rate Water Tests • Testing at AES Facilities	• Verify Hydrodynamic Performance • Verify Mechanical Integrity
Hybrid/Steam Turbo-pump Drive System	• Steam Generator Drive System • Pump Tested in Water	• Verify Ceramic/Metal Brazed-Joint Torque Capacity • Verify Ceramic Compatibility With Temperature Levels
Hot-Gas Driven Cryogenic Tests	• Turbine Driven With Oxygen-Rich Hot Gas • Pump Tested in Lox • Testing at MSFC	• Verify Ceramic Turbopump Compatibility With High-Thermal Gradients • Demonstrate Ceramic Turbopump Under Simulated Engine Conditions

accommodate thermal-expansion mismatch.

Sponsor: Aerospace Industry Technology Program through Technology Investment Office

Industry Involvement: Allied Signal Aerospace Equipment Systems and Allied Signal Ceramic Components, Torrance, California; Allied Signal Research and Technology, Morristown, Nevada; Lockheed Martin Manned Space Systems, New Orleans, Louisiana

New Technology Targets Eye Disease

Robert J. Lessels/LA02
205–544–6539

A 1980 NASA Technology Utilization Grant to Dr. S. Hutson Hay, a Huntsville, Alabama, eye surgeon, has led to the development of a diagnostic system with potential to benefit physicians around the world.

Dr. Hay has established Kudi Kali, Inc., a new biomedical firm, which has received permission from the U.S. Food and Drug Administration to begin marketing an invention that could enable physicians to instantly diagnose many eye diseases and disorders. Known as a "digital retinoscopic photometer," it is the result of work that began with a NASA Technology Utilization Grant. MSFC, through its Technology Transfer Office, funded an experiment (May 13, 1980, to November 13, 1981) that attempted to detect amblyopia through the use of generated retinal reflexes. The results of that study, combined with technological innovations, medical discoveries, and his own insights during the past 15 years, have enabled Dr. Hay to develop the digital retinoscopic photometer.

The concept behind the tool is simple: an optical disease that distorts light passing from the outside, through the eye, to the retina—thereby impairing vision— equally degrades the reflected light going back in the other direction. A major problem arises in getting light to pass from inside the eye, out. Reflecting light off the retina accomplishes this. These reflected images can then be captured, digitized, and analyzed on a computer. Just as an animal's eyes reflect the light of automobile headlights at night, human eyes can be made to do the same thing.

Findings indicate that each eye disease seems to have a unique reflection "signature"—a signature that changes in a set pattern as the disease progresses. Many patterns and signatures can now be recognized and understood. Other patterns can be recognized, but not enough data have been collected for them to be understood yet. This understanding may come as more information is obtained through expanded use of the system as a diagnostic tool. As examples, myopia (nearsightedness) has a characteristic pattern that shows a bright crescent at the top of the pupil, hypermetropia (farsightedness) has a pattern with a bright spot at the bottom of the pupil, and patients with a form of myopic astigmatism characteristically have patterns with a flattened horizontal bright spot. Other disorders have equally distinct patterns.

At present, enough information has been compiled to permit Dr. Hay to determine the optical quality of the eye and the quality of binocular vision in children and adults. Of particular importance is the device's ability to evaluate the vision of children too young to speak, thereby enabling the physician to detect and treat conditions such as amblyopia and crossed eyes earlier in life.

Tests are absolutely painless, are totally objective, and require no response from patients other than keeping their eyes open. It is also safe,

noninvasive, fast, and inexpensive. As data are accumulated from clinical trials which began this fall, Dr. Hay expects the device could also enable him and other physicians to assess the size of cataracts and to monitor their growth. The information will also permit the physician to make a more informed assessment in determining the need for surgery.

The data base showing the reflected light patterns of different types of eye diseases at various stages of development is being compiled. As use of the new system expands, additional data will be accumulated and the computer will "learn" to associate distinct patterns with individual diseases and disorders. With a large enough data base, Dr. Hay says it should be possible to have a computerized instrument able to provide highly accurate diagnoses that electronically assess different stages of a disease's development.

Benefiting physicians around the world, the data base could enable a doctor examining a patient in India or Africa to transmit the digitized image of the patient's eyes to Huntsville via satellite. Trained personnel at Kudi Kali, Inc., could immediately enter the digitized image into the computer and have the computer compare the image against the known patterns for various disorders and diseases. The computer would then provide a diagnosis—along with a probability rating of its accuracy—in seconds. This data could then be transmitted via satellite back to the physician requesting assistance.

The prototype is about the size of a personal computer and fits easily into a small examining room. Institutions such as the Smith Kettlewell Eye Research Institute in San Francisco, California, and NASA's MSFC have been instrumental in its development. The assistance of several individuals has proven invaluable, including: Austin Jennings, president of the International Lions Club; Dr. Philip Reiner of AIMM, Inc., in Huntsville; doctors Chen Feng and Anees Ahmad of the Center for Applied Optics at the University of Alabama in Huntsville; Dr. Jean-Andre DeGroot in Montreal, Canada; and Richard Bryant at Vanderbilt University Medical School in Nashville, Tennessee.

Dr. Hay welcomes having his system tested by independent scientific investigators. Their corroboration will lead to further improvements and a more precise definition of the disease states that can be evaluated.

Sponsor: Office of Space Access and Technology

Industry Involvement: Kudi Kali, Inc.; Smith Kittlewell Eye Research Institute, San Francisco, California

Space-Age Training Program Technologies Offered to Commercial Industries

Robert J. Lessels/LA02
205–544–6539

Teledyne Brown Engineering, in cooperation with NASA, has developed a new tool to train astronauts, ground controllers, and principal investigators on scientific experiment operations for SpaceLab missions. "Interactive Multimedia Training" is finding applications with private industries seeking to train new employees and certify the job skills of experienced workers.

At present, SpaceLab training programs use manuals, briefings, high-fidelity simulators, and flight simulations. Trainees must travel to a training site where they learn to operate in-flight experiments aboard the space shuttle. Personnel who will remain on the ground in support of those in space are also trained in this manner. A typical training program requires an average of 2 years to prepare and conduct, and commands the participation of instructors and trainees located around the world.

In view of accelerated launch schedules, increasing demands, reduced training time, budget reductions, and the rising costs of traveling to training sites, NASA and Teledyne Brown Engineering have been seeking a better way to train space operations teams. Interactive Multimedia Training provides one such solution by merging the best communication techniques and technologies in one

powerful, complete package. It reaches each trainee with the same information every time and allows trainees to set the pace at which the information is presented. Students use a computer mouse or enter appropriate keyboard commands as they proceed through the training program. Students may repeat various portions of the training program as many times as necessary to gain a complete understanding. When the course is completed, students are provided with immediate feedback to evaluate their performance.

Interactive Multimedia Training stimulates the senses with color, motion, sound, and touch to increase comprehension and maximize the effectiveness of available learning time. The course content is easily customized and updated on compact disk/read-only memory disks. The updated materials can then be sent to trainees who may proceed through the new material at their convenience.

Teledyne Brown developed its pathfinder course to train NASA personnel who were involved in operating the crystal-growth furnace to be flown on the second United States Microgravity Laboratory SpaceLab mission. The new approach trained operations personnel in how to operate the furnace's hardware/software systems and science and operations procedures. It also reviewed "lessons learned" from previous missions. This effort has been a successful "proof of concept" in establishing the value of Interactive Multimedia Training as an effective, efficient training tool.

After Teledyne Brown developed this new training concept, the firm became aware of a need existing in the commercial market for quality training on specialized systems at a reasonable price. The company combined its expertise in training with its ability to package interactive multimedia courses, enabling it to offer industry a method of qualifying and certifying new employees and recertifying experienced workers.

A major Huntsville manufacturer requested that Teledyne Brown develop an interactive training program for its own employees. Training courses were developed to teach newly hired workers the proper method of performing their jobs, emphasizing the proper use of safety equipment, and explaining how a worker's job is integrated into the overall production of the product and operation of the industry. In addition, the manufacturer has been provided with a means of testing new workers to ensure they are qualified to operate expensive equipment and are aware of proper safety precautions to prevent injury to themselves and damage to equipment. Employees are also shown various types of problems encountered in manufacturing the product and the proper way of correcting them.

The finished program benefits the company's employees by providing them with a means of improving their skills, thereby enhancing their opportunities for promotion and higher wages. Additionally, managers have found the program offers a new way of upgrading veteran employees' skills as new equipment is introduced or improved manufacturing methods are introduced.

Local employers who have implemented the training program are finding that fully trained and certified workers ensure a maximum flow of quality products without bottlenecks. Better quality controls reduce the number of rejected parts. Both factors contribute to increased production and lower costs.

Sponsor: Office of Commercial Development and Technology Transfer

Industry Involvement: Teledyne Brown Engineering

NASA Welding Technology Transfer to Private Industry

Robert J. Lessels/LA02
205–544–6539

The transfer of NASA- and NASA contractor-derived welding technology (fig. 117) by MSFC is benefiting three firms in the Southeast:

- Headquartered in Louisiana, Frymaster Corporation, the world's largest manufacturer of commercial deep-fat fryers, is using remote weld-bead seam-tracking technology originally developed for use on the external fuel tank of the space shuttle. The technology was developed for NASA at the Michoud Assembly Facility by Martin Marietta, the plant's contractor operator.

- The robotic weld-bead seam-tracker sensor technology has also been used at a major Alabama manufacturer of air conditioners. The technology proved successful when applied to girth-welding operations on air-conditioner compressors. During the first day of operation, 320 compressors were manufactured with only two incidents being reported—both of which were attributable to operator inexperience with the system.

- Memphis Drum Service, Inc., in Tennessee has studied using the robotic weld-bead seam-tracker sensor technology in recycling 55-gallon drums. The company had been having a problem with intense heat (required for cleaning and sterilization of the drums) destroying the rubber seals between the inside of the drum lid and the outside flanges, which caused drums to leak when filled with certain liquids. The options of using another recycled type of lid-flange configuration or purchasing a new lid were both expensive. MSFC identified a method of restoring the seal through robotic welding system technology.

Sponsor: Office of Commercial Development and Technology Transfer

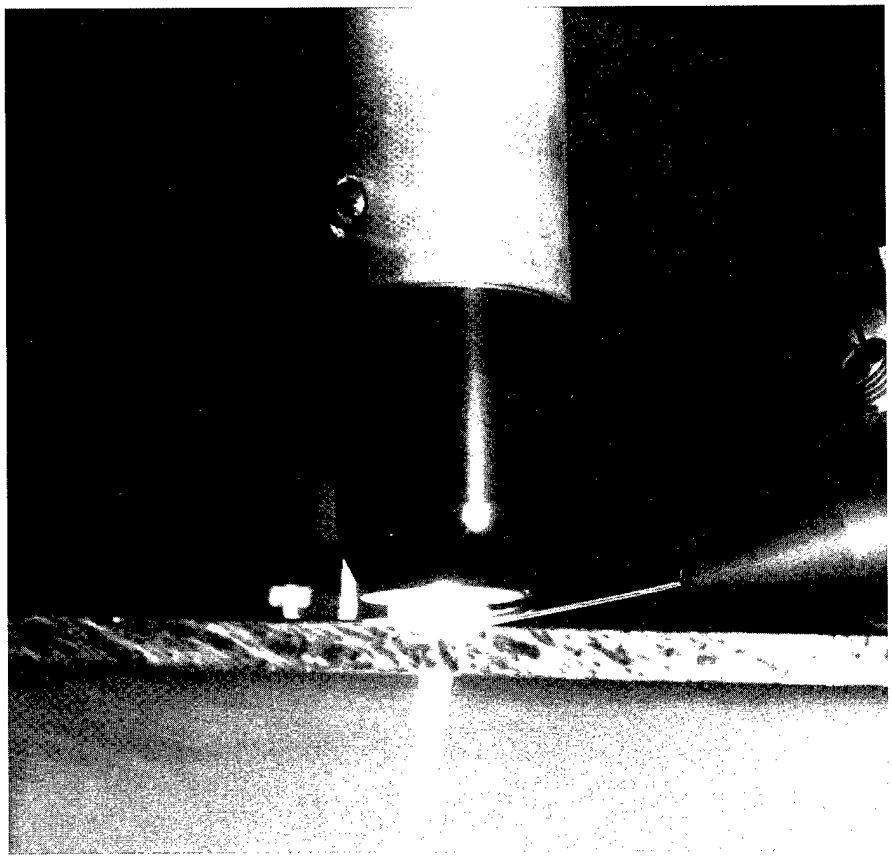

FIGURE 117.—Vertical welding tool of the Productivity Enhancement Complex.

Industry Involvement: Frymaster Corporation, Louisiana; Memphis Drum Service, Inc., Memphis, Tennessee; Martin Marietta

Waterjet-Stripping Technology

Robert J. Lessels/LA02
205–544–6539

Work completed by MSFC to improve waterjet-stripping technology is paying dividends to the aviation and shipyard industries.

Initially, MSFC developed hand-held waterjets to remove thermal ablative coatings from the solid rocket motors used to launch the space shuttles. While effective, the work was tiring. Robotics seemed to offer a viable alternative. The practicality of robotic waterjet-stripping systems was proven at MSFC's Productivity Enhancement Complex. The first fully automated system went into service at Kennedy Space Center in 1985.

The technology breakthrough led to the establishment of Pratt & Whitney Waterjet Systems. Today, four major airlines use the technology to clean aircraft engines, using 55,000 pounds per square inch of pressure to quickly remove gaskets, seals, abradable rub-strips, and metal- and plasma-sprayed coatings from engine parts. These parts range from shafts 6 inches in diameter to fan-engine inlet casings 120 inches in diameter. Most airlines expect the system to pay for itself in the first year of operation.

Work is ongoing to enhance the system and expand its potential applications. The U.S. Air Force is studying the possibility of using it to remove paint from combat aircraft as they undergo regular refurbishment. The U.S. Navy and other maritime interests are examining the potential of using the high-pressure streams of water to remove barnacles and other encrustations from the hulls of ships, which could result in better fuel economy and better operational performance.

The system poses no ecological concerns. A means has been devised to capture all material removed by the jets for proper disposal, and the water itself is cleaned and recycled within the system. Only filtered, pure water is ever returned to the environment. Reference figure 118.

Sponsor: Office of Commercial Development and Technology Transfer

Industry Involvement: Pratt & Whitney Waterjet Systems, Huntsville, Alabama

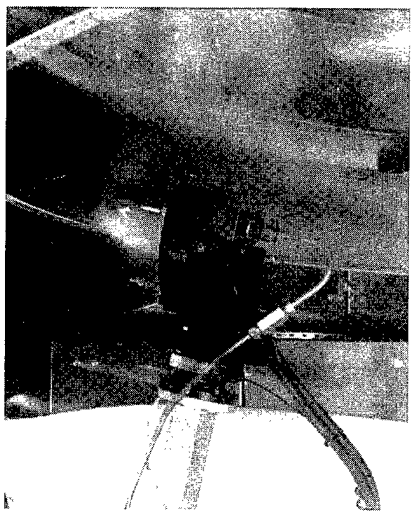

FIGURE 118.—Waterjet stripping.

Rapid Prototyping

Robert J. Lessels/LA02
205–544–6539

Rapid prototyping, in its most general form, involves the direct production of a prototype in three dimensions from a computer-aided drawing. MSFC is directed at integrating rapid-prototyping technologies with current manufacturing practices and developing rapid-prototyping processes to manufacture complex materials needed in future NASA programs. Growing in its ability to cut the design-to-product development cycle, the process enables manufacturers to shorten prototype development costs by orders of magnitude. As an example, MSFC is producing wind-tunnel models for $400 that once would have cost $40,000.

The net-shape master and mold-complex geometry-fabrication technologies employed by rapid prototyping are reaching into the production environment, reducing costs, improving reliability, and providing additional—or exclusive—fabrication routes for the introduction of complex, lightweight materials into future products. These products will include the next generation of space vehicles, such as the X–33 and X–34, and will also include various "down-to-Earth" products that will simply benefit from being lighter, yet stronger.

At present, MSFC's Rapid Prototyping Center uses a variety of machinery to complete its tasks: a fused deposition modeler, used to make investment master castings, particularly of wind-

tunnel models; a Sanders three-dimensional printer to produce high-detail, high-surface-finished investment master castings; and a stereolithography device that produces wind-tunnel models and other visual aids. A fourth device, a ballistic particle machine to be used in rapidly making inexpensive concept models, is coming on-line.

Traditionally, prototypes cost many thousands of dollars, and it is only by commercially marketing a design that costs can be recovered by industry. Cutting the costs of prototype fabrication by a factor of 10 or 100 will result in enormous savings in product development and may encourage firms to explore alternative, potentially better designs. Extrapolating this to the consumer, the price paid for a new or improved product may be substantially lower since the manufacturer does not have to recoup high research and development costs. A number of major firms in the United States are experimenting with various aspects of rapid prototyping, and MSFC is poised to assist the small-business person in deciding on how to invest in the technology.

Sponsor: Office of Commercial Development and Technology Transfer

Composites Technologies

Robert J. Lessels/LA02
205–544–6539

Manmade composite materials technologies offer significant advantages over metals when applied to structural programs and to programs where thermal problems are anticipated. Ongoing efforts at MSFC to develop composite materials and technologies for use in the DC–X/X–33/X–34 space shuttle follow-on vehicle program should pay a number of dividends for American industries.

Various composite materials have different properties that can be tailored to suit the needs of the user. For structural applications where high strength and stiffness are most desirable, carbon or graphite fibers are combined with resins to achieve the desired results with the least weight. This, however, is the most costly approach. In situations where damage resistance is paramount and weight is not a major concern, Kevlar may be substituted for carbon or graphite. The most economical material is fiberglass, but it normally has the lowest strength-to-weight ratio. Being silica-based, fiberglass works very well for thermal extremes, as the substance has a low coefficient of expansion. Regardless of the type of fiber selected, each would be combined with an epoxy or polyester resin to hold the fibers in place. A number of advanced resins have been developed for use in high-heat/cryogenic applications.

Scientists have already used composites to fabricate cryogenic fuel-pressure vessels for the Reusable Launch Vehicle program. Some of the technologies employed for this effort may soon show up in the family automobile, as attention is given to using liquefied natural gas as a low-emission fuel. Being extremely cold in its liquid state, liquefied natural gas will require an insulated, pressurized fuel tank. Insulation will probably be similar to the spray-on foam insulation now in use on the space shuttle's external fuel tank. Some work—with Thiokol Corporation, through MSFC's Technology Transfer Office—has already been completed for developing a cryogenic fuel tank for use on a minivan. Scientists are also looking at composites for use in Chrysler Corporation's proposed Patriot II Formula One racing car (which is also expected to use liquefied natural gas as a fuel contained in an insulated pressurized tank made of composite materials).

MSFC's efforts in developing composites technologies involve a number of specialized machines:

- A filament-winding machine lays down resin/fiber-composite ribbons that are built up layer by layer until a desired thickness and degree of strength is achieved. Computer directed, the device is used to make pressure vessels and similar items which have symmetrical shapes. As with many metal-working machine tools, the filament-winding machine was designed to do one job, but has been adapted to perform others.
- A pultrusion machine is similar to an extrusion machine. (Pultrusion technologies lend themselves to

making long, continuous geometry tubes. Unlike metals, resin fibers cannot be pushed through a machine. It is like trying to push a rope. A strand of epoxy-impregnated resin must be pulled through the die to shape it.) A pultrusion machine is a continuously operating machine in that, once set up, it can be run for long periods of time. Pultrusion techniques have a number of structural applications; all types of fibers—carbon/graphite, Kevlar, or fiberglass—can be used, depending on the desired physical properties of the finished composite item.

- A tape-laying machine enables engineers to fabricate very large, somewhat contoured structures with asymmetrical geometries.
- A fiber-placement machine—employing a very sophisticated, computer-controlled robotic system—is the first of its kind ever built. MSFC and Cincinnati Milacron Corporation shared development costs of the device, which was initially used to make inlet ducts for the XF–22 jet-fighter prototypes. MSFC has been a leader in testing its potential applications in manufacturing composite parts with extremely complex geometries. Resin/fiber tapes can be deposited in patterns that can be narrowed or expanded.
- A tape-wrapping machine was designed to build nozzles for solid rocket motors used on the space shuttle, and it has been adapted to make nozzles for engines that burn hybrid (solid-propellant/liquid-oxydizer) fuels and liquid fuels.

Commercial applications of composites technologies include the development of obstetrical forceps to enable physicians to position fetuses in the womb more safely in instrument-assisted deliveries. Gauges on the instrument will enable the physician to avoid placing too much pressure or stress on the infant. Also, several MSFC materials engineers have recently worked on the development of a racing wheelchair design made of composites that is now being manufactured commercially.

Sponsor: Office of Commercial Development and Technology Transfer

Industry Involvement: Thiokol Corporation, Chrysler Corporation, Cincinnati Milacron Corporation

Composite Piping For Offshore Oil and Gas Industry

Robert J. Lessels/LA02
205–544–6539

MSFC is slated to work with the Department of Mechanical Engineering at Louisiana State University to assist Specialty Plastics, Inc., of Baton Rouge, Louisiana, in developing innovative joining and fitting technologies for advanced composite piping systems for the offshore oil and gas industry in Louisiana. The U.S. Department of Commerce's National Institute of Standards and Technology has announced the awarding of a $1.8 million advanced technology program grant to the Louisiana firm to help finance research in this "high-risk" area of technology. (The grant makes possible the undertaking of research and development projects that otherwise would not be pursued—or to which sufficient resources would not be dedicated—because of the financial and/or technical risks involved in pursuing such leading-edge technologies.) This particular effort will seek to develop high-performance composite materials (e.g., combining polymers with glass or carbon fibers) to achieve such enhanced physical properties as strength and durability.

Regarding the offshore oil and gas industry, the cost of manufacturing and erecting offshore production platforms could be reduced significantly if even a portion of the heavy metal pipelines could be replaced with lighter-weight pipeline systems made of composite materials.

By reducing the topside weight of offshore oil and gas rigs (known as tension-leg platforms in the industry) that are required to access deep-water reserves in the Gulf of Mexico, an estimated $250,000 could be saved per meter of water depth—about $150 million per offshore platform. The composite pipe could be used for fire-water piping, sea-water cooling, and drainage systems and sewerage, if the design team can adequately develop methods of joining pipe segments and manufacturing low-cost, high-strength pipe fittings. Accessing deep-water oil resources in the Gulf of Mexico could help reduce excessive U.S. dependence ($1 billion per week) on foreign oil.

Making advanced composite piping economically feasible could benefit other industries as well. About $20 billion is spent annually by the petrochemical, pulp and paper, and marine industries in combating the corrosion of pipes made with present-day materials.

This project has an estimated completion date of September 1998.

Sponsor: Office of Commercial Development and Technology Transfer

University Involvement: Louisiana State University

Industry Involvement: Specialty Plastics, Inc., Baton Rouge, Louisiana

■■■■■

NASA Assistance to the Physically Challenged

Robert J. Lessels/LA02
205–544–6539

MSFC has a long history of helping physically challenged individuals overcoming limitations imposed by their handicaps and enjoying an enhanced quality of life.

One such success story began with the Technology Transfer Office's participation in an exhibit sponsored by the Alabama Department of Education's Division of Rehabilitative Services. Subsequently, a request for assistance was referred to MSFC's Technology Applications Board for the design of a specially designed water ski for use by wheelchair-confined persons. Specifications dictated a seat that would provide a softer ride and that would not sway to the side.

Engineer Bruce Weddendorf of the Structures and Dynamics Laboratory's Special Projects Design Branch led the design effort, which culminated in a modified framework for a seat with a special shock absorber to eliminate side sway. The seat mounts to a water ski on four tracks, along which the seat can be moved to suit the preferences of the skier.

Steven Hamilton recently used the preliminary seat design to win the U.S. national competition in his division (fig. 119). He then took an upgraded water-ski seat to Australia, where he won the world water-skiing championship in his class.

Sponsor: Office of Commercial Development and Technology Transfer

■■■■■

FIGURE 119.—MSFC-designed water ski for the physically challenged.

Marine Jet-Propulsion Technology

Robert J. Lessels/LA02
205–544–6539

MSFC is NASA's leader for the development and management of the space shuttle's propulsion elements, has developed the Saturn series of rockets that took man to the Moon, and is managing the development of propulsion systems for the next generation of space vehicles being developed by NASA. Arkansas-based North American Marine Jet, Inc., has tapped into this vast reservoir of experience in hopes of repositioning the company's global marketplace. At present, the ship jet-propulsion engine market is dominated by manufacturers in Europe and New Zealand. However, NASA technology may help U.S. firms compete more successfully, and marine jet-propulsion technology may also find its way into U.S. Navy propulsion systems later this year.

When company president Leonard Hill and his design staff from North American Marine Jet first met with Robert Garcia of the Computational Fluid Dynamics Branch of MSFC's Structures and Dynamics Laboratory, Garcia used the branch's analytical systems to reveal that the Arkansas firm's proposed design for an improved impeller would not meet desired performance requirements. Garcia, Hill, and the firm's design team then discussed possible design modifications, which Garcia then analyzed. His calculations correctly predicted a new design would meet or exceed all requirements, resulting in an overall improved design and the creation of a new product line for the firm.

Garcia's three-dimensional computer model of the impeller design enabled Paul Gill of MSFC's Materials and Processes Laboratory and NASA contractor engineers at Rocketdyne to use rapid-prototyping systems to make a solid polycarbonate model, allowing the engineers to optimize the improved impeller's production process. Ordinarily, the firm would have had to produce a wooden "master" of the impeller blade, make an epoxy mold and then wax impeller blades from the epoxy mold, machine an impeller hub, precisely attach four

FIGURE 120.—A new MSFC-designed impeller.

FIGURE 121.—Jet-propulsion technology in action.

sets of impeller blades to the hub, dip the wax model to form a ceramic mold, melt out the wax, and, finally, pour metal into the ceramic mold. Gill's work allowed the mold to be made directly, avoiding many time-consuming and costly steps. Reference figures 120 and 121.

Sponsor: Office of Commercial Development and Technology Transfer

Industry Involvement: North American Marine Jet, Inc.; Rocketdyne Division of Rockwell International

■■■■■

Portable Lifting Seat

Robert J. Lessels/LA02
205–544–6539

Licensing to manufacture a portable lifting seat developed and patented by MSFC in Huntsville, Alabama, is underway. For individuals with degenerative knee or hip-joint diseases or injuries, the easily carried device offers a new degree of freedom, including the ability to attend movies and go out to dinner, among other things.

Using funds provided by the Technology Utilization Office, a team of engineers from MSFC's Structures and Dynamics Laboratory—with medical guidance from an orthopedic surgeon from Southern Hills Medical Center in Nashville, Tennessee—developed a lightweight, battery-powered lifting device capable of assisting individuals weighing up to 300 pounds with severe degenerative conditions in their knees, hips, and/or backs with sitting down or standing up. At the time work began on the effort in 1991, an estimated 8 million individuals could benefit from the seat.

The device consists of a battery-powered motor that drives a gear train and crank assembly. The gears and crank lift up and push forward simultaneously, ensuring the padded seat remains at a proper angle to maintain contact with the individual being assisted. A three-position switch enables the user to raise, lower, or stop the seat. A carrying handle completes the device.

Nurses and orderlies in hospitals and nursing homes could find the seat useful in protecting themselves from back strain incurred when lifting patients and in assisting them in sitting down. The seat carries the weight of the patient, as the nurse or orderly safely guides and steadies the patient.

Sponsor: Office of Commercial Development and Technology Transfer

Industry Involvement: Southern Hills Medical Center, Nashville, Tennessee

Ocular Screening System

Robert J. Lessels/LA02
205–544–6539

An ocular screening system developed at MSFC is helping to detect vision abnormalities and diseases—some of which can lead to blindness if left untreated—in children as young as 6 months of age. The technology, developed by the late John Richardson, formerly the biomedical applications manager for the Technology Transfer Office, and Joseph H. Kerr, an engineer in the Space Systems Chief Engineer's Office, involves simply photographing the children's eyes and analyzing the patterns of light reflected from them. As different eye abnormalities and diseases cause the eyes to reflect light in different ways, each abnormality has a reflection "signature," thus permitting immediate diagnosis of a problem.

In a statewide test of more than 170,000 Alabama elementary school students in kindergarten through second grade, more than 10 percent were found to have eye diseases or defects requiring medical attention (fig. 122). The difficulties ranged from simple nearsightedness and farsightedness to much more serious diseases that required immediate treatment if the children's vision were to be saved. The tests were conducted under license by the Birmingham, Alabama-based, Vision Research Corporation. Funding for the testing was provided by the State of Alabama ($600,000), the Russell Corporation ($100,000), and the Alabama Power Company ($100,000)—approximately $4.70 per child.

FIGURE 122.—A student being tested using the ocular-screening system.

The results of the 1994–95 school year Alabama testing have impressed the education commissioners in 24 other states, which are now following Alabama's example and scheduling testing of their own school children. Since vision abnormalities can affect a child's performance and self-esteem in school, educators hope students whose eye defects are detected and corrected as a result of the test will earn better grades, improve his or her comprehension of subject material, and enjoy a better quality of life—both while in school and after graduation.

Sponsor: Office of Commercial Development and Technology Transfer

Industry Involvement: Russell Corporation, Alabama Power Company

Other Involvement: State of Alabama

Hybrid Rocket Motor Technology

Robert J. Lessels/LA02
205–544–6539

MSFC is preparing to test a new rocket motor that will combine the safety features of a liquid-propulsion system with the cost savings of a solid-propulsion system to achieve a full-scale, 250,000-pound-thrust hybrid rocket motor. It will be designed, fabricated, and tested under a multipartner effort called the Hybrid Propulsion Demonstration Program. Developmental testing will be performed at MSFC's test stand 500 beginning in December 1996.

The goal of the program is to demonstrate critical hybrid-propulsion technologies and enable manufacturing of large hybrid boosters for current and future space launch vehicles. Preliminary concepts show promise for application on both the X–33 Advanced Technology Demonstrator and the Atlas launch vehicle. The hybrid motors can be used independently, such as for sounding rockets, or for thrust augmentation on an expendable or reusable launch vehicle.

Safety, the most critical factor for any propulsion system, is the key feature of the hybrid rocket motor: hybrid motors employ an inert solid fuel and a liquid oxidizer which are physically separated until ignition. The motor throttle can be controlled to enable on-pad checkout, thrust tailoring, and abort options.

MSFC's role will include providing test facilities, test operations support, and test analysis. Modifications to test stand 500 are being made to accommodate motor development, including expansions in the feed, ignition, pressurization, and purge systems.

The Hybrid Propulsion Demonstration Program is an excellent example of partnership between government and industry participants working together to enhance and mature technologies for future applications. The effort combines the resources and funding of NASA; the Advanced Research Project Agency in Washington, D.C.; Phillips Laboratory at Edwards Air-Force Base, California; and members of an industry consortium that includes Lockheed Martin, Thiokol Corporation, United Technologies, the Rocketdyne Division of Rockwell International, Allied Signal, and Environmental Aerosciences.

Sponsor: Office of Commercial Development and Technology Transfer

Industry Involvement: Lockheed Martin, Thiokol Corporation, United Technologies, the Rocketdyne Division of Rockwell International, Allied Signal, Environmental Aerosciences

Other Government Involvement: Advanced Research Project Agency, Washington, D.C.; Phillips Laboratory, Edwards Air Force Base, California

■■■■■

Quick-Connect Nut and Bolt

Robert J. Lessels/LA02
205–544–6539

An engineer in MSFC's Structures and Dynamics Laboratory has invented a quick-connect, slow-disconnect nut and bolt. Used in the same manner as regular fasteners, the quick-connect nut and bolt are of special benefit in situations where connections must be made quickly.

The bolt has circumferential shells designed to constitute a standard external thread. Clips and springs hold the shells against the conical surface of the shank. When the bolt is pushed into a threaded hole, the bolt's threads are engaged within the nut, and the bolt is positively retained in the hole. Pulling the bolt only seats the shells more firmly into the thread. Reference figures 123 and 124.

Possible use scenarios include making emergency repairs to damaged vessels, reinforcing damaged structures, and working in hazardous environments in which a maximum amount of work must be performed in a very limited time (such as in the vacuum of space).

Licensing information on this patented fastening system is available by writing: Patent Counsel, Mail Code CC01, MSFC, AL, 35812, or by calling 205–544–0021.

Sponsor: Office of Commercial Development and Technology Transfer

■■■■■

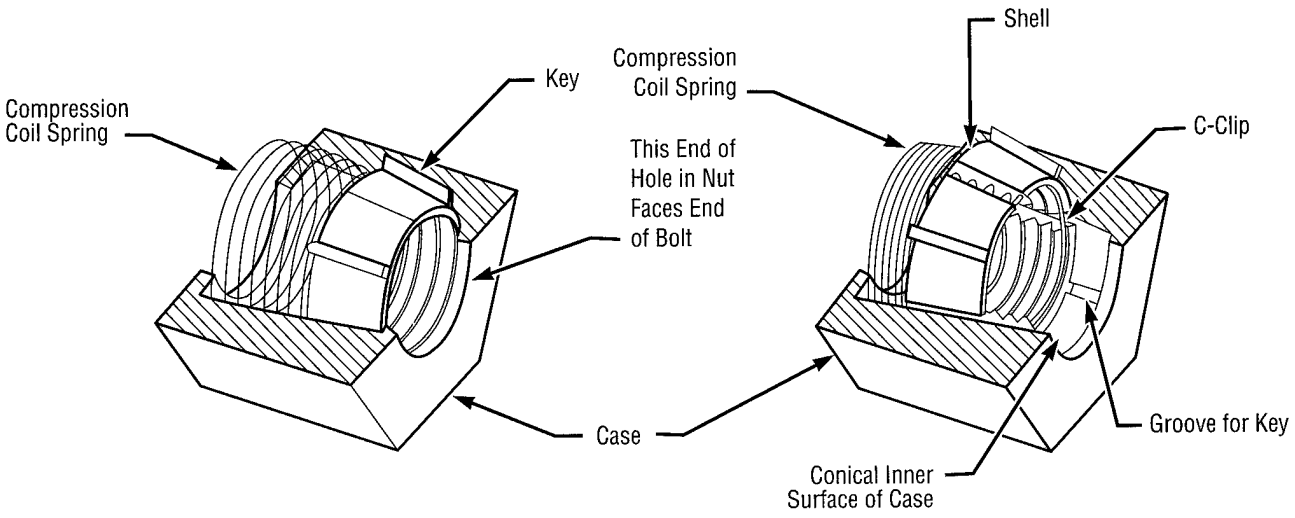

FIGURE 123.—Left, shells shown in normal position; right, shells shown pushed axially against coil spring.

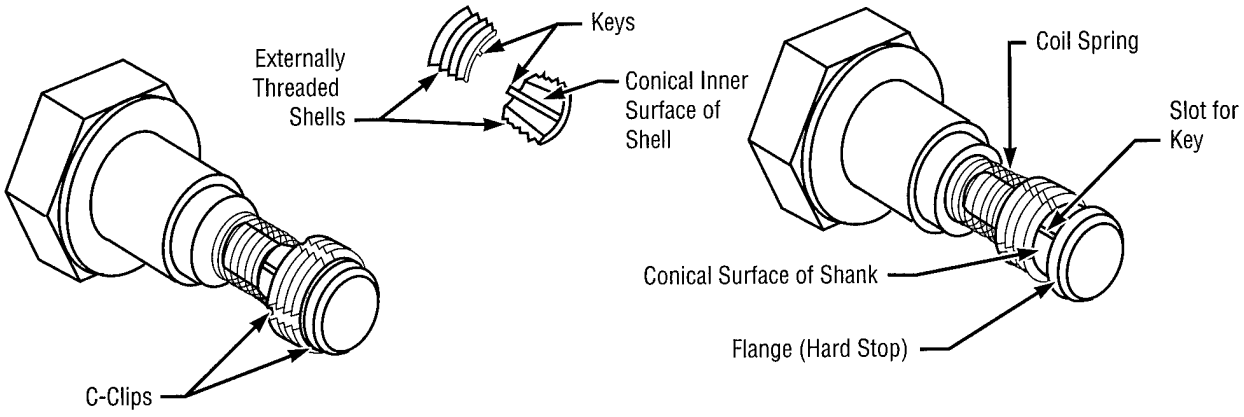

FIGURE 124.—Left, threads in normal position, as when standing freely or during engagement in thread hole; right, threads pushed back, as during insertion into threaded hole.

Improvements for Firefighters

Robert J. Lessels/LA02
205–544–6539

A Memorandum of Understanding has opened the door for NASA, led by MSFC and in collaboration with other NASA centers, to work with the Chicago Fire Department in applying NASA technologies to improve fire fighting and other emergency services.

Chicago Mayor Richard M. Dailey and Fire Commissioner Raymond E. Orosco met with NASA Administrator Daniel Goldin and the director of MSFC on April 19, 1995, in Chicago to sign a Space Act Agreement. They also began discussing various technologies that could be transferred to the department to enhance fire and other emergency services.

" The Chicago Fire Department is a strong innovator in testing, developing and adopting new methodologies and technologies," said Goldin. "NASA is looking forward to working with them to explore ways space technology can be used to enchance emergency services. Ultimately, it will be the American people who benefit from what we accomplish here." A number of candidate activities have already been identified for joint study, including:

- Development of a personnel locator system that will enable on-scene authorities to locate, track, and—if necessary—rescue firefighters within a 2,400-square-foot area of operations
- Possible modification of MSFC's dynamic structural analysis techniques to determine if a structure is in imminent danger of collapsing
- Development of a new, portable air-breathing apparatus for use by firefighters that would incorporate NASA's knowledge of liquid-oxygen technology
- Development of an emergency vehicle alerting system to warn hearing-impaired drivers (or those in a high-noise environment) of an approaching emergency vehicle.

The MSFC's Technology Transfer Office is responsible for the direct transfer of NASA-inspired ideas and solutions to businesses throughout the Southeast. The office also interacts with companies and government organizations around the country, providing assistance for a variety of technology challenges.

Sponsor: Office of Commercial Development and Technology Transfer

Other Involvement: Chicago Fire Department, Chicago, Illinois

MSFC Propulsion Center of Excellence is Built on Solid Foundation

MSFC's propulsion expertise continued in 1995, as the launch of STS–70 in 1995 marked the first flight of an upgraded version of the space shuttle main engine. Managed by MSFC, the new Block 1 engine featured such improvements as a new liquid-oxidizer turbopump built by Pratt & Whitney. Many of the turbopump parts were produced through a casting process designed to eliminate all but six of the more than 300 welds that had existed in the previously used turbopump. "The engine performed just as expected," said Otto Goetz, deputy manager of the Space Shuttle Main Engine Project.[1]

The successful flight of the new engine was in keeping with MSFC's historic role as NASA's primary propulsion development center. 1995 marked MSFC's 35th anniversary, but the roots of its propulsion expertise run to the latter half of the 1940's and to the New Mexico desert. There, members of a German V–2 rocket team, originally assembled by Wernher von Braun in Germany, reassembled to work on missile and rocket developments under contract to the U.S. Army. In 1950, the Army transferred the Von Braun team to Huntsville and expanded its membership. Throughout the 1950's, engineers and scientists on Redstone Arsenal made new strides in rocket and missile development for the Army. On September 8, 1960, President Eisenhower came to Huntsville to dedicate the new George C. Marshall Space Flight Center, where hundreds of those same engineers and scientists who had worked for the Army formed the nucleus of the new NASA center.

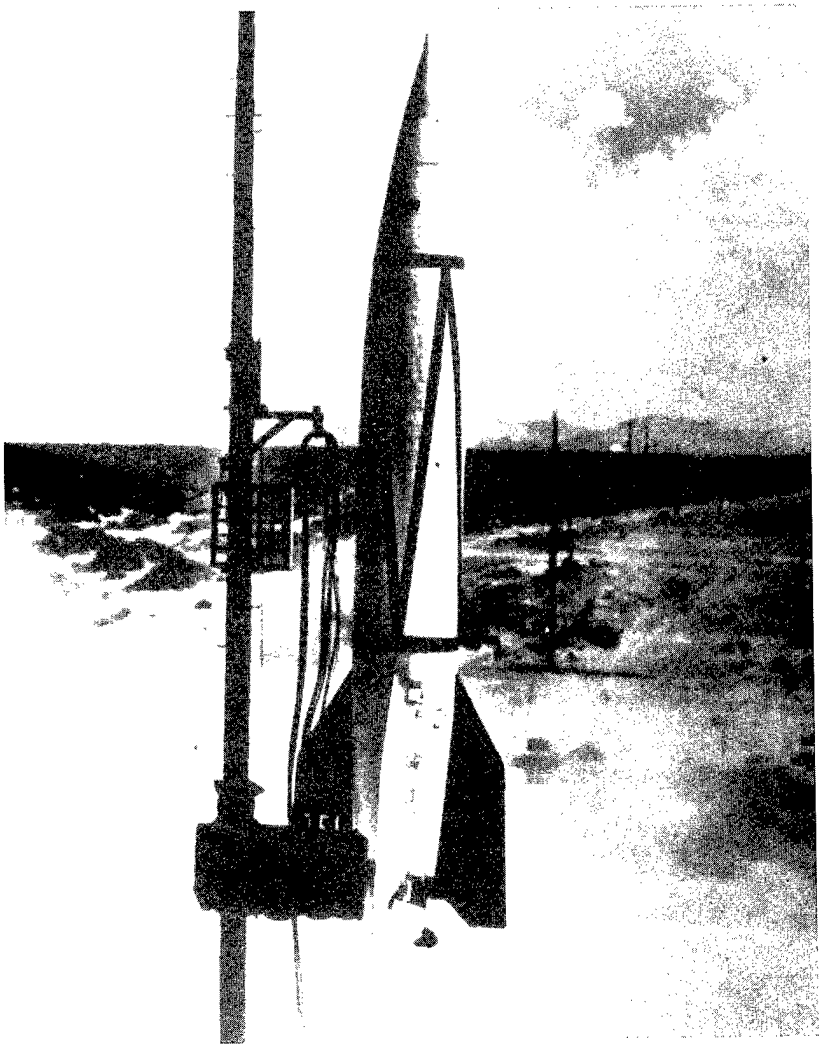

Launch of V–2 rocket.

■ The V–2 Rocket Motor

The V–2 rocket motor has been called "the immediate ancestor of many of the American rockets to follow."[2] The 46-foot V–2 rocket could carry a 1,650-pound warhead 225 miles. During World War II, an estimated 1,115 V–2 rockets were successfully fired against England and 1,675 against continental targets.[3] After World War II, more than 100 V–2 missiles were launched at White Sands, where they provided invaluable data in the beginning of America's missile program.

The engine for the V–2 used a 5,000-revolutions-per-minute turbine to develop 504 kilowatts (675 horsepower). The rocket produced a thrust of 59,500 pounds at sea level and 70,000 pounds at altitudes above 25 miles. According to rocket and space historian Willy Ley, the fuel for the V–2 "was ordinary ethyl alcohol—in this case made from potatoes—to which enough water had been added to bring its strength down to 75 percent by volume." Liquid oxygen was used as the oxidizer. For the first time a turbopump was incorporated,

powered by an 80-percent hydrogen-peroxide steam generator.[4] In the late 1940's and throughout the 1950's, V–2 rocket motor technology directly influenced plans for the development of missiles and rockets in the United States.

■ Engine Proposals for Hermes C

After World War II, American rocket experts at White Sands were anxious to exploit German V–2 rocket motor technology. For example, they initiated the Hermes program, actually a conglomeration of different projects and proposals. For a while, engineers proposed building a three-stage Hermes C rocket using six rocket motors in clusters of two in its first stage. These motors would be designed to develop a total of 600,000 pounds of thrust during a burning time of 1 minute. After jettisoning the first stage, the second-stage motors would provide an additional 100,000 pounds of thrust during a 1-minute burning time. A winged third stage would have given Hermes C a range of about 2,000 miles. Hermes C, and an even smaller version known as Hermes C–2, turned out to be too ambitious, and the project was scaled back.[5] Nevertheless, Hermes research conducted by General Electric contributed to the advancing state of the art in rocket motor design, especially for the Redstone. "The Hermes C–1 study was handed to our team, and the design and development of the new rocket with a 500-mile range was given a very high priority by the Chief of Ordnance in the fall of 1950," Von Braun said.[6]

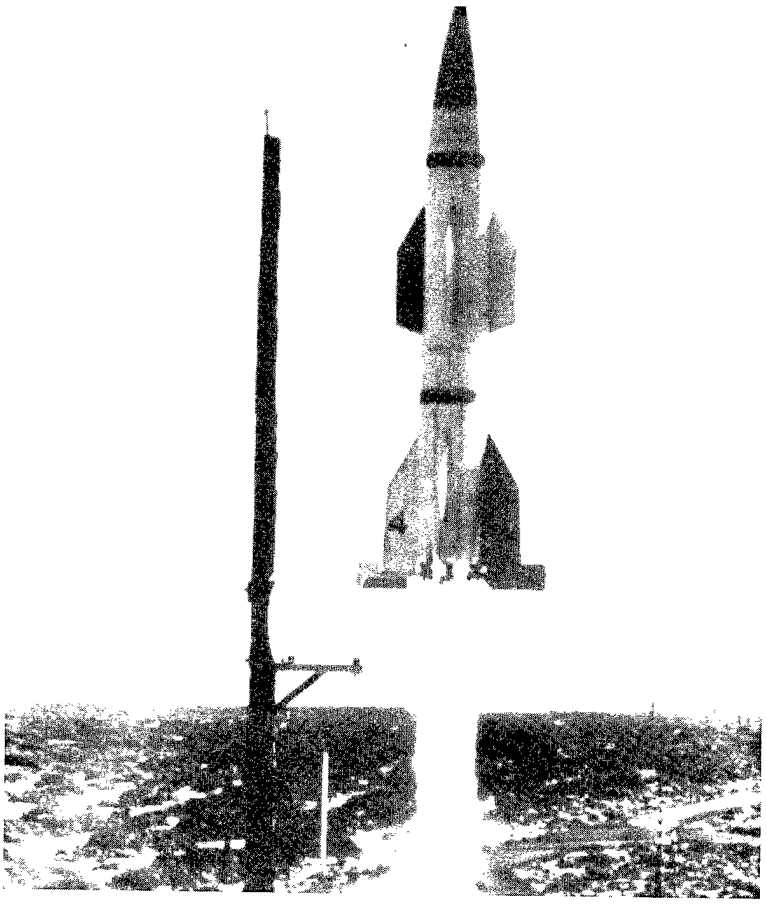

Hermes A–1 launch.

■ Navaho Booster Engines

The development of the propulsion system for Redstone was also directly linked to an Air Force project, i.e., Navaho, which had roots in the V–2 engine. Before the Air Force became convinced that ballistic missiles represented the most effective approach to unmanned strategic long-range weapons, it developed early air-breathing cruise missiles. Even though it used a ramjet engine for sustained flight to the target, the Navaho was boosted into the air by three liquid-propellant rocket engines originally designed with 75,000 pounds of thrust.[7] MSFC engineers Alex McCool and Keith B. Chandler traced the development trends of early liquid-propellant engines and noted that while early V–2 concepts were incorporated in these engines, many new design features and improvements were also brought in for the Navaho. A new thrust-chamber design provided better cooling for the higher heat-transfer rate and an improved single injector replaced 18 separate injectors.[8] Eventually the engine was updated to 135,000 pounds of thrust.

■ The Redstone NAA 75–110

The Navaho production contract was later canceled, but its research and development effort directly influenced future rocket engines, including the engine for the Redstone. The Navaho XLR43–NA–1 engine, basically a redesigned version of the V–2, came nearer than any other engine did to meeting the special requirements for the Redstone. "We decided to adapt to our purpose the liquid-propulsion system then used in the Navaho test missile—a North American Aviation engine," Von Braun wrote.[9] The Redstone engine was designated "NAA 75–110" and rated at 75,000 pounds of

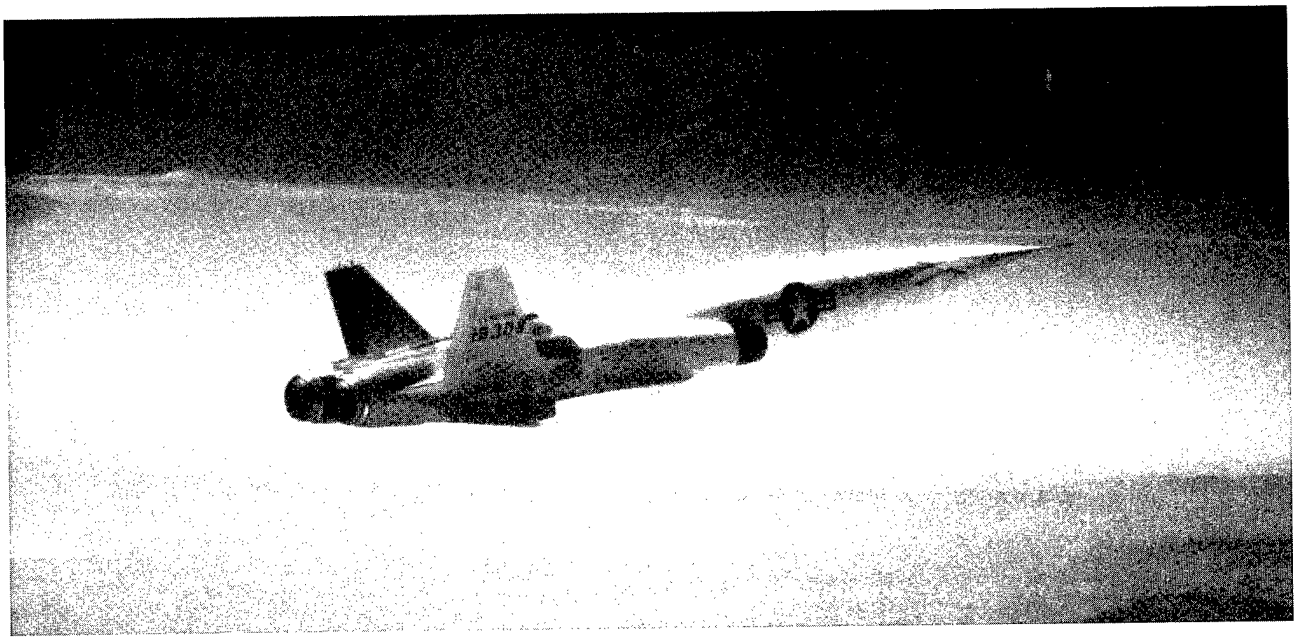

Navaho in flight.

thrust at sea level, with a thrust-burning time of 110 seconds.[10] Improvements in the performance features and components of the engine yielded seven different engine types, A–1 through A–7. The A–7 engine was the power plant for the Mercury-Redstone launch vehicles. Basically, it was the same power plant used in the latest tactical Redstone ballistic missiles with modifications to improve overall efficiency and safety. The engine generated 78,000 pounds of thrust at sea level.[11] In May 1961, a Mercury-Redstone designed by the Von Braun team in Huntsville and managed by the new Marshall Center launched Alan B. Shepard, the first American astronaut, into space.[12]

■ Jupiter S–3D Engine

On May 31, 1957, an Army Jupiter Intermediate-Range Ballistic Missile was fired to an altitude of 250 to 350 miles and to a range of 1,500 miles, marking the limit of its design capability and the first successful flight of such a missile.[13] The success was tied to Huntsville where members of the Von Braun team at Redstone Arsenal had modified existing engine hardware to meet new requirements. Like the Redstone, the Jupiter missile drew power from a V–2 engine originally adapted for the Navaho.[14] For the Jupiter, however, the engine was scaled up to a thrust of 150,000 pounds. The engine was also designed to operate on liquid oxygen and kerosene (RP–1) instead of the liquid oxygen and ethyl alcohol used in the Redstone, resulting in about a 7-percent gain in propellant performance. The engine also utilized a tubular-wall, regeneratively cooled thrust chamber that provided a major reduction in weight, cost, and fabrication, as compared to previous double-walled chambers.[15] The Rocketdyne Division of North American Aviation supplied the S–3D engine. The Jupiter space flight that probably attracted more public attention than any other came on May 28, 1959, when two primates, Able and Baker, rode in a capsule aboard a nose cone and survived the flight in spite of reentry temperatures of approximately 5,000 °F.[16]

■ Jupiter C Engine

Other launch vehicles, including the Jupiter C, developed by the Army missile team in Huntsville also received their inheritance from the experience the team had acquired on the V–2, the Hermes, and the Redstone. On August 7, 1957, an Army Jupiter C, developed by the Von Braun team in Huntsville, fired a one-third-scale model nose cone 1,200 miles down range from a Florida launch site. The nose cone reached a summit altitude of 600 miles and was recovered the next day. On November 7, the nose cone was shown on television by President Eisenhower as evidence that the United States had marked another milestone in the missile and space race.[17] Engineers at Redstone Arsenal had solved the reentry heating problem for the Jupiter missile. They had also modified the Redstone and designed it to serve as the first stage for the Jupiter C. Two clustered stages of solid-propellant motors

developed by the Jet Propulsion Laboratory in California served as the second and third stages for the vehicle. Changes to the Jupiter C stage included increasing the tankage so that it could hold more fuel and oxidizer, thus extending engine burning time. The engine itself was also modified to burn a more powerful fuel, Hydyne (unsymmetrical dimethylhydrazine and diethylene triamine), boosting the first-stage thrust to 83,000 pounds.[18] On January 31, 1958, the engineers from Huntsville used the Jupiter C to tackle the biggest test of all: they used the Jupiter C rocket to launch Explorer I, the first U.S. satellite, into orbit.[19]

■ H–1 Engines for Saturn I and Saturn IB

As the United States planned for the decade of the 1960's, its missile and space experts reviewed their existing inventory of launch vehicles. The review demonstrated the clear need to develop a large-scale engine that could be arranged in a cluster in the first stage to launch communications satellites and other scientific payloads, including weather satellites and instrumented probes.[20] The engine would eventually boost the Saturn launch vehicle. The history of the Saturn program began in the Spring of 1957; Wernher von Braun recalled, "Our preliminary designers were studying a large, clustered-engine, first-stage arrangement. In the late summer of 1958, we were authorized to proceed with the design and development of a 1.5-million-pound thrust stage based on this bunching concept." The H–1 engine based on the Jupiter S–3D engine was selected for the new booster that would eventually be known as Saturn I.[21] The S–I stage for the Saturn I became the S–IB first stage for the Saturn IB. The design used Von Braun's clustering concept. This involved using former Redstone and Jupiter tanks, which were lengthened to carry added propellant, while the basic diameter of the 70-inch Redstone and the 105-inch Jupiter tanks were retained. The tank arrangement gave an alternate pattern of the four fuel and four oxidizer tanks, clustered around the 105-inch center oxidizer tank.

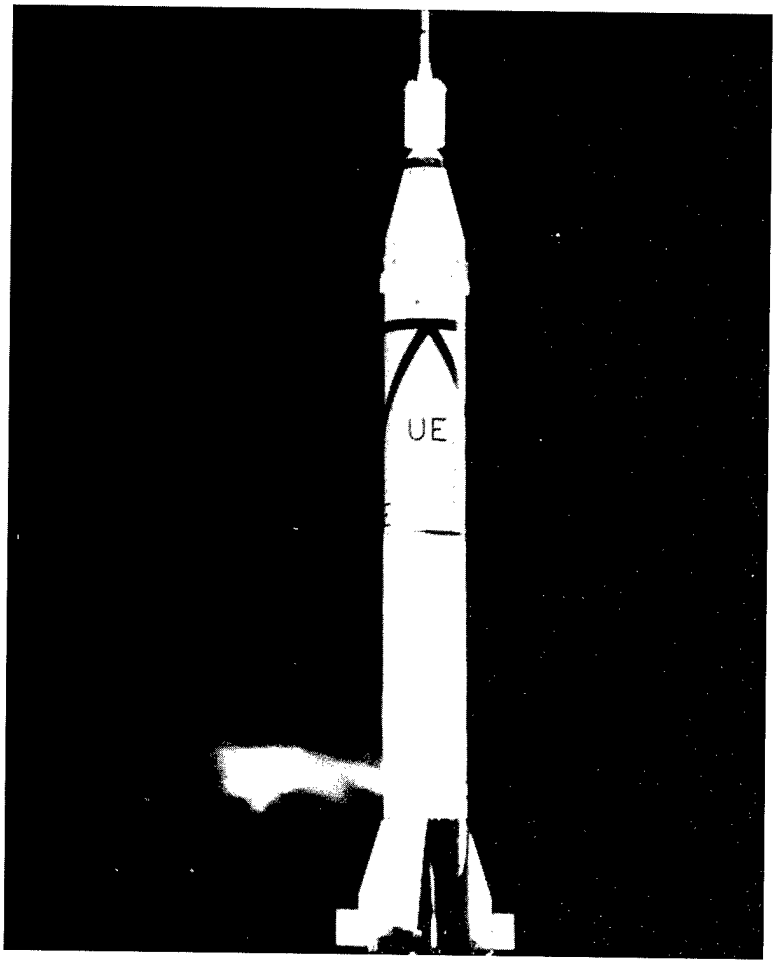

Jupiter C.

Rocketdyne was selected as the contractor to modify the S–3D design for the H–1, which would use liquid oxygen and RP–1.[22] "The H–1 also shed a number of accessories carried over from the Jupiter engine system," wrote Saturn historian Roger Bilstein. "Early versions of the H–1 relied on the Jupiter's lubrication system, which featured a 73-liter (20-gallon) oil tank. The H–1 designers arranged for the vehicle's own fuel, RP–1 (along with some additives), to do the same job. This arrangement eliminated not only the oil tankage, but also a potential source of contamination."[23] Rocketdyne's Edward E. Straub also reviewed the modifications made to the H–1. Two ground start tanks (with complex accessories) for the Jupiter engine were replaced on the H–1 by a simple solid-propellant cartridge starter. In addition, a complex thrust-level control system for the Jupiter engine was modified for the H–1.[24] Initial versions of the Saturn I vehicle, called "Block I," had eight H–1 engines—each producing 165,000

pounds of thrust. H–1 engines were also used in a Block II design that increased thrust to 188,000 pounds each. By the time the tenth and last Saturn I vehicle lifted off on July 30, 1965, the United States had clearly committed itself to President Kennedy's challenge to land a man on the Moon by the end of the decade. The final Saturn I flight climaxed with what MSFC officials termed as a "program which started the U.S. on the road to the Moon with 10 straight successes."[25]

■ RL–10 Upper-Stage Engines

During the 1960's, many MSFC efforts were directed toward advanced engine technology and higher energy propellants. Fuel-efficiency assessments pointed to liquefied gases as the promising new propellants for advanced missions, and to liquid hydrogen, in particular, for the Saturn upper stages.[26] Liquid hydrogen, however, introduced even more risk and danger into missile and space research. Joel E. Tucker, who has traced the history of Pratt & Whitney's RL–10 upper-stage rocket engine, has noted that the company's key engineers and researchers were introduced to hydrogen-fueled projects in 1956, with a sketch of the Hindenburg's last fateful moments and a report on an explosion of a hydrogen lab.[27] Undaunted, but cautious, industry and government rocket experts were drawn by what Saturn historian Roger Bilstein has called the "lure of liquid hydrogen." Studies showed that "compared to an RP–1-fueled engine of similar size, liquid-hydrogen fuel could increase the specific impulse of an engine by 40 percent," Bilstein noted.[28] The RL–10 engine was rooted in liquid-hydrogen engine research. Pratt & Whitney had explored liquid hydrogen for the Air Force for the super-secret high-altitude reconnaissance aircraft known later as the "SR71 Blackbird." The Air Force was also interested in a liquid-hydrogen engine that would enable it to launch heavier payloads, such as communications satellites.[29] NASA eventually inherited responsibility for the RL–10 engine under development by Pratt & Whitney—and destined for use in the Saturn I upper stages. The first flight of the engine occurred in 1964 after engineers at MSFC and Pratt & Whitney logged hours of engine testing in Huntsville and at other sites. The tests helped score hundreds of innovative design breakthroughs in cryogenic pumps, the thrust chamber, the injector face, and the lubrication system.[30]

■ J–2 Engines for Saturn IB and Saturn V

The selected configuration for the Saturn I second stage, the S–IV stage, was a cluster of six RL–10 engines, each having 15,000 pounds of thrust. But as NASA looked beyond Saturn I to large launch vehicles for future missions, clustering the RL–10

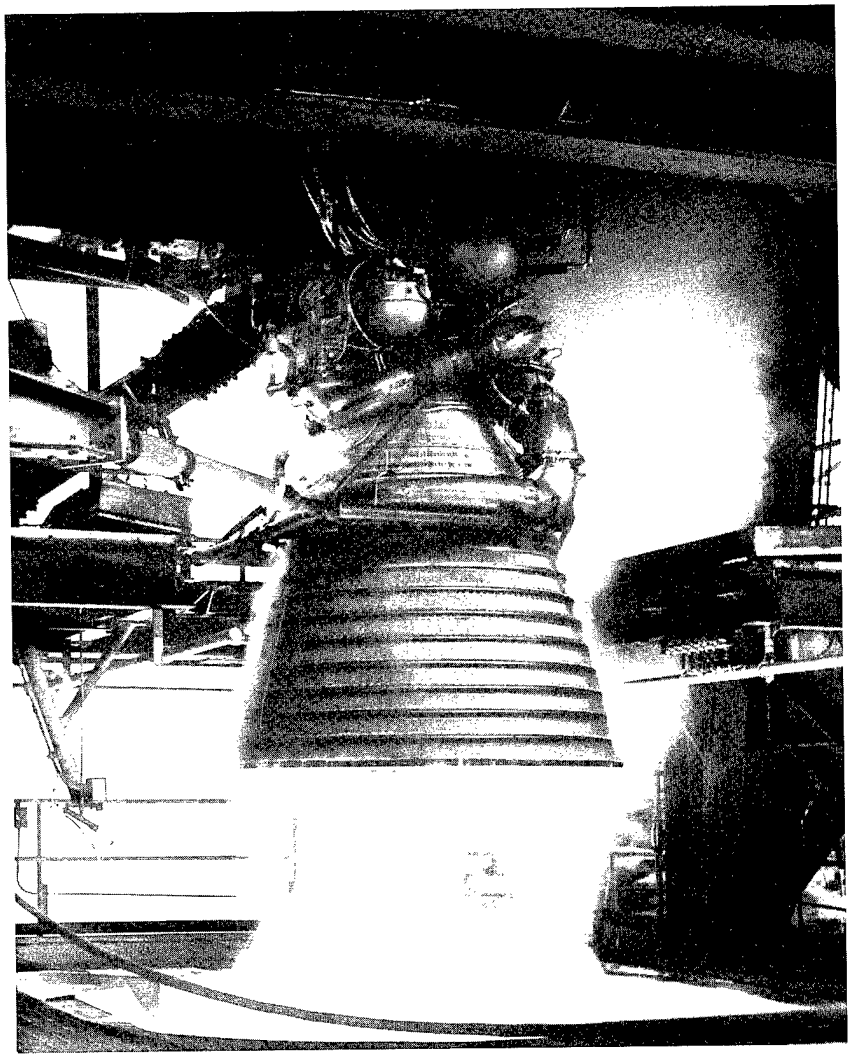

J–2 engine static firing.

was not enough. Beginning in 1960, development of the J–2 engine, a single-chamber hydrogen/oxygen engine of 200,000 pounds thrust was underway.[31] By late 1960, the first experimental components for the J–2 were being fabricated and assembled by a research and development team. Like the RL–10, the development of the J–2 engine was dependent on innovation and design simplicity. For example, engineers had to design a system for forming some 600 uniform posts on the face of the J–2 injector, and they had to tackle new problems of insulation, metals embrittlement, and sealing. In addition, engineers had to develop a new method of brazing high-strength stainless-steel tubing to form the J–2's regeneratively cooled thrust chamber.[32] These huge engines, built by Rocketdyne for MSFC, became the powerhouse for Saturn IB and Saturn V upper stages. A single J–2 was used in the Saturn IB second stage and Saturn V third stage. Five J–2 engines were clustered in the Saturn V second stage for a million pounds of thrust.

F–1 engine static firing at MSFC.

■ Saturn V F–1 Engine

The origins of the Saturn launch vehicle concept are rooted in the research conducted within the Army Ballistic Missile Agency in the late 1950's. However, interest in the program moved well beyond the borders of Redstone Arsenal after President Kennedy's challenge in 1961 to land a man on the Moon before the end of the decade. In reality, the Von Braun team had recognized early on that a rocket engine of tremendous capabilities would be needed if man ever embarked on lunar journeys or sent probes into deep space. As a result, development started in the 1950's on the 1.5-million-pound-thrust F–1 engine even before a vehicle was designed for it. The F–1 would burn the familiar liquid oxygen and RP–1, and had roots in the Air Force Navaho program. The F–1 was based on an initial concept for a 360,000-pound-thrust E–1 engine that would burn liquid oxygen and RP–1.[33]

Rocketdyne was selected as the contractor for the F–1, and—for a brief while—NASA considered using the F–1 on a vehicle of tremendous size, the Nova, which would be capable of direct flights to the Moon. The Nova never materialized, but the F–1 did and would eventually be used in the first stage (S–IC) of the vehicle that would launch men on their way to the Moon. Five F–1 engines would provide a total thrust of 7.5 million pounds in the Saturn V S–IDC stage.

Rocketdyne's Bob Biggs has pointed out that although the giant F–1 engine was simple, it was not developed without problems. "Its very 'bigness' created a brand-new territory for technical problems." According to Biggs, the most

significant problem was also the one most expected and the most difficult to solve—combustion instability. The engine was designed to the man-rated safety concept, which required that it be dynamically stable. If any engine system was disturbed from any source, the system was required to automatically overcome the disturbance and return to stable operations.[34] Saturn historian Roger Bilstein has recounted the efforts that Rocketdyne and MSFC engineers used to solve the stiff challenge of combustion instability. "The most bizarre aspect of F–1 testing (like the H–1) involved the use of small bombs to upset the thrust exhaust pattern to measure the engine's ability to recover from disturbance."[35] Biggs has termed the F–1 as "the No-Frills Giant."[36] NASA and Rocketdyne news releases often tried to put the size and power of the engine in perspective by pointing out, for example, that "the fuel pump of the Rocketdyne F–1 pushes fuel with the force of 30 diesel locomotives," or that the five engines generated "double the amount of potential hydroelectric power that would be available at any given moment if all the moving waters of North America were channeled through turbines."[37] Of course, those who watched the launch of Apollo 11 on July 15, 1969, understood the power of the Saturn V vehicle that Wernher von Braun called the "Giant."[38]

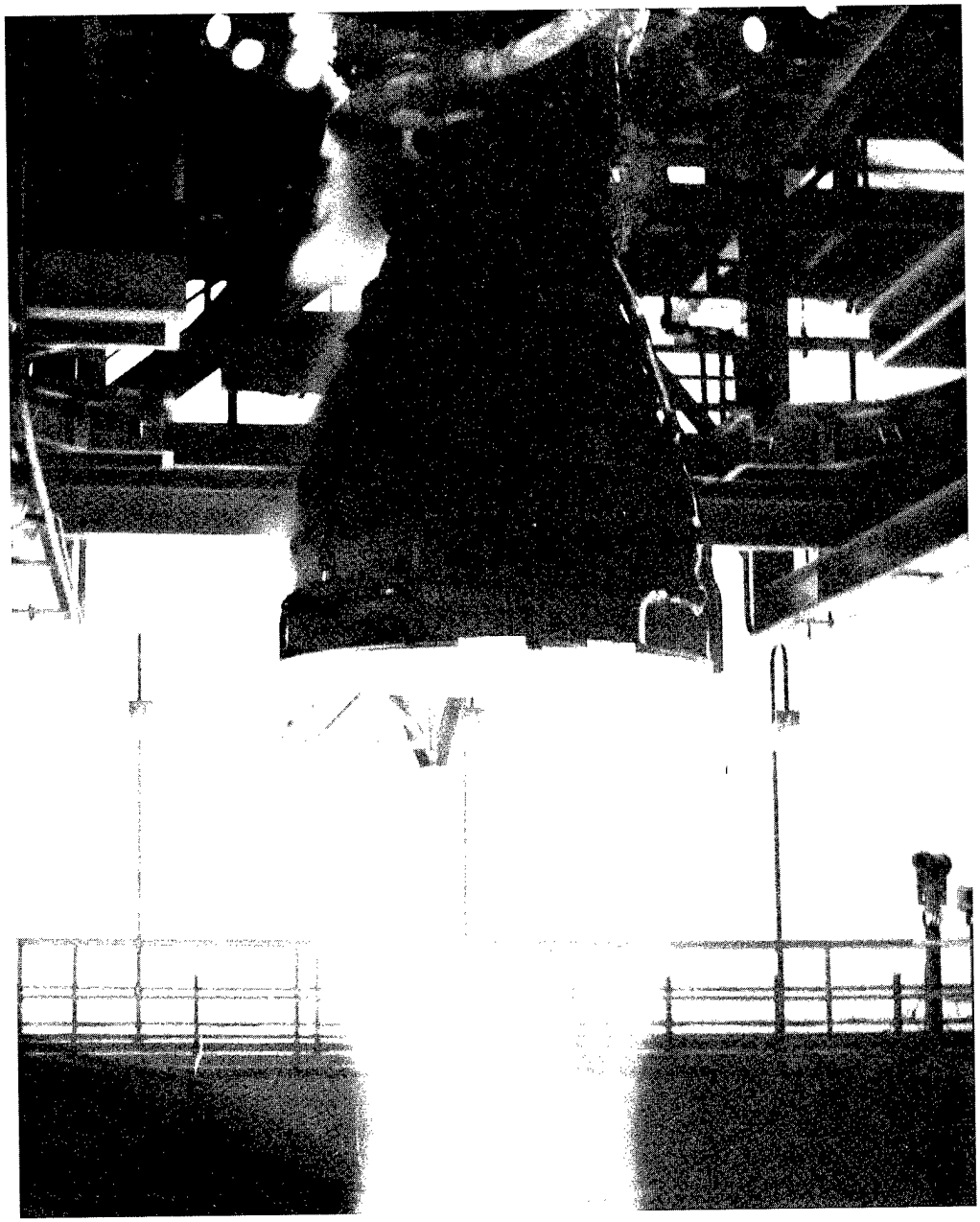

Space shuttle main engine testing.

■ Space Shuttle Main Engine

The last Saturn F–1's that NASA employed helped lift *Skylab* into orbit in 1973. By then, NASA engineers were already deep into the design for the space shuttle main engine, a concept that broke with the past, according to shuttle historian Dennis R. Jenkins. The challenge, Jenkins said, was "not to build a larger, more powerful engine, but to build a small, compact engine that could be throttled during ascent to provide some measure of control over the maximum dynamic pressure and speed of the vehicle."[39] MSFC engineers who have traced the technology projects leading to the development of the space shuttle main engine have pointed to an "aggressive technology program in high-pressure tubomachinery initiated in the 1960's." They point out that much of the work was done by Pratt & Whitney under MSFC's sponsorship, with the

outgrowth known in-house as the concept for the HG–3, a 350,000-pound-thrust engine named after Hans G. Paul, the long-time chief of the Propulsion Division. In essence, the HG–3 concept eventually became the space shuttle main engine.[40]

The main engines would become the most advanced cryogenic liquid-fueled rocket engines ever built. To get very high performance from an engine compact enough that it could not encumber the orbiter or diminish its desired payload capability, MSFC worked closely with its prime contractor, the Rocketdyne Division of Rockwell International. The greatest problem was to develop the combustion devices and complex turbomachinery—the pumps, turbines, seals, and bearings—that could contain and deliver propellants to the engines at pressures several times greater than in the Saturn engines. The shuttle main engine was also designed as the first propulsion system with a computer mounted directly on the engine to control operation and automatically make corrective adjustments or shut down the engine safely. For improved fuel efficiency, engineers developed an ingenious, staged combustion cycle never before used in rocket engines.[41] Rocketdyne's Bob Biggs has reported on the first 10 years of the shuttle main engine and has traced the technical hurdles and challenges that engineers at Rocketdyne and MSFC faced during the development period. These included predicting the transient behavior of the propellants and engine hardware during start and shutdown. Rocketdyne engineers and officials, such as Rocketdyne Vice President Matt Eck, also sought solutions to concerns with high-pressure fuel turbopump bearing instability problems, explosions, and blade failures. On various occasions during different tests, engineers confronted a fire that started in the engine's main oxidizer valve, a major fracture in the housing for the main fuel valve, the rupture of a nozzle fuel coolant feedline, and a fire that burned through the engine's fuel preburner. Solutions were also sought to heat-exchanger failures, weld cracks in the main combustion chamber, and problems with the main injector posts. A major portion of the problems were answered by conducting ground test after ground test. In fact, a goal of 65,000 seconds of total ground testings was reached during an engine test on March 24, 1980—a little more than a year before the first space shuttle was launched on April 12, 1981.[42]

It is possible to draw charts and diagrams that trace the origins of MSFC's expertise in liquid-propulsion systems all the way back to the days of the V–2 or the Navaho missile. Unfortunately, charts and diagrams do not adequately convey the thousands of hours engineers at MSFC and its contractor sites have spent year after year, studying, designing, analyzing, testing, and dissecting pumps, bearings, valves, insulation, fuel mixtures, nozzles, feedlines, and thousands of other rocket engine components. Better evidence of that expertise came this year when NASA launched the first flight of the upgraded space shuttle main engine and marked more than 200 main engine flights overall.*

Michael D. Wright/CN31S
205–544–6840

* Bibliographic references provided on page 220.

References

[1]July 19, 1995. STS–70 Sees First Use of New Space Shuttle Main Engine: Inertial Upper Stage Deploys Last Tracking and Data Relay Satellite System. *Marshall Star.*

[2]Science Policy Research Division, Congressional Research Service, Library of Congress, Serial D, Volume I. *United States Civilian Space Programs 1958–1978.* 1981. Report Prepared for the Subcommittee on Space Science and Applications of the Committee on Science and Technology, U.S. House of Representatives (Washington), 166.

[3]Emme, E.M., ed. 1961. *Aeronautics and Astronautics: An American Chronology of Science and Technology in the Exploration of Space, 1915–1960* (Washington), 50.

[4]Ley, W. 1968. *Rockets, Missiles, and Men in Space.* Viking Press (New York), 498–499; Schulze, H.A. 1965. Technical Data on the Development of the A–4, V–2. Historical Office, Management Services Office, MSFC, 22.

[5]Bullard, J.W. *History of the Redstone Missile System.* October 15, 1965. Historical Monograph Project Number: AMC 23M, U.S. Army Missile Command, Redstone Arsenal, Alabama, 13; *United States Civilian Space Programs 1958–78*, 167.

[6]Von Braun, W. Fall 1963. The Redstone, Jupiter, and Juno (reprint). *Technology and Culture*, vol. IV., no. 4, 454.

[7]*United States Civilian Space Programs 1958–1978*, 166–167.

[8]Chandler, K.B., and McCool, A.A. March 23, 1962. Development Trends in Liquid-Propellant Rocket Engines. *From Peenemuende to Outer Space, Commemorating the Fiftieth Birthday of Wernher von Braun.* Edited by Stuhlinger, E.; Ordway, F.I., III; McCall, J.C.; and Bucher, G.C. MSFC, 292.

[9]The Redstone, Jupiter, and Juno, 454.

[10]*History of the Redstone Missile System*, 54.

[11]*United States Civilian Space Programs 1958–1978*, 186.

[12]Bilstein, R.E. 1980. *Stages to Saturn, A Technological History of the Apollo/Saturn Launch Vehicle.* NASA SP–4206 (Washington), 19–20.

[13]*Aeronautics and Astronautics*, 86.

[14]*United States Civilian Space Programs 1958–1978*, 168.

[15]Development Trends in Liquid-Propellant Rocket Engines, 294.

[16]*Aeronautics and Astronautics*, 109.

[17]*Aeronautics and Astronautics*, 87.

[18]The Redstone, Jupiter, and Juno, 457.

[19]*Aeronautics and Astronautics*, 95.

[20]Lange, O.H. March 23, 1962. Development of the Saturn Space Vehicle. *From Peenemuende to Outer Space, Commemorating the Fiftieth Birthday of Wernher von Braun.* Edited by Stuhlinger, E.; Ordway, F.I., III; McCall, J.C.; and Bucher, G.C. MSFC, 6.

[21]Von Braun, W. June 1963. Saturn, Our Best Hope. *Space World*, 13.

[22]Development Trends in Liquid-Propellant Rocket Engines, 294.

[23]*Stages to Saturn*, 99.

[24]Straub, E.E. February 1962. H–1 Engine. *Astronautics, A Publication of the American Rocket Society*, vol. 7, no. 2, 39.

[25]August 4, 1965. Saturn I Program Closes. *Marshall Star.*

[26]*Marshall Space Flight Center, 1960–1985 Anniversary Report.* 1985. NASA (Washington), 9–10.

[27]Tucker, J.E. 1989. The History of the RL–10 Upper-Stage Rocket Engine. *History of Liquid Rocket Engine Development in the United States.* Liquid Rocket Propulsion History Colloquium, American Association for the Advancement of Science Annual Meeting, Los Angeles. Doyle, S.E., vol. ed.; Hall, R.C., series ed. History Series, vol. 13, A Supplement to Advances in the Astronautical Sciences, 123.

[28]*Stages to Saturn*, 129–130.

[29]Jones, L.W.; Fisher, M.F.; McCool, A.A.; and McCarty, J.P. June 24–26, 1991. Propulsion at the Marshall Space Flight Center. American Institute of Aeronautics and Astronautics, AIAA–91–2553. Presented at the American Institute of Aeronautics and Astronautics/Social of Automotive Engineers /American Society of Mechanical Engineers, 27th Joint Propulsion Conference, Sacramento, California, 6.

[30]The History of the RL–10 Upper-Stage Rocket Engine. 123–151.

[31]*United States Civilian Space Programs 1958–1978*, 171.

[32]News from Rocketdyne, J–2 Rocket Engine Background Information, 4.

[33]Propulsion at the Marshall Space Flight Center, 8.

[34]Biggs, B. Spring 1992. F–1, The No-Frills Giant. *Threshold*, 22–31.

[35]*Stages to Saturn*, 115.

[36]The No-Frills Giant, 22–31.

[37]Did You Know That???? Rocketdyne Division, North American Rockwell Corporation.

[38]Von Braun, W. 1975. Saturn, The Giant. *Apollo Expeditions to the Moon.* Edited by Cortright, E.M. NASA SP–350 (Washington), 41.

[39]Jenkins, D.R. The History of Developing the National Space Transportation System, the Beginning Through STS–50. 1992. Broadfield Publishing (Melbourne, Florida), 75.

[40]Propulsion at the Marshall Space Flight Center, 11.

[41]*Marshall Space Flight Center, 1960–1985 Anniversary Report*, 22.

[42]Biggs, R. 1989. Space Shuttle Main Engine, the First Ten Years. *History of Liquid Rocket Engine Development in the United States*. Liquid Rocket Propulsion History Colloquium, American Association for the Advancement of Science Annual Meeting, Los Angeles. Doyle, S.E., vol. ed.; Hall, R.C., series ed. History Series, vol. 13, A Supplement to Advances in the Astronautical Sciences, 69–110.

Abbreviations and Acronyms

AADSF	Advanced Automated Directional Solidification Furnace
AAS	American Astronomical Society
ACES	advanced control evaluation for structures
ACTIS	Advanced Computed Tomography Inspection System
AEOLUS	Autonomous Earth Orbiting Lidar Utility Sensor
AETF	Advanced Engine Test Facility
AFM	advancing front method
AFSIG	Ascent Flight System Integration Group
Ag-MH	silver-metal hydride
Ag-Zn	silver-zinc
AGU	American Geophysical Union
AI	artificial intelligence
AIAA	American Institute of Aeronautics and Astronautics
AITP	Aerospace Industry Technology Program
albedo	reflected solar energy
AMCC	advanced main combustion chamber
AMPR	Advanced Microwave Precipitation Radiometer
ANOVA	analysis of variance
AOPL	Aerosol Optical Properties Laboratory
AR&C	automated rendezvous and capture
ARC	Aerophysics Research Center
ARCS	Argon Release for Controlled Studies sounding rocket
ASCA	Advanced Satellite for Cosmology and Astrophysics
ASRM	advanced solid rocket motor
ASTEX	Atlantic Stratocumulus Transition Experiment
ASTM	American Society for Testing Materials
ATD	alternate turbopump development
ATLAS–3	Third Atmospheric Laboratory for Applications and Science Mission
ATMOS	Atmospheric Trace Molecules Observed By Spectroscopy
ATS	automated torque sensor
AXAF–I	Advanced X-Ray Astrophysics Facility—Imaging
BATSE	Burst and Transient Source Experiment
blisk	integrally bladed turbine disk
BOL	beginning-of-life
BTOS	Beam Transmission Optical System
CA	clocking angle
CAD	computer-aided design
CAGI	computer-aided grid interface
CAMEX	Convection and Moisture Experiment
CaPE	Convection and Precipitation/ Electrification
CAR	critical area response
CASE	computer-aided software engineering
CAVE	Computer Applications and Virtual Environments Laboratory
CBL	convective boundary layer
CCD	charge-coupled device
CCP	center cracked panel
CCT	cognitive computing techniques
Cd	cadmium
CDDF	Center Director's Discretionary Fund
CEC	Chemical Equilibrium Computer
CEETC3	Combined Environmental Effects Test-Cell 3 system
CFC	chlorofluorocarbon
CFD	computational fluid dynamics
CFE	continuous-flow electrophoresis
CGRO	Compton Gamma Ray Observatory
CHymP	CaPE Hydrometeorology Project
CICM	coaxial injection combustion model
CIRS	composite infrared spectrometer
CLR	coherent laser radar
cm	centimeter
CO	carbon monoxide
CO_2	carbon dioxide
codecs	compressor-decompressors
COHMEX	Cooperative Huntsville Meteorological Experiment
CORSSTol	Cylinder Optimization of Rings, Skin, and Stringers with Tolerance sensitivity
COST	controls, optics, structures, and thermal
COTS	commercial off-the-shelf
CRES	corrosion-resistant steel
CSC	Computer Science Corporation
CSI	controls/structures interaction
CSI/GTF	Controls/Structures Interaction Ground Test Facility
CTOD	crack-tip opening displacement
CTTP	Cryogenic Tank Technology Program
Cu	copper
CW	continuous wave
DAAC	Distributed Active Archive Center
dc	direct current
DC-X	delta clipper experimental vehicle
dc/dc	direct current/direct current
DCE	DC electric field instrument

DMSP SSM/I	Defense Meteorological Satellite Program Special Sensor Microwave/Imager
DOD	Department of Defense
DOE	Department of Energy
DSMC	direct simulation Monte Carlo analysis
DTM	digital transient model
DTO	demonstration test objective
ECMWF	European Center for Medium-range Weather Forecasting
EDO	extended-duration orbiter
ELV	expendable launch vehicles
EOL	end-of-life
EOS	Earth Observation System
EPA	Environmental Protection Agency
EPFCG	elastic-plastic fatigue crack growth
EPRI	Electric Power Research Institute
EPS	electrical power system
ERBE	Earth Radiation Budget Experiment
ESA	European Space Agency
ET	elapsed time
ETO	Earth-to-Orbit
EUV	extreme ultraviolet
eV	electron volts
EVA	extravehicular activity
EVM	Experimental Vector Magnetograph (also EXVM)
f#	focal ratio
FACE	Florida Area Cumulus Experiment
FAD	failure assessment diagram
FDIR	fault detection, isolation, and recovery
FDNS	Finite-Difference, Navier-Stokes
FEM	finite element model
FOV	field of view
fps	frames per second
FRL	Flight Robotics Laboratory
FSSP	Forward-Scattering Spectrometer Probe
ftp	file transfer protocol
FUV	far ultraviolet
G	units of gravitational force
g/cm^3	grams per cubic centimeter
Ga	gallium
GASP	General Aerodynamic Simulation Program
GATV	ground-to-air television
GC	generic card
GCIP	GEWEX Continental Scale International Project
GCM	general circulation model
GDSS	General Dynamics Space Systems
Ge	germanium
GENIE	general grid generation system
GEO	geosynchronous orbit
GEOSIM	GEOphysical fluid-flow SIMulator
GEOWARN	Global Emergency Observation Warning and Relief Network
GEWEX	Global Energy and Water Cycle Experiment
GGOT	Gas Generator Oxidizer Turbine
GGS	Global Geospace Study
GHC	generalized hyper-coherence
GHe	gaseous helium
GIS	geographic information system
GLOBE	GLObal Backscatter Experiment
GN&C	guidance, navigation, and control
GOES	Geostationary Operational Environmental Satellite
GONG	Global Oscillations Network Group
GPC	Gravity Probe B
GPS	Global Positioning System
GRAM	Global Reference Atmospheric Model
GSFC	Goddard Space Flight Center
GST	glutathione S-transferase
GTF	ground test facility
GVaP	Global Energy and Water Cycle Experiment Water Vapor Project
H^+	hydrogen ion
HBMS	Hirshfelder-Buehler-McGee-Sutton
HCF	high-cycle fatigue
HCF	hydrogen cold flow
HDOS	Hughes Danbury Optical Systems
He	helium
He^+	helium ion
He-Cd	helium-cadmium
He-Ne	helium-neon
HEE	hydrogen environmental embrittlement
HESI	High-Energy Solar Imager
Hex	heat exchanger
Hg	mercury
Hg-Xe	mercury-xenon
HH-PCAM	hand-held protein crystallization in microgravity hardware
HI-PAC DTV	high-packed digital television (also HI-PAC)
HIP	hot isostatic pressing
HIV	human immunodeficiency virus
Ho, Tm:YAG	holmium, thulium: yttrium aluminum garnet

HOMO–LUMO	highest occupied molecular orbital-lowest unoccupied molecular orbital
HOSC	Huntsville Operations Support Center
HPFT	high-pressure fuel turbine
HPFTP	high-pressure fuel turbopump
HPOPTP	high-pressure oxygen turbopump
HPOTP	high-pressure oxidizer turbopump
HRDM	high-rate demultiplexer
HRM	high-rate multiplexer
HRV	highly reusable vehicles
HSL	Huntsville Simulation Laboratory
HST	Hubble Space Telescope
Hz	hertz
IAU	International Astronomical Union
ICD	interface control document
IDNDR	International Decade for National Disaster Reduction
IECEC	Intersociety Energy Conversion and Engineering Conference
IFM	in-flight maintenance
IGES	Initial Graphics Exchange Specification
ILC	intelligent load controller
IMF	interplanetary magnetic field
IML–2	International Microgravity Laboratory 2
INS	inertial navigation system
InSb	indium antimonide
IPC	intelligent power controller
IR	infrared
IRAD	industrial research and development
IRAS	Infrared Astronomy Satellite
IRTF	Infrared Telescope Facility
ISCCP	International Satellite Cloud Climatology Project
ISO	Infrared Space Observatory
ISOPHOT	Infrared Space Observatory spectrophotometer
ITCZ	InterTropical Convergence Zone
ITL	Inducer Test Loop
IV	independent variable
IWC	integrated water content
J	joule
JANNAF	Joint Army, Navy, NASA, and Air Force
JIRAD	joint independent research and development
JPEG	Joint Photographic Experts Group
JPL	Jet Propulsion Laboratory
JSC	Johnson Space Center
K	Kelvin
KAO	Kuiper Airborne Observatory
KATE	Knowledge-based Autonomous Test Engineer
kbps	kilobits per second
keV	kiloelectron volts
kHz	kilohertz
km	kilometer
km/s	kilometers per second
KSC	Kennedy Space Center
Ku-band	15.250 to 17.250 gigahertz
kWh	kilowatt hours
L-O-L	like-on-like
LAD	liquid acquisition device
LALMM	load-allowable load minimum margin
LaRC	Langley Research Center
LAWS	Laser Atmospheric Wind Sounder
lbm/sec	pound mass per second
LCF	low-cycle fatigue
LDV	laser Doppler velocimeter
LEIF	Low-Energy Ion Facility
LEO	low-Earth orbit
LIS	Lightning Imaging Sensor
LLPC	liquid-liquid partition chromotography
LMM	load minimum margin
LMSC	Lockheed Missiles and Space Corporation
LN_2	liquid nitrogen
LO_2	liquid oxygen (also lox)
LO_2-LH_2	liquid oxygen-liquid hydrogen
LOLC	Laser Optical Particle Counter
lox	liquid oxygen (also LO_2)
LPFTP	low-pressure fuel turbopump
LTC	low thermal conductivity
LUTE	Lunar Ultraviolet Telescope Experiment
m	meter
MACAWS	Multi-center Airborne Coherent Atmospheric Wing Sensor
maglev	magnetically levitated
MARCSIM	MSFC automated rendezvous and capture simulation
MB/s	megabits per second
MCC	main combustion chamber
MCP	microchannel plates
MCPT	multicycle proof test
MECO	main engine cutoff
MeV	million electron volts
MHD	magnetohydrodynamic
MHz	megahertz
MI	Magnetosphere Imager
MIMR	Multifrequency Imaging Microwave Radiometer

MIXE	Marshall Imaging X-Ray Experiment
MLT	magnetic local time
MNA	2-methyl-4-nitroniline
MOSFET	metal oxide semiconductor field-effect transistor
MPa	megaPascal
MPEG	Motion Picture Experts Group
MR	mixture ratio
MSCSurv	Manned Spacecraft Crew Survivability
MSU	microwave sounding unit
MTPE	Mission to Planet Earth
mV/m	millivolts per meter
ν	frequency
NAOMI	National Adaptive Optics Mission Initiative
NARC	North American Rayon Corporation
NASCAP/GEO	NASA Analyzer Program for Geosynchronous Orbit
NASCAP/LEO	NASA Analyzer Program for Low-Earth Orbit
NASP	National Aerospace Plane
NAVC	Northeast Alternative Vehicle Consortium
NBS	Neutral Buoyancy Simulator
NCAR	National Center for Atmospheric Research
NDE	nondestructive evaluation
Ne	neon
NESDIS	National Environmental Satellite Data Information Service
Ni	nickel
Ni-Cd	nickel-cadmium
Ni-MH	nickel-metal hydride
NiH_2	nickel-hydrogen
NIR	near-infrared
NIST	National Institute for Standards and Technology
NITROX	increased oxygen/reduced nitrogen
NLO	nonlinear optical
NLS	National Launch System
nm	nanometer
NOAA	National Oceanic and Atmospheric Administration
NOx	nitric oxide
NS	neutron star
NSTS	National Space Transportation System
NTSC	National Television Standards Committee
NURBS	non-uniform rational B-splines
NUV	near-ultraviolet
O^+	oxygen ion
OACT	Office of Advanced Concepts and Technology
OLR	outgoing longwave radiation
OMV	orbital maneuvering vehicle
OSEE	optically simulated electron emission
OSHA	Occupational Safety and Health Administration
OTD	Optical Transient Detector
OTTR	Oxidizer Technology Turbine Rig
P&W	Pratt and Whitney
P-T	pressure-temperature
PAM	portable automated mesonet
PAMELA	Phased-Array Mirror, Extendible Large Aperture
PAN	polyacrylonitrile
PBL	planetary boundary layer
PCC	Precision Castparts Corporation
PCR	payload control room
PCR	principal component regression
PDF	probability distribution function
PEG	polyethylene glycol
PI	principal investigator
PL	peak load
PLS	partial least squares
PMD	propellant management device
PMM	probability matching method
POLAR	Potentials of Large Spacecraft in Auroral Regions
PRF	pulse repetition frequency
PRISM	Passively Cooled Reconnaissance of the Interstellar Medium
PSD	power spectral density
PSEM	phase-synchronized enhancement method
PSI	phase-shifting interferometry
PSI	plasma source instrument
psia	pounds per square inch absolute
PSW	physical split-window
PTDS	Post-Test Diagnostic System
QE	quantum efficiency
QN	quadravariate normal
R-curves	resistance curves
R/S	range over standard
REFLEQS	REactive FLow EQuation Solver
RGB	red, green, blue
RIMS	retarding ion mass spectrometer
RLV	reusable launch vehicle
RMS	remote manipulator system
rms	root-mean-square
RNTS	Rocket Nozzle Technology Subcommittee

ROSETA	range over standard deviation experimental trend analysis
RPC	remote power controller
RSRM	redesigned solid rocket motor
RTG	radioisotope thermoelectric generator
RTLS	return-to-launch site
SAFD	System for Anomaly and Failure Detection
SAO	Smithsonian Astrophysical Observatory
SBIR	Small Business Innovative Research
SBTD	space booster technology demonstrator
SCIFER	Sounding of the Cleft Ion Fountain Energization Region
SCIM	standard cubic inches per minute
SCN/H_20	succinonitrile/water
SDIO	Strategic Defense Initiative Organization
SDT	science definition team
SEDS	Students for the Exploration and Development of Space
SEDSAT	Students for the Exploration and Development of Space Satellite
SEEF	Space Environments Effects Facility
SHEELS	Simulator for Hydrology and Energy Exchange at Land Surface
SHG	second harmonic generation
Si	silicon
SIM	simulation control room
*Sj*GST	Schistosoma japonicum
SLA	stereolithography
SNR	signal-to-noise ratio
SNTP	space nuclear thermal propulsion
SOF	scintillating optical fibers
SOFIC	Scintillating Optical Fiber Ionization Calorimeter
SOHO	Solar and Heliospheric Observatory
SPIE	Society of Photo-optical Instrumentation Engineers
SPIP	Solid Propulsion Integrity Program
SPSR	space-portable spectroreflectometer
SRM	solid rocket motor
SSA	Space Suit Assembly
SSM/I	Special Sensor Microwave/Imager
SSM/PMAD	Space Station Module Power Management and Distribution
SSME	space shuttle main engine
SSTO	single-stage-to-orbit
STICS	super thermal ion composition spectrometer
STME	space transportation main engine
STS	space transportation system
STV	space transfer vehicle
SWRI	Southwest Research Institute
SXI	Solar X-Ray Imager
TAL	time after launch
TAL	trans-Atlantic landing
TAL	transoceanic abort landing
TAPP	Twin Auroral Plasma Probes
TCA	thrust chamber assembly
τ_{decay}	time constant
Te	tellurium
TEM	transition electron microscope
THM	traveling heater method
TIDE	Thermal Ion Dynamics Experiment
TIPS	Thermal Input Printing System
Tm, Ho: YLF	thulium, holmium: yttrium lithium fluorine
TMI	Tropical Rainfall Measuring Mission Microwave Imager
TOA	top-of-atmosphere
TOGA COARE	Tropical Ocean Global Atmosphere Coupled Ocean Atmosphere Response Experiment
TPS	thermal protection system
τ_{rise}	rise time
TRMM	Tropical Rainfall Measuring Mission
TRP	Technology Reinvestment Project
TTA	turbine test article
TTB	Technology Test-Bed
TTE	turbine test equipment
UAH	University of Alabama in Huntsville
UAH-ARC	University of Alabama in Huntsville's Aerophysics Research Center
ULE	ultra-low expansion
UPS	uninterruptible power supply
USML–2	U.S. Microgravity Laboratory–2
USMP–2	Second United States Microgravity Payload
USNAWC	U.S. Navy Air-Warfare Center
UTC	universal time coordinated
UV	ultraviolet
UVI	Ultraviolet Imager
V	volt
Vac	volts, alternating current
VAS	Visible Infrared Spin-Scan Radiometer Atmospheric Sounder
VDA	video decoder assembly
Vdc	volts, direct current
VEA	video encoder assembly
VETA–I	Verification Engineering Test Article I

VGS	video guidance sensor
VI	virtual instrument
VISSR	Visible Infrared Spin-Scan Radiometer
VPCR	virtual payload control room
VPPA	variable polarity plasma arc
VR	virtual reality
VSIM	virtual simulation control room
VUV	vacuum ultraviolet
VWM	vector wind model
WTA	West Test Area
XUV	x-ray ultraviolet
Z-R	reflectivity-rain rate
Zn	zinc
°C	degrees Celsius
µm	micrometer

Index of Contacts

Adams, Alan	Solar Thermal Propulsion	17
Barret, Chris	Flight-Control Augmentation for Aft Center-of-Gravity Launch Vehicles	112
Beckham, Richard H.	Modular Rocket Engine Control Software	182
Bramon, Christopher J.	Dual-Use Hydrostatic Bearing Technology	190
	Structural Ceramics for Advanced Turbomachinery Applications	195
Bukley, Angelia P.	Global Emergency Observation Warning and Relief Network	7
Burns, Morrison R., Jr.	Installation Integrity Measurement for Various Sensors	176
Campbell, Jonathan W.	Passively Cooled Reconnaissance of the Interstellar Medium	11
	Hard X-Ray and Gamma-Ray Imaging System	12
Carrigan, Robert W.	Determination of Composite Material Sensitivity to Permeability Depending Upon Lay-Up Configuration	138
Carter, Daniel C.	High-Brilliance X-Ray Source for Protein Crystallography	25
	Protein Crystal-Growth Apparatus for Microgravity Facility Hardware	26
Chandler, Michael O.	Quantitative Determination of the Rate of Hydrogen-Ion Heating by an Argon-Ion Beam	61
Clinton, Raymond G., Jr.	Development of Low Thermal Conductivity, Polyacrylonitrile-Based Fibers	164
Coffey, Victoria N.	Absolute Sensitivity Measurement for the Thermal Ion Dynamics Experiment	67
Coughlin, Dan J.	Reusable Launch Vehicle Vertical Lander Guidance and Control Research	102
Craven, Paul D.	Helium- to Hydrogen-Ion Ratios in the Inner Magnetosphere	62
Cruit, Wendy	Hybrid Rocket Cold-Flow Modeling	91
Dabney, Richard W.	Automated Rendezvous and Capture Technology Description	107
Danford, Merlin D.	Localized Corrosion in Aluminum Alloys by the Scanning Reference Electrode Technique	162

Denniston, Charles L.	Development of State-of-the-Art Proof-Test Methodology	122
Derrickson, James H.	Measurements With a Superconducting Magnet Spectrometer	41
Earhart, Eric M.	Experimental Determination of Preswirl Effects on Damping Seal Performance	111
Finckenor, Jeffrey L.	Nonautoclave Curing of Composite Flight Structures	143
Fiorucci, Tony R.	Synchronous Phase-Averaging Method for Machinery Diagnostics	119
Fitzjarrald, Daniel E.	Global Modeling of Surface Boundary Forcing	35
Ford, Donald B.	Composite Intertank	138
Fox, Thomas H.	System for Anomaly and Failure Detection	112
Frazier, Donald O.	Investigation of Local Effects on Microstructure Evolution	29
	Polydiacetylene Thin Films for Photonic Applications	31
Funkhouser, John O.	Solid Rocket Motor Asbestos-Free Insulation	90
Gaddis, Stephen W.	Investigation of Inducer Steady and Unsteady Blade Loads	134
Gallagher, Dennis L.	Cold Plasma in the Earth's Magnetosphere	57
Gallaher, Michael W.	Reusable Launch Vehicle Lander Guidance and Control Research	102
Gary, G. Allen	Three-Dimensional Rendering and Image Analysis of Coronal Loops	52
Genge, Gary G.	Structural Ceramics for Advanced Turbomachinery Applications	195
Giles, Barbara L.	Particle Transport From the Magnetosphere's Low-Latitude Boundary Layer	54
Gregg, Wayne	Elastic-Plastic and Fully Plastic Crack Growth	129
Hagyard, Mona J.	Solar Magnetic Fields	47
Hale, Joseph P., II	The Use of Virtual Reality in the Design Analysis of a Space Station Control Room	183
Harris, Donald L.	Damping Measurement of Advanced Composite Materials for Turbomachinery Applications	117

Hastings, Leon J.	Solar Thermal Propulsion Thrusters and Cryogenic Fluid Management	96
Hathaway, David H.	Newly Discovered Flows on the Sun's Surface	44
Holt, Dan M.	Ultrasonic Fuel-Regression Measurement in Hybrid Rocket Motors	84
	Pressure Oscillations in Hybrid Rocket Motors	88
	Development and Demonstration of a 250-Kilopound-Force Hybrid Rocket Test-Bed	92
	Solid Rocket Combustion Simulation Using the Hybrid Combustion Process	94
Horack, John M.	Gamma-Ray Bursts As A Tool For Cosmology	39
Howell, Joe T.	MagLifer	13
Hutchens, Cindy F.	Urine Pretreatment Methods for Microgravity	152
Hutt, John	Main and Preburner Injector Technology	78
Jacobs, William	Flight-Qualifiable, Three-Point Docking Mechanism Control Electronics for Automated Docking	181
Johnson, C. Les	Atmospheric and Ionispheric Research Using a Small Expendable Deployed Satellite	2
	Very Fine-Line Lithography for Extreme Ultraviolet and Soft X-Ray Optics	3
	The Magnetosphere Imager Mission	10
Keller, Vernon W.	Tether Applications on the Space Station	5
Kim, Jonnathan	Virtual Keyboard for Hands-Free Operations	18
Knox, James C.	Development of a Packed-Bed Adsorption Model With Predictive Capabilities	156
Krupp, Don R.	Reusable Launch Vehicle Lander Guidance and Control Research	102
Lee, Henry M.	Single-Cycle Versus Multicycle Proof Testing	122
Lee, Jonathan A.	Development of a High-Strength, Low-Cost Aluminum Piston Alloy	170

Lessels, Robert J.	New Technology Targets Eye Disease	197
	Space-Age Training Program Technologies Offered to Commercial Industries	198
	NASA Welding Technology Transfer to Private Industry	200
	Waterjet-Stripping Technology	201
	Rapid Prototyping	201
	Composites Technologies	202
	Composite Piping for Offshore Oil and Gas Industry	203
	NASA Assistance to the Physically Challenged	204
	Marine Jet-Propulsion Technology	205
	Portable Lifting Seat	207
	Ocular Screening System	207
	Hybrid Rocket Motor Technology	209
	Quick-Connect Nut and Bolt	209
	Improvements for Firefighters	211
Marsh, Matthew W.	Low-Cost Turbomachinery Technology	72
Martin, Charles	Results of an 11-Inch Liquid-Oxygen Hybrid Rocket Motor Combustion Instability Study	86
McMillan, Vernotto C.	Space Vehicle to Save Launch Costs	193
Meegan, Charles A.	The Third Burst and Transient Source Experiment Catalog of Gamma-Ray Bursts	38
Miller, Timothy L.	Numerical Modeling of Nonlinear Baroclinic Fluids Systems	34
Mims, Katherine K.	Composite Integrally Bladed Turbine	116
Min, James B.	Life Prediction of Ceramic- and Metal-Matrix Composites	127
Montgomery, Edward E.	Ultra-Lightweight Telescope, Integrated Missions for Astronomy	4
Moore, Craig E.	Prediction of Nonlinear Optical Properties of Organic Materials	32

Moore, Ronald L.	Solar Flares	51
Moore, Thomas E.	Plasma Tornadoes	65
Myers, George	TREETOPS Structural Dynamics and Controls Simulation System Upgrade	104
Nesman, Tom E.	Coherent-Phase Cavitation Monitoring System for Turbomachinery	131
Nunes, Arthur C., Jr.	Characterizing Metal Brittleness	168
Nurre, Gerald S.	Suppression of Transient Acceleration by Levitation Evaluation	101
Ortega, Rene	Life-Prediction Methodology for Ceramic-Matrix Composites	130
Parnell, Thomas A.	Measurements With a Superconducting Magnet Spectrometer	41
Perry, Jay L.	Poisoning Characteristics of a Palladium-Based Trace Contaminant Control System Catalyst	147
	Trace Chemical Contaminant Control System Performance Simulation	148
	Small, Efficient Metal-Substrate Catalytic Converter for Trace Contaminant Control	149
	Catalysts for the Oxidation of Trace Contaminants	151
	Trace Chemical Contaminant Generation Rates for System Design of Closed Habitats	151
Pollock, Craig J.	MSFC Thermal Plasma Instrumentation Probing the Topside, Cleft Ionosphere	55
Porter, Jason G.	Heating Magnetic Structures in the Solar Corona	45
Powers, William T.	Clamp-On Flow-Velocity and Density Transducers for Cryofluids in Thin-Walled Conduits	171
	Ground-Based Optical Leak Detection	172
	In-Flight Leak Detection: a Hydrogen/Oxygen Leak-Imaging Sensor	174
	Optical Plume Anomaly Detection Engine Diagnostic Filtering System	178

Rakoczy, John M.	Segmented Mirror Adaptive Optics	105
Ray, Charles	Trace Contaminant System Performance Simulation	148
Robertson, Franklin R.	Global Modeling of Surface Boundary Forcing	35
	Global Multiphase Water Analysis	36
Robinson, Jennifer H.	Orbital Debris Penetration Resistance of Reusable Launch Vehicles	144
Rodriguez, Pete I.	Composite Intertank	138
Roman, Monserrate C.	Developing a Microbial Monitor With Polymerase Chain-Reaction Technology	154
Rupp, Charles C.	Survivable Space Tethers	8
Schmidt, Deborah D.	Improved Single-Crystal Superalloys Tailored for Hydrogen Service	167
Schmidt, George	Magnetically Actuated Propellant Orientation	76
Self, Timothy A.	MSFC Small Business Innovation Research	188
Skelley, Stephen E.	Investigation of Flow Through a Power-Steering Flow-Control Valve	135
Smeltzer, Stan S. III	Composite Redesign of Obstetrical Forceps	145
	Composite Dome and Polar-Boss Leakage Validation	146
Smith, Andrew W.	Experimental Microthruster Evaluation at Simulated Orbital Conditions	136
Spann, James F.	The Dusty Plasma Experiment	59
Sparks, David L.	Low-Cost Combustion Devices Component Design Verification	73
Stinson, Helen C.	MSFC Small Business Innovation Research	188
Suess, Steven T.	The Fine-Scale Structure of the Interplanetary Magnetic Field	48
	Three-Dimensional Magnetic Field-Line Topology in the Outer Heliosphere	49
Szofran, Frank R.	Magnetic-Damping Test of Convective Flows in Microgravity	23

Traweek, Mary S..	Poisoning Characteristics of a Palladium-Based Trace Contaminant Control System Catalyst	147
Tinker, Michael L.	Hybrid Method for Measurement of Rotational Structural Dynamic Properties	125
Trinh, Huu P.	Tripropellant Injector and Combustion Technology	79
Trinh, Huu P.	Effects of Hydrogen Addition on RP–1 Droplet Burning in Oxygen Environment	80
Trinh, Huu P.	Unielement, Oxygen-Rich Preburner	82
Tygielski, Philip	A Lightweight, Composite, Liquid-Hydrogen Feedline	98
Volz, Martin P.	Electromagnetic Field Effects in Semiconductor Crystal Growth	22
Wells, Douglas N.	Casting Modeling Technology	169
Westra, Douglas G.	Pulse-Tube Refrigeration for Spacecraft and Commercial Applications	158
	Low-Temperature Stirling-Cycle Refrigerator for Spacecraft Refrigeration Systems	159
Williamsen, Joel E.	Orbital Debris Penetration Effects in Spacecraft Interiors	140
Witherow, William K.	Phase-Shifting Interferometric Analysis of Protein Crystal-Growth Boundaries and Convective Flows	27
	Diode-Laser Holographic-Imaging System Applied to the Study of Fluids in Microgravity	28
Wright, Michael D.	MSFC Propulsion Center of Excellence is Built on Solid Foundation	212

Index of Key Words

About Key Words
To broaden the availability of this report, this publication has been linked to the World-Wide Web at http://techtran.msfc.nasa.gov/95R&T/R&T.html. This enhances the opportunities for technology transfer.

ablative 74
ablative combustion chamber 73
absorber/thruster 96, 97
acrylonitrile butadiene rubber 90
active regions 53
adaptive 4
adaptive optics 105, 106
adsorption 148, 156, 157
Aerospace Industry Technology Program 193
alignment 181
aluminum alloys 162
aluminum-silicon 170
Aramid 90
atmosphere 34
aurora 65, 66
bearings 190, 191
blade 134
blisk 116, 117, 118
bonded 143, 144
bonded composite 143
brittle 168
Burst and Transient Source Experiment 38, 39, 40
capture 181
carbon monoxide 151
carbon-dioxide removal 156
casting 169
casting modeling 169
catalyst 151
catalyst system 149
catalytic oxidation 147, 148
cavitation 131, 132
center of gravity 113, 114
ceramic 195, 196
ceramic turbine 195
ceramic-matrix composites 127, 128, 130
chamber pressure 86, 88
charging mechanisms 59, 60
chlorofluorocarbon 158, 159
clamp-on transducer 172
climate variability 35, 36
cloud microphysical processes 37
coherent-phase wide-band demodulation 131, 132
combustion 78
combustion chamber 73
combustion efficiency 80
combustion simulator 94
combustion stability 78
communication 198
composite feedlines 98
composite honeycomb structures 143
composite intertank 139
composite piping 203
composite structures 138, 139, 143
composites 98, 100, 116, 117, 118, 119, 127, 138, 143, 144, 146, 147, 202, 203
compressors 190
Compton Gamma-Ray Observatory 38
computational fluid dynamics 136
Consortium on Casting of Aerospace Alloys 169
control 102, 103
control electronics 181
control room 183, 184, 185
controller 181
controls-Optics-structures-thermal 105
convection 23, 24, 27, 28
cooling 158, 159, 160
corona 52, 53
cracks 168
Cryogenic Fluid Management Subsystem 97
cryogenic 138, 146
cryogenic fluid management 96
crystals 22, 25
damping 111, 116, 117, 118, 119
damping seal 111
DC–X 202
deboost 5
design 138, 139
diamagnetism 76
diffraction 3, 25
diffusion 29, 30
diode-laser 29
disaster 7
docking 107, 181
ductile tearing 122
dusty plasma 59, 60

Earth system 34
effervescent atomizer 79
electroencephalogram 19
electromagnetic actuators 101
emissions 149, 150
ethylene propylene diene monomer 90
exhaust emissions 170
eye diseases 197, 198
eye disorders 197, 198
eye tracking 18, 19
fabrication 201, 202
Failure Assessment Diagram 122
feedline 98
ferrofluid 77
fiber optic 145
fiber-optic strain 145
fiber-reinforced polymer 145
film cooling 74
flares 46
flaw 129
flight-control augmentors 113, 114
flow 91
flow patterns 44
flow-control valve 135, 136
fluid density 171, 172
fluid-borne noise 135
fluids 29
fracture mechanics 122
frequency response functions 125, 126
full-wave rectification 131
gamma rays 12
gamma-ray bursts 38, 39, 40
gaseous hydrogen 80
generation rates 151
geometric factor 67, 68
Global Emergency Observation Warning and Relief System 7
Global Oscillations Network Group 44
global climate models 37
graphite/epoxy 98
graphite/epoxy composite feedlines 98
gratings 3
guidance 102, 103
Hard X-Ray and Gamma-Ray Imaging System 12
hard x rays 12, 51
heat transfer 78
heliosphere 49, 50
helium 158, 159, 160, 161
high brilliance 25
holography 28, 30
hot-fire test 112
human factors 183, 184
human metabolism 151
Hybrid Propulsion Demonstration Program 92
hybrid 84, 85, 88, 89, 92, 93, 94, 95
hybrid motor 86
hybrid motor chamber pressure oscillations 86
hybrid propulsion 92, 93
hybrid rocket motor 91, 209
hydrostatic 190, 192
hydrostatic bearings 190, 191
hypervelocity impact 144
inducer 134
inducer unsteady blade loads 134
infants 145
injector 78, 79
installation 177
installation integrity 176, 177
integrity 176
Interactive Multimedia Training 198, 199
International Space Station 152,153, 154, 155, 156
interplanetary magnetic field 48
interstellar medium 11
intertank 138, 139
ion density 62, 63, 64
ion heating 61
ionosphere 2
ions 59
J-integral 122, 129
Japanese/American Cooperative Emulsion Experiment 41
jet propulsion 205
kerosene 74
landing 102, 103
Large Subscale Solid Rocket Combustion Simulator 94, 95
large-aperture space telescope 105
launch vehicles 13, 112, 113
leak detection 175
leak rates 172
leakage 145, 147

life prediction 128
life-prediction methodology 130
liquid oxygen 76, 77, 78
lithography 3
loads 134
local effects 30
localized corrosion 162, 163
low cost 72, 73
low thermal conductivity 164, 165
low-latitude boundary layer 54
MagLifter 13
magnet spectrometer 41
magnetic 22, 23
magnetic fields 23, 24, 47, 48, 51,52,53,76
magnetohydrodynamic turbulence 51
magnetosheath 54, 57
Magnetosphere Imager 10
magnetosphere 2, 54, 62, 64
manufacturing 144
Marshall Avionics System Test-Bed 182
mass flow rate 171
mass-additive approach 126
measurement 176
metal substrates 151
metal-matrix composites 127, 128
metal-oxide catalyst 151
microbial monitor 155
microgravity 29, 101
microstructure evolution 29
microstructures 167
microthrusters 136, 137
modal testing 125
modeling 58, 169
Modular Combustion Test Article 78, 79
Modular Rocket Engine Control Software 182
modulation 131
multicycle 122
multicycle proof testing 122
NASA/FLAGRO 129, 130
near-stoichiometric/dilution injection 82, 84
nonlinear 32
nonlinear optical organic compounds 32
nonlinear optics 31
oceans 34
ocular screening system 207
offgassing 151
offshore oil 203, 204
Optical Plume Anomaly Detection 178
Optical Plume Anomaly Detection Engine Diagnostic Filtering System 178
optical 32
optical leak detection 172, 173
optical leak sensors 174
optics 4
optimization 138, 139
orbital debris 140, 144, 145
orbital simulation 137
oscillations 86, 87, 88, 89
overpressure 140, 141
oxygen 89
oxygen-rich preburner 82
paramagnetism 76
Passively Cooled Reconnaissance of the Interstellar Medium 11
penetration 140, 141
permeability 138
phase-shifting interferometry 27, 28
phase-synchronized enhancement method 119, 120, 129
photodeposition 31
photometer 197
photopolymerization 31
physically challenged 204
pistons 170
plasma 2
plasma tornadoes 65
plasmasphere 62, 63, 64
poisoning 147, 148
polar boss 146, 147
polyacrylonitrile 164, 165, 166
polydiacetylene 31
polymerase chain reaction 154, 155
portable lifting seat 207
power generation 5, 7
presence 181
presence sensors 181
preswirl 111
pretreatment 152, 153
proof tests 122
propellant injection 80
propellant orientation 78
propulsion 17, 92, 98
propulsion feed systems 98
protein 25
protein crystal growth 28
protein crystals 26

pulse-tube refrigerator 158, 159
quick-connect nut and bolt 209
Raman scattering 174
rapid prototyping 201, 202, 205
reboost 5, 6, 7
reconnection 51, 52
reduced gravity 23
reference stress method 129
regression 84, 85
regression rate 81
reliability 122
rendezvous 107
residual flexibility method 126
return capsules 5, 6
reusable launch vehicles 102, 144, 145
reusable solid rocket motor 90
Scanning Reference Electrode Technique 162, 163
Scanning Thermal Ion-Composition Spectrometer 55, 56
seals 111
semiconductor 22
sensors 181
SIMPLEX 72, 73
simulators 95
single crystal 167
single cycle 122
single cycle proof testing 122
single-stage-to-orbit 102
Small Business Innovation Research 188, 189, 190
Small Business Technology Transfer 188
Small Expendable Deployer System 8
soap leak inspection 174
soil moisture 36
Solar Oscillations Investigation-Michelson Doppler Imager 44
Solar Test Facility 97
Solar Thermal Upper Stage 193
Solar Thermal Upper-Stage Technology Program 17
solar corona 45
solar flares 47, 51
solar propulsion 96
solar thermal propulsion 17, 96
solar wind 48
Solid Propulsion Integrity Program 164, 166
solidification 169
Sounding of the Cleft Ion-Fountain Energization Region 55, 57
space shuttle main engine 182
space weather 57, 58
stabilization 88, 89
Stirling-cycle refrigerator 159, 160
strains 134, 145
stress intensity 129
structures 138, 139
subflares 46
subrack isolation 101
subsynchronous whirl 111
Sun 47, 48, 49, 50, 52, 53
superalloys 167
superthermal ion-mass spectrometer 61, 62
Suppression of Transient Acceleration by Levitation Evaluation 101
survivability 8
swirl coaxial injector 84
synchronous phase averaging 119, 120, 121
synchronous time averaging 119, 120
System for Anomaly and Failure Detection 112
Technology Test-Bed 112
telescope 4, 5
termination shock 49, 50
tether 2, 5, 6, 8, 9
Thermal Electron Capped-Hemisphere Spectrometer 55, 56, 57
Thermal Ion Dynamics Experiment 67, 68
thermal protection system 144, 145
thermocouple 176
thermoelectromagnetic convection 24
thin-film growth 31
three-point docking mechanism 107, 181
time domain averaging 119, 120
trace contaminant control 148, 151
transducers 84, 85
tree topology 104
TREETOPS 104
tricoaxial swirl injector 79
tripropellant 79, 80, 81
turbine 195, 196
turbine gas 72, 73
turbomachinery 72, 73, 117, 119
turbopumps 190,195, 196

ultrasonic 85
ultrasonic transducers 84
ultraviolet 31
Ulysses 48
unielement combustor 80
unsteady 134
unsteady blade loads 134
upper atmosphere 2
urine 152, 153
urine pretreatment 152, 153
vacuum chamber 136
Van Allen 10
vector magnetograph 47
vertical 102, 103
vertical landing 102
virtual keyboard 18
virtual reality 183, 184
vortex 65, 66
Voyagers 49, 50
water recovery 152
water ski 204
water-recovery system 154, 155
water-vapor feedback 35
waterjet-stripping technology 201
wavefront sensor 105, 106
weld-bead seam tracker 200
welding 168, 200
whirl 111
X–33 ..... 201, 202
X–34 ..... 201, 202